INFORMATION TO USERS

This manuscript has been reproduced from the microfilm master. UMI films the text directly from the original or copy submitted. Thus, some thesis and dissertation copies are in typewriter face, while others may be from any type of computer printer.

The quality of this reproduction is dependent upon the quality of the copy submitted. Broken or indistinct print, colored or poor quality illustrations and photographs, print bleedthrough, substandard margins, and improper alignment can adversely affect reproduction.

In the unlikely event that the author did not send UMI a complete manuscript and there are missing pages, these will be noted. Also, if unauthorized copyright material had to be removed, a note will indicate the deletion.

Oversize materials (e.g., maps, drawings, charts) are reproduced by sectioning the original, beginning at the upper left-hand corner and continuing from left to right in equal sections with small overlaps.

Photographs included in the original manuscript have been reproduced xerographically in this copy. Higher quality 6" x 9" black and white photographic prints are available for any photographs or illustrations appearing in this copy for an additional charge. Contact UMI directly to order.

ProQuest Information and Learning
300 North Zeeb Road, Ann Arbor, MI 48106-1346 USA
800-521-0600

NOTE TO USERS

This reproduction is the best copy available.

UMI®

University of Alberta

PRENATAL DEVELOPMENT OF THE RAT PHRENIC NERVE AND DIAPHRAGM: BASIC EMBRYOLOGY, ROLE OF PSA-NCAM AND THE PATHOGENESIS OF CONGENITAL DIAPHRAGMATIC HERNIA

by

DOUGLAS WATT ALLAN

A thesis submitted to the Faculty of Graduate Studies and Research in partial fulfilment of the requirements for the degree of Doctor of Philosophy.

Department of Physiology

Edmonton, Alberta

Spring 2000

University of Alberta

Library Release Form

Name of Author: Douglas Watt Allan

Title of Thesis: PRENATAL DEVELOPMENT OF THE RAT PHRENIC NERVE AND DIAPHRAGM: BASIC EMBRYOLOGY, ROLE OF PSA-NCAM AND THE PATHOGENESIS OF CONGENITAL DIAPHRAGMATIC HERNIA.

Degree: Doctor of Philosophy.

Year This Degree Granted: 2000

4 Southpark Court
Hay Street
Elgin, Morayshire, IV30 1NJ
Scotland

MAR 24, 2000

University of Alberta

Faculty of Graduate Studies and Research

The undersigned certify that they have read, and recommend to the Faculty of Graduate Studies and Research for acceptance, a thesis entitled **Prenatal Development of the Rat Phrenic Nerve and Diaphragm: Basic Embryology, Role of PSA-NCAM and the Pathogenesis of Congenital Diaphragmatic Hernia** submitted by **Douglas Watt Allan** in partial fulfilment of the requirements for the degree of Doctor of Philosophy.

Dr. John Greer

Dr. Lynn Landmesser

Dr. Robert Campenot

Dr. Tessa Gordon

Dr. Warren Gallin

Dr. Esmond Sanders.

Feb 9, 2000
Date

For Mum and all my family:

Hey mum, yir loon didna dae aw that bad!!

ABSTRACT

The phrenic nerve and diaphragm constitute the major neuromuscular system of the respiratory network, and its proper development is critical for survival at birth. However, data regarding the prenatal development of the phrenic nerve and diaphragm are inconsistent and incomplete. Studies performed here have: 1) Described the embryogenesis of the phrenic nerve and diaphragm and the maturation of phrenic motoneuron morphology throughout prenatal development, 2) Examined the molecular control of certain aspects of phrenic-diaphragm morphogenesis. 3) Performed parallel studies investigating the pathogenesis of congenital diaphragmatic hernia in a rodent model of this developmental anomaly.

These studies identify the primordial diaphragm (the pleuroperitoneal fold) and describe phrenic axon outgrowth and the formation of the diaphragm neuromusculature from the time of initial axonal outgrowth (E11) to birth in the rat. This offers substantive understanding of phrenic-diaphragm development and demonstrates that many text-book descriptions are likely incorrect. These studies have also found that expression of the anti-adhesive polysialylated (PSA) form of neural cell adhesion molecule (NCAM) implicates its role in selective guidance of phrenic axons as they diverge from brachial axons at the brachial plexus. A whole embryo culture system has been adopted for future testing of this hypothesis. PSA-NCAM has also been found to be a potential modulator of myotube separation during muscle morphogenesis; its expression is concentrated to juxtaposed membranes of separating myotubes and evidence suggests that its enzymatic removal inhibits myotube separation in the rat diaphragm. Retrograde labelling with the lipophilic dye, DiI, of phrenic motoneurons which analysed somatodendritic morphology throughout embryonic development showed that major morphological reorganisation and maturation occurs subsequent to the onset of functional respiratory drive, implicating this drive in these modifications.

Congenital diaphragmatic hernia (CDH) is an often fatal developmental disorder in which a large region of the diaphragm is missing. How it arises embryologically is poorly understood. Using a well-established nitrofen-induced rodent model of CDH, we have performed the first systematic assessment of prevalent hypotheses regarding CDH pathogenesis. Results indicate that these theories are incorrect and refocus the field to an examination of early developmental events during formation of the pleuroperitoneal fold.

ACKNOWLEDGEMENTS

A special thanks to **Dr. John Greer**, my supervisor. First and foremost, he showed me the trust that enabled us to continually try new things all the way along, and his scientific guidance made this the rewarding learning experience that it has been.

Thanks to the technicians over the years, **Jody Carter, Brian Parsons** and **Wei Zhang**. They have been a huge help, taking the load off my back and making this an easier process.

Thanks to the Grad Students in the lab, **Zaidoon Al-Zubaidy, Miguel Martin-Caraballo** and **Randy Babiuk**. I'd also like to thank **Dr. Robert Lemke** and the new post-doc, **Dr. Calvin Wong** for rekindling my excitement about this work and science in general when I was wilting under the pressure of getting this finished.

Thanks also to all the summer and rotation undergraduate students. Each one worked closely with me, often for long long hours, and helped me generate the body of grunt work that was essential to getting this data together. Each one also kept my spirits up with their humour and sense of fun and were patient while I slowly learnt how to teach. Many are now long term friends and that says it all. **Alex Gill, Robbie 'The Jobbie' Erickson, Megan Lalonde** and **Linh Li, David Cote, Marieke Schoenmakers** and of course **Rob 'Jobman' Stack** and **Kelly Santarossa**.

I'd also like to say a special thanks to **Dr. Keith Bagnall** for constant support of my work and helping us sort out the anatomical aspects of normal and defective diaphragm formation. Also, **Dr. Victor Rafuse** for his constant help on the PSA-NCAM project. Also, **Neil Tyreman** for constant help and for letting me nick things from his lab. **Dr. David Olson**, who was always supportive and helped financially with travel awards.

Also, I would like to thank those who provided great support at specific points of my research. **Dr. Warren Gallin** who gave so much of his time to hold my hand through manufacture of the endoN enzyme. **Dr. Esmond Sanders** and **Bill Keyes** for help with getting the chick work started. **Dr. Susan Fu** who contributed with very insightful conversations over my first couple of years when we were trying to find our way. **Dr. Marc Ridyard** for help with the Westerns. **Dr. Theodore Petrov** for advice on the immunohisto over my first year. **Honey Chan** basically did the electron microscopy. **Robert Rolf**, the department computer guy who always gave his time to keep the computers ticking. **Vera Chlumecky** for teaching us how to work a confocal microscope.

I also want to thank those who have been on my committee, who all were people I respected and learnt a lot from. **Dr. Tessa Gordon, Dr. Robert Campenot, Dr. Kier Pearson, Dr. Warren Gallin, Dr. Esmond Sanders**. And I would also like to extend my great appreciation to **Dr. Lynn Landmesser** for agreeing to be my external and being such a cool

person when she was here.

I also have to think past and present members and the secretarial staff of the Departments of **Neuroscience, Physiology** and the **Perinatal Research Centre.** It was these people who made it fun and smoother than it would have been without them.

There are many people who were great friends throughout and through parts of this last 6 years, but I'd like to especially mention a few people who have been great pals over a long period. Of course **Lenka,** my girlfriend, I love you very much. And her cat, **Mickey** (who liked to sit on my papers when I was working at home). Also, Lenka's family who made me so welcome at their homes and fed me so many times. **Marc 'Rocco' Ridyard** who kept Pierre to himself but got a 180 in anger. **Leo 'Sol' Sanelli** You're OK buddy, I don't care what everyone else on this list says!! **Alex 'Igor' Gill** and **California Mark,** who are both very wierd. **Brian** who was always up for a pint. **Bag o' Doughnuts,** I knew I'd leave as soon as the Oilers got good, I was accurate to a couple of months!! Also, all those people on my various football and volleyball teams, all those I got to know in the various pubs and restaurants (especially **Milan the Czech)** I hung out in, and all those who basically made my life more fun, especially **Calum** and **Kirsty, Bill, Debs, Gayle, Karen, Paul, Abdul, Wale, Dave** and **Monica, Sharla, Gordie, Pete** and **Sandra, Stuart, Mike** and **Catherine, Di, Costas, Anna,** (and **Emma, Elspeth, Virginia, Jock** and **Sheila**) and too many others.

I would also like to thank the following for supporting my research over the years. The **Alberta Heritage Fund for Medical Research,** the **Izaak Walton Killam Foundation** and **The University of Alberta** (U of A PhD Scholarship, Dissertation Fellowship).

TABLE OF CONTENTS

LIST OF FIGURES

LIST OF TABLES.

LIST OF ABBREVIATIONS

BrdU, bromodinated uridine

C3-C6, cervical spinal segments 3-6.

CDH, congenital diaphragmatic hernia.

DAB, 3,3-diaminobenzidine tetrahydrochloride

DAPI, 4',6-Diamidino-2-phenylindole

DiI, 1,1'-dilinoleyl-3,3,3',3'-tetramethylindicarbocyanine perchlorate.

DREZ, dorsal root entry zone

DRG, dorsal root ganglion.

E0-E22, embryonic day 0 to 22

ECM, extracellular matrix.

ECL, enhanced chemiluminescence

endoN, α-2,8-endoneuraminidase N

FGFR, fibroblast growth factor receptor.

GAP-43, growth associated protein.

GPI, glycosylphosphatidylinositol

H&E, haematoxylin and eosin

HGF/SF, hepatocyte growth factor/scatter factor

HRP, horseradish peroxidase.

IgG, immunoglobulin type G

IgM, immunoglobulin type M.

IgCAM, immunoglobulin-like cell adhesion molecule.

LIM, denotes a family of genes/proteins originally defined by *C. elegans* Lin-11, rat Isl-1 and *C. elegans* Mec-3.

Mab, monoclonal antibody

MHC, myosin heavy chain

M-cadherin, muscle cadherin

N-cadherin, neural cadherin.

NCAM, neural cell adhesion molecule.

P0, postnatal day 0 (the day of birth).

p75, low affinity nerve growth factor receptor.

Pab, polyclonal antibody.

PBS, phosphate-buffered saline.

PCM, pleuropericardial membrane.

PCNA, proliferating cell nuclear antigen

PHMP, posthepatic mesenchymal plate.

PPC, pleuroperitoneal canal.

PPF, pleuroperitoneal fold.

PSA, polysialic acid

PSA-NCAM, polysialylated neural cell adhesion molecule.

St 30-40, chick developmental stage 30-40, according to Hamilton-Hamburger Staging.

SDS-PAGE, sodium dodecyl sulphate-polyacrylamide gel electrophoresis

TLC, thin liquid chromatography.

TTX, tetrodotoxin

Chapter 1

GENERAL INTRODUCTION

General Aims

The goals of these studies were: 1) to describe key developmental steps in the formation of a single well-defined mammalian motor system essential to respiratory function from the initiation of spinal nerve outgrowth at E11 up to birth, 2) to start examining aspects of the molecular regulation of phrenic axon outgrowth and myogenesis, and 3) to start applying this knowledge towards a fundamental understanding of the pathogenesis underlying a high incidence congenital abnormality affecting respiratory function with 50% mortality. The studies fall into three general categories.

1) ***Embryology:*** 1) How do the phrenic nerve and diaphragm arise embryologically? The literature regarding prenatal development of the phrenic nerve and diaphragm has been largely inconclusive and has proven insufficient to offer any substantive understanding of relevant congenital abnormalities. Further, even modern embryological and medical texts derive their explanation of diaphragmatic development from assumptions based upon gross anatomical dissection of a small number of human fetuses in the first half of the century. This is somewhat surprising given the critical importance of the respiratory system to survival at birth and the implications to respiratory disorders in human perinates. This thesis describes work examining the formation of the phrenic nerve and diaphragmatic musculature as well as the identity and formation of the primordial diaphragm. Definitive information regarding the development of the major effector of the respiratory system is of interest to those working in the field of respiratory system development and to clinicians treating infants with respiratory disorders. 2) How does phrenic motoneuron somatodendritic morphology arise? Phrenic motoneurons have a characteristic morphology, postulated to be directly related to their function, that is essentially intact by birth. Studies presented here have directly examined phrenic morphology from the initiation of neuromuscular formation up to birth. A critical time has been identified in which dramatic somatodendritic reorganisation leads to the attainment of the characteristic mature phrenic motoneuron morphology.

2) ***Neuromuscular Development:*** What factors play a role in the formation of the neuromusculature? Many molecules have been identified which have been demonstrated or

implicated to have particular roles in neuromuscular morphogenesis. This thesis describes initial attempts to utilise our new understanding of diaphragm embryology to understand the molecular modulation of phrenic axon guidance and diaphragm muscle formation. These studies implicate a role for the polysialylated form of the neural cell adhesion molecule (PSA-NCAM) in selective phrenic axon guidance and specific phases of muscle morphogenesis.

3) ***Clinical Relevance:*** How does the pathology of congenital diaphragmatic hernia (CDH) arise? CDH is a developmental anomaly in which entire regions of the diaphragm fail to form. Resultant herniation of abdominal contents into the thoracic cavity retards lung development to the extent that pulmonary compromise leads to ~50% mortality, despite modern intervention. Despite the prevalence (1:2000 conceptuses and 1:3000 births) of CDH and the extent of cardio-respiratory sequalae in survivors, the understanding and treatment of CDH is surprisingly rudimentary at best. Theories pertaining to the pathogenesis and the treatment of CDH are almost as numerous as those participating in both pursuits. There is general agreement that an inadequate understanding of normal diaphragmatic development has been a major contributor to our ignorance concerning the pathogenic mechanism of CDH. We have applied our new understanding of the normal development of the diaphragm to examine the underlying causes for CDH in a well established rodent model. We have systematically examined the prevalent theories and discounted them as secondary to the diaphragmatic defect. Instead, we propose a novel mechanism for the genesis of CDH which refocuses the field on the aberrant formation of the pleuroperitoneal fold.

General Introduction

One key feature of the studies described here has been to integrate these goals, so that no one aspect stands alone and each contributes to a larger picture. Essentially, these studies would be rightly viewed as an initial attempt to come to grips with a previously poorly understood system and to use it to obtain information of specific and general interest as outlined above. The following introductory text shall be devoted to a brief review of respiratory function and then a focussed review of these categories. This background text is not intended to be exhaustive, but to provide a general context for the work performed.

General Considerations Regarding Respiration

Respiration, or eupnea, is a neurogenic motor behaviour generated within brainstem ponto-medullary circuits. The rhythm generated by these circuits is under strict modulation by sensory feedback from peripheral mechanoreceptors and central and peripheral chemoreceptors, in particular. Together with input from higher brain centres, these match the activity of respiratory neuromusculature to the ventilatory demands of homeostatic regulation and physical activity. Further, respiratory pattern and rhythm are significantly modulated during such tasks as phonation, swallowing, vomiting, physical tasks, defaecation, coughing and sneezing etc, likely at a central level. Respiratory pattern and rhythm output from these centres imposes highly coordinated inspiratory and expiratory phase activity on spinal and cranial motoneurons that innervate the muscles of respiration. The major neuromuscular component of the respiratory network is the phrenic nerve and diaphragm. This motor system receives monosynaptic inspiratory drive via bulbospinal premotor interneurons whose somata reside adjacent to respiratory generating circuits within the ventrolateral medulla.

Unlike other motor systems, that controlling respiration must be fully functional by birth to ensure viability. Although significant maturational changes do occur in the respiratory system of all mammals from birth into the first few weeks of life and into adulthood, a neuronal network which controls breathing is essentially intact by birth (Hilaire and Duron, 1999). In fact, respiratory-related movements commence prior to birth and appear to be crucial for aspects of *in utero* fetal development, perhaps even beyond that promoting

respiratory neuromuscular maturation (see Navarette and Vrbova, 1993). For example, prenatal lung maturation is dependant upon respiratory-related movements (Harding et al., 1993; Harding 1994). Rhythmic fetal respiratory movements are a common feature of mammalian fetal development (Jansen and Chernick, 1991), commencing in humans at the start of the third month (nine month gestation) (De Vries et al., 1982), in lambs at embryonic day (E) 65 (147 day gestation) (Cooke and Berger, 1996), in mice at E15.5 (19 days gestation) (Suzue, 1984), and in rats at E17 (21 day gestation) (Greer et al., 1992; DiPasquale et al., 1992).

The Central Pattern Generator of Respiration

Several brainstem sites in the pons and medulla possess respiratory-related activity compatible with a role in the generation of respiratory rhythm and pattern (refer to recent reviews for details: Funk and Feldman, 1995; Rekling and Feldman, 1998; St. John, 1998). Studies by Smith et al. (1991) identified a region intersecting the rostral extent of the VRG and the Bötzinger complex, the pre-Bötzinger complex, which appears responsible for respiratory rhythmogenesis (reviewed in Funk and Feldman, 1995; Rekling and Feldman, 1998). Electrophysiological studies and calcium imaging of propriobulbar neurons in the pre-Bötzinger complex have identified numerous cellular properties which are consistent with a role in the generation of phases of the respiratory cycle (Koyisha and Smith, 1999; reviewed by Funk and Feldman, 1995; Rekling and Feldman, 1998). These neurons display either tonic, phase-spanning, inspiratory or expiratory-related patterns of discharge (Smith et al., 1990, 1991; Onimaru and Homma, 1992; DiPasquale et al., 1994; Paton, 1996; reviewed in Funk and Feldman, 1995; Rekling and Feldman, 1998). However, as noted by Funk and Feldman (1995) "...no causal relationship between any neuron type and respiratory rhythm has been established". Much of the debate regarding rhythm generation has surrounded whether respiratory rhythm is generated by a network of interacting inhibitory and excitatory neurons, a population of pacemaker cells or a hybrid of these two models (Richter et al., 1992; Smith et al., 1995; Funk and Feldman, 1995; Rekling and Feldman, 1998). Currently, the hybrid model seems to be favoured. It should be emphasised that whereas many of the key studies regarding respiratory rhythmogenesis have come from

examination of the pre-Bötzinger complex, reports emphasise that further sites, most notably the pneumotaxic centre of the pons, may contribute to the generation and/or modulation of respiratory pattern and rhythm (reviewed by St.-John, 1998).

Muscles and Work of Respiration

The muscles of respiration constitute two primary groups, those of the pump which generate the work of breathing, supplied by spinal innervation, and those of its valve which regulate upper airway resistance, supplied by cranial innervation. The pump comprises the muscles of inspiration and expiration which regulate intrathoracic volume. Mechanical coupling of the lungs to increases-decreases in intrathoracic volume results in the influx-efflux of air in the lung for gaseous exchange. The valve is composed of upper airway muscles which regulate airway resistance in the larynx and pharynx. At rest, inspiration is the primary drive for ventilation, expiration being a passive activity marked by the relaxation of the muscles of inspiration. Inspiration results from the contraction of the diaphragm, which increases volume axially, and a contribution (which varies with ventilatory demand) from the external intercostal and parasternal muscles which lift the ribcage, increasing volume radially. Increasing ventilatory demand enhances inspiratory muscle recruitment. Additional contribution from internal intercostal and abdominal muscles during forced expiration acts to constrict intrathoracic volume. Other motor activities for which these muscles are recruited include vomiting, coughing, hiccuping, postural shifts, defaecation, phonation.

Phrenic nerve and Diaphragm

The phrenic nerve and diaphragm constitute the major neuromuscular system of the respiratory pump, contributing about 80% of respiratory load in animals (Sant'Ambrogio and Camporesi, 1973). For a review of the neural control of the diaphragm, see Sieck (1991). The diaphragm is composed of bilaterally identical muscles, commonly termed hemidiaphragms, each comprising two muscles, the costal and the crural. The costal is composed of bilateral flat sheets of muscle separated by a central tendon which fully separates the abdominal and thoracic cavities. The costal muscle sheets intercalate laterally with the ribcage, ventrally

with the sternum and dorsally with a short tendinous zone separating the costal and crural regions. The crural is a thicker muscle encapsulating the oesophagus. For comprehensive reviews of diaphragm morphology, function and ultrastructure, see Leak (1979), Sieck, 1988 and Skandalakis et al. (1994).

Bilateral phrenic nerves innervate the ipsilateral hemidiaphragm. Phrenic motoneuron somata reside in bilateral clusters within a narrow ventromedial column through cervical spinal segments C3-C6 (rat: Kuzuhara and Chou, 1980; Goshgarian and Rafols, 1981). They possess a characteristically dense rostrocaudal dendritic tree which runs the entirety of the motor nucleus and is postulated to synchronise discharge (rat: Furicchia and Goshgarian, 1987; Torikai et al., 1996). Innervation of the diaphragm comprises ~240α-motoneurons, ~9 γ-motoneurons and ~120 sensory neurons in the rat. The paucity of γ-motoneurons reflects the virtual absence of muscle spindles and fusimotor drive, perhaps in order to limit reflex feedback which may interfere with the generation of repetitious muscle function throughout life. Golgi tendon organs and small calibre fibres account for a greater proportion of sensory feedback. However, despite projections to phrenic motoneurons and numerous supraspinal centres including respiratory-related centres, their influence during the normal ventilatory pattern is generally considered to be slight (reviewed in Monteau and Hilaire, 1991).

The phrenic nerve enters each hemidiaphragm at a central point, adjacent to the inferior vena cava on the right side, and trifurcation of the phrenic nerve provides separate innervation to the sternal costal, dorsolateral costal and crural areas. During respiratory activity, both costal and crural muscles are co-activated, but functional differentiation is observed during postural change (Lunteren et al., 1985) and the crural muscle is silenced when swallowing and vomiting (Monges et al., 1978; Aziz and Rex, 1984). This functional differentiation is consistent with the compartmentalisation of motor units into costal and crural units (Ogawa, 1959; Hammond et al., 1989). In fact, the costal diaphragm is likewise segmented into distinct motor unit territories. The rostrocaudal position of phrenic motoneuron soma in the cervical spinal cord is faithfully represented as a somatotopic map of innervation across the costal surface (Landau et al., 1962; Duron et al., 1979a, b; Laskowski and Sanes, 1987; Fournier and Sieck, 1988; Hammond et al., 1989; Gordon and Richmond, 1990). Such somatotopy is a general feature of neuromuscular systems (Sanes,

1993) and may reflect an efficiency of organisation in addition to any potential functional significance (Roussos et al., 1976).

Studies of development of the phrenic nerve and diaphragm

In relation to the general study of neuromuscular system development, that controlling diaphragmatic function is particularly amenable for addressing a number of developmental issues in a number of regards:

1) The neuromusculature is small, a bilaterally paired muscle innervated by ~220 motoneurons as opposed to 40 muscles innervated by ~20,000 motoneurons in the chick hindlimb (Landmesser, 1992a).

2) The phrenic nerve and diaphragm is anatomically isolated throughout development. In the vertebrate limb, individual muscles form by subtractive segregation of primordial ventral and dorsal muscle pools. Motoneuron nerve trunks sequentially segregate down to individual muscle nerves that branch into their specific muscles. These factors limit analysis of early events in neuromuscular formation to mixed populations of neurons and muscles when examining targeting of neurons and muscles to specific embryonic locations and early neuromuscular interactions. In contrast, from early in its development (see Chapter 4), the diaphragm is anatomically isolated from other motor systems, providing unambiguous discrimination of an identified muscle and its nerve as they migrate to the target embryonic region and initiate neuromuscular formation.

3) Unlike the majority of limb muscles which form with a roughly cylindrical geometry, the diaphragmatic musculature develops in an essentially two dimensional geometry, across which the phrenic axons traverse, emanating from a single, central innervation point (see Chapter 4). These factors make the delineation of axonal growth and muscle formation very simple at all developmental stages, and provide an ideal format for correlating key developmental events with the expression of molecules of interest towards the eventual goal of understanding mammalian neuromuscular development at the molecular level.

4) The respiratory network is simple: i) the primary motoneuron population is unambiguously identifiable from E13.5, both morphologically (backlabelling) and electrophysiologically (antidromic stimulation), ii) the central pattern generating core resides within a known region

of the medulla at a distance from the motoneuron pool in cervical segments C3-C6, 4) phrenic motoneurons receive monosynaptic input from a known source, 5) the pattern consists of a single repetitious inspiratory discharge which evokes a single contraction of the diaphragm, 6) the time of the onset of functional drive is known, and 7) experimentally, function is spontaneously maintained *in vitro* in a variety of reduced preparations and the advent of murine genetic technologies will permit a molecular dissection of respiratory system development.

These shall be discussed in their relevant context throughout this thesis. A time line has been provided (Fig. 1.1) to orient the reader to the major developmental events of phrenic nerve and diaphragm development in the rat. An additional timeline comparing aspects of these events to equivalent events in human development is provided (Fig. 1.2).

Fig. 1.1: Timeline of Rat Phrenic Nerve-Diaphragm Development

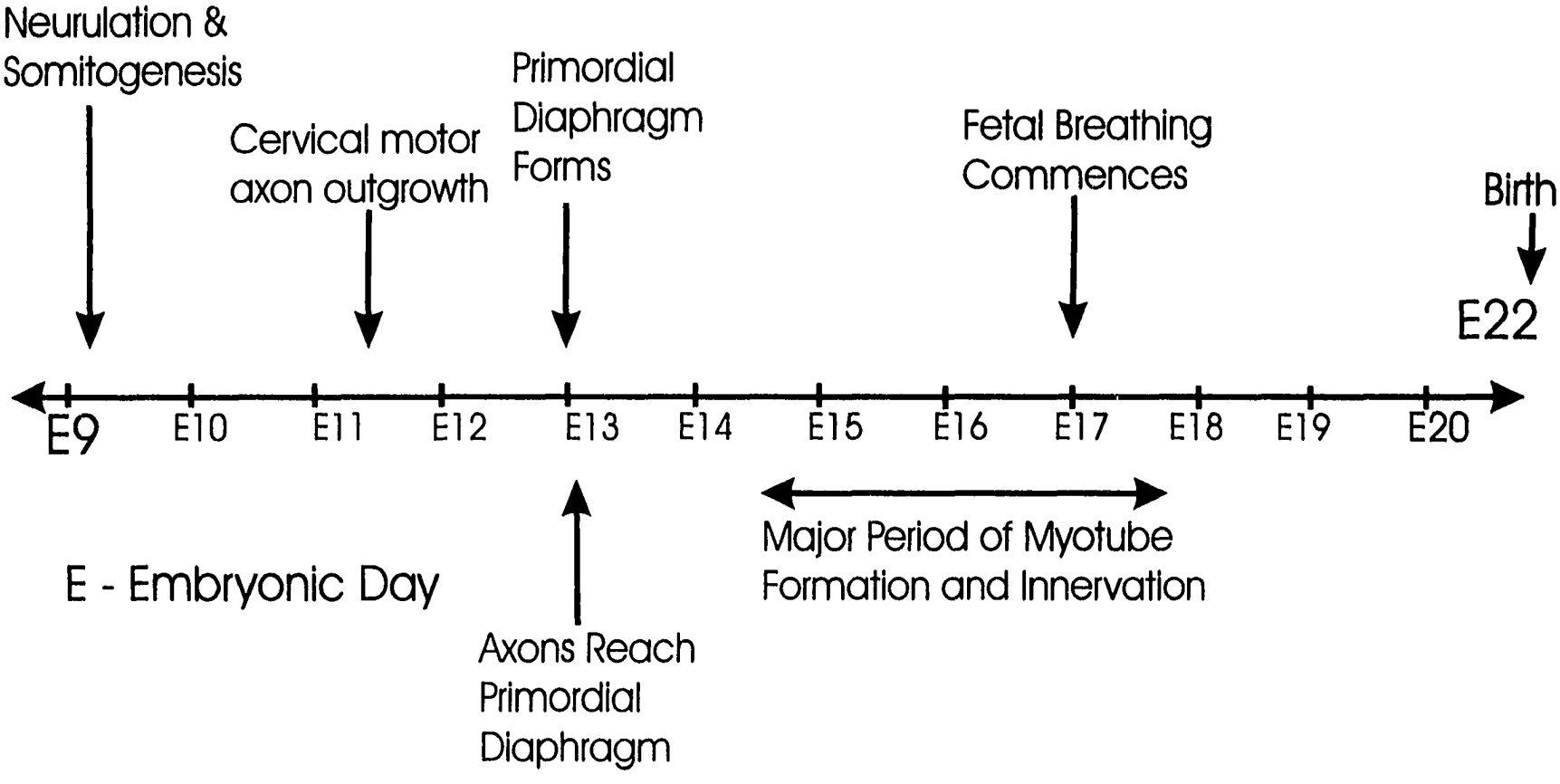

Fig. 1.2: Relative Timelines of Human And Rat Development

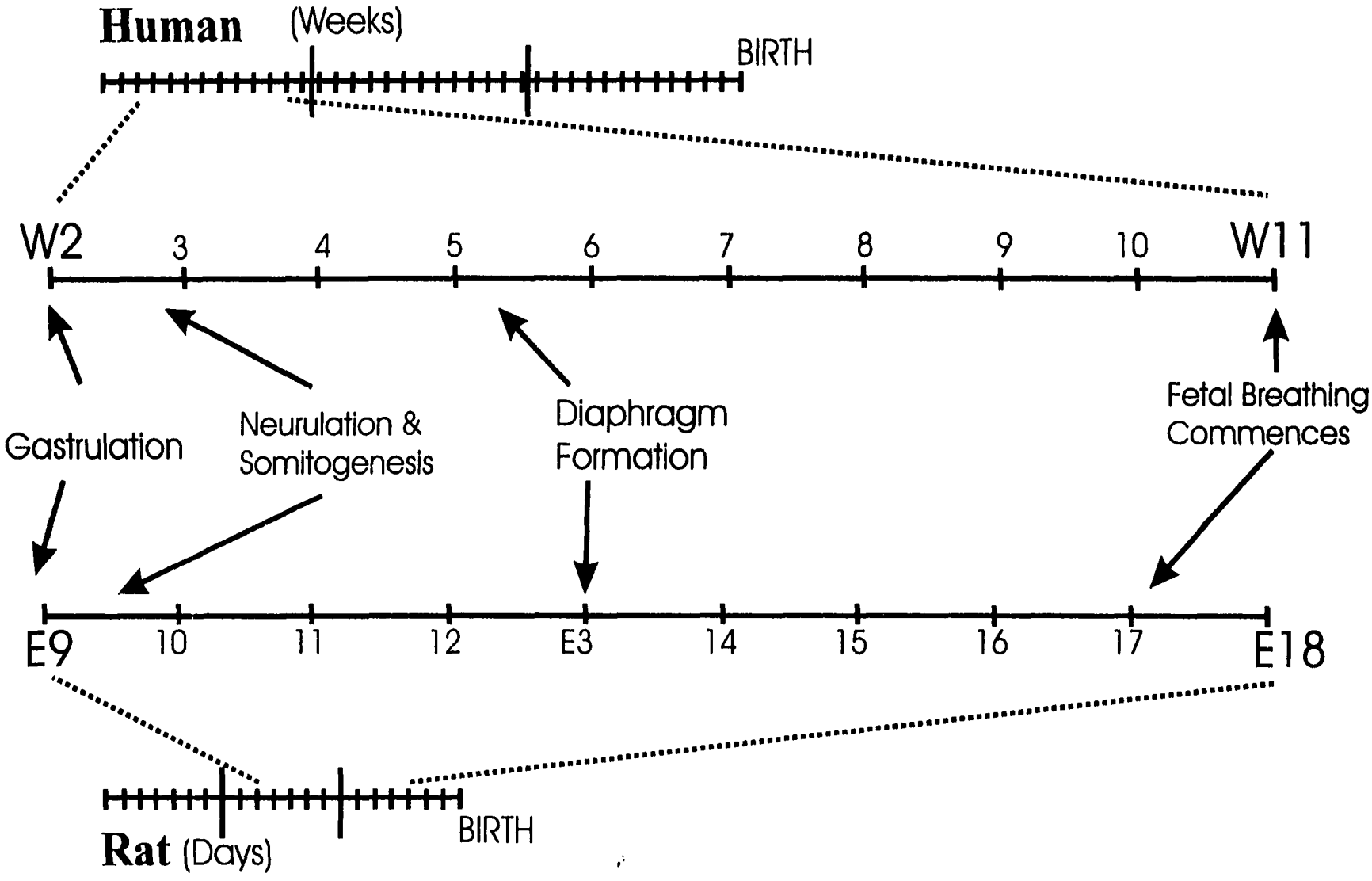

Embryology of the phrenic nerve and diaphragm

In contrast to the dogmatic approach taken in the majority of medical texts and textbooks of embryology, the scientific literature concerning phrenic nerve and diaphragm ontogeny has been controversial, often contradictory and lacking in rigorous systematic study. This is somewhat surprising for a two primary reasons: 1) the importance of diaphragmatic function for fetal lung development and neonatal breathing, and 2) an understanding of the pathogenesis of congenital diaphragmatic hernia would undoubtedly benefit from an understanding of phrenic-diaphragm embryogenesis. Essentially, much of the dogma regarding phrenic-diaphragm development has derived from standard drawings and texts (as fully depicted in Skandalakis et al., 1994), based upon interpretations of gross anatomical dissections of human fetal tissue in the first half of the century (eg. Mall, 1910; Wells, 1954). Their findings have been faithfully propagated to this day in the medical and scientific literature, with only the best texts noting that there has been very little data upon which to base these assumptions (eg. Kluth et al., 1989, Skandalakis et al., 1994). Even Wells (1954) noted that the earlier attempts "had to contend with a scarcity of good specimens". Yet he only used 12 preserved human embryos of uncontrolled age to gauge the complete aetiology of the diaphragm and the pathogenesis of congenital diaphragmatic hernia. In deciding which specimens to use, he noted, "it had been decided not to use the very best embryos'. Such a situation prompted Professor J.C. McLachlan (1996) to succinctly comment, "I would be happy to give a pound to everyone who really understands the development of the diaphragm, if in return I received a pound from everyone who has merely committed the official description (and those diagrams) to memory".

Much of the ambiguity regarding phrenic-diaphragm development has been due to the difficulty of experimental study of neuromuscular development in uterine animals. It should be stressed here that the diaphragm is an exclusively mammalian adaptation, although it is typical of the majority of skeletal muscles. The application of techniques developed over the last 20 years in particular now enable a rigorous examination of phrenic nerve and diaphragm development. In the 70's and 80's, technical advances led to a number of publications which dealt with various aspects of rodent diaphragmatic neuromuscular

development (most notably Bennett and Pettigrew, 1974; Harris 1981a-c; Noakes et al., 1983; Harris and McCaig, 1984; Laskowski and Sanes, 1987; Harris et al., 1989). However, despite their contribution to our general knowledge concerning neuromuscular development, they did not resolve any of the longstanding issues regarding the origins of the diaphragmatic tissues. Both embryologists and clinicians still had many important questions unanswered.

Studies performed in chapter 4 discuss our data regarding the embryogenesis of the diaphragm. These initial studies have been expanded upon in subsequent chapters. We anticipate that future discussion of phrenic nerve and diaphragm development shall draw a large component of its support from these studies.

Neuromuscular Development

The following chapters frequently refer to multiple aspects of neuromuscular development. To put these into context, this introductory section describes key aspects of the development of nerve and muscle in the embryo. To avoid reviewing what is a very large literature, this section is presented from the perspective of factors of potential relevance to the developing phrenic nerve and diaphragm. How neurons and muscles are generated, specified, positioned and appropriately connected is the focus of tremendous investigative effort. Given the complexity of the nervous system and the musculature, this is an intimidating task. However, progress has been rapid, primarily because of the growing repertoire of experimental models and techniques. The three primary embryonic structures underlying the formation of the phrenic nerve and diaphragm are; 1) the neural tube, of ectodermal origin, which gives rise to spinal neurons including motoneurons, and the neural crest which provides peripheral neurons and Schwann cells, 2) the somites, of mesodermal origin, which gives rise to several structures including the musculature, and 3) the somatopleure, or somatic mesoderm, which gives rise to the mesenchymal substructure upon which the neuromuscular components of the limb and diaphragm develop, and which contributes non-neuronal and non-muscular tissues such as blood vessels, bone etc. An excellent resource which reviews basic vertebrate embryology can be found on the world wide web (www.med.unc.edu/embryo_images).

Specification of Motoneurons

Rat phrenic motoneuron soma reside within a tightly aligned ventromedial nucleus running through cervical spinal segments C3-C6 (Kuzuhara and Chou, 1980; Goshgarian and Rafols, 1981). In fact, during development, it is neuronal position along both rostrocaudal and dorsoventral axes that appears to specify neuronal identity. These positional cues encode differentially expressed combinations of transcription factors that specify neuronal identity throughout the central nervous system (reviewed by Eisen, 1998, 1999; Pfaff and Kintner, 1998). In the spinal cord, motoneuron identity is generated by sonic hedgehog signalling ventrally and the paraxial mesoderm rostrocaudally (Ericson et al., 1996; Chiang et al., 1996; Appel et al., 1995; Itasaki et al., 1996; Matise and Lance-Jones, 1996; Dale et al., 1997; Muir et al., 1997; Ensini et al., 1998). Motoneuron fate becomes progressively restricted, initially by *mnr2* and *islet-1* expression (Tanabe et al., 1998; Pfaff et al., 1996), and then by the differential combinatorial expression of LIM homeodomain transcription factors which generate incomplete, yet substantial, motoneuron subtype specification (Tsuchida et al., 1994; Appel et al., 1995; reviewed by Pfaff and Kintner, 1998). With regards to phrenic nerve specification, differences between the medial phrenic population and more lateral populations such as the subclavian, sternomastoid and brachial motoneurons may be generated by retinoid signalling from phrenic motoneurons as the later born lateral populations migrate in their more lateral location (Sockanathan and Jessell, 1998). Further, selective deletion of the phrenic nerve implicates the LIM homeobox genes *Hb9*, and potentially *Lhx3 and Lhx4* in the specification of phrenic motoneuron identity and selective pathfinding (Sharma et al., 1998; Thaler et al., 1999; Arber et al., 1999).

Axonal Guidance

Debate as to whether axonal pathfinding is a matter of specific guidance or selective pruning of more randomly distributed projections (reviewed in Landmesser, 1992a; Goodman and Shatz, 1993) has found its ultimate answer, as LIM homeodomain transcription factors appear to encode at least part of the specific guidance properties of neurons from the onset of pathfinding (Thor and Thomas, 1997; Sharma et al., 1998; Thor et al., 1999). The environment can modulate this 'program' to effect relevant changes in

protein expression and/or mobilisation during active pathfinding (Tang et al., 1992; Dodd et al., 1988; Kidd et al., 1998). The task of axonal guidance is performed at the tip of the axon, the growth cone, which is equipped with lamellipodial and filopodial sensors that probe the environment for guidance cues (Davenport et al., 1993; Chien et al., 1993; Kater and Rehder, 1995). The growth cone receives multiple attractive and repulsive guidance cues which interact with receptor molecules on the growth cone surface. Although still poorly understood, the growth cone seems to integrate these combined cues into a response which modulates the cytoskeletal architecture to effect directed growth of the axon (Winberg et al., 1998; reviewed by Hall, 1998; Suter and Forscher, 1998; Song and Poo, 1999; Mueller, 1999). Recent evidence points to the central role of cyclic nucleotides as a potential point of convergence for multiple guidance cues and in discriminating whether any particular guidance cue is attractive or repulsive (Ming et al., 1997; Song et al., 1998).

The list of molecules which influence the guidance of growing axons is becoming extensive and many demonstrate remarkable conservation (Chisholm and Tessier-Lavigne, 1999). These cues can be either attractive/permissive or repulsive/inhibitory and can act over a distance (chemo) or upon contact (general reviews include: Goodman and Shatz, 1993; Goodman, 1996; Tessier-Lavigne and Goodman, 1996; Cook et al., 1998; Stoeckli and Landmesser, 1998; Holt and Harris, 1998; Mueller, 1999; Chisholm and Tessier-Lavigne, 1999; Song and Poo, 1999).

Guidance cues include:

1) the netrins, bifunctional molecules which mediate long and short range attractive and repulsive cues depending upon the receptor complement on growth cones and the status of their cyclic nucleotides (reviewed in Culotti and Kolodkin, 1996; Culotti and Merz, 1998; Chisholm and Tessier-Lavigne, 1999; Mueller, 1999).

2) the semaphorins, which are long and short range repulsive molecules that mediate their effects via neuropilin and plexin receptors on growth cones (reviewed in Culotti and Kolodkin, 1996; Fujisawa and Kitsukawa, 1998; Chisholm and Tessier-Lavigne, 1999; Mueller, 1999).

3) the ephrins, which mediate contact repulsion via Eph tyrosine kinases on the growth cone, generate bidirectional signalling complexes important in the formation of topographic maps,

cell sorting and axonal fasciculation (reviewed in Flanagan and Vanderhaeghen, 1998; Bruckner and Klein, 1998; O'Leary and Wilkinson, 1999; Holder and Klein, 1999; Chisholm and Tessier-Lavigne, 1999; Mueller, 1999).

4) tyrosine phosphatases, which are still poorly understood, although a laminin-nidogen complex has been identified as a ligand, are implicated in axonal guidance, and defasciculation in particular (O'Grady et al., 1998; reviewed in Desai et al., 1996; Van Vactor, 1998a; Stoker and Dutta, 1998). 5) Slit, which is a contact repulsive molecule operating via the Robo receptor on growth cones and promotes axonal branching, potentially linking these two mechanistically (reviewed in Chisholm and Tessier-Lavigne, 1999; Song and Poo, 1999).

The above lists more recently discovered specific guidance molecules. Certain families of longer established globally and restrictively expressed molecules modulate contact cellular adhesion and/or inhibition. These are involved in such processes as: 1) general and selective axonal fasciculation and defasciculation, 2) cellular recognition and selective synaptogenesis, 3) the formation of permissive and/or attractive substrates for the modulation of the axonal traction necessary for growth (reviewed in Hynes and Lander 1992; Martini 1994; Rosales et al., 1995; Müller and Kypta, 1995; Tessier-Lavgne and Goodman, 1996; Schachner, 1997; Viollet and Doherty, 1997; Suter and Forscher, 1998; Alpin et al., 1998; Van Vactor, 1998b). These include:

1) extracellular matrix (ECM) molecules such as laminin, fibronectin, collagen, tenascin, thrombospondin and proteoglycans and their various isoforms which can be either adhesive or inhibitory to growth and modulate the guidance of neurons by passive and active mechanisms upon contact, primarily via integrins on the neuronal surface (reviews by Sanes, 1989; Venstrom and Reichardt, 1993; Letourneau et al., 1994).

2) subgroups of immunoglobulin cell adhesion molecules (IgCAMs) such as those of neural cell adhesion molecule (NCAM) and L1. These have been implicated in both *cis*- and *trans*-acting Ca^{2+}-independent homophilic and heterophilic interactions that contribute to selective and global adhesion during outgrowth, target interaction and synaptic plasticity. Promiscuous interactions of IgCAMs, such as with proteoglycans and the fibroblast growth factor receptor (FGFR), increases the repertoire of IgCAM activity and underscores the intracellular

signalling generated by IgCAM engagement (Hortsch, 1996; Walsh and Doherty, 1997; Viollet and Doherty, 1997; Brümmendorf et al., 1998; Alpin et al., 1998; Davis and Goodman, 1998).

3) cadherins, which mediate Ca^{2+}-dependent cellular adhesion primarily by homophilic interaction with like-cadherin isoforms but also more promiscuously with FGFR. Intracellular coupling of cadherins with catenins emphasises the role of cadherins, not only in selective adhesion and synapse formation, but also in gene regulation and differentiation (Knudsen et al., 1998; Shapiro and Colman, 1998, 1999; Vleminckx and Kemler, 1999).

Motor axon pathfinding: Lessons from the chick

Motor axons leaving the developing spinal cord (E11-E11.5 in rat cervical cord) first grow into the somite-derived sclerotome. Axons preferentially grow into the anterior half of the sclerotome (Keynes and Stern, 1984). This is primarily due to the posterior sclerotome being inhibitory to axonal growth due to the restricted expression of such molecules as T-cadherin (Ranscht and Bronner-Fraser, 1991; Fredette and Ranscht, 1994; Fredette et al., 1996), semaphorin III (Wright et al., 1995, but see Behar et al., 1996), chondroitin-6-sulphate and at least two peanut agglutinin binding glycoproteins (Stern et al., 1986; Davies et al., 1990; Oakley and Tosney, 1991), and versican (Landolt et al., 1995). Such repulsive cues locally paralyse the growth cone and enhanced branching in the other direction promotes avoidance behaviour (Oakley and Tosney, 1993). The perinotochordal mesenchyme and other chondrogenic tissues such as the presumptive pelvic girdle and femur represent further inhibitory zones which shape the basic nerve projections (reviewed by Landmesser, 1992a; Tosney, 1992).

Axons derived from rat cervical ventral roots co-mingle at the brachial plexus at E12-E12.5 (Chapters 4 and 5). This is the first major decision point for many motor axons, including the phrenic and brachial axons, and is reminiscent of the well studied chick crural and sciatic plexuses (reviewed by Landmesser, 1992a, see chapter 5). A series of surgical deletions and rotations demonstrated that intermingled axons sort out non-competitively into segregated nerve trunks at the plexus in response to guidance cues within the plexus and hindlimb (Lance-Jones and Landmesser, 1980a,b, 1981; Whitelaw and Hollyday, 1983;

Tosney and Landmesser, 1984, 1985). Thus, motor axons respond differentially to guidance cues common to all plexus axons, implicating differences in the repertoire of receptors and/or adhesion molecules on motor axons as providing guidance. This certainly seems to be the case with regards to sensory axons which follow motor axons, as differences in the expression of IgCAMs and N-cadherin between sensory axon populations have been observed (Landmesser and Honig, 1986; Honig and Rutishauser, 1996; Scott et al., 1996). Whereas known differences in the combination of LIM homeodomain transcription factors likely prescribes differential motor axon guidance at the plexus (Tsuchida et al., 1994; Appel et al., 1995; Sharma et al., 1998; reviewed by Pfaff and Kintner, 1998), no differences in guidance molecules have been found between these motor populations. The mesenchymal tissue of the plexus and limb appears to provide the primary guidance substrate for axons within the plexus (Lance-Jones and Dias, 1991), potentially due to expression of hepatocyte growth factor, or scatter factor (HGF/SF) which may be an attractive substrate for *met*-expressing axons (Ebens et al., 1996; Yang et al., 1998; reviewed by Maina and Klein, 1999). However, expression of HGF/SF along all motor axon pathways implicates a more global than selective role. In the chick hindlimb, the expression of the anti-adhesive, polysialylated form of NCAM (PSA-NCAM) along axons facilitates axonal sorting at the plexus, presumably by reducing axonal interaction and thereby improving the capacity for axonal response to the appropriate guidance cues (see chapter 5; Tang et al., 1992, 1994). However, as yet, the mechanism underlying specific nerve trunk guidance for motor axons is unknown. Chemo-attractant cues from the muscle may help refine the guidance system (McCaig, 1986; Lance-Jones and Landmesser, 1981; Tosney and Landmesser, 1984), but axonal guidance is surprisingly normal in amuscular limbs as only intramuscular branching appears to be grossly abnormal (Phelan and Hollyday, 1990). In the chick crural plexus, axons segregate into two nerve trunks, dorsal and ventral. At the rat brachial plexus (see Chapter 4), axons segregate into three trunks, the dorsal and ventral brachial trunks and the phrenic nerve. Studies performed in Chapter 5 explored whether the same rules apply to the role of PSA-NCAM where three populations segregate, instead of two, adding a extra layer of complexity. Unlike at the chick crural plexus, the expression pattern of PSA-NCAM at the rodent brachial plexus is more consistent with a selective pathfinding role for phrenic axons. This is more

reminiscent of defasciculation in *Drosophila*, where PSA-NCAM is not expressed, but where *beaten path* regulates selective axonal defasciculation (Van Vactor et al., 1993; Fambrough and Goodman, 1996; Holmes and Heilig, 1999). Ongoing studies are aimed at testing the functional role of PSA-NCAM in selective phrenic axon guidance

Muscle precursor migration

The following chapters frequently refer to myogenic precursor cell migration from the somite to the diaphragm. The condensation of paraxial mesoderm into the bilateral somites is the first morphological indication of segmentation in the embryonic body. They arise in a rostrocaudal progression lateral to the neural tube, and then break up into the dermomyotome and sclerotome. In cervical and limb regions, the ventrolateral lip of the epithelial dermomyotome delaminates and a migratory population of muscle precursor cells migrate out to form the dorsal and ventral limb muscle masses, as well as the diaphragm in the rodent (reviewed in Christ and Ordahl, 1995). This conversion from an epithelial to a migratory state occurs in response to HGF/SF signalling from the presumptive limb (and diaphragm?) mesoderm (Hayashi and Ozawa, 1995; Bladt et al., 1995; Brand-Saberi et al., 1996) which induces delamination of this *met*-expressing ventrolateral cell population. A number of gene products are postulated to control aspects of myogenic cell migration, including *Lbx1* (Dietrich et al., 1998; Mennerich et al., 1998; Schäfer and Braun, 1999) and *pax-3* (Goulding et al., 1994; Bober, 1994; Williams and Ordahl, 1994), whereas the expression of myogenic genes is delayed until they reach their prospective muscle regions (Bober et al., 1991; Pownall and Emerson, 1992; Smith et al., 1994; Williams and Ordahl, 1994), potentially due to influence of *msx1* expression during the migratory phase (Houzelstein et al., 1999; Bendall et al., 1999).

The mechanism(s) underlying segregation of migrating muscle precursors into dorsal and ventral muscle masses in limbs, as well as the diaphragm at the level of the rodent forelimb, are unknown. It is generally believed that gradients of certain molecules generates a positional mapping system throughout the limb bud mesoderm (general review by Ng et al., 1999). Muscle precursors are postulated to read this molecular map and differentiate into muscle at their appropriate region (Robson et al., 1994; Riddle et al., 1995; Parr and

McMahon, 1995). The dynamic expression of *Hoxa-11* and *Hoxa-13* in normal and manipulated chick wing bud suggests that these genes may pattern muscle formation in response to signals from the mesoderm (Yamamoto et al., 1999). However, are migrating precursors specifically targeted to one of the primordial masses? Circumstantial evidence supports this hypothesis. Myosin phenotype is may be specified during migration in the chick limb (Van Swearingen and Lance-Jones, 1995), avian myoblasts remain clonally committed to a specific fate *in vitro* (Miler and Stockdale, 1986; DiMario et al., 1993), and muscles with distinct MHC expression arise in certain locations of the limb (Fredette and Landmesser, 1991a). The link between early phenotype specification, targeted migration and muscle deposition has been described in zebrafish (Devoto et al., 1996). Further, *Lbx1* null mutant mice have specific defects in dorsal forelimb muscle precursor migration (Schäfer and Braun, 1999). The total absence of migration into the hindlimb in these null mutants may suggest that the additional pathway (to the diaphragm) at the forelimb has necessitated a higher degree of specification in migration. This is consistent with the more global expression of PSA-NCAM at a bifurcation (Tang and Landmesser, 1992) but its more restricted expression at a trifurcation (Chapter 5). Whatever the mechanism(s) that generate(s) segregation and position of muscle masses actually turns out to be, it may well be related to that which generates neuronal segregation, given that the mesoderm appears to provide guidance information to both populations of cells.

Myogenesis and formation of the motor unit

The following chapters deal with various aspects of muscle formation and nerve-muscle interaction. Here I shall briefly outline major events during vertebrate neuromuscular formation from inception to the establishment of the motor unit.

Once migrating muscle precursors reach the appropriate location, they rapidly proliferate to form a large pool of prospective myoblasts. Upon exit from the cell cycle, they differentiate into myoblasts, under the transcriptional control of the myogenic regulatory factors Myf-5, Myo-D, MRF-4 and myogenin (reviewed by Lassar and Münsterberg, 1994; Buckingham, 1994; Rudnicki and Jaenisch, 1995; Ordahl and Williams, 1998). Myogenesis is characterised by two temporally separated phases of proliferation and fusion of distinct

populations of precursors termed primary and secondary myogenesis (see Kelly, 1983). Primary myoblasts fuse to form multinucleated primary myotubes which then separate and become ensheathed within their own basal lamina. Subsequently, secondary myoblasts align themselves along the 'scaffold' of the primary myotubes and fuse to form secondary myotubes (which contribute up to 80% of the muscle), which subsequently separate. Muscle fusion activates many muscle-specific genes (Ontell and Ontell, 1995). Waves of fusion and separation are controlled by the regulated expression of cell adhesion molecules such as integrins, neural cell adhesion molecule (NCAM) and N-cadherin (reviewed by McDonald et al., 1995). These shall be considered in depth in chapter 5 and 6 where the putative role of the polysialylated form of NCAM in muscle morphogenesis is considered.

Innervation plays a major role in myogenesis. Chemical and activity-based antero-and retrograde interactions at the developing neuromuscular junction (NMJ) bring about the maturation of both pre- and post-synaptic elements (reviewed in Navarette and Vrbova, 1993; Connor and Smith, 1994; Dan and Poo, 1994; Keshishian et al., 1996; Davis and Goodman, 1998; Meier and Wallace, 1998; Sanes and Lichtman, 1999). Innervation is precise from its onset as both the topographic projection of the nerve and the matching of motoneurons to either fast or slow fibres are observed from the onset of myogenesis (Laskowski and Owens, 1994; Rafuse et al., 1996; Milner et al., 1998). Both phases of myogenesis, as well as early differentiation of fibre MHC phenotype, occurs in the absence of the nerve or nerve activity. However, the nerve and its activity is required for the survival of the majority of the muscle, muscle morphogenesis, the expression and/or upregulation of many muscle-specific genes, and development of the neuromuscular junction (Condon et al., 1990; Harris, 1981 a,b,c; Fredette and Landmesser, 1991b, Fredette et al., 1993; reviewed by Navarrete and Vrbova, 1993; Sanes and Lichtman, 1999; Buonanno and Fields, 1999). NMJs are initially hyperinnervated, but motoneuron programmed cell death prior to secondary myogenesis and synapse elimination into the postnatal period cull presynaptic numbers until the NMJ becomes monoinnervated and the mature motor unit is attained (Oppenheim, 1991; 1996; Navarrete and Vrbova, 1993; Nguyen and Lichtman, 1996). Programmed cell death roughly matches motoneuron numbers to available muscle, as determined by access to trophic factors at the synapse (Landmesser, 1992b; Oppenheim, 1991, 1996). Synapse elimination refines

the motor unit by eliminating inappropriate or out-competed axons from the synapse (Nguyen and Lichtman, 1996).

Clinical Relevance

Congenital diaphragmatic hernia (CDH) is a relatively common (1:3000 human births and 1:2000 conceptuses) congenital anomaly characterised by the developmental formation of a diaphragm which has regions of varying size entirely missing (Harrison et al., 1994; Harding, 1994; Skandalakis et al., 1994). Abdominal contents (liver, intestines and stomach) migrate through this missing region into the thorax, occupying space normally reserved for the developing lungs. As a result, the newborn lungs are hypoplastic, hypertensive and surfactant-deficient (Torfs et al., 1992). Even when diagnosed prenatally and delivery is in a fully-equipped neonatal care facility, infants presenting with CDH have ~50% mortality (see Harrison et al., 1994), treatment is expensive, over $200,000 per patient (Metkus et al., 1995), and many survivors have persistent sequalae such as chronic lung disease, abnormal lung growth and function, cardiac compromise, spinal deformities and gastrointestinal complications (Thurlbeck et al., 1979;Vanamo et al., 1996a, b; Lund et al., 1994; Nobuhara et al., 1996; Ijsselstijn et al., 1997). For a historical perspective of CDH, refer to Irish et al. (1996).

Due to the lack of impact of postnatal treatment, attempts are being made to intervene *in utero* to prevent or alleviate the development of immature lungs. These include: 1) Return of the viscera and patching the defect *in utero* but this resulted in obstruction of umbilical venous flow and consequential death (Harrison et al., 1993; MacGillivray et al., 1994). 2) Tracheal occlusion which allows type II alveolar cells to fill the lungs with fluid, thereby inflating the lungs and outcompeting the viscera for space in the thorax (DiFiore et al., 1994; Kitano et al., 1999). However, human trials have not shown any consistent benefits and a high incidence of fetal complications persists (Harrison et al., 1998). 3) Drug treatments aimed at improving lung development include the use of glucocorticoids (Liggins and Howie, 1972; Kitterman et al., 1981; Okoye et al., 1998; Tannuri et al., 1998). However, concern over their efficacy and side-effects have prevented their widespread use (Massaro and

Massaro, 1992; Ng, 1993; Stewart et al., 1997; Gramsbergen and Mulder, 1998).

The pathogenesis of human CDH is incredibly difficult to study directly; the first indication of human CDH is visualisation of herniated viscera by ultrasound, which is obviously too late to examine factors contributing to the anomaly, and fetal tissue of the relevant age with relevant anomalies is rare. Fortunately, a rodent model for CDH exists (see chapters 7 and 8). Remarkably, partly due to the emphasis on lung hypoplasia and hypertension (motivated by clinical concerns at birth), no systematic study has previously been undertaken to determine the abnormal formation of the diaphragm. Simply put, studies have been hampered by the previously limited and contradictory literature regarding phrenic and diaphragm development. We have used the well established nitrofen-induced rodent model to systematically test the relative contribution of each of the prevalent theories regarding CDH pathogenesis in an attempt to uncover the pathogenic mechanism leading to CDH. These are fully discussed in the following chapters.

REFERENCES

Alpin AE, Howe A, Alahari SK and Juliano RL (1998) Signal transduction and signal modulation by cell adhesion receptors: the role of integrins, cadherins, immunoglobulin-cell adhesion molecules, and selectins. *Pharmacological Reviews.* 50: 197-263.

Appel B, Korzh V, Glasgow E, Thor S, Edlund T, Dawid IB and Eisen JS (1995) Motoneuron fate specification revealed by patterned LIM homeobox gene expression in embryonic zebrafish. *Development.* 121: 4117-4125.

Arber S, Han B, Mendelsohn M, Smith M, Jessell TM and Sockanathan S (1999) Requirement for the homeobox gene *Hb9* in the consolidation of motor neuron identity. *Neuron* 23: 659-674.

Aziz HA and Rex MAE (1984) Electromyographic study of the cat's diaphragm during oesophageal distension. *Aust. Vet.J.* 61: 254-256.

Behar O, Golden JA, Mashimo H, Schoen FJ, Fishman MC (1996) Semaphorin III is needed for normal patterning and growth of nerves, bones and heart. *Nature.* 383: 525-528.

Bendall AJ, Ding J, Hu G, Shen MM and Abate-Shen C (1999) Msx1 antagonizes the myogenic activity of Pax3 in migrating limb muscle precursors. *Development.* 126: 4965-4976.

Bennett MR, and Pettigrew AG (1974) The formation of synapses in striated muscle during development. *J. Physiol. (Lond.)* 241: 515-545.

Bladt F, Riethmacher D, Isenmann S, Aguzzi A, Birchmeier C (1995) Essential role for the c-Met receptor iin the migration of myogenic precursor cells into the limb bud. *Nature.* 376: 768-771.

Bober E, Lyons GE, Braun T, Cossu G, Buckingham M, and Arnold HH (1991) The muscle regulatory gene, Myf-5 has a biphasic pattern of expression during early mouse development. *J. Cell Biol.* 113: 1255-1265.

Brand-Saberi B, Muller TS, Wilting J, Christ B and Birchmeier C (1996) Scatter factor/ hepatocyte growth factor (SF/HGF) induces emigration of myogenic cells at interlimb levels i vivo. *Dev. Biol.* 179: 160-173.

Bruckner K and Klein R (1998) Signalling by Eph receptors and theri ephrin ligands. *Curr. Opin. Neurobiol.* 8: 375-382.

Brümmendorf T, Kenwrick S and Rathjen FG (1998) Neural cell recognition molecule L1: from cell biology to human hereditary brain malformations.*Curr. Opin. Neurobiol.* 8: 87-97.

Buckingham M (1994) Molecular biology of muscle development. *Cell.* 78: 15-21.

Buonanno A and Fields RD (1999) Gene regulation by patterned electrical activity during neural and skeletal development. *Curr. Opin. Neurobiol.* 9: 110-120.

Chiang C, Litingtung Y, Lee E, Young KE, Corden JL, Westphal H and Beachy PA (1996) Cyclopia and defective axial patterning in mice lacking sonic hedgehog gene function. *Nature.* 383: 407-413.

Chien C-B, Rosenthal DE, Harris WA and Holt CE (1993) Navigational errors made by growth cones without filopodia in the embryonic Xenopus brain. *Neuron.* 11: 237-251.

Chisholm A and Tessier-Lavigne M (1999) Conservation and divergence of axon guidance mechanisms. *Curr. Opin. Neurobiol.* 9: 603-615.

Christ B and Ordahl CP (1995) Early stages of chick somite development. *Anat. Embryol.* 191: 381-396.

Condon K, Silberstein L, Blau HM and Thompson WJ (1990) Differentiation of fiber types in aneural musculature of the prenatal rat hindlimb. *Dev. Biol.* 138: 275-295.

Connor EA and Smith MA (1994) Retrograde signalling in the formation and maintenance of the neuromuscular junction. *J. Neurobiol.* 25: 722-739.

Cooke IRC and Berger PJ (1996) Development of patterns of activity in diaphragm of fetal lamb early in gestation.

Cook G, Tannahill D and Keynes R (1998) Axon guidance to and from choice points. *Curr. Opin. Neurobiol.* 8: 64-72.

Culotti JG and Kolodkin AL (1996) Functions of netrins and semaphorins in axon guidance. *Curr. Opin. Neurobiol.* 6: 81-88.

Culotti JG and Merz DC (1998) DCC and netrins. *Curr. Opin. Cell Biol.* 10: 609-613.

Dale JK, Vesque C, Lints TJ, Sampath TK, Furley A, Dodd J and Placzek M (1997) Cooperation of BMP7 and SHH in the induction of forebrain ventral midline cells by prechordal mesoderm. *Cell.* 90: 257-269.

Dan Y and Poo M-M (1994) Retrograde interactions during formation and elimination of neuromuscular synapses. *Curr. Opin. Neurobiol.* 4: 95-100.

Davenport RW, Dou P, Rehder V and Kater SB (1993) A sensory role for neuronal growth cone filopodia. *Nature.* 721-724.

Davies JA, Cook GM, Stern CD, Keynes RJ (1990) Isolation from chick somites of a glycoprotein fraction that causes collapse of dorsal root ganglion growth cones. *Neuron.* 2: 11-20.

Davis GW and Goodman, CS (1998) Genetic and synaptic development and plasticity: homeostatic regulation of synaptic efficacy. *Curr. Opin. Neurobiol.* 8: 149-156.

Desai CJ, Gindhart JG, Goldstein LSB and Zinn K (1996) Receptor tyrosine phosphatases are required for motr axon guidance in the *Drosophila* embryo. *Cell.* 84: 599-609.

Devoto SH, Melançon E, Eisen JS and Westerfield M (1996) Identification of separate slow and fast muscle precursor cells in vivo, prior to somite formation. *Development.* 122: 3371-3380.

De Vries JIP, Visser GHA and Prechtl HFR (1982) The emergence of fetal behaviour. I. Qualitative Aspects. *Early Hum. Dev.* 7: 301-322.

Dietrich S, Schubert FR, Healy C, Sharpe PT, Lumsden A (1998) Specification of the hypaxial musculature. *Development.* 125: 2235-2249.

DiFiore JW, Fauza DO, Slavin R, Peters CA, Fackler JC and Wilson JM (1994) Experimental fetal tracheal ligation reverses the structural and physiological effects of pulmonary hypoplasia in congenital diaphragmatic hernia. *J. Paediatr. Surg.* 29: 248-256.

DiMario JX, Fernyack SE and Stockdale FE (1993) Myoblasts transferred to the limbs of embryos are committed to specific fibre fates. *Nature.* 362: 165-167.

Di Pasquale E, Monteau R, Hilaire G (1992) In vitro study of central respiratory-like activity of the fetal rat. *Exp. Brain Res.* 89: 459-464.

Di Pasquale E, Monteau R, Hilaire G (1994) Involvement of the rostral ventro-lateral medulla in respiratory rhythm genesis during the pernatal period: an in vitro study in newborn and fetal rats. *Dev. Brain Res.* 78: 243-252.

Di Pasquale E, Monteau R, Hilaire G (1996) Perinatal developmental changes in respiratory activity of medullary and spinal neurons: an in vitro study on fetal and newborn rats. *Dev. Brain Res.* 91: 121-130.

Dodd J, Morton SB, Karagogeos D, Yamamoto M, Jessell TM (1988) Spatial regulation of axonal glycoprotein expression on subsets of embryonic spinla neurons. *Neuron.* 1: 105-116.

Duron B, Marlot D, Larnicol N, Jung-Caillol MC and Macron JM (1979a) Somatotopy in the phrenic motor nucleus of the cat as revealed by retrograde transport of horseradish peroxidase. *Neurosci. Lett.* 14: 159-163.

Duron B, Marlot D and Macron JM (1979b) Segmental motor innervation of the diaphragm. *Neurosci. Lett.* 15: 93-96.

Ebens A, Brose K, Leonardo ED, Hanson MG Jr, Bladt F, Birchmeier C, Barres BA, Tessier-Lavigne M (1996) Hepatocyte growth factor/scatter factor is an axonal chemoattractant and a neurtrophic for spinal motor neurons. *Neuron* 17: 1157-1172.

Eisen JS (1998) Genetaic and molecular analyses of motoneuron development. *Curr. Opin. Neurobiol.* 8: 697-704.

Eisen JS (1999) Patterning motoneurons in the vertebrate nervous system. *TINS.* 22: 321-326.

Ensini M, Tsuchida TN, Belting H-G and Jessell TM (1998) The control of rostrocaudal pattern in the developing spinal cord: specification of motor neuron subtype identity is initiated by signals from paraxial mesoderm. *Development* 125: 969-982.

Ericson J, Morotn S, Kawakami A, Roelink H and Jessell TM (1996) Two critical periods of Sonic Hedgehog signalling required for the specification of motor neuron identity. *Cell* 87: 661-673.

Fambrough D and Goodman CS (1996) The *Drosophila beaten path* gene encodes a novel secreted protein that regulates defasciculation at motor axon choice points. *Cell.* 87: 1049-1058.

Flanagan JG and Vanderhaeghen P (1998) The ephrins and Eph receptors in neural development. *Curr. Opin. Neurobiol.* 21: 309-345.

Fournier M and Sieck GC (1988) Somatotopy in the segmental innervation of the cat diaphragm. *J. Appl. Physiol.* 64: 291-298.

Fredette BJ and Landmesser LT (1991a) Relationship of primary and secondary myogenesis to fiber type development in embryonic chick muscle. *Dev. Biol.* 143: 1-18.

Fredette BJ and Landmesser LT (1991b) A reevaluation of the role of innervation in primary and secondary myogenesis in developing chick muscle. *Dev. Biol.* 143: 19-35.

Fredette BJ, Rutishauser U and Landmesser L (1993) Regulation and activity-dependence of N-cadherin, NCAM isoforms and polysialic acid on chick myotubes during development. *J. Cell. Biol.* 6: 1867-1888

Fredette BJ and Ranscht B (1994) T-cadherin expression delineates specific regions of the developing motor axon-hindlimb projection pathway. *J. Neurosci.* 14: 7331-7346.

Fredette BJ, Miller J and Ranscht B (1996) Inhibition of motor axon growth by T-cadherin substrata. *Development.* 122: 3163-3171.

Funk GD and Feldman JL (1995) Generation of respiratory rhythm and pattern in mammals: insights from developmental studies. *Curr. Opin. Neurobiol.* 5: 778-785.

Furicchia JV and Goshgarian HG (1987) Dendritic organisation of phrenic motoneurons in the adult rat. *Exp. Neurol.* 96: 621-634.

Goodman CS and Spitzer NC (1979) Embryonic development of identified neurones: differentiation from neuroblast to neurone. *Nature.* 280: 208-214.

Goodman CS and Shatz CJ (1993) Developmental mechanisms that generate precise patterns of neuronal connectivity. *Cell.* 72: 77-98.

Gordon DC and Richmond FJR (1990) Topography in the phrenic motoneuron nucleus demonstrated by retrograde multiple-labelling techniques. *J. Comp. Neurol.* 292:424-434

Goshgarian HG and Rafols JA (1981) The phrenic nucleus of the Albino rat: a correlative HRP and Golgi study. *J. Comp. Neurol.* 201: 441-456.

Goulding M, Lumsden A and Paquette AJ (1994) Regulation of Pax-3 expression in the dermamyotome and its role in muscle development. *Development.* 120: 957-971.

Gramsbergen A and Mulder EJH (1998) The influence of betamethasone and dexamethasone on motor development in young rats. *Pediatr. Res.* 44: 105-110.

Greer JJ, Smith JC and Feldman JL (1992) Respiratory and locomotor patterns generated in

the fetal rat brain stem-spinal cord in vitro. *J. Neurophysiol.* 67: 996-999.

Hall A (1998) Rho GTPases and the actin cytoskeleton. *Science.* 279: 509-514.

Hammond CGM, Gordon DC, Fisher JT and Richmond FJR (1989) Motor unit territories supplied by primary branches of the phrenic nerve. *J. Appl. Physiol.* 66: 61-71.

Harding R (1994) Development of the respoiratory system. In *Textbook of Fetal Physiology.* Edited by: Thorburn GD and Harding R. New York, Oxford. pp 140-167.

Harding R, Hooper SB and Van VK. (1993) Abolition of fetal breathing movements by spinal cord transection leads to reductions in fetal lung volume, lung growth and IGF-II gene expression. *Pediatric Res.* 34: 148-153

Harris AJ (1981a) Embryonic growth and innervation of rat skeletal muscles. I. Neural regulation of muscle fiber numbers. *Phil. Trans. R. Soc. Lond. B* 293:257-277.

Harris AJ (1981b) Embryonic growth and innervation of rat skeletal muscles. II. Neural regulation of muscle cholinesterase. *Phil. Trans. R. Soc. Lond. B* 293: 279-286.

Harris AJ (1981c) Embryonic growth and innervation of rat skeletal muscles. III. Neural regulation of junctional and extra-junctional acetylcholine receptor clusters. *Phil. Trans. R. Soc. London B* 293:287-314.

Harris AJ and McCaig CD (1984) Motoneuron death and motor size during embryonic development of the rat. *J. Neurosci.* 4: 13-24.

Harris AJ, Fitzsimons RB and McEwan JC (1989) Neural control of the sequence of expression of myosin heavy chain isoforms in foetal mammalian muscles. *Development* 107:751-769.

Harrison MR, Adzick NS, Flake AW, Jennings RW, Estes JM, MacGillivray TE, Chueh JT, Goldberg JD, Filly RA and Goldstein RB (1993) Correction of congenital diaphragmatic hernia in utero VI. Hard-earned lessons. *J. Paediatr. Surg.* 28: 1411-1417.

Harrison M, Adzick N, Estes J and Howell L (1994) A prospective study of the outcome for fetuses with diaphragmatic hernia. *J. Am. Med. Assoc.* 271: 382-384.

Harrison MR, Mychaliska GB, Albanese CT, Jennings RW, Farrell JA, Hawgood S, Sandberg P, Levine AH, Lobo E and Filly RA (1998) Correction of congenital daphragmatic hernia in utero IX. Fetuses with poor prognmosis (liver herniation and low lung-to-head

ratio) can be saved by fetoscopic temporary tracheal ligation. *J. Paediatr. Surg.* 33: 1017-1022.

Hayashi K and Ozawa E (1995) Myogenic cell migration from somites is induced by tissue contact with medial region of the presumptive limb mesoderm in chick embryos. *Development.* 121: 661-669.

Hilaire G and Duron B (1999) Maturation of the mammalian respiratory system. *Physiol. Rev.* 79: 325-360.

Holder N and Klein R (1999) Eph receptors and ephrins: effectors of morphogenesis. *Development.* 126: 2033-2044.

Holmes AL and Heilig JS (1999) Fasciclin II and Beaten path modulate intercellular adhesion in *Drosophila* larval visual organ development. *Development.* 126: 261-272.

Holt CE and Harris WA (1998) Target selection: invasion, mapping and cell choice. *Curr. Opin. Neurobiol.* 8: 98-105.

Honig MG and Rutishauser US (1996) Changes in the segmental patternof sensory neuron projections in the chick hindlimb under conditions of altered cell adhesion molecule function. *Dev. Biol.* 175: 325-337.

Hortsch M (1996) The L1 family of neural cell adhesion molecules: old proteins performing new tricks. *Neuron* 17: 587-593.

Houzelstein D, Auda-Boucher G, Chéraud Y, Rouaud T, Blanc I, Tajbakhsh S, Buckingham ME,
Fontaine-Perus J and Robert B (1999) The homeobox gene Msx1 is expressed in a subset of somites, and in muscle progenitor cells migrating into the forelimb. *Development.* 126: 2689-2701.

Hynes RO and Lander AD (1992) Contact and adhesive specificities in the associations, migrations and targeting of cells and axons. *Cell.* 303-322.

Irish MS, Holm BA and Glick PL (1996) Congenital diaphragmatic hernia: A historical review. In: *Clinics in Perinatology*. Congenital Diaphragmatic Hernia. 23: 625-654.

Ijsselstijn H, Tibboel D, Hop WJC, Molenaar JC and de Jongste JC (1997) Long term pulmonary sequelae in children with congenital diaphragmatic hernia. *Am. J. Respir. Crit. Care Med.* 155: 174-180.

Itasaki N, Sharpe J, Morrison A and Krumlauf R (1996) Reprogramming Hox expression in the vertebrate hindbrain: influence of paraxial and rhombomere transposition. *Neuron.* 16: 487-500.

Jansen AH and Chernick V (1991) Fetal breathing and development of control of breathing. *J. Appl. Physiol.* 70: 1431-1446

Kater SB and Rehder V (1995) The sensory-motor role of growth cone filopodia. *Curr. Opin. Neurobiol.* 5: 68-74.

Kelly AM (1983) Emergence of specialisation of skeletal muscle. In *Handbook of Physiology, section 10.* Edited by: LD Peachey, Waverley Press. Pp507-537.

Keshishian H, Broadie K, Chiba A and Bate M (1996) The *Drosophila* neuromuscular junction: A model system for studying synapse development and function. *Annu. Rev. Neurosci.* 19: 545-575.

Keynes RJ and Stern CD (1984) Segmentation in the vertebrate nervous system. *Nature.* 310: 786-789.

Kidd T, Brose K, Mitchell KJ, Fetter RD, Tessier-Lavigne M, Goodman CS, Tear G (1998) Roundabout controls axon crossing of the CNS midline and defines a novel subfamily of evolutionarily conserved guidance receptors. *Cell.* 92: 205-215.

Kitano Y, Davies P, Von Allmen, Adzick NS, Flake AW (1999) Fetal tracheal occlusion in the rat model of nitrofen-induced congenital diaphragmatic hernia. *J. Appl. Physiol.* 87: 769-775.

Kitterman JA, Liggins GC, Campos GA, Clements JA, Forster C, Lee CH and Creasy RK (1981) Prepartum maturation of the lung in fetal sheep: relation to cortisol. *J. Appl. Physiol.* 51: 384-390.

Kluth D, Peterson C and Zimmerman HJ (1989) The embryology of congenital diaphragmatic hernia. In *Congenital Diaphragmatic Hernia. Mod. Probl. Paediatr. Vol 24.* Edited by P Puri. Basel, Switzerland, Karger 7-21.

Knudsen KA, Frankowski C, Johnson KR and Wheelock MJ (1998) A role for cadherins in cellular signalling and differentiation. *J. Cell Biochem - Suppl.* 30-31: 168-176.

Koyisha N and Smith JC (1999) Neuronal pacemaker for breathing visualized *in vitro*.

Nature. 400: 360-363.

Kuzuhara S and Chou SM (1980) Localisation of the phrenic nucleus in the rat: a HRP study. *Neurosc. Lett.* 16: 119-124.

Lance-Jones C and Landmesser LT (1980a) Motoneurone projection patterns in embryonic chick limb following partial deletions of the spinal cord. *J. Physiol. (Lond)*. 302: 559-580.

Lance-Jones C and Landmesser LT (1980b) Motoneurone projection patterns in the chick hindlimb following early partial reversals of the spinal cord. *J. Physiol. (Lond)*. 302: 2518-2527.

Lance-Jones C and Landmesser LT (1981) Pathway selection by embryonic chick motoneurons in an experimentally altered environment. *Proc. R Soc. Lond. B* 214: 119-152.

Lance-Jones C and Dias M (1991) The influence of presumptive limb connective tissue on motoneuron axon guidance. *Dev. Biol.* 143: 93-110.

Landau BR, Akert K and Roberts TS (1962) Studies on the innervation of the diaphragm. *J. Comp. Neurol.* 119: 1-10.

Landolt RM, Vaughan L, Winterhalter KH and Zimmerman DR (1995) Versican is selectively expressed in embryonic tissues that act as barriers to neural crest cell migration and axon outgrowth. *Development.* 121: 2303-2312.

Landmesser LT and Honig MG (1986) Altered sensory projections in the chick hindlimb following the early removal of motoneurons. *Dev. Biol.* 118: 511-531.

Landmesser LT (1992a) Growth cone guidance in the avian limb: a search for cellular and molecular mechanisms. In: *The nerve growth cone*, edited by PC Letourneau, SB Kater and ER Macagno, New York: Raven 373-386.

Landmesser LT (1992b) The relationship of intramuscular nerve branching and synaptogenesis to motoneuron survival. *J. Neurobiol.* 23: 1131-1139.

Laskowski MB and Sanes JR (1987) Topographic mapping of motor pools onto skeletal muscles. *J. Neursoci.* 7: 252-260.

Laskowski MB and Owens JL (1994) Embryonic expression of motoneuron topography in the rat diaphragm muscle. *Dev. Biol.* 166: 502-508.

Lassar A and Müunsterberg A (1994) Wiring diagrams: regulatory circuits and the control of skeletal myogenesis. *Curr. Opin. Cell Biol.* 6: 432-442.

Leak LV (1979) Gross and ultrastructural morphological features of the diaphragm. *Am. Rev. Respir. Dis.* Anatomy, Mechanics. A. Anatomy of the Diaphragm. 119 Suppl.: 3-21.

Letouneau PC, Condic ML and Snow DM (1994) Interactions of developng neurons with the extracellular matrix. *J. Neurosci.* 14: 915-928.

Liggins GC and Howie RN (1972) A controlled trial of antepartum corticosteroid treatment for prevention of the respiratory distress syndrome in premature infants. *Pediatrics.* 50: 515-525.

Lund DP, Mitchell J, Kharasch V, Quigley S, Kuehn M and Wilson JM (1994) Congenital diaphragmatic hernia: The hidden morbidity. *J. Paediatr. Surg.* 29: 258-264.

Lunteren EV, Haxhiu MA, Cherniack NS and Goldman MD (1985) Differential costal and crural diaphragm compensation of posture changes. *J. Appl. Physiol.* 58: 1895-1900.

MacGillivray TE, Jennings RW, Rudolph AM, Ring EJ, Adzick NS and Harrison MR (1994) Vascular changes with in utero correction of diaphragmatic hernia. *J. Paediatr. Surg.* 29: 992-996.

Maina F and Klein R (1999) Hepatocyte growth factor, a versatile signal for developing neurons. *Nature Neurosci.* 2: 213-217.

Mall FP (1910) Coelem and diaphragm. In *Manual of Human Embryology. Volume I.* Edited by Keibel and Mall. Philadelphia. 523-548.

Martini R (1994) Expression and functional roles of neural cell surface molecules and extracellular matrix components during development and regeneration of peripheral nerves. *J. Neurocytol.* 23: 1-28.

Massaro GD and Massaro D (1992) Formation of alveoli in rats: postnatal effects of prenatal dexamethasone. *Am J. Physiol.* 263 (Lung Cell. Mol. Physiol. 7) L37-L41.

Matise MP and Lance-Jones C (1996) A critical period for the specification of motor pools in the chick lumboscral spinal cord. *Development* 122: 659-669

McCaig (1986) Myoblasts and myoblast-conditioned medium attract the earliest spinal

neurites from frog embryos. *J. Physiol.* 375: 39-54.

McDonald, K.A., A.F. Horwitz, and K.A. Knudsen (1995) Adhesion molecules and skeletal myogenesis. Semin. Dev. Biol. *6*: 105-116

McLachlan JC (1996) *Anat. Soc. Of Great Britain and Ireland Newsletter.* Summer Issue: 2-4.

Meier T and Wallace BG (1998) Formation of the neuromuscular junction: molecules and mechanisms. *BioEssays.* 20: 819-829.

Mennerich D, Schäfer K and Braun T (1998) Pax-3 is necessary but not sufficient for lbx1 expression in myogenic precursor cells of the limb. *Mech. Dev.* 73: 147-158.

Metkus AP, Esserman L, Sola A, Harrison MR and Adzick NS (1995) Cost per anomaly: what does diaphragmctic hernia cost? *J. Paediatr. Surg.* 30: 226-230.

Miller JB and Stockdale FE (1986) Developmental origins of skeletal muscle fibers: Clonal analysis of myogenic cell lineages based on expression of fast and slow myosin heavy chains. *Proc. Natl. Acad. Sci. USA.* 83: 3860-3864.

Milner LD, Rafuse VF and Landmesser LT (1998) Selective fasciculation and divergent pathfinding decisions of embryonic chick motor axons projecting to fast and slow muscle regions. *J. Neurosci.* 18: 3297-3313.

Ming GL, Song H-J, Berninger B, Holt CE, Tessier-Lavigne M and Poo M-M (1997) cAMP-dependent growth cone guidance by netrin-1. *Neuron.* 19: 1225-1235.

Monges H, Salducci J and Naudy B (1978) Dissociation between the elctrical activity of the diaphragmatic dome and crura muscular fibres during oesophageal distension, vomiting and eructation. *J. Physiol.* 74: 541-554.

Monteau R and Hilaire G (1991) Spinal respiratory motoneurons. *Prog. Neurobiol* 37: 83-144.

Mueller BK (1999) Growth cone guidance: first steps towards a deeper understanding. *Annu. Rev. Neurosci.* 22: 351-388.

Muir J, Jessell TM and Edlund T (1997) Assignment of early caudal identity to neural plate cells by a signal from caudal paraxial mesoderm. *Neuron.* 19: 487-502.

Müller W and Connor JA (1991) Dendritic spines as individual neuronal compartments for synaptic Ca^{2+} responses. *Nature.* 354: 73-76.

Müller U and Kypta R (1995) Molecular genetics of neuronal adhesion. *Curr. Opin. Neurobiol.* 5: 36-41.

Navarrete R and Vrbová G (1993) Activity-dependent interactions between motoneurones and muscles: their role in the development of the motor unit. *Prog. Neurobiol.* 41: 93-124.

Ng P (1993) The effectiveness and side effects of dexamethasone in preterm infants with bronchopulmonary dysplasia. *Arch. Dis. Child.* 68: 330-336.

Ng JK, Tamura K, Büscher D and Izpisúa-Belmonte JG (1999) Molecular and cellular basis of pattern formation during vertebrate limb development. *Curr. Topics Dev. Biol.* 41: 37-66.

Nguyen QT and Lichtman JW (1996) Mechanism of synapse disassembly at the developing neuuromuscular junction. *Curr. Opin. Neurobiol.* 6: 104-112.

Noakes PG, Bennett MR and Davey DF (1983) Growth of segmental nerves to the developing rat diaphragm: absence of pioneer axons. *J. Comp. Neurol.* 218:365-377.

Nobuhara KK, Lund DP, Mitchell J and Wilson JM (1996) Long-term outlook for survivors of congenital diaphragmatic hernia. In: *Clinics in Perinatology.* Congenital Diaphragmatic Hernia. Vol 23. pp 873-887.

Oakley RA and Tosney KW (1991) Peanut agglutinin and chondroitin-6-sulfate are molecular markers for tissues that act as barriers to axon advance in the avian embryo. *Dev. Biol.* 147: 187-206.

Oakley RA and Tosney KW (1993) Contact-mediated mechanisms of motor axon segmentation. *J. Neurosci.* 13: 3773-3792.

Ogawa, T (1959) Studies on the phrenic nerve and the diaphragm of the dog. *Am. J. Surg.* 97: 744-748.

O'Grady P, Thai TC and Saito H (1998) The laminin-nidogen complex is a ligand for a specific splice isoform of the transmembrane protein tyrosine phosphatase LAR. *J. Cell. Biol.* 141: 1675-1684.

Okoye BO, Losty PD, lloyd DA and Gosney JR (1998) Effect of prenatal glucocorticoids on

pulmonary vascular muscularisation in nitrofen-induced congenital diaphragmatic hernia. *J. Pediatr. Surg.* 33: 76-80.

O'Leary DD and Wilkinson DG (1999) Eph receptors and ephrins in neural development. *Curr. Opin. Neurobiol.* 9: 65-73.

Onimaru H and Homma I (1992) Whole cell recordings from respiratory neurons in the medulla of brain stem spinal cord preparations isolated from newborn rats. *Pflügers Arch.* 420: 399-406.

Ontell M and Ontell MP (1995) Muscle-specific gene expression during myogenesis in the mouse. *Microsc. Res. Tech.* 30: 354-365.

Oppenheim RW (1991) Cell death during development of the nervous system. *Annu. Rev. Neurosci.* 14: 453-501.

Oppenheim RW (1996) Neurotrophic survival molecules for motoneurons: an embarrassment of riches. *Neuron.* 17: 195-197.

Ordahl CP and Williams BA (1998) Knowing chops from chuck: roasting MyoD redundancy. *BioEssays.* 20: 357-362.

Parr BA and McMahon AP (1995) Dorsalizing signal Wnt-7a required for normal polarity of D-V and A-P axes in the vertebrate limb. *Cell.* 83: 631-640.

Paton J. (1996) The ventral medulary respiratory network of the mature mouse studied in a working heart-brainstem preparation. *J. Physiol.* 493: 819-831.

Pfaff S and Kintner C (1998) Neuronal diversification: development of motor neuron subtypes. *Curr. Opin. Neurobiol.* 8: 27-36.

Pfaff, SL, Mendelsohn M, Stewart CL, Edlund T and Jessell TM (1996) Requirement for LIM homeobox gene *Isl1* in motor neuron generation reveals a motor neuron-dependent step in interneuron differentiation. *Cell.* 84: 309-320.

Phelan KA and Hollyday M (1990) Axon guidance in muscleless chick wings: the role of muscle cells in motoneuronal pathway selection and muscle nerve formation. *J. Neurosci.* 10: 2699-2716.

Pownall ME and Emerson CP (1992) Sequential activation of three myogenic regulatory

genes during somite morphogenesis in quail embryos. *Dev. Biol.* 151: 67-79.

Rafuse VF, Milner LD and Landmesser (1996) Selective nnervation of fast and slow muscle regions during early chick neuromuscular development. *J. Neurosci.* 16: 6864-6877.

Ranscht B and Bronner-Fraser M (1991) T-cadherin expression alternates with migrating neural crest cells in the trunk of the avian embryo. *Development.* 111: 15-22.

Rekling JC and Feldman JL (1998) PreBötzinger complex and pacemaker neurons: Hypothesized site and kernel for respiratory rhythm generation. *Annu. Rev. Physiol.* 60: 385-405.

Richter DW, Ballanyi K and Schwarzacher S (1992) Mechanisms of respiratory rhythm generation. *Curr. Opin. Neurobiol.* 2:788-793.

Riddle RD, Ensini M, Nelson C, Tsuchida T, Jessell T, Tabin C (1995) Induction of the LIM homeobox gene *Lmx-1* by *Wnt-7a* establishes dorsoventral pattern in the vertebrate limb. *Cell.* 83: 631-640.

Robson LG, Kara T, Crawley A and Tickle C (1994) Tissue and cellular patterning of the musculature in chick wings. *Development.* 120: 1265-1276.

Rosales C, O'Brien V, Kornberg L and Juliano R (1995) Signal transduction by cell adhesion receptors. *Bioch. Biophys. Acta* 1242: 77-98.

Roussos CS, Fukichi Y, Macklem PT and Engl LA (1976) Influence of diaphragmatic contraction on ventilation distribution in horizontal man. *J. Appl. Physiol.* 40: 417-424.

Rudnicki MA and Jaenisch R (1995) The MyoD family of transcription factors and skeletal myogenesis. *BioEssays.* 17: 203-209.

Sanes JR (1989) Extracellular matrix molecules that influence neural development. *Annu. Rev. Neurosci.* 12: 491-516.

Sanes JR (1993) Topographic maps and molecular gradients. *Curr. Opin. Neurobiol.* 3: 67-74.

Sanes JR and Lichtman JW (1999) Development of the vertebratye neuromuscular junction. *Annu. Rev. Neurosci.* 22: 389-442.

Sant'Ambrogio G and Camporesi E (1973) Contribution of various inspiratory muscles to ventilation and the immediate and distant effect of diaphragmatic paralysis. *Acta. Neurobiol. Exp.* 33: 401-409.

Schachner M (1997) Neural recognition molecules and synaptic plasticity. *Curr. Opin. Cell Biol.* 9: 627-634.

Schäfer K and Braun T (1999) Early specification of limb precursor cells by the homeobox gene *Lbx1h. Nature Gen.* 23: 213-216.

Scott SA, Chau CA, Randazzo KF, Stone R and Cahoon SM (1996) Differential expression of cell adhesion molecules on trigeminal cutaneous and muscle afferents. *Dev. Biol.* 178: 101-112.

Sharma K, Sheng HZ, Lettieri K, Li H, Karavanov, Potter S, Westphal H and Pfaff SL (1998) LIM homeodomain factors LHX3 and LHX4 assign subtype identities for motor neurons. *Cell.* 95: 817-828.

Sieck GC (1988) Diaphragm muscle: structural and functional organisation. *Clin. Chest Med.* 9: 195-210.

Sieck GC (1991) Neural control of the inspiratory pump. *NIPS.* 6: 260-264.

Skandalakis JE, Gray SW and Ricketts RR (1994) The diaphragm. In *Embryology for Surgeons.* Edited by JE Skandalakis and SW Gray. Chpt 15.

Smith J, Greer JJ, Liu G and Feldman JL (1990) Neural mechanisms generating respiratory pattern in mammalian brainstem-spinal cord in vitro I. Spatiotemporal patterns of motor and medullary neuron activity. *J. Neurophysiol.* 64: 1149-1169.

Smith J, Ellenberger H, Ballanyi K, Richter D and Feldman JL (1991) Pre-Bötzinger complex: a brainstem region that may generate respiratory rhythm in mammals. *Science.* 254: 726-729.

Smith JC, Funk GD, Johnson SM and Feldman JL (1995) Cellular and synaptic mechanisms generating respiratory rhythm: insights from *in vitro* and computational studies. In: *Ventral Brainstem Mechanisms and Control of Respiration and Blood Pressure.* Edited by CO Trouth, R Millis, H Kiwull-Schone, M Scolofke. New York: M. Dekker. 463-496.

Smith TH, Kachinsky AM and Miller JB (1994) Somite subdomains, muscle cell origins, and

the four muscle regulatory factor proteins. *J. Cell Biol.* 127: 95-105.

Sockanathan S and Jessell TM (1998) Motor neuron-derived retinoid signals determine the number and subtype identity of motor neurons in the developing spinal cord. *Cell.* 94: 503-514.

Song H-J, Ming GL, He Z, Lehmann M, Tessier-Lavigne M and Poo M-M (1998) Conversion of neuronal growth cone responses from repulsion to attraction by cyclic nucleotides. *Science.* 281: 1515-1518.

Song H-J and Poo M-M (1999) Signal transduction underlying growth cone guidance by diffusible factors. *Curr. Opin. Neurobiol.* 9: 355-363.

Stewart JD, Gonzalez CL, Christensen HD and Rayburn WF (1997) Impact of multiple antenatal doses of betamethasone on groath and development of mice offspring. *Am. J. Obstet. Gynecol.* 177: 1138-1144.

St. John WM (1998) Neurogenesis of patterns of automatic ventilatory activity. *Prog. Neurobiol.* 56: 97-117.

Stoeckli ET and Landmesser LT (1998) Axon guidance at choice points. *Curr. Opin. Neurobiol.* 8: 73-79.

Stern CD, Sisoyida Sm and Keynes RJ (1986) Interactions between neurites and somite cells: inhibition and stimulation of nerve growth in the chick embryo. *J. Embryol. Exp. Morph.* 91: 209-226.

Stoker A and Dutta R (1998) Protein tyrosine phosphatases and neural development. *BioEssays.* 20: 463-472.

Suter DM and Forscher P (1998) An emerging link between cytoskeletal dynamics and cell adhesion molecules in growth cone guidance. *Curr. Opin. Neurobiol.* 8: 106-116.

Suzue T (1984) Respiratory rhythm generation in the in vitro brainstem-spinal cord preparation of the neonatal rat. *J. Physiol.Lond.* 354: 173-183.

Tanabe Y, Williams C and Jessell TM (1998) Specification of motor neuron identity by the MNR2 homeodomain protein. *Cell.* 95: 67-80.

Tang J, Landmesser LT and Rutishauser U (1992) Polysialic acid influences specific

pathfinding by avian motoneurons. *Neuron.* 8: 1031-1044.

Tang J, Rutishauser U and Landmesser LT(1994) Polysialic acid regulates growth cone behaviour during sorting of motor axons in the plexus region *Neuron.* 13: 405-414.

Tannuri U, Rodrigues CJ, Maksoud-Filho JG, Santos MM, Tannuri ACA and Rodrigues AJ Jr (1998) The effects of prenatal intraamniotic surfactant or dexamethasone administration on lung development are comparable to changes induced by tracheal ligation in an animal model of congenital diaphragmatic hernia: Studies on lung glycogen content, elastic fiber density and collagen content. *J. Paediatr. Surg.* 33: 1776-1783.

Tessier-Lavigne M and Goodman CS (1996) The molecular biology of axon guidance. Science. 274: 1123-1133.

Thaler J, Harrison K, Sharma K, Lettieri K, Kehrl J and Pfaff SL (1999) Active suppression of interneuron within developing motor neurons revealed by analysis of homeodomain factor HB9. Neuron. 23: 675-687.

Thor S and Thomas JB (1997) The Drosophila islet gene governs axon pathfindign and neurotransmitter identity. Neuron. 18: 397-409.

Thor S, Andersson SGE, Tomlinson A and Thomas JB (1999) A LIM-homeodomain combinatorial code for motor-neuron pathway selection. Nature. 397: 76-80.

Thurlbeck WM, Kida K, Langston C, Cowan MJ, Kitterman JA, Tooley WH and Bryan H (1979) Postnatal lung growth after repair of diaphragmatic hernia. *Thorax.* 34: 338-343.

Torikai H, Hayashi F, Tanaka K, Chiba T, Fukada Y and Moriya H (1996) Recruitment order and dendritic morphology of rat phrenic motoneurons. J. Comp. Neurol. 366: 231-243.

Torfs CD, Cury CJR, Bateson TF and Honoré LH (1992) A population based study of congenital diaphragmatic hernia. *Teratology.* 46: 555-565.

Tosney KW (1992) Growth cone navigation in the proximal environment of the chick embryo. In: *The nerve growth cone*, edited by PC Letourneau, SB Kater and ER Macagno, New York: Raven 387-403

Tosney KW and Landmesser LT(1984) Pattern and specificity of axonal outgrowth following varying degrees of chick limbud ablation. *J. Neurosci.* 4: 2518-2527.

Tosney KW and Landmesser LT (1985) Specificity of early motoneuron growth cone outgrowth in the chick embryo. *J. Neurosci.* 5: 2336-2344.

Tsuchida T, Ensini M, Morton SB, Baldassare M, Edlund T, Jessell TM and Pfaff SL (1994) Topographic organisation of embryonic motor neurons defined by expression of LIM homeobox genes. *Cell.* 79: 957-970.

Van Swearingen J and Lance-Jones C (1995) Slow and fast muscle fibres are preferentially derived from myoblasts migrating into chick limb at different developmental times. Dev. Biol. 170: 321-337.

Van Vactor D, Sink H, Fambrough D, Tsoo R and Goodman CS (1993) Genes that control neuromuscular specificity in Drosophila. Cell. 73: 1137-1153.

Van Vactor D (1998a) Protein tyrosine phosphatases in developing neurons. Curr. Opin. Cell Biol. 10: 174-181.

Van Vactor D (1998b) Adhesion and signalling in axonal fasciculation. Curr. Opin. Neurobiol. 8: 80-86.

Vanamo K, Rintala RJ, Lindahl H and Louhimo I (1996a) Long-term gastrointestinal morbidity in patients with congenital diaphragmtic defects. *J. Paediatr. Surg.* 31: 551-554.

Vanamo K, Peltonen J, Rintala R, Lindahl H, Jaaskelainen J and Louhimo I (1996b) Chest wall and spinal deformities in adults with congenital diaphragmatic defects. *J. Paediatr. Surg.* 31: 851-854.

Venstrom KA and Reichardt LF (1993) Extracellular matrix 2: role of extracellular matrix molecules and their receptors in the nervous system. FASEB J. 7: 737-743.

Viollet C and Doherty P (1997) CAMs and the FGF receptor: an interacting role in axonal growth. Cell Tissue Res. 290: 451-455.

Vlemminckx K and Kemler R (1999) Cadherins and tissue formation: integrating adhesion and signaling. Bioessaysi 21: 211-220.

Walsh FS and Doherty P (1997) Neural cell adhesion molecules of the immunoglobulin superfamily: role in axon growth and guidance. Annu. Rev. Cell Dev. Biol. 13: 425-456.

Wellik DM, Norback DH and DeLuca HF 91997) Retinol is specifically required during

midgestation for neonatal survival. *Am. J. Physiol. (Endocrinol. Metab.* 35:) 272: E25-29.

Wells LJ. (1954) Development of the human diaphragm and pleural sacs. *Cont. Embryol.* 35:107-134.

Whitelaw V and Hollyday M (1983) Neural pathway constraints in the motor innervation of the chick hindlimb following dorsoventral rotation of distal limb segments. J. Neurosci. 3: 1226-1233.

Williams BA and Ordahl CP (1994) Pax-3 expression in segmental mesoderm marks early stages in myogenic cell specification. Development. 120: 785-796.

Winberg ML, Mitchell KJ and Goodman CS (1998) Genetic analysis of the mechanisms controlling target selection: complementary and combinatorial functions of netrins, semaphorins and IgCAMs. Cell 93: 581-591.

Wright DE, White FA, Gerfen RW, Silos-Santiago I and Snider WD (1995) The guidance molecule semaphorin III is expressed in regions of spinal cord and periphery avoided by growing sensory axons. *J. Comp. Neurol.* 361: 321-333.

Yamamoto M, Gotoh Y, Tamura K, Tanaka M, Kawakami A, Ide H and Kuroiwa A (1999) Coordinated expression of Hoxa-11 and Hoxa-13 during limb muscle patterning. Development. 125: 1325-1335.

Yang X-M, Toma JG, Bamji SX, Belliveau DJ, Kohn J, Park M and Miller FD (1998) Autocrine hepatocyte growth factor provides a local mechanism for promoting axonal growth. J. Neurosci. 18: 8369-8381.

Chapter 2

GENERAL MATERIALS AND METHODS

Caesarean Section and Fixation

Fetal rats were delivered from timed-pregnant Sprague-Dawley rats anaesthetised with halothane (1.25-1.5% delivered in 95%0_2 and 5%CO_2) and maintained at 37°C by radiant heat. The timing of dam pregnancies was determined from the appearance of sperm plugs in the morning (designated as E0). Fetal age was confirmed by comparison of their crown-rump length measurements with those published by Angulo y González (1932). Newborn rats (P0) taken within 3 hours of birth were anaesthetised via inhalation of metofane gas. Embryonic rats up to E15 were immediately placed in 4% paraformaldehyde and dissected to expose the diaphragm and neuraxis to fixative, depending upon the tissue being examined. Fetal rats of E16 and above were initially perfused with 1ml of PBS, followed by up to 15ml of 4% paraformaldehyde. Perfusion was performed by insertion of a needle (16 - 30 gauge depending upon age) into the left ventricle. A snipped right atrium provided drainage. The needle was attached to the end of an IV drip attached to an upturned 60cc graduated syringe.

Buffers and Fixative

The buffer commonly used throughout these studies for washing and storing tissue, as well as for antibody dilutions, was a 0.1M sodium phosphate buffer containing 0.9% NaCl (PBS), pH 7.4. In all cases, 4% paraformaldehyde in a 0.1M sodium phosphate buffer (pH 7.4) was the primary fixative used. New fixative was prepared on a regular basis.

Whole embryo sections

Vibratome Sections: After fixation, fetuses were washed in PBS and placed in a 7.5% gelatin solution maintained at 30°C for 1 hour. They were then embedded in a 20% gelatin/glycerol solution which was hardened by cooling. A small block containing the fetus was excised and fixed overnight. The block was appropriately oriented (for either sagittal or transverse sectioning) and vibratome sectioned at 50-70 μm (Pelco Series 1000 and Leica VT1000S). Serial sections were washed in PBS, immunostained free floating and then mounted onto gelatin-subbed or Superfrost Plus (Fisher Scientific) slides, dried, cover-slipped, and examined by standard light microscopy.

Due to the low density of axons within the phrenic nerve during E11.5-E13.5, cutting sections much thinner than 40μm typically did not provide for a clear visualisation of the respective immunolabelled axonal populations. The best resolution for determining immunolabelling patterns within brachial and phrenic axonal populations was obtained by comparing immunolabels between thick sections taken from the same region of different fetuses of the same age (often from the same litter).

Cryostat Sections: After fixation, tissues were placed in PBS containing 30% sucrose overnight. Tissues were then placed on a strip of aluminium foil and this was placed on a metal block frozen with liquid nitrogen. Tissues were then stored in a -70°C freezer until use. The day before use, tissues were sectioned on a Jung CM3000 cryostat at between -23 to -25°C, thaw mounted onto Superfrost Plus slides and dried on a slide dryer overnight.

Microtome Sections: After fixation, serial dehydration through graded ethanol series was followed by three incubations in xylene. Tissues were then placed in liquid paraffin wax and left over one to two days in an incubator set to 55°C. Tissues were then oriented and wax was hardened by cooling in ice. Blocks were stored until sectioning. After embedding, the paraffin block containing the tissue was trimmed and mounted on a rotary microtome (Lipshaw Co, Model 45) equipped with standard knife holder and forward-moving block holder. Sections were cut at 5μm at ribbons were placed on warm water at approximately 40°C. Sections were then mounted onto Superfrost Plus slides and dried on a slide dryer overnight. Sections were then stored until use.

Diaphragm wholemounts

E14-E15: Fetuses were dissected so as to allow exposure of the diaphragm to fixative while maintaining the muscle in its natural extended state. This mostly involved numerous cuts in the body wall. After an hour of fixation, the liver was removed and a small cut was made in the thoracic body wall, and the embryo was fixed for 2 to 24 hours. Diaphragms were subsequently isolated. Prior to immunohistochemical staining, diaphragms were thoroughly washed in three changes of PBS, immunostained free floating and mounted on chrome-alum gelatin subbed slides.

E16 to Birth: Fetuses were perfusion fixed, dissected immediately and processed as for

younger diaphragms.

Immunolabelling

Antibodies: All primary antibodies used were diluted in PBS with 1% goat serum and 0.1% NaN_3. Secondary antibodies were diluted into PBS containing 1% goat serum. Details and dilutions of antibodies used are outlined for each study.

Immunohistochemistry

Immunohistochemical protocols were essentially the same for all studies. Tissues for all immunolabelling, unless otherwise stated, were immersed in methanol containing 0.3% hydrogen peroxide; 20-45 minutes for gelatin sections and 10 minutes for cryostat and microtome sections. This was followed by incubation in 1:20 goat serum (Sigma) in PBS for 1 hour. After 3 x 10 minute PBS washes, all tissues were incubated in diluted primary antibody over 1 night for gelatin sections (4°C), 1-2 nights for diaphragm whole mounts (4°C) and 2-3 hours for cryostat and microtome sections (RT). After 3 x 30 minute PBS washes, tissues were incubated in the appropriate secondary antibody for 1-2 hours at room temperature. Tissues treated with biotinylated secondary antibodies were further washed in PBS, then incubated in an avidin biotinylated-peroxidase solution (Vectastain ABC kit, PK-4000, Vector Lab.) for 1-2 hours at room temperature. Antigen labelling was then revealed by a DAB (3,3-diaminobenzidine tetrahydrochloride) product intensified with nickel ions [0.1M Tris buffered solution (pH 8) containing 0.04% DAB with 0.04% H_2O_2 and 0.6% nickel ammonium sulphate] for 5-15 minutes at room temperature. This produced an intense purple-black precipitate. After thorough washing, tissues were mounted and examined as above. Controls were provided by primary antibody omission or by use of an inappropriate secondary antibody.

Microscopy

Throughout these studies, images of embryonic tissues were obtained on a Leitz Diaplan microscope attached to a camera and Image Pro imaging software. For photomicrographs, colour pictures taken on an automated timer were processed by commercial film developers.

Images were scanned into the Scan Jet Image Software Program and stored on Iomega Zip 100MB discs. For image capture using the Image Pro software package, a MCI 3CCD camera was attached to the microscope was used. Images were subsequently stored on Zip disks. All images were imported into CorelDraw 6-8 (over the years), converted into grayscale if necessary, and oriented with other figures. In all cases, a microscope graticule was obtained for each magnification used and this was processed identically to fetal images to maintain appropriate scale.

REFERENCES

Angulo y González AW (1932) The prenatal growth of the albino rat. *Anat. Embryol.* 52: 117-138.

Chapter 3

DEVELOPMENT OF PHRENIC MOTONEURON MORPHOLOGY IN THE FETAL RAT

Adapted from the Original Publication:
Douglas W. Allan and John J. Greer
J. Comp. Neurol. 382: 469-479 (1997)

INTRODUCTION

The major neuromuscular component of the respiratory system comprises the phrenic nerve and diaphragm, responsible for expanding the thorax during the inspiratory phase of the breathing cycle. Unlike other motor systems, that controlling breathing must be fully functional by birth to ensure viability. In fact, phrenic motoneurons and the diaphragmatic musculature must be functional *in utero*, as respiratory-related movements are thought to be essential for normal growth of the lungs in the fetus (Jansen & Chernick, 1991; Harding et al., 1993; Harding, 1994). The early maturation of phrenic motoneurons is apparent from two lines of evidence: a) rhythmic respiratory phrenic discharge commences at approximately E17, four days prior to birth (Greer et al., 1992), and b) phrenic morphology has reached a state similar to that observed in the adult by birth (Lindsay et al. 1991). Therefore, to examine the developmental changes underlying the inception of respiratory discharge and morphogenesis of phrenic motoneurons, one must study events occurring prenatally.

In the present study, we describe the developmental profile of rat phrenic motoneuron morphology from E13.5 (two days after motoneuron generation) up to birth (~E21). The entire extent of phrenic motoneuron and afferent morphology was visualised following retrograde labelling of the phrenic nerve with the carbocyanine dye, DiI (Honig & Hume, 1989). Thus, we could determine the development of the phrenic motor pool, its dendritic arborisations and the arrival of afferent input. Further, we correlate these factors with the timing and extent of phrenic axon intramuscular branching and synaptogenesis with diaphragmatic musculature (E14-E19), the inception of respiratory drive to phrenic motoneurons (E17), and the final stages of maturation before birth (Bennett & Pettigrew, 1974; Noakes et al., 1983, Greer et al., 1992).

By E14, phrenic soma had aggregated within the ventral horn of cervical segments C3-C6 in the same location and relative segmental density as in the adult. However, maturation of a morphology characteristic of newborn and adult phrenic motoneurons did not occur until after E17, after the onset of phrenic respiratory motor discharge, the approximation of the complete intramuscular branching pattern, and the arrival of afferent fibres. These morphological changes include loss of close contact (gap junctions) between soma which had been established from the onset of motoneuron migration, and a radical

reorganisation of dendritic arborisations with the formation of the characteristic rostrocaudally-projecting phrenic dendritic tree. By birth, the phrenic motoneuron pool has attained the major morphological characteristics of the adult pool. A few remaining immature features do persist, including extensive neuritic projections into the white matter and floor plate region and the persistence of growth cones on a number of dendritic processes.

METHODS

DiI labelling and tissue processing

Tissue was postfixed in 4% paraformaldehyde for 2-4 days. The phrenic nerve was cut at the level of the atria for E13.5-E15 fetuses, at the level of the thymus for E16-E17.5 fetuses and at the level of thoracic spinal level T1-T2 for E18-newborn pups. The distal end of the nerve was stripped of connective tissue and cuffed in a small crystal of Fast DiI (Molecular Probes). The cut end of the phrenic nerve and DiI crystal was sealed in a strip of parafilm to prevent DiI diffusion into other tissues. Tissues were placed in 1.2% paraformaldehyde, pH 9.5 for 2 months at 37°C to allow time for complete neuronal labelling. The cervical spinal cord with dorsal root ganglia and ventral roots attached were isolated and maintained in cold 4% paraformaldehyde prior to a brief wash in PBS and embedded in 3.5% agar. A block containing the tissue was excised and fixed for up to 3 days. Vibratome serial sections of 50-80 μm in horizontal and transverse planes were collected and washed in PBS. Sections were mounted onto chrome-alum subbed microscope slides and coverslipped so as to keep the sections moist. Slides were stored at 4°C in a humid chamber.

Microscopy

Photographs of labelled neurons were taken with a camera attached to a Leitz Diaplan epifluorescent microscope, or from images generated with a confocal laser scanning system, consisting of a Leitz Aristoplan fluorescence microscope illuminated by a 100 W HBO mercury burner for direct observation and an argon-krypton laser with emission of 568 nm for scanning. Confocal images were processed utilising image analysis software developed by Leica Lasertechnick GmbH (Heidelberg) run on a Motorola 68030 CPU workstation, using the OS-9 operating system. Measurements of somal diameter and number were made from horizontal sections using an image analysis system (JAVA; Jandel Inc.). Diameters and numbers are expressed as mean ± standard deviation. Differences between mediolateral and rostrocaudal diameters for each age calculated using an unpaired t-test in the SigmaStat statistics package.

RESULTS

Cell bodies

We began our studies at embryonic day (E)13.5, two days after the onset of motoneuron generation and the first age at which the distal end of the phrenic nerve could be successfully isolated and specifically labelled without diffusion of dye into other neuronal populations. Fig. 3.1C illustrates that, at this age, phrenic soma had reached their approximate final position within the ventral horn. Phrenic soma were clustered into tightly clustered groups along mediolaterally-projecting neuritic processes, likely composed of bundles of phrenic axons. By E14, the majority of phrenic motoneurons had coalesced within the ventro-medial ventral horn of cervical segments C3-C6, with the greatest density of soma being throughout C4 and C5 (Fig. 3.1D). This location and relative segmental density of soma was maintained up to birth (Figs. 3.1-3.8, horizontal sections), and in the adult (Goshgarian and Rafols, 1981).

Between E14 and E18, closely apposed phrenic soma undergo compaction into a more tightly aligned motor column (compare Figs. 3.1A,B with Figs. 3.5A-C). Fig. 3.2C clearly demonstrates the mediolateral distribution of soma within the motor pool at E15, prior to compaction of the motor pool (see below). This confocal image shows that closely associated soma are spread along common mediolaterally-oriented neuritic bundles. Two processes likely contribute to somal compaction. First, neuronal cell death occurring during E15 and E16 (Harris and McCaig, 1984) will alleviate spatial limitations to cellular compaction. The reduction in labelling density, indicative of a decrease in motoneuron number, is evident from comparisons of the phrenic pool at similar cervical levels at E15 (Fig. 3.2B), E16 (Fig. 3.3D) and at E17 (Fig. 3.4B). Second, continued somal migratory activity must occur. High magnification confocal images of soma at E15 ($P<.0001$) (Fig. 3.2C) and E17 ($P<.05$) (Fig. 3.4C) demonstrate that their shape is characteristic of migratory neurons, longer along the axis of migration. Fig. 3.6C illustrates that this elongated morphology is no longer as apparent by E19. Interestingly, however, the rostrocaudal diameter becomes statistically larger than the mediolateral diameter during E19-E21. These changes in somal diameter are shown in Table 3.1.

Contralateral retrograde labelling of forelimb (brachial) and phrenic motoneurons allowed for a clear delineation of the relative positioning of the respective motor pools (Fig. 6E). The relative positioning of the two motoneuron pools was attained as early as E14. Brachial motoneurons were located laterally and dorsally of the phrenic motoneuron pool.

Dendritic arborisation

DiI labelling extended throughout the entire length of dendrites, as evidenced by the labelling of growth cones at the tips of the longer dendrites (Fig. 8E). Short dendritic arbors could be observed as early as E14 throughout the ventral horn (Fig. 1D). In horizontal sections, neurites were observed to extend medially and laterally from the motor column to the ventricular zone (Figs. 1A,B). By E15 phrenic dendrites had fanned out dorsolaterally to ventromedially of the phrenic nucleus, extensively penetrating the white matter and the floor plate, crossing contralaterally (Fig. 2D). These dendrites were highly defasciculated, and in horizontal section (Figs. 2A,B) spanned the entire mediolateral breadth of the ipsilateral spinal cord. From E16 to E18, dendritic morphology did not change significantly, in relation to further growth of the spinal cord. By E17, the decline in the numbers of somata due to cell death (E15-E16) results in an apparent decrease in dendritic density (compare Fig. 2B - E15 with Fig. 4B - E17). It should be noted, however, that by the onset of respiratory activity (at E17), phrenic dendritic morphology was essentially immature.

After the inception of phrenic rhythmic respiratory discharge at E17, a radical reorganisation of dendritic morphology occurred, which approximated that observed in the newborn and adult (Furicchia & Goshgarian, 1987; Lindsay et al. 1991) by E19. Dendrites projecting within the transverse plane began to retract (Fig. 6D) and fasciculate (Fig. 6A) and the rostrocaudally-projecting dendrites believed to synchronise phrenic motoneuron discharge began to form (Fig. 6C). From the period E18-P0, there was continuing retraction and bundling of transversely-oriented dendrites and an increasing presence of rostrocaudally-projecting dendrites which were organised into tight fascicles (Figs. 5-8). By birth, there were still quite extensive neuritic projections into the white matter and medially towards the floor plate region where contralaterally-derived dendrites were in close proximity within the floor plate region (Figs. 8D-G). Moreover, growth cones could still be visualised on dendritic tips

within the white matter at P0 (Fig. 8E), suggesting that neuritic reorganisation continued postnatally.

Afferents

Cell bodies within the dorsal root ganglion (DRG) were observed as early as E13.5. Further, even at this early age, the relative segmental distribution of sensory soma was attained, primarily being contained within C5 dorsal root ganglion (most heavily labelled DRG in all figures: Gottschall, 1981). However, projections of afferent fibres within the dorsal horn were not observed until age E15–E16. Previous to that age, the nerve terminals of afferent fibres converged and stayed in position at the perimeter of dorsal horn in what has been referred to as the dorsal root entry zone (DREZ). The first afferent fibres to reach the vicinity of phrenic motoneuron dendrites were observed at age E17.

Fig. 3.1 E13.5-14: A,B illustrate the labelled phrenic motoneuron pool in the coronal plane at E14. A few cells are also labelled in the DRG of C4 and C5 which sit lateral (left) of the spinal cord. Neurites can be seen projecting mediolaterally from the central canal into the white matter. Dotted line represents central canal in A. C shows phrenic motoneurons at age E13.5 in the coronal plane. This confocal image shows that phrenic motoneurons are still migrating from the medial region of the spinal cord (left) towards the final positioning within the phrenic nucleus. D illustrates a rather diffuse cluster of phrenic motoneurons in a transverse section from an E14 fetal rat cervical cord, dotted line representing lateral and ventral extent of spinal cord. Cells in the DRG located laterally (left) to the phrenic nucleus can also be seen. Scale bars (μm): A=100, B=50, C=20, D=50.

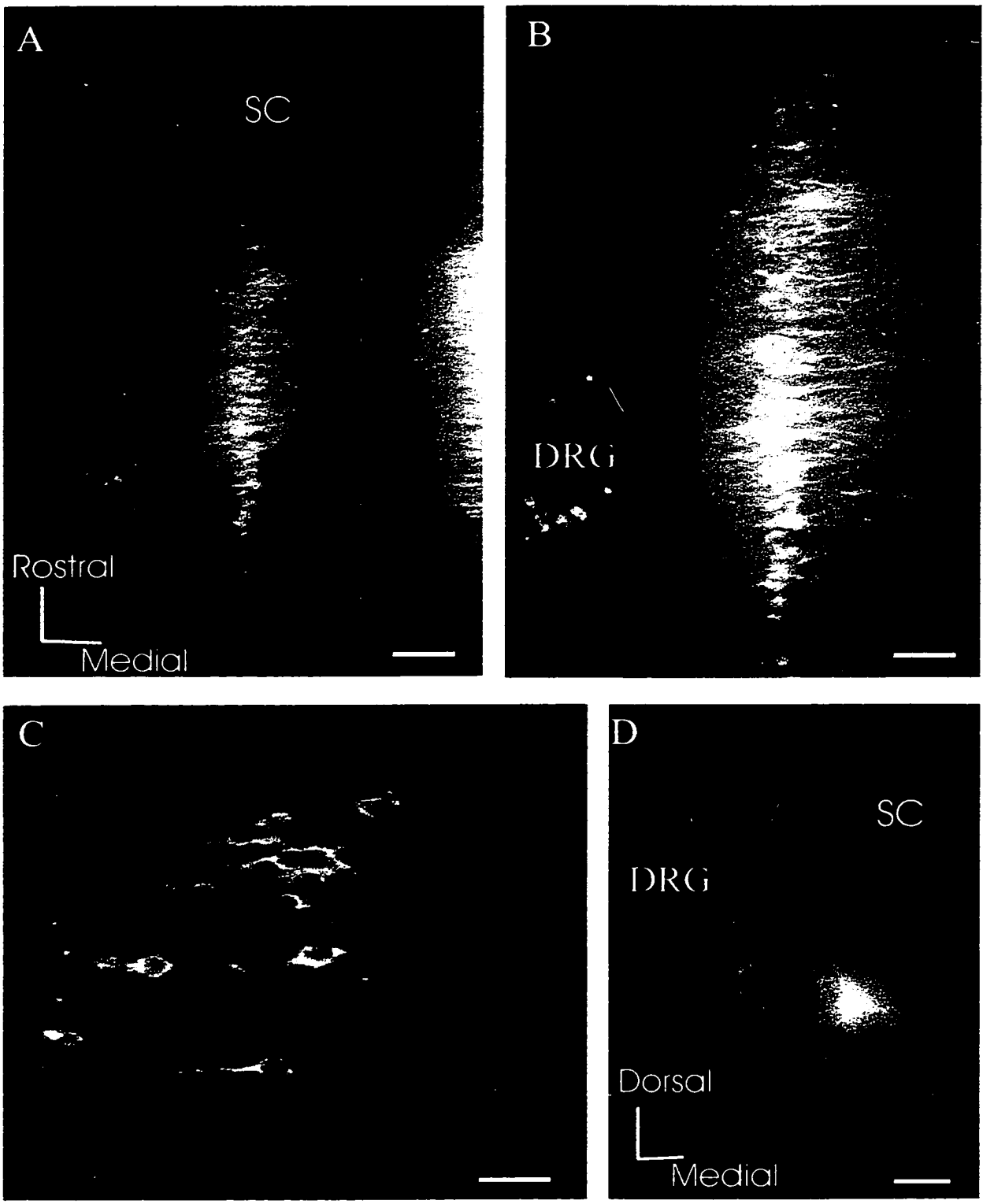

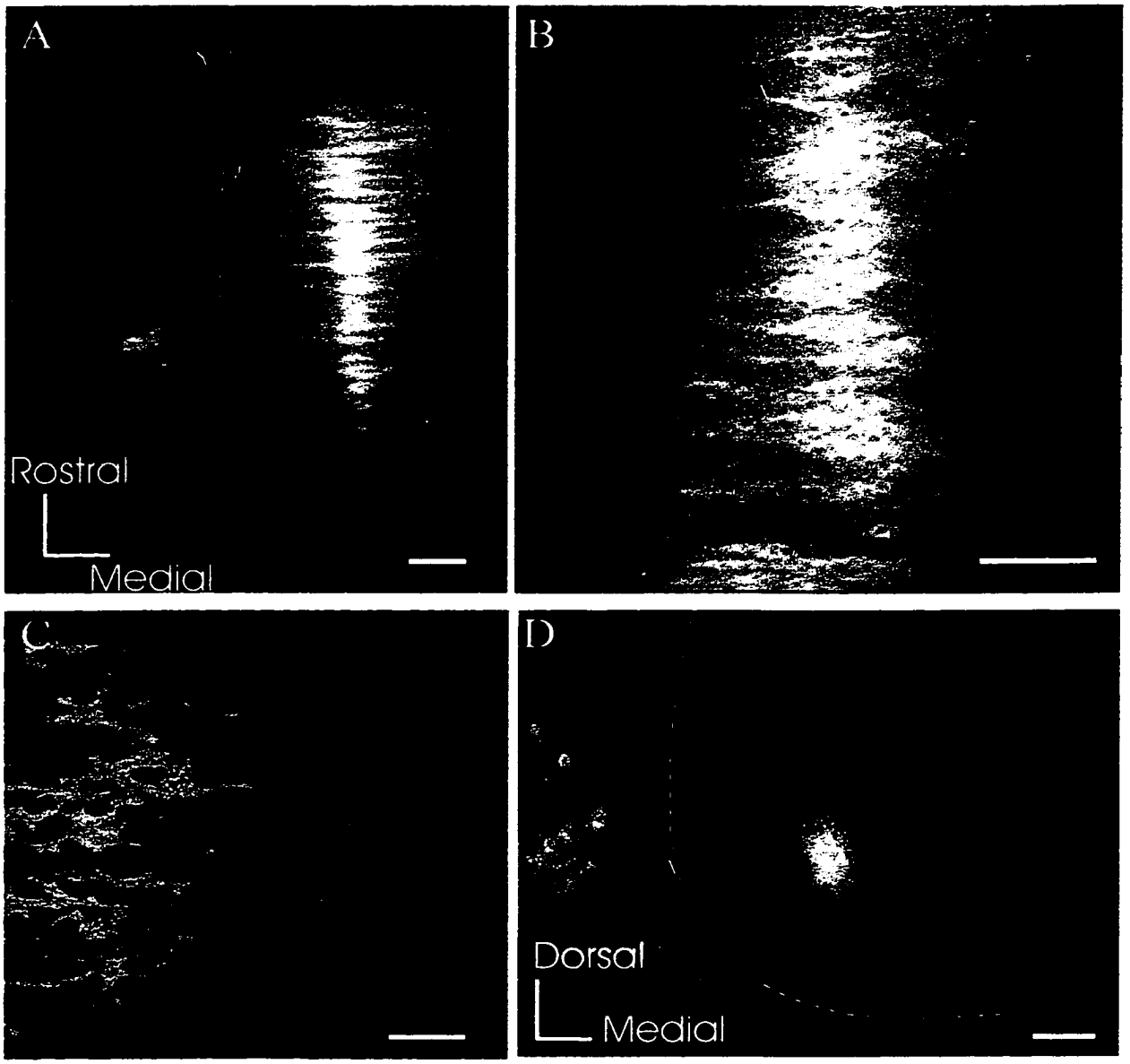

Fig. 3.2 E15: A, B, C illustrate labelled phrenic motoneurons in the horizontal plane at E15. A shows labelling of C5 phrenic afferent soma in dorsal root ganglion. Phrenic motoneurons appear similar to those observed at E14, with the neurites projecting mediolaterally towards the central canal and the white matter. C shows a confocal image of phrenic motoneurons located in clusters with their membranes closely apposed and their neurites trailing medially (right) towards the ventricular zone. From B&C it is apparent that the mediolateral spread of soma is quite high at this age. D shows a cluster of phrenic motoneurons in the transverse plane with dendrites radiating dorsolaterally, ventrolaterally and ventromedially to a greater extent than that seen at age E14. Dotted lines represent outer limit of spinal cord. Axes equivalent to those in Fig. 3.1.Scale bars (μm): A=100, B, D=50, C=25.

Fig. 3.3 E16: A-D show the phrenic motor column in the coronal plane. Neurons are not so diffusely distributed mediolaterally within the motor column. Further, ongoing programmed cell death is resulting in fewer labelled neurons. E shows the phrenic motoneurons in the transverse plane with the neurites projecting in a similar pattern as seen at E15. Dotted line in A&B represent lateral extent and in E represents lateral and ventral edge of spinal cord. Scale bars (μm): A=100, B,C,E=50, D=25.

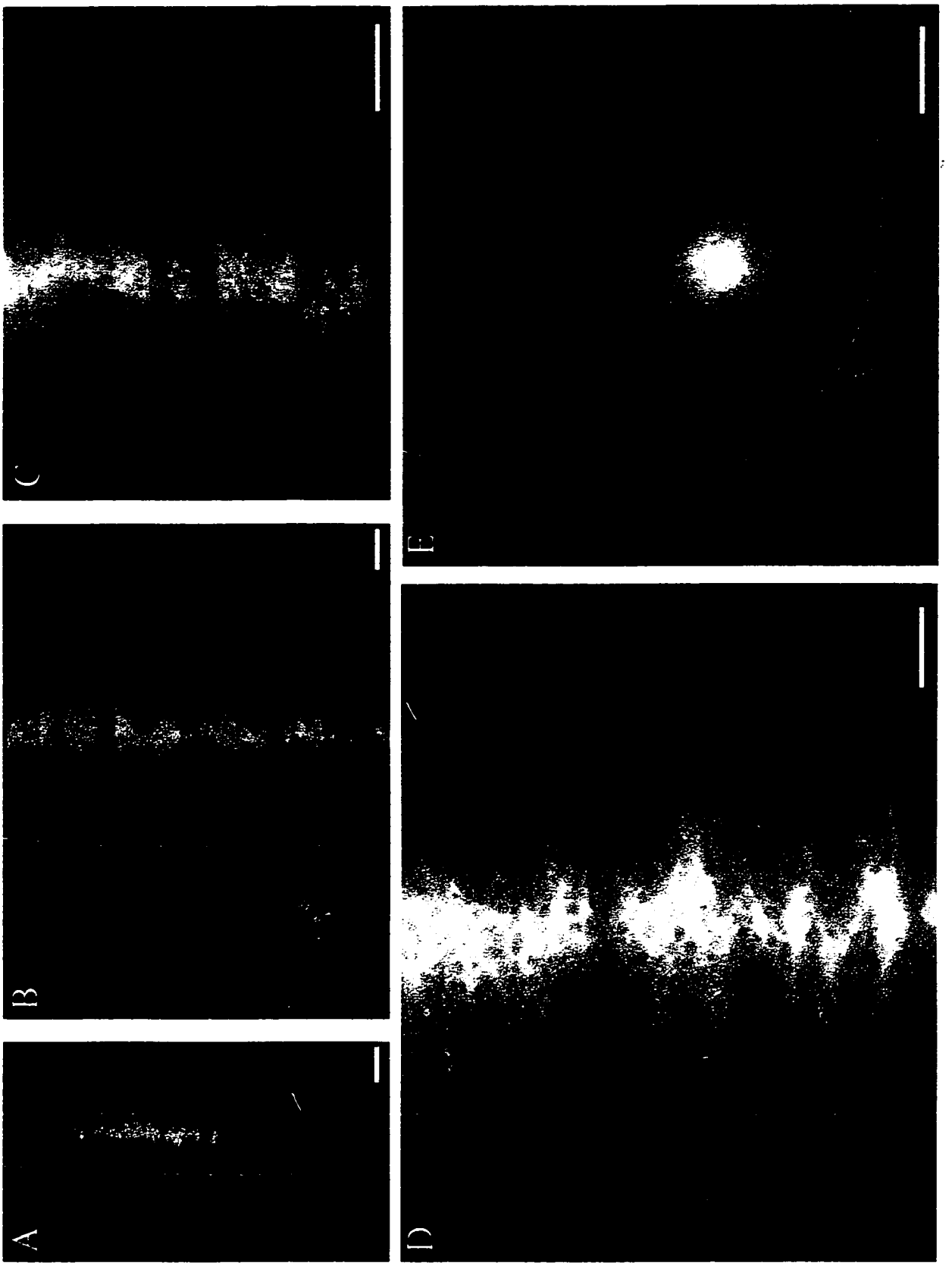

Fig. 3.4 E17: A,B demonstrate the absence of rostrocaudally-projecting dendritic arbors at the onset of rhythmic respiratory activity. Further, fewer neurons label compared to the previous day and somata in the phrenic nucleus appear more clustered into separate groups as compared with earlier ages. Fig. C shows a confocal image of two very closely apposed phrenic somata with their neurites projecting mediolaterally which retain the morphology of migrating neurons. D shows the phrenic motoneurons in the transverse plane with the neurites projecting well into the white matter. Dotted line in A&B represent lateral extent and in D represents lateral and ventral edge of spinal cord. Scale bars (μm): A,B,D=50,C=10.

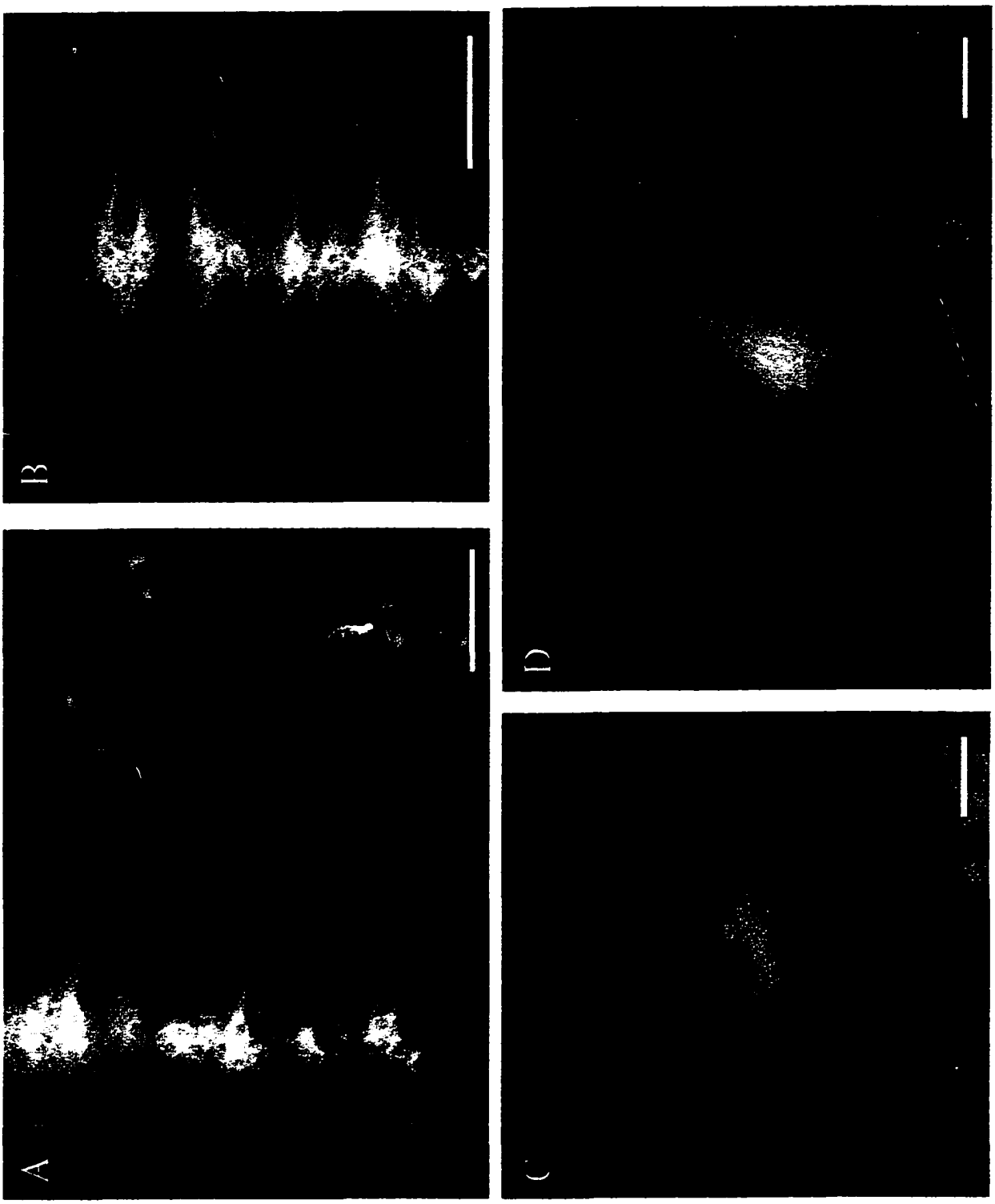

Fig. 3.5 E18: A-C show that by E18 the first signs of rostrocaudally directed neurites are visible and that a tightly aligned motor pool has developed. D shows the phrenic motoneurons in the transverse plane and their persistence in the white matter. Dotted line in A&C represent lateral extent and in D represents lateral and ventral edge of spinal cord Scale bars (μm): A-D=50.

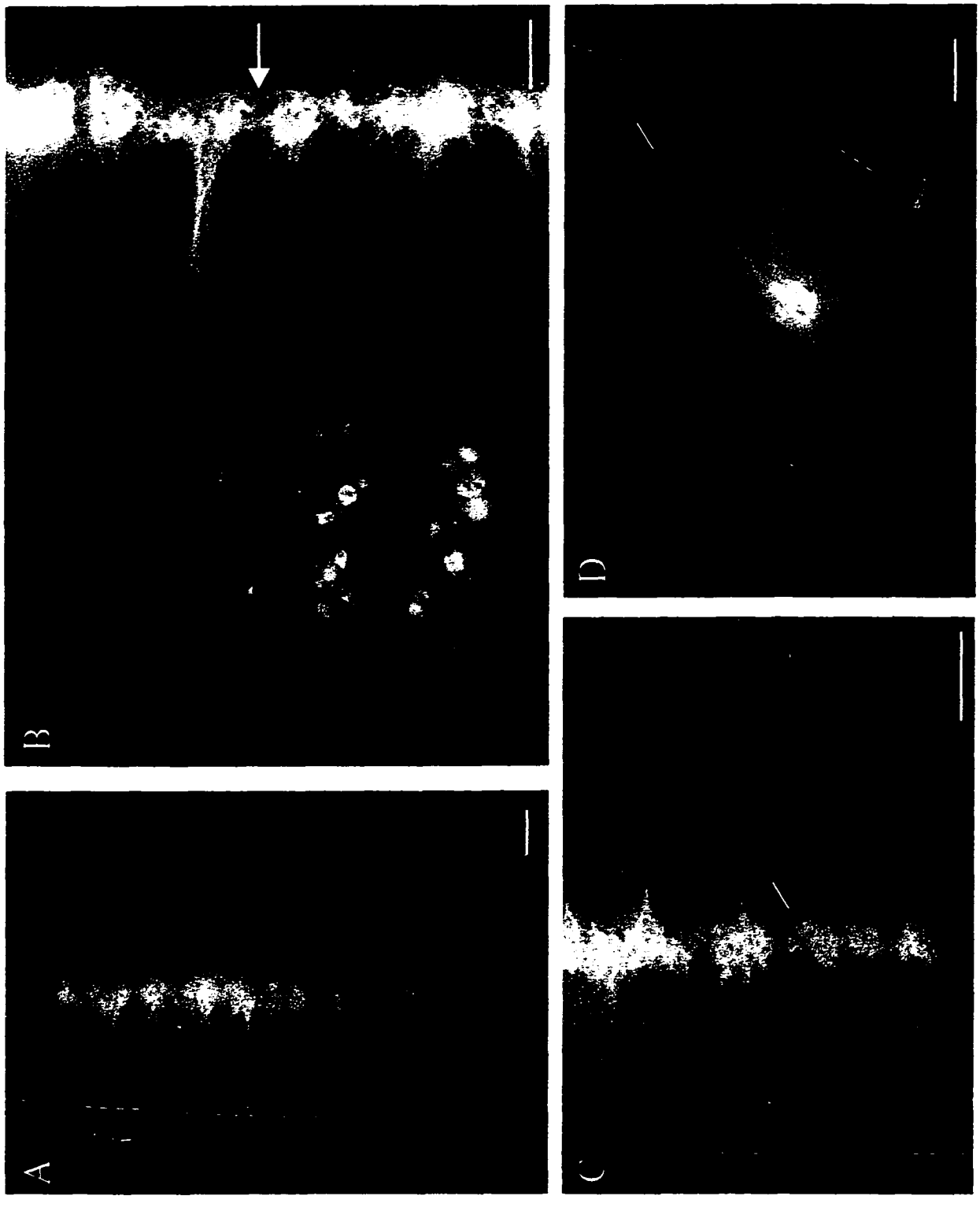

Fig. 3.6 E19: The mature state is approximated during E19. A-C show the continuing increase in the formation of rostrocaudal dendrites (arrow in C) within the phrenic motoneuron pool and the increase in bundling of mediolaterally-directed dendrites. D demonstrates the start of dendritic retraction, particularly of the laterally-projecting populations. Differences in the positioning of phrenic (D) and brachial (E) motoneuron pools are shown in the transverse plane. Afferent fibres are particularly obvious as they project to brachial motoneurons in E. Dotted line in A&B represent lateral extent of spinal cord and in E the lateral and ventral extents, round to the floor plate. Scale bars (μm): A,B,D,E = 50, C=25.

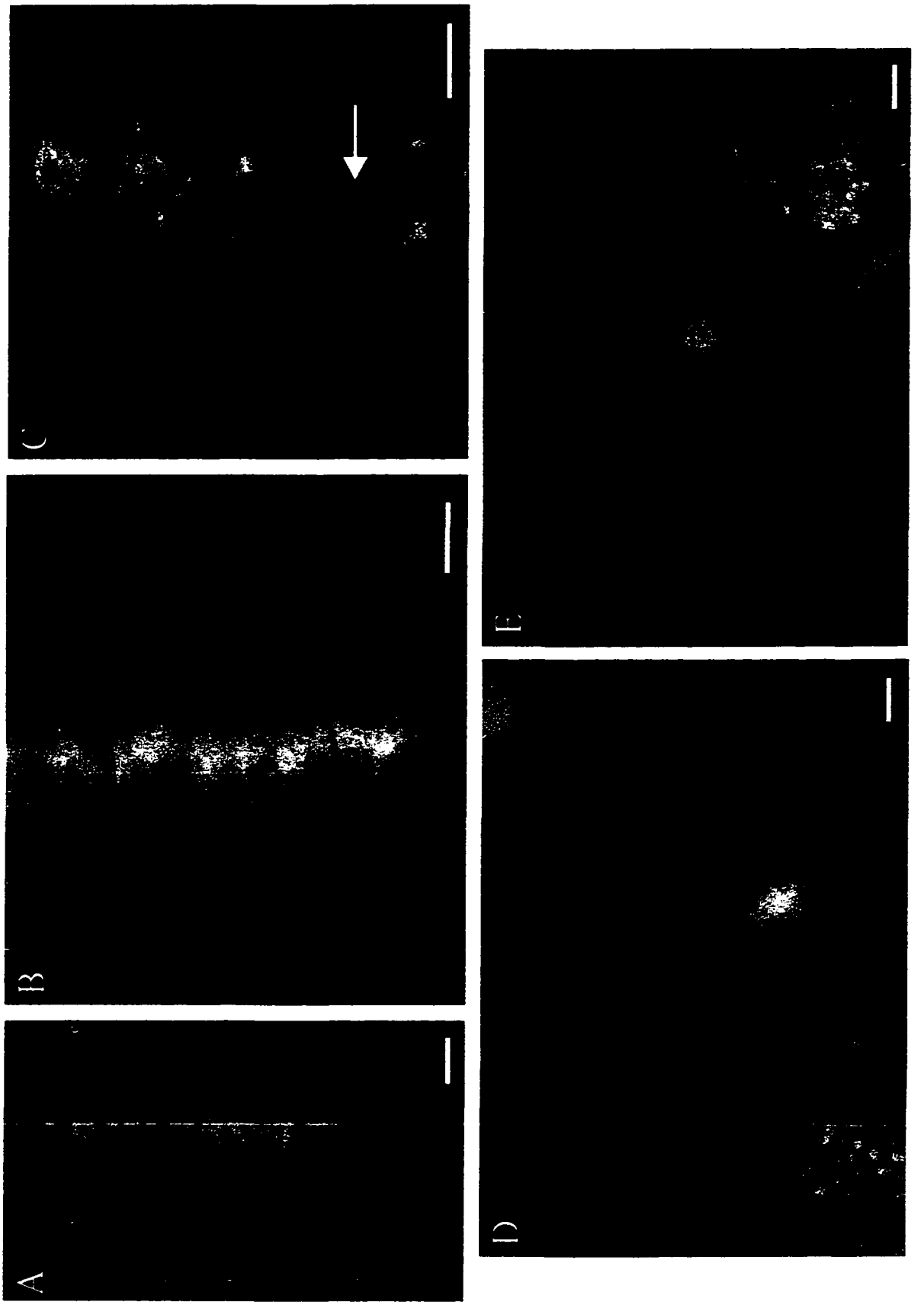

Fig. 3.7: E21. As illustrated in A-C, phrenic motoneurons are tightly clustered into small groups, and the rostrocaudal dendritic projections (indicated by arrows in C) are similar to those in the mature state. D illustrates the neuritic projections in the transverse plane are also less extensive and more highly bundled than at earlier ages. Dotted line in A and B represents the lateral extent of the spinal cord. Scale bars = 50μm in A,B,D, 25μm in C.

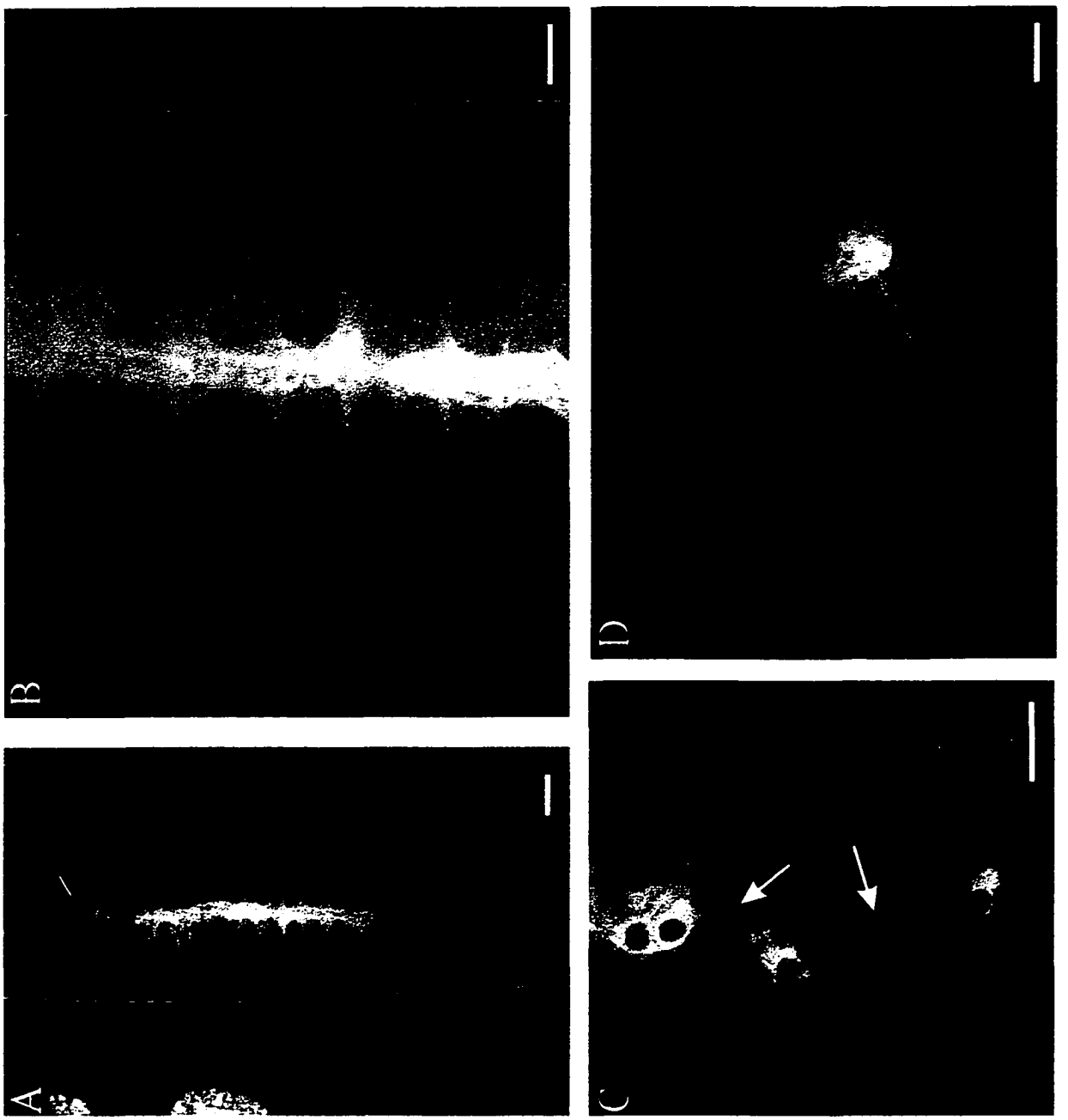

Fig. 3.8 P0: A,B show the distribution of phrenic motoneurons within the motor column at birth. C is a confocal image of a cluster of neurons in the sagittal plane with the arrow pointing at rostrocaudally-directed dendrites. Fig. D shows the tightly clustered neurites of the right phrenic motoneuron pool in the transverse plane. E is a confocal image of a growth cone located at the tip of a dorsoventrally projecting dendrite which is in the white matter. F illustrates the medially-projecting neurites in the left and right phrenic pools which are co-localized at the floor plate of the spinal cord. G is a higher magnification from a different animal showing the medially projecting neurites from left and right phrenic nuclei converging at, and in some instances, crossing the floor plate. Dotted line in A&B represent lateral extent and in D represents lateral and ventral edge of spinal cord. Further, in F, dotted line shows ventral extent of spinal cord with floor plate in middle. Scale bars (μm): A=100, B,D=50, C,F,G=20, D=10.

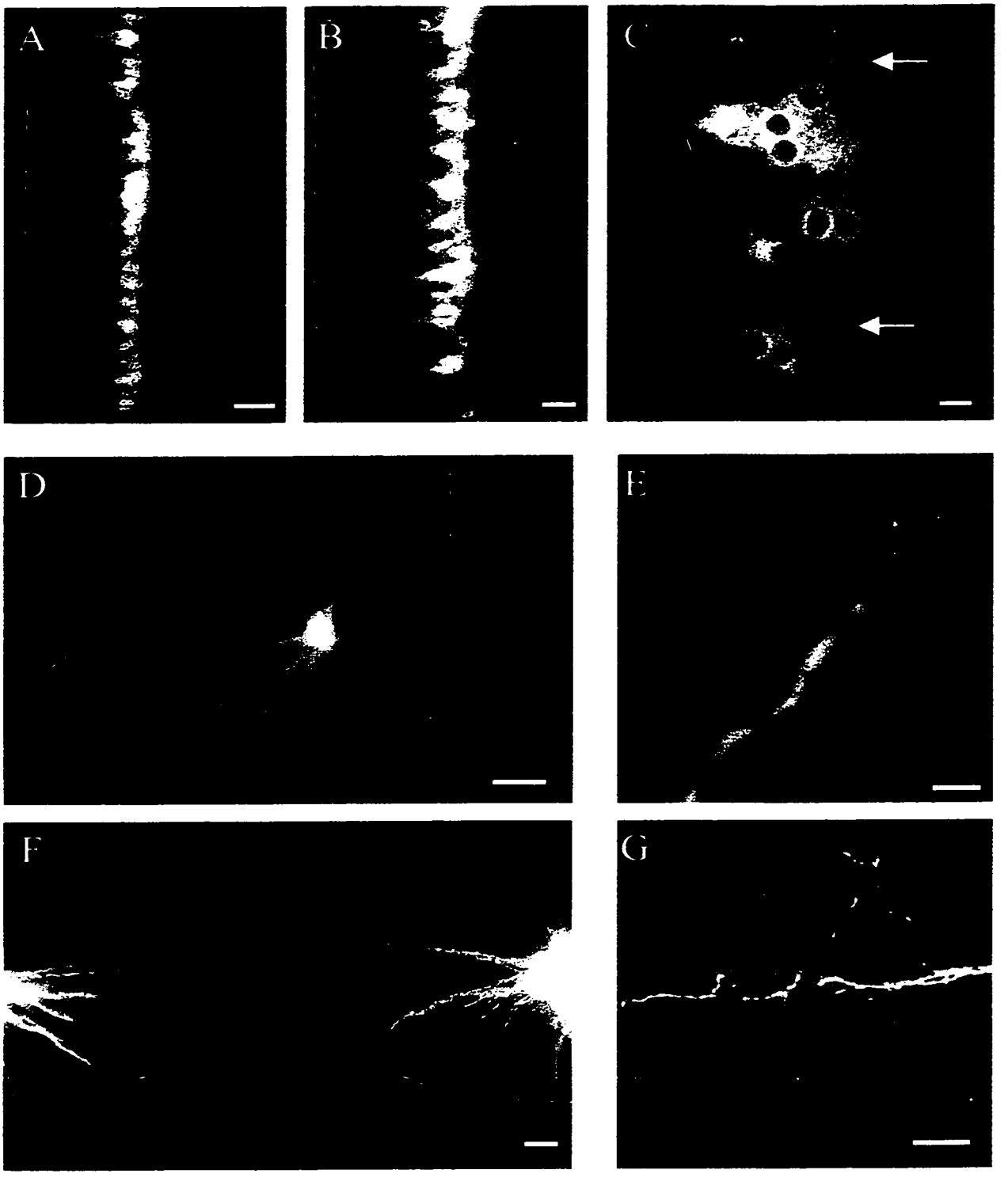

Table 3.1: Phrenic Motoneuron Diameter

Age	E14	E15	E16	E17	E18	E19	E21	P0
Diameter (mediolateral)	8.4±1.8 (n=195)	**10.7±2.1*** (n=335)	**11.1±1.9*** (n=238)	**12.4±2.1†** (n=147)	13.2±2.5 (n=119)	13.4±1.7 (n=112)	15.6±2.6 (n=145)	15.8±1.8 (n=158)
Diameter (rostrocaudal)	8.1±1.5 (n=73)	9.1±1.6 (n=90)	10.3±1.8 (n=233)	11.9±1.9 (n=130)	13.7±1.8 (n=114)	**14.0±2.1†** (n=112)	**16.3±2.3†** (n=144)	16.1±2.0 (n=148)

Values are mean ± standard deviation. n = number of samples.
* Significant difference of P<.0001 between diameters for same age. Figures in bold font are significantly larger.
† Significant difference of P<.05 between diameters for same age. Figures in bold font are significantly larger.

DISCUSSION

Retrograde labelling of phrenic motoneurons with horseradish peroxidase (HRP) in a previous study demonstrated that phrenic motoneuron morphology was essentially mature by birth, outside of a persistence of neuritic projections into the white matter (Lindsay et al. 1991). In this study, we describe the morphogenesis of phrenic neurons prenatally, and demonstrate that many of the maturational changes occur subsequently to the onset of respiratory motor discharge at E17 (Greer et al., 1992). A more recent publication by Song et al. (1999) has detailed a number of features of the developing phrenic nerve in Wistar rat through the perinatal period, most notably axonal number, myelination, and further details concerning afferent penetration into the cervical cord. Where this publication overlaps ours, similar data was obtained.

Phrenic motoneurons reach the motor column by E13.5

At the earliest age studied (E13.5), phrenic motoneurons were going through the final stages of radially-oriented migration from the ventricular zone, where they are generated between E11 and E12 (Altman & Bayer, 1984). During migration, phrenic motoneurons were organised into tightly packed clusters, perhaps linked by gap junctions (see below). Gap junctions are common to early neurons and have been demonstrated to contribute to their migration and differentiation (see Kandler and Katz, 1995). Another distinguishing feature of phrenic motoneurons at E13.5 is the very simple mediolateral projection of neurites. Further, it is important to note that while all of the motoneurons at E13.5 have approximated their final position within the spinal cord, their axons have reached their primordial target, the pleuroperitoneal fold (chapter 4). The laterally-directed neurites observed extending from the phrenic soma at E13.5 appear to be the proximal extent of their axonal processes, although it is most likely that radial glia mediated phrenic motoneuron migration to their appropriate position within the spinal cord (Ono & Camera, 1989).

The onset of respiratory drive and phrenic maturation

Bulbospinal premotor neurons reach the phrenic motor nucleus between E16 and E17 (Ellenberger & Feldman, 1988; Lakke, 1997). At approximately E17, rhythmic respiratory

motor discharge of the phrenic nerve commences (Greer et al., 1992), indicating that inspiratory drive from bulbospinal pre-motor to phrenic motor neurons is transmitted from the onset of their synaptis contact. This study demonstrates, however, that phrenic motoneuron morphology is still immature at this time. Gap junctions appear prevalent between motoneurons (confirmed by Martin-Caraballo and Greer, 1999; utilising intracellular fills with Lucifer Yellow and neurobiotin as well as electrophysiologically), cell body shape is reflective of migratory activity, extensive phrenic dendritic branches penetrate the white matter and the characteristic rostrocaudally-extending dendritic tree has not formed. Thus, the onset of functional inspiratory recruitment is clearly not limited by the morphological maturation of the phrenic motor pool. Subsequently, dramatic remodelling of the phrenic dendritic arbor to approximate that of the adult by E19 implies that maturation of the phrenic motor pool may be coupled to the descending drive. By birth, the phrenic motor pool is essentially morphologically mature. Such precocious development is reflective of its critical function upon birth. In comparison, locomotor function appears over the next two to three weeks postnatally (Westerga and Gramsbergen, 1990). The gradual maturation of somatodendritic morphology over this same period (2-3 weeks) correlates with the attainment of locomotor function (Schiebel and Schiebel, 1970; Ulfhake et al., 1988; Westerga and Gramsbergen, 1992).

Gap junctions in phrenic motoneuron development

Spontaneous electrical activity of neurons is an important component of the initial modelling of the nervous system. The onset of subsequent function (experience)-related activity fine tunes connectivity to attain an appropriately wired nervous system (general review by Katz and Shatz, 1996). Gap junctions are postulated to synchronise the electrical and biochemical activities of functionally-related populations of neurons in order to promote population-specific development and refinement of afferent and efferent projections (general review Kandler and Katz, 1995). Cellular coupling during development and its subsequent loss postnatally is a feature common to spinal (Fulton et al., 1980; Walton and Navarrete, 1991; Chang et al., 1999) and brainstem motoneurons (Mazza et al., 1992). At all ages examined, we observed close apposition between motoneuron soma. A parallel study by

Martin-Caraballo and Greer (1999) demonstrates electrotonic and dye-coupling between phrenic motoneurons from E16 up to P0-P1 (the entire period under study). Adult phrenic motoneurons are not coupled and thus gap junctions must disappear postnatally (Lipski, 1984).

Phrenic motoneurons are spontaneously active from E13 (Greer et al., 1992) and are capable of eliciting diaphragm myotube activity from the onset of neuromuscular formation at E14-E15 (Laskowski and Owens, 1994). Prior to the establishment of coordinated supraspinal input, gap junctions may help generate, synchronise and augment firing in order to elicit optimal, concerted contractile activity of the diaphragm throughout development. This would be particularly important when respiratory movements commence, where an initially weak descending drive (DiPasquale et al., 1994) and limited phrenic firing properties (Martin-Caraballo and Greer, 1999) may otherwise hinder optimal diaphragmatic activity. Further, slight differences in timing between gap junction-linked phrenic motor subpopulations may promote two processes: 1) establishment of a somatotopic map on the diaphragmatic surface (Laskowski and Owens, 1994) and 2) a higher degree of specificity in the establishment of synaptic connectivity with descending input.

Postnatally, the loss of gap junctions is likely functionally linked to the marked reduction in motoneurons recruited during resting respiratory effort, where extensive coupling may be detrimental to fine motor control (Cameron et al., 1991; Torikai et al., 1996). Further, the loss of hyperinnervated diaphragmatic neuromuscular junctions and refinement of the topographic projection postnatally (Bennett and Pettigrew, 1974; Laskowski and High, 1989) may be related to a loss of electrical coupling between phrenic motoneurons, in a mechanism where subtle asynchronisation between motoneuron firing promotes the stabilisation of one favoured input along Hebbian principles (see Balice-Gordon and Lichtman, 1994; Chang et al, 1999).

The establishment of medullary drive and phrenic dendritic remodelling

It would appear that from early in development, the extensive projection of phrenic dendrites into the white matter would ideally position them for interaction with descending fibres in these tracts. It is tempting to speculate that these dendrites in some way assist the

guidance of migrating axons of descending medullary neurons into the phrenic motor pool, where they terminate on soma and dendritic processes (Ellenberger and Feldman, 1988). The retraction of phrenic dendrites from the white matter commences at approximately E19 but is not yet fully complete by birth. Further, the fact that growth cones were observed on dendrites within the white matter at birth, suggests that there was active remodelling of dendritic arborisations at that stage. The purpose of such remodelling is unclear but is likely related to continued synaptogenesis and/or synaptic reorganisation with descending medullary input. Evidence from studies of hippocampal dendritic arborisation in *in vitro* slices indicates that the presence of dendritic growth cones during dendritic reorganisation reflect ongoing synaptogenesis between hippocampal and afferent neurons (Dailey and Smith, 1996; Kossel et al., 1997)

The morphological substrate believed responsible for the synchronisation of mature phrenic motor output is the branching of medullary bulbospinal respiratory axons onto the extensive rostrocaudally-oriented dendritic branches of phrenic motoneurons (Goshgarian and Rafols, 1981; Furicchia and Goshgarian, 1987; Lipski et al., 1994). This is established by birth (Lindsay et al., 1991). We have found that the rostrocaudally-projecting dendrites do not form until E19, 2 days after the onset of phrenic respiratory discharge. Thus, synchronised phrenic activity during E17 and E18 likely involves either one or both of: a) medullary axon branching onto multiple mediolaterally-projecting dendritic branches, and b) gap junctional electrotonic coupling which may induce firing in neighbouring neurons and/or prevent asynchronous firing.

Considerable evidence points to the role of afferent input in dendritic morphology, in the hippocampus (Dailey and Smith, 1996; Kossel et al., 1997) and lumbar spinal cord (O'Hanlon and Lowrie, 1994). Thus, we hypothesise that phrenic motoneuron dendritic morphology is remodelled during E17-E19 by the monosynaptic bulbospinal input. The synaptotrophic model of Vaughn (1989) suggests that somatodendritic maturation may be mediated by signalling through newly established synaptic input, perhaps via the influence of neurotrophins (reviewed in Theonen, 1995; McAllister et al., 1999), and the local morphoregulatory influence of Ca^{2+} transients (Müller and Connor, 1991; Guthrie et al., 1991). However, as opposed to lumbar motoneurons, which are coupled to local central

pattern generators and receive considerable sensory input, phrenic motoneurons receive their major functional input from a supraspinal source. Thus, phrenic maturation may be particularly sensitive to this descending input. We are currently testing this hypothesis by attempting to remove descending drive during the critical period E17-E19.

Programmed cell death

DiI retrograde labelling of soma is not ideal for a quantitative analysis of motoneuron number, as it is not possible to determine with certainty whether the dye transports along all axons. However, it was obvious that the density of cell bodies was higher at E14 and E15 compared with older ages. This likely reflects the fact that the majority of naturally occurring cell death occurs at approximately E16, resulting in an approximately 50% reduction in the number of phrenic motoneurons (Harris and McCaig, 1984). Recent evidence from Song et al. (1999) establishes that phrenic axon number falls from ~950 at E15 to ~550 at E19, supporting the original estimations of Harris and McCaig (1984). We counted ~1065 axons from electron micrographs of the phrenic nerve at E18 (chapter 7) in Sprague-Dawley rats. Whether the differences in axonal count are reflective of differences between strains of rat used is unclear, although this would appear to be the most likely explanation for the discrepancy.

Electrophysiological correlates

The conversion from immature to mature function, such as at the onset of inspiratory drive to phrenic motoneurons, is an important time in the development of neurons. The onset of respiratory drive commences at E17 and robust respiratory activity is established by E20 (Greer et al., 1992; DiPasquale et al., 1994). The current study indicates that the period encompassing E16 to E19/20 is a pivotal time for the maturation of phrenic motoneurons. Coincidental with the onset of functional recruitment at E17, phrenic afferent axons reach the dendritic arbors of phrenic motoneurons, and the neuromusculature has approximated its adult extent (see chapter 4). Thus, the entire network is essentially in place for the onset of function. Further maturation can thus play out over an interconnected network, where functional drive can modulate the maturation of this motor system (see Navarette and

Vrbova, 1993; Katz and Shatz, 1996). Parallel studies have demonstrated that after the inception of inspiratory drive, major maturational changes in phrenic motoneuron electrophysiological properties develop concomitantly with the major morphological changes described here (Martin-Caraballo and Greer, 1999, 2000 in press A, 2000 in preparation). Maturational changes occur in passive membrane properties, and action potential properties and firing characteristics. These factors demonstrate that at E16, motoneurons are more excitable and elicit longer lasting but less frequent or robust bursts than at birth. These factors correlate functionally with the developmental profile of diaphragm contractile and fatigue properties (Martin-Caraballo et al., 2000 in press B). From E18 to birth, the diaphragm exhibits maturational changes in twitch and tetanic properties as well as changes in half-relaxation time and increased resistance to fatigue. Importantly, developmental changes in phrenic nerve and diaphragm properties appear to be mutually tuned in order to elicit optimal neuromuscular activity at all developmental ages in order to produce fetal breathing movements throughout the perinatal period (see Greer et al., 1999 for detailed review). The extent to which components of a motor network that are to function together either develop in an interdependent or independent/coincidental fashion is currently unclear. Accumulating evidence presented here certainly implies that maturation of phrenic motoneurons may be coupled to descending drive. Current studies within the laboratory are aimed at removing this functional drive in an attempt to determine which aspects of phrenic development are altered.

REFERENCES

Altman J and Bayer SA (1984) The development of the rat spinal cord. *Adv. Anat. Embryol. Cell Biol.* 85: 1-164.

Balice-Gordon RJ and Lichtman RW (1994) Long-term synapse loss induced by focal blockade of postsynaptic receptors. *Nature.* 372: 519-524.

Bennett MR and Pettigrew AG (1974) The formation of synapses in striated muscle during development. *J. Physiol.* 241: 515-545.

Cameron WE, Jodkowski JS, Fang H and Guthrie RD (1991) Electrophysiological properties of developing phrenic motoneurons in the cat. *J. Neurophysiol.* 65: 671-679.

Chang Q, Gonzalez M, Pinter MJ and Balice-Gordon RJ (1999) Gap junctional coupling and patterns of connexin expression among neonatal rat lumbar spinal motor neurons. *J. Neurosci.* 19: 10813-10828.

Dailey ME and Smith SJ (1996) The dynamics of dendritic structure in developing hippocampal slices. *J. Neurosci.* 16: 2983-2994.

Di Pasquale E, Monteau R, Hilaire G (1994) Involvement of the rostral ventro-lateral medulla in respiratory rhythm genesis during the prenatal period: an in vitro study in newborn and fetal rats. *Dev. Brain Res.* 78: 243-252.

Ellenberger HH. and Feldman JL (1988) Monosynaptic transmission of respiratory drive to phrenic motoneurons from brainstem bulbospinal neurons in rats. *J. Comp. Neurol. 269*:47-57.

Fulton BP, Miledi R, and Takahashi T (1980) Electrical synapses between motoneurons in the spinal cord of the newborn rat. *Proc. R. Soc. Lond. B* 208: 115-120.

Furicchia JV and Goshgarian HG (1987) Dendritic organization of phrenic motoneurons in the adult rat. *Exp. Neurol.* 69:621-634.

Goshgarian HG and Rafols JA (1981) The ultrastructure and synaptic architecture of phrenic motoneurons in the spinal cord of the adult rat. *J. Neurocytol.* 13:85-109.

Gottschall J (1981) The diaphragm of the rat and its innervation. Muscle fibre composition; perikarya and axons of efferent and afferent neurons. *Anat. Embryol.* 161:405-417

Greer JJ, Smith JC and Feldman JL (1992) Respiratory and locomotor patterns generated in the fetal rat brain-stem spinal cord in vitro. *J. Neurophysiol.* 67:996-999.

Greer JJ, Allan DW, Martin-Caraballo M and Lemke RP (1999) An overview of phrenic

nerve and diaphragm muscle development in the perinatal rat. Invited Review. *J. Appl. Physiol.* 86: 779-786.

Guthrie PB, Segal M and Kater SB (1991) Independent regulation of calcium revealed by imaging dendritic spines. *Nature.* 354: 76-80.

Harding R (1994) Development of the respoiratory system. In *Textbook of Fetal Physiology.* Edited by: Thorburn GD and Harding R. New York, Oxford. pp 140-167.

Harding R, Hooper SB and Van VK. (1993) Abolition of fetal breathing movements by spinal cord transection leads to reductions in fetal lung volume, lung growth and IGF-II gene expression. *Pediatric Res.* 34: 148-153

Harris AJ and McCaig CD (1984) Motoneuron death and motor unit size during embryonic development of the rat. *J. Neurosci.* 4:13-24

Honig MG. and Hume RI (1989) DiI and DiO: versatile fluorescent dyes for neuronal labelling and pathway tracing. *TINS.* 12:333-341.

Jansen, A.H. and V. Chernick (1991) Fetal breathing and development of control of breathing. *J. Appl. Physiol.* 70:1431-1446.

Johnson BD, Wilson LE, Zhan WZ, Watchko JF, Daood MJ and Sieck GC (1994) Contractile properties of the developing diaphragm correlate with myosin heavy chain phenotype. *J. Appl. Phyiol.* 77: 481-487.

Kandler K and Katz LC (1995) Neuronal coupling and uncoupling in the developing nervous system. *Curr. Opin. Neurobiol.* 5:98-105.

Katz LC and Shatz CJ (1996) Synaptic activity and the construction of cortical circuits. *Science.* 274: 1133-1138.

Kossel AH, Williams CV, Schweizer M and Kater SB (1997) Afferent innervation influences the development of dendritic branches and spines via both activity-dependent and non-activity-dependent mechanisms. *J. Neurosci.* 17: 6314-6324.

Lakke EAJF (1997) The projections to the spinal cord of the rat during development. A timetable of descent. In: *Advances in Anatomy, embryology and cell biology.* Vol. 135. Springer-Verlag. pp1-143.

Laskowski MB and High JA (1989) Expression of nerve-muscle topography during development. *J. Neurosci.* 9: 175-182.

Laskowski MB and Owens JL (1994) Embryonic expression of motoneuron topography in the rat diaphragm muscle. *Dev. Biol.* 166: 502-508.

Lindsay AD, Greer JJ and Feldman JL (1991) Phrenic motoneuron morphology in the neonatal rat. *J. Comp. Neurol.* 308:169-179.

Lipski J (1984) Is there electrical coupling between phrenic motoneurons in cats? *Neurosci. Lett.* 46: 229-234.

Lipski J, Zhang X, Kruszewska B and Kanjhan R (1994) Morphological study of long axonal projections of ventral medullary inspiratory neurons in the rat. *Brain Res.* 640:171-184.

Martin-Caraballo M and Greer JJ (1999) Electrophysiological properties of rat phrenic motoneurons during perinatal development. *J. Neurophysiol.* 81: 1365-1378.

Martin-Caraballo M and Greer JJ (2000, in press A) Development of potassium conductances in perinatal rat phrenic motoneurons. *J. Neurophysiol.*

Martin-Caraballo M, Campagnaro PA, Gao Y and Greer JJ (2000, in press B) Contractile and fatigue properties of the rat diaphragm musculature during the perinatal period. *J. Appl. Physiol*

Martin-Caraballo M and Greer JJ (in preparation) Calcium conductances and their functional role in the maturation of rat phrenic motoneurons.

Mazza E, Nunez-Abades PA, Spielmann JM and Cameron WE (1992) Anatomical and electrotonic coupling in developing genioglossal motoneurons of the rat. *Brain. Res.* 598:127-137.

McAllister AK, Katz LC and Lo DC (1999) Neurotrophins and synaptic plasticity. *Annu. Rev. Neurosci.* 22: 295-318.

Müller W and Connor JA (1991) Dendritic spines as individual neuronal compartments for synaptic Ca^{2+} responses. *Nature.* 354: 73-76.

Navarrete R and Vrbová G (1993) Activity-dependent interactions between motoneurones and muscles: their role in the development of the motor unit. *Prog. Neurobiol.* 41: 93-124.

Noakes, PG, Bennett MR and Davey DF (1983) Growth of segmental nerves to the developing rat diaphragm: absence of pioneer axons. *J. Comp. Neurol. 218*:365-377.

O'Hanlon GM and Lowrie MB (1994) Both afferent and efferent connections influence postnatal growth of motoneuron dendrites in the rat. *Dev. Neurosci.* 16: 100-107

Ono, K. and K. Camera (1989) Migration of immature neurons along tangentially oriented fibres in the subpial part of the fetal mouse medulla oblongata. *Exp. Brain Res.* 78:290-300.

Scheibel ME and Scheibel AB (1970) Developmental relationship between spinal

motoneuron dendrite bundles and patterned activity in the hindlimb of cats. *Exp. Neurol.* 29: 328-335.

Song A, Tracey DJ and Ashwell KWS (1999) Development of the rat phrenic nerve and terminal distribution of phrenic afferents in the cervical cord. *Anat. Embryol.* 200: 625-644.

Theonen H (1995) Neurotrophins and neuronal plasticity. *Science.* 270: 593-598.

Torikai H, Hayashi F, Tanaka K, Chiba T, Fukada Y and Moriya H (1996) Recruitment order and dendritic morphology of rat phrenic motoneurons. *J. Comp. Neurol.* 366: 231-243.

Ulfhake B, Cullheim S and Franson P (1988) Postnatal development of cat hind limb motoneurons. I: Changes in length, branching structure, and spatial distribution of dendrites of at triceps surae motoneurons. *J. Comp. Neurol.* 278: 69-87.

Vaughn JE (1989) Review: fine structure of synaptogenesis in the vertebrate central nervous system. *Synapse.* 3: 255-285.

Walton KD and Navarrete R (1991) Postnatal changes in motoneurone electrotonic coupling studied in the *in vitro* rat lumbar spinal cord. *J. Physiol. (London)* 433:283-305.

Westerga J and Gramsbergen A (1990) The development of locomotion in the rat. *Dev. Brain Res.* 57: 163-174.

Westerga J and Gramsbergen A (1992) Structural changes of the soleus and the tibialis anterior motoneuron pool during development in the rat. *J. Comp. Neurol.* 319: 406-416.

Chapter 4

EMBRYOGENESIS OF THE PHRENIC NERVE AND DIAPHRAGM IN THE FETAL RAT

Adapted from the original publication:
Douglas W. Allan and John J. Greer
J. Comp. Neurol. 382(4): 459-468 (1997)

INTRODUCTION

This study provides a detailed description of phrenic nerve and diaphragm development in fetal rats from ages E11.5, when motor axons first exit the cervical spinal cord, through to E17 when the diaphragmatic neuromusculature approximates its mature extent. We addressed four contentious issues regarding the embryogenesis of the phrenic nerve and diaphragm. 1) What is the migratory path and primordial target of growing phrenic axons? 2) What is the embryological origin for the diaphragm? 3) What is the relationship between the phrenic nerve and primordial diaphragm during descent from the cervical to the thoracic spinal cord levels? 4) How does the intramuscular branching of the phrenic nerve correlate with the onset of diaphragmatic muscle formation? In order to observe the extent of phrenic axon growth at each age, we immunolabelled for growth associated protein (GAP-43), a protein expressed by growing axons and the growth cone (Reynolds et al., 1991; Strittmatter et al., 19995). Moreover, double immunolabelling for GAP-43 in the nerve and for desmin (an intermediate filament protein specific to muscle, see Capetanaki et al., 1997) in the muscle provided a means of determining the relationship between intramuscular nerve branching and diaphragmatic myotube formation. In chapter 5, we show that immunolabelling for PSA-NCAM actually provides a clearer outline of axon-muscle development. Immunolabelling for neural cell adhesion molecule (NCAM) and the low affinity nerve growth factor receptor (p75) was utilised to demonstrate the presence of a well-defined track of cells which precede, and may direct, migrating phrenic axons towards the primordial diaphragm, the pleuroperitoneal fold. Further, p75 immunolabelling aided in defining the origin, identity and ontogeny of the mesodermal substrate for the diaphragmatic neuromusculature.

The classical view of phrenic nerve-diaphragm embryology states that phrenic axons migrate from the cervical spinal cord to innervate the dorsal portion of the septum transversum, located at approximately the same rostrocaudal level as the emerging phrenic axons. Subsequently, the septum transversum and the attached phrenic nerve descend to the lower level of the thorax as the heart and lung enlarge within the thoracic cavity (Lewis, 1910). However, these ideas were challenged by Noakes et al. (1983) who proposed that the septum transversum descends to the lower thoracic cavity prior to innervation by phrenic

axons (E14.5). Moreover, they proposed that phrenic axons migrate caudally *en masse*, adjacent to the cardinal vein, without any clear indication of leading axons which could act as pioneers towards the target.

According to standard embryological texts, the septum transversum develops as an endodermal ridge adjacent to the cardiac splanchnic mesoderm at the anterior end of the embryo, prior to gut formation. Cephalocaudal flexure of the embryo swings the anterior heart tissue and its underlying endoderm (including the septum transversum) ventrally during formation of the foregut. The liver subsequently develops within the septum transversum with contribution from the foregut endoderm. At approximately the same time, the embryonic coelem is formed. As the liver and foregut develops, the coelomic channels running dorsal to the septum transversum and liver on either side of the foregut are referred to as the pleuroperitoneal canals. These form a channel linking the future abdominal and pleural cavities. This channel is understood to be closed by the expansion of the somatic mesodermal pleuroperitoneal folds.

The septum transversum has classically been viewed as the initial target for growing phrenic axons (see above and Skandalakis et al., 1994). This hypothesis persists into the modern literature. Further, the contribution of the septum transversum to the formation of the diaphragm seems to depend more upon the bias of the author than to any specific evidence. However, these hypotheses are ultimately based upon gross embryological dissections in the first half of the century with very little consistent scientific data to support them (see general introduction). From our examination of the projection of phrenic axons and the development of the diaphragm, we propose that their primordial target is the pleuroperitoneal fold, which protrudes from the lateral body wall, rather than the septum transversum. The septum transversum appears to contribute to the central tendon of the diaphragm. Further, our data indicate that pioneering phrenic axons may be guided to the pleuroperitoneal fold by a track of p75-expressing cells which extend from the brachial plexus to the primordial pleuroperitoneal fold. Strikingly, this p75-expressing population apparently expands to form the pleuroperitoneal fold and, subsequently, the mesodermal substrate for the development of the neuromusculature of the diaphragm. In agreement with the classical view, we find that the primordial target for phrenic nerve outgrowth is initially

positioned rostrocaudally at the approximate level of emerging phrenic axons from the cervical spinal cord (E13), and then remain attached as the liver and primordial diaphragm descend to the level of the lower thorax.

The third issue examined, namely the nature and origin of the intramuscular branching of phrenic axons and diaphragmatic myotube formation, has also been controversial. As discussed in the general introduction, persistent reports hold that muscle is contributed from the lateral body wall, the septum transversum, the pleuroperitoneal fold and the dorsal mesentery (likely derived from lumbar somites). In this study, however, we find no evidence for any contribution of diaphragmatic neuromusculature from any sources other than the pleuroperitoneal fold. Bennett & Pettigrew (1974) initially reported that primary myotubes formed in the diaphragm in a sequential fashion which parallelled the extent of outgrowth of primary phrenic intramuscular branching. However, later reports by Harris (1981) suggested that primary myotube formation within the diaphragm occurred throughout the muscle mass with no apparent relationship between the arrival of the growing phrenic intramuscular branching and myotube formation. Our current results favour the interpretation of Bennett & Pettigrew (1974). We observed a clear correlation between intramuscular axon growth and myotube formation.

METHODS

Immunolabelling

Antibodies: Detection of GAP-43 was performed using the mouse anti-GAP-43 IgG MAb (Sigma, St. Louis, Mo) at a dilution of 1:1000. Desmin was detected using the mouse anti-desmin IgG MAb (Sigma; clone DE-U-10) at a dilution of 1:25. Total-NCAM was detected using a rabbit polyclonal IgG antisera (a generous gift from E. Bock; University of Copenhagen) which detected the three major isoforms of rat NCAM (~120, 140, 180 kDa; Andersson et al. 1993). It was used at a dilution of 1:2,000-3,000. Low affinity nerve growth factor receptor (p75) was detected using a mouse anti-p75 IgG MAb at a dilution of 1:75 (Boehringer Manheim, Laval, Quebec). Dilutions of anti-P75 were made with 0.4% Triton X-100. All secondary antibodies were diluted to 1:200. Secondary antibodies used for GAP-43, desmin and p75 receptor was biotinylated goat anti-mouse IgG (Sigma: whole molecule), for NCAM was peroxidase-conjugated goat anti-rabbit IgG (Sigma: whole molecule).

Immunohistochemistry: As in the methods section except that all steps for anti-P75 immunolabelling were done with buffers containing 0.4% Triton X-100.

Double immunohistochemistry: Tissues were incubated in a cocktail of anti-GAP-43 and anti-desmin. Both antibodies were then detected as described above as if for one antibody. The distinctive cellular populations stained by these antibodies allowed clear visualisation of both in relation to one another using the same secondary antibody and one DAB reaction to reveal both staining patterns.

RESULTS

Fig. 4.1 is included to orient the reader to the basic anatomy of the primordial diaphragm in relation to other features at approximately E13 (Fig. 4.1B) and E13.5 (Fig. 4.1A), as determined in this study. This figure is intended to emphasise a number of key features and is thus not accurate in every regard.

Fig. 4.1: Schematic diagram of early phrenic nerve-diaphragm development.
A) The phrenic nerve exits the cervical roots and follows a track of p75-expressing cells along the medial aspect of the lateral body wall to innervate the pleuroperitoneal fold. At age E13, when contact is made, the pleuroperitoneal fold is at the level of the cervical spinal cord. The septum transversum is fused with the ventral aspect of the pleuroperitoneal fold and is adherent to the dorsal aspect of the liver. The pleuroperitoneal canals can be viewed (long arrows) running dorsally of the pleuroperitoneal folds, connecting the pleural and peritoneal cavities. B) Transverse view demonstrates the separation of phrenic and brachial axons at the brachial plexus and the path of phrenic axons from the plexus to the pleuroperitoneal fold. In this figure, the relative size of the septum transversum and liver have been reduced. Original illustrations, as specified by the authors, by Rafe McNabb

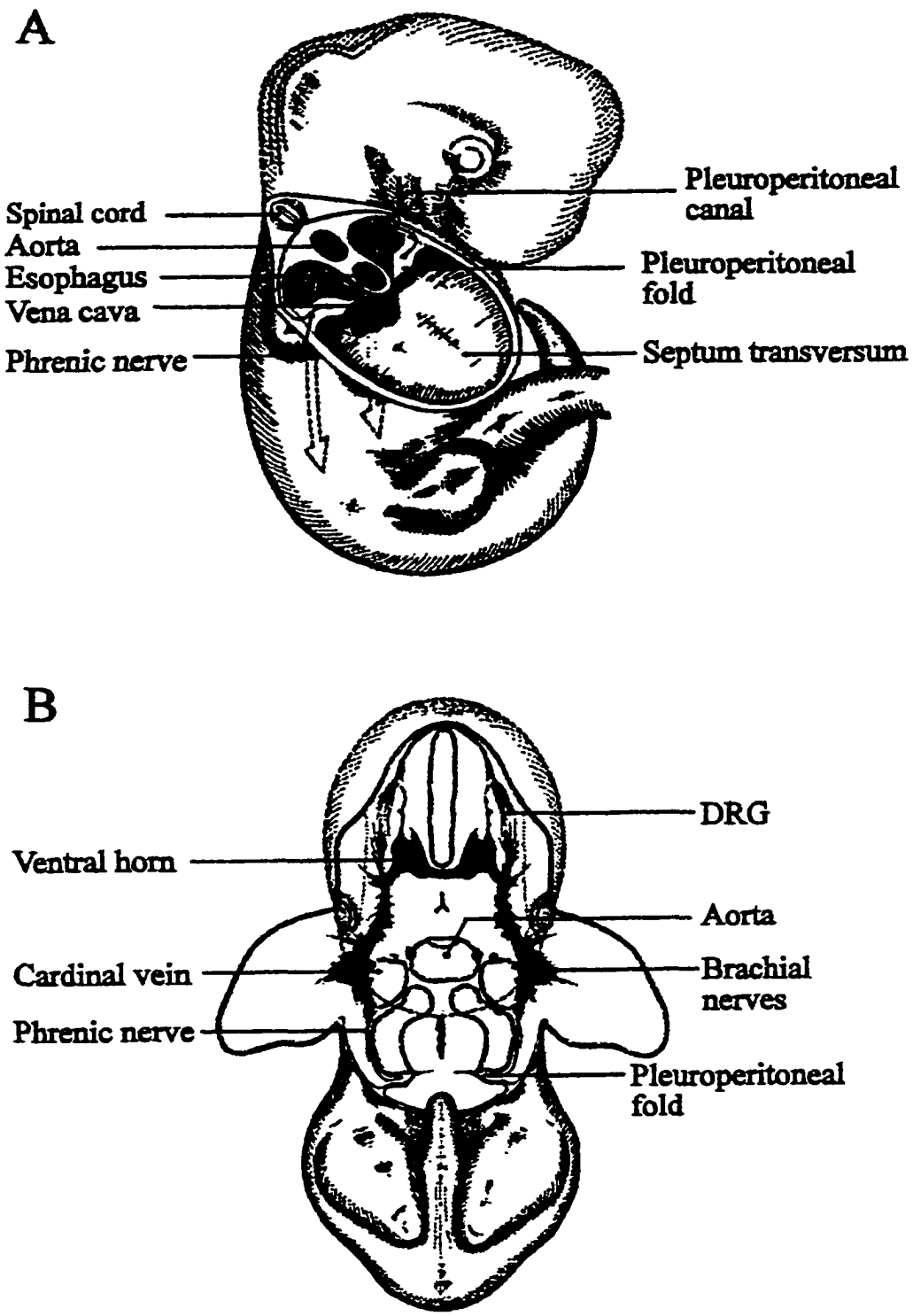

Outgrowth of phrenic axons towards the primordial diaphragm.

Cervical motor axons, likely including the phrenic axons, emerge from the cervical spinal cord at E11.5. They migrate along a dorsoventral path, slightly obliquely, to merge with other cervical axons and form the brachial plexus by E12.5 (Fig. 4.2A-C). During E12.5-E13, the plexus is situated at the level of cervical segments C6-C7 (Fig. 4.3A) at the base of the forelimb bud, dorsal and lateral to the anterior cardinal vein (Fig. 4.3B,D). Three nerve trunks emerge from the brachial plexus during E12.5-E13, the dorsal and ventral brachial trunks and the phrenic nerve (Figs. 4.3C, 4.3A-C, 4.4). Once separated, phrenic axons continued to migrate, through the medial aspect of the lateral body wall (Figs. 4.2, 4.4). The migratory pathway runs lateral to the rostral extent of the lung.

With regards to the vasculature, phrenic axons extend along the caudal aspect of the ventrally projecting common cardinal veins. Bilaterally, these veins branch from the anterior cardinal veins to fuse medially at the sinus venosus caudal to the heart. Throughout this time, the spread of growing axons is up to 50μm and 200μm in the mediolateral (Figs. 4.2, 4.4) and rostrocaudal axes (Fig. 4.3A-C), respectively. In all fetuses examined, there was a group of axons which had grown ahead of the remaining population. Such 'pioneering' axons, often travelling singly or in small groups of 2-3 axons, were observed up to 100μm ahead of the bulk of growing phrenic axons (Figs. 4.2C, 4.3D, 4.4). During E13, migrating axons reach their primordial target, a triangular shaped protrusion of the body wall referred to as the pleuroperitoneal fold (PPF) (Figs. 4.2-4.7). Phrenic axons terminate in the medial aspect of this structure bilaterally (see Fig. 4.2D).

Fig. 4.2: Migration to and initial contact of the phrenic nerve with the primordial diaphragm.
Transverse sections (50-70μm) through the whole fetal rat at E11.75 - E14 immunolabelled for GAP-43. A) E11.75 fetal section at the cervical level showing cervical motor axons exiting the spinal cord (SC) to form ventral roots (VR). B) E12.25 fetal section through the cervical level demonstrating the growth of motor axons to the brachial plexus (BP). As axons reach this region, their growing tips start to defasciculate from one another. C) E12.5 fetal section through the cervical level demonstrating the segregation of motor axons at the brachial plexus into brachial (Br) and phrenic (Ph) populations. The brachial axons have turned to grow into the forelimb bud (FL) whereas the phrenic axons continue to grow ventrally along the medial aspect of the lateral body wall. D) E14 fetal sections through the thoracic level showing the medial location of phrenic axons within the pleuroperitoneal folds (*). Abbreviations: A (aorta), ST (septum transversum), Ph (phrenic), Li (Liver), H (heart), Lu (lung), S (stomach), G (foregut), D (dorsal), L (left). Scale bars = 500 μm.

Fig. 4.3: Migration to the primordial diaphragm. Sagittal sections (70 μm) through the E13 whole rat fetus immunolabelled for GAP-43. A) Phrenic nerve (arrow) at E13 in relation to the whole fetus. The brachial plexus and segregated phrenic axons are at the lower cervical level. B,C) Close-ups of the brachial plexus and the phrenic nerve are shown in consecutive sagittal sections (the section in B is immediately lateral to that shown in C). In C it can be observed that pioneering phrenic axons have grown towards and made initial contact with the pleuroperitoneal fold (PF). D) A high magnification view of the leading process of the phrenic nerve shows the growing tip of a pioneering axon growing into the PF. At this stage, the septum transversum (ST) is a thin membrane separating the liver and heart whereas the PF is an expanded mesodermal plate at the dorsal and rostral aspect of the liver. Abbreviations: Ph (phrenic), Li (Liver), ST (septum transversum), H (heart), PF (pleuroperitoneal fold), Lu (lung), S (stomach), R (rostral), V (ventral). Scale bars = 500 μm (A) 200 μm (B,C), 10 μm (D).

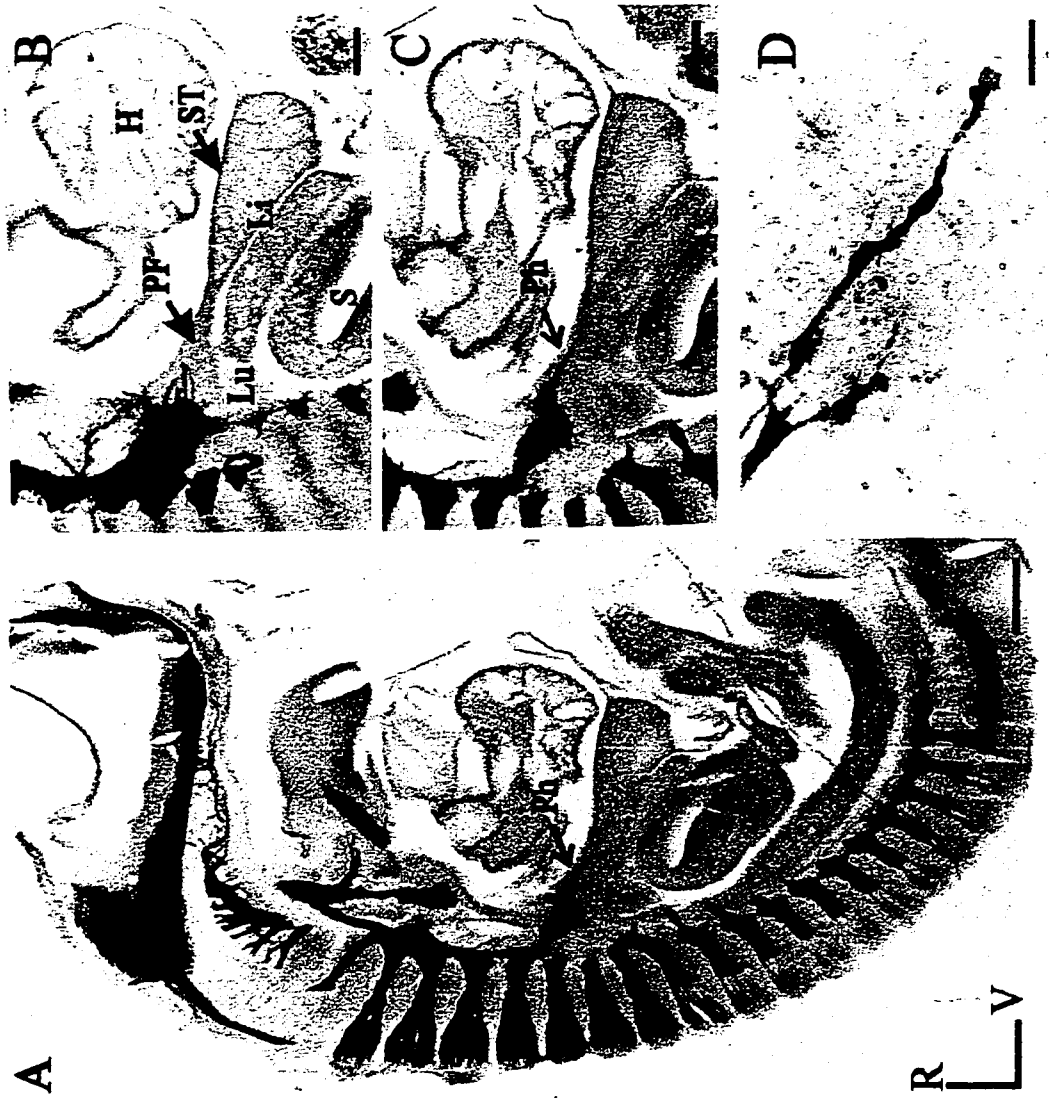

Immunologically-defined track of cells along the phrenic axon migratory pathway.

Fig. 4.4 B,C shows a well-defined track of p75- and NCAM-expressing cells through which phrenic axons traverse towards the primordial diaphragm. Axons are also visualised within these sections due to co-labelling of axons and 'track' cells by both antibody labels. This was confirmed by double labelling for GAP-43 and either p75 or NCAM (not shown). This track extends for up to approximately 50μm in its mediolateral and 200-300μm in its rostrocaudal extent (refer to scale bars in Figs. 4.3B,C and 4.4). Note that these parameters are equivalent to those for growing phrenic axons, as determined by GAP-43 immunolabelling. Indeed, in the multiple fetuses examined, no axons were observed to stray from this track. This cellular track extends from the brachial plexus, up to and throughout the fold of tissue which forms the primordial diaphragm (see below). We postulate that this track represents a selective guidance substrate for phrenic axons, although it is currently unclear as to the roles that are being played by either p75 or NCAM within the track. Thus, these immunolabels are merely utilised to demonstrate an immunologically distinct population of cells which are ideally spatiotemporally placed to perform a selective pathfinding role for phrenic axons.

We initially hypothesised that at least some of the p75-expressing cells appeared to be either migrating myoblasts or muscle precursor cells, primarily due to the intradiaphragmatic p75 labelling which would be consistent with myoblast populations (see Fig. 4.7). However, we now believe that the p75-expressing cells are more likely to be mesenchyme derived from the somatopleure (or somatic mesoderm) which forms the structural foundation for the pleuroperitoneal fold. This notion is supported by recent labelling for specific markers of migrating (met, pax-3) and differentiating (MyoD and myogenin) muscle populations (Babiuk, Allan and Greer, unpublished) which demonstrate that these populations are more restricted than the p75 labelling. Attempts to verify the mesenchymal identity of this p75-expressing population is awaiting satisfactory co-labelling for hepatocyte growth factor/scatter factor (see Ebens et al., 1996).

Fig. 4.4: A track of p75 and NCAM immunopositive cells precedes the migrating phrenic axons into the pleuroperitoneal fold. Transverse cervical level sections (50μm) from aged matched (E12.75-E13) rat fetuses immunolabelled for GAP-43 (A), p75 (B) and NCAM (C). A) GAP-43 labelling illustrates the migratory path of phrenic axons (Ph) towards the pleuroperitoneal fold (* indicates right PPF). Note pioneer axons indicated by arrow. B) p75 immunolabelling of E12.75 fetal rat. Phrenic and brachial (Br) axons express p75. A well-defined track of p75-expressing tissue approximately 50 μm in diameter is situated along the migratory path of phrenic axons from the brachial plexus to the PPF. This tissue obscures the phrenic axons within the track at the magnification shown. Double labelling confirms that phrenic axons do not stray from the track (not shown). C) Similarly, an E13 fetal rat immunolabelled for NCAM illustrates the presence of the track. Higher density staining of axons allows co-visualisation of axons and track. It also apparent from A and C that a subpopulation of phrenic axons migrate ahead of the majority remaining axons (arrow). Scale bars = 50 μm. Abbreviations: D (dorsal), L (left), CV (anterior cardinal vein), FL (forelimb bud), Lu (lung).

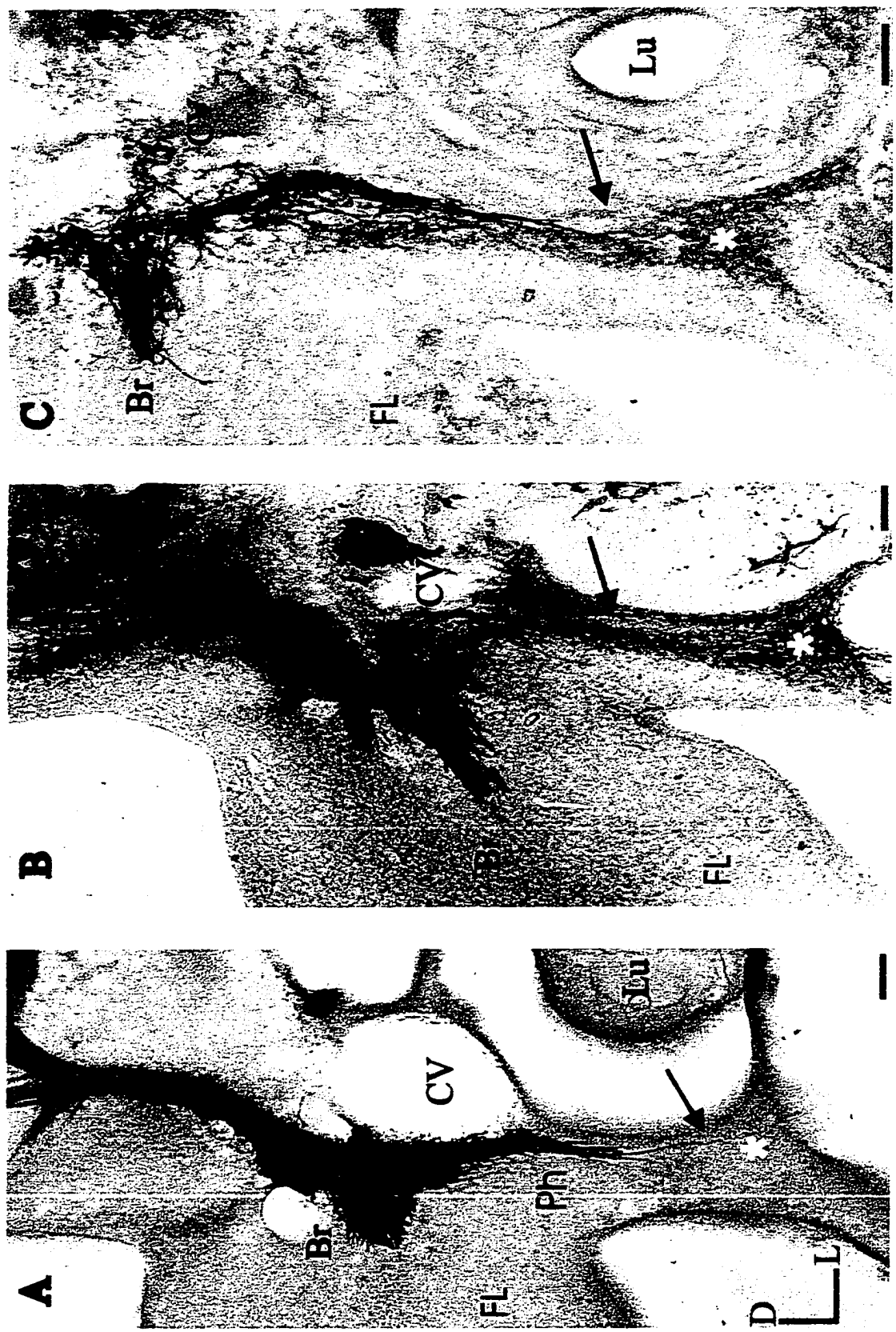

P75 immunolabelling and the identification and tracing of the primordial diaphragm.

Our finding that p75 immunolabelling defined a population of cells which is appropriately placed to perform a guidance role for phrenic axons prompted us to investigate the origin and fate of this labelling pattern. Figs. 4.4, 4.5 and 4.7 D-F show labelling patterns pertinent to phrenic axon guidance from E11.5 to E17. At E11.5, tissues of both somitic (sclerotome) and somatopleural (limb bud mesoderm) origin express p75 in a pattern which approximates presumptive axonal tracks and the pattern of HGF/SF expression published by Ebens et al. (1996). By E12.5, the p75-labelled phrenic track has formed and p75 expression has been down-regulated within the limb bud. By E13.5, the population of p75-expressing cells within the track has expanded medially and ventrally to form p75-positive bilateral triangular pleuroperitoneal folds (PPFs) (Figs. 4.5C and 4.6). These taper medially towards the eosophageal mesentery and contain the phrenic nerve endings (Figs. 4.2D and 4.5C). P75 immunolabelling of serial sections in both E12.5 and E13.5 fetuses (Fig. 4.6) emphasises that the densely p75-expressing PPF is positioned at the dorsal and rostral extent of the liver. Further, it is morphologically distinct from the underlying liver, which originates from the septum transversum. The developing liver cords give the liver a 'spongy' appearance, as opposed to the more solid PPF.

In Figs. 4.3 and 4.7, a thin membranous tissue which separates the liver from the heart corresponds to the septum transversum. At E11.5, the septum transversum expresses low levels of p75 in an intermittent pattern (Fig 4.4A). This pattern is very similar to that observed in the liver at E12.5 and E13.5 (Fig. 4.6), but is very distinct from that of the PPF. By E13.5, however, the thin membranous septum transversum residing at the rostral aspect of the liver does not express p75 (not shown in sagittal section in Fig. 4.7A). Tracing the progression of p75 labelling from E12.5 to E13.5 and on to E15.5 (Fig. 4.5) appears to preclude the septum transversum from contributing to the diaphragmatic neuromusculature. The lateral somatic mesodermal origin of the PPF and its subsequent expansion to form the primordial diaphragmatic tissue and the neuromusculature suggests that it is quite different from the septum transversum of anterior endodermal origin. It appears that the p75-positive PPF utilises the dorsal aspect of the septum transversum and liver as a platform upon which to elaborate the diaphragm. Discussion of the expansion of diaphragmatic neuromusculature

below picks up this point and stresses that it appears to derive solely from the pleuroperitoneal fold.

By E15.5, p75 labelling within the isolated diaphragm corresponds to regions of diaphragmatic neuromusculature formation and is absent from the membranous septum transversum (Figs. 4.5D, 4.8). The asterisks in Fig. 4.5 denotes the point of origin for the PPF on each hemi-diaphragm. These are the points at which the nerve enters the PPF and remains the point of neural entry throughout development (Fig. 4.8). Expansion of the PPF to form the diaphragmatic neuromusculature proceeds in three principle directions, as indicated by p75 labelling here (and direction of arrows in Fig. 4.5C,D; see also chapter 5 and 7 for specific details). From the central PPF region (asterisk in fig 4.5), expansion proceeds: 1) Ventrally to form the sternal region that reaches the sternum by E17 (Fig. 4.8B,E). 2) Dorsolaterally, across the dorsal aspect of the liver to fuse with the body wall caudal to the lung to close the pleuroperitoneal canals by E15. This expansion is more fully considered in following chapters but can be observed in sagittal section in Fig 4.7. 3) Dorsomedially, to form the crural musculature. Following p75, nerve and muscle labelling into the crural region as well as its absence in severe instances of diaphragmatic hernia indicates the crus' PPF-derived origin. This discounts previous theories that the crus develops from the eosophageal mesentery and lumbar somites.

Without experimentally tracing the fate of the p75-expressing track by such methods as dye application, we cannot conclusively demonstrate that the population of cells within the track expands to form the mesodermal substrate for the diaphragmatic neuromusculature. However, there is a compelling continuity of p75 labelling with morphological development within a putatively immunologically-defined cellular population, as demonstrated in Fig 4.5 and the many samples not shown here. We postulate that this labelling delineates the diaphragmatic tissue as it develops, and propose that this labelling can be used to discriminate the embryological development of the diaphragm. Further, tracing p75 labelling back to the somatic mesoderm not only provides evidence indicative of a non-septum transversum origin for the diaphragm, but also provides a satisfactorily mechanism whereby phrenic axons and diaphragmatic myogenic cells can be guided to the diaphragm primordium in a manner equivalent to that proposed for limb musculature and innervation.

Fig. 4.5: p75 labelling and formation of the diaphragm. 50μm transverse sections of whole rat fetuses and whole diaphragm labelled for p75 at E11.5, E12.5, E13.5 and at E15.5. A) At E11.5, as motor axons are first exiting the spinal cord (SC), p75 labelling extends imprecisely throughout presumptive axonal pathways, including the sclerotome, the brachial plexus and the forelimb bud. B) By E12.5, expression has been reduced within the forelimb bud but heavily up-regulated within the phrenic track, bilaterally. C) At E13.5, p75 expression further delineates regions of axonal growth, including the pleuroperitoneal fold (PPF) (*). Densely labelled phrenic axons can be observed at the medial extent of the PPF (compare to Fig. 4.2D) whereas general p75 expression extends throughout the PPF. It should be noted, however, that p75 labelling extends beyond axonal pathways in most cases. D) By E15.5, p75 expression within the diaphragm extends throughout the neuromusculature. (Compare with Fig. 4.8). Labelling for the aorta (A), the developing eosophageal mesentary (E), the approximate positioning of the septum transversum (ST) and the vena cava (VC) emphasises that the progression of p75 labelling appears to delineate the developing diaphragmatic tissue from E11.5 up to E15.5. The asterisk (*) in B-D indicates the same region in each figure. Comparison of B and C demonstrates that a tissue of somatic mesodermal origin has expanded to form the PPF between E13 and E13.5, bilaterally. The arrows in C indicate the progressive expansion of this tissue as it migrates ventrally between the lateral body wall and the septum transversum to form the substrate for the sternal diaphragmatic neuromusculature. Further expansion of the tissue dorso-caudally separates the abdominal and pleural cavities and forms the dorsolateral and crural musculature of the diaphragm. Abbreviations: D (dorsal), L (left). Scale bars = 500μm.

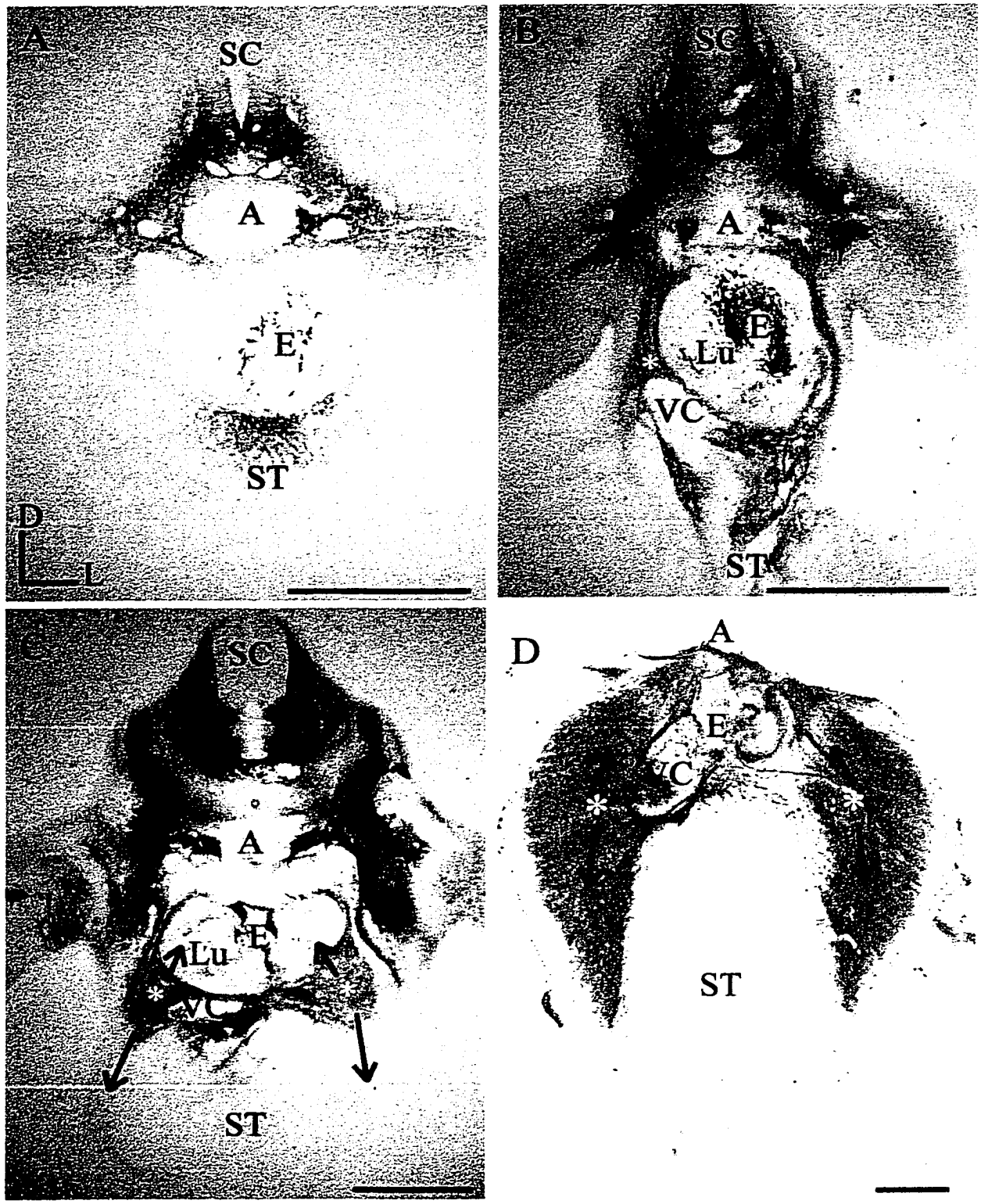

Fig. 4.6: Comparison of the primordial diaphragm and the liver. Comparison of p75 labelling from the same fetus at different rostrocaudal levels. 50μm transverse sections of whole rat fetuses labelled for p75 at E12.5 (A,B) and E13.5 (C,D). A,B) A is approximately 100μm rostral to B and shows that the densely-p75 labelled PPF is quite distinct from the more loosely defined p75 labelled septum transversum-derived liver tissue underneath. Reference to fig 4.5A shows that septum transversum labelling for p75 is likewise less dense than the track or PPF. At this age, it can be observed that the developing PPF is consistent with, and extends from, the lateral body wall and thus would appear to be of somatic mesodermal origin. C,D) C is approximately 200μm rostral to D and shows that the expanded PPF is rostral to the liver, but now has begun to expand over the top of the liver, notable on the right side. Further expansion, as shown in Fig. 4.5D proceeds on top of the liver, without the two tissues ever being fused. Abbreviations: D (dorsal), L (left). Scale bars = 500μm.

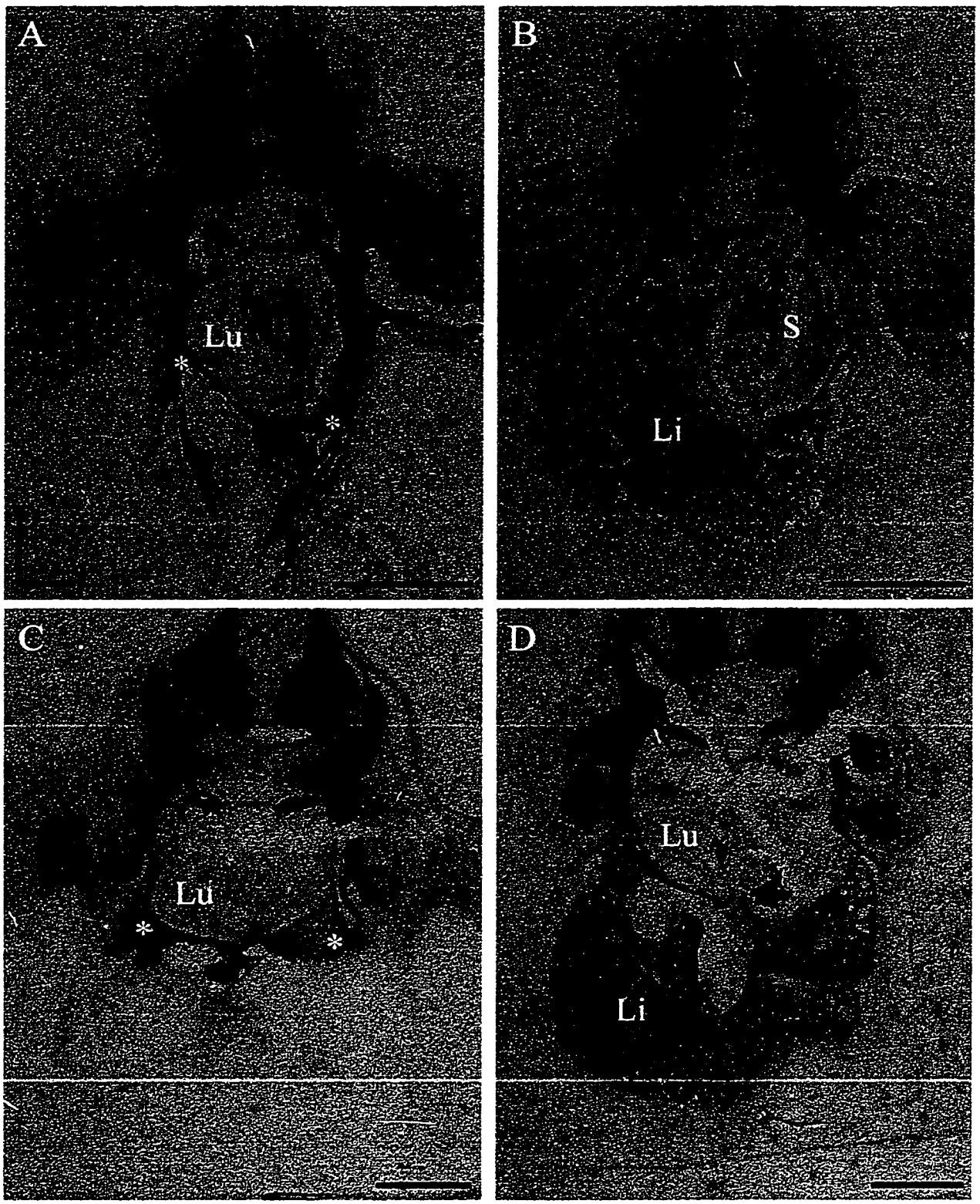

The pleuroperitoneal fold descends caudally with the liver, forms the primordial diaphragm and the pleuropericardial membrane.

By E13.5, phrenic axons had converged at a position medially within the pleuroperitoneal fold (see Figs. 4.2D and 4.5C). Note that between E13 and E13.5, the PPF had maintained its rostrocaudal level, ie. adjacent to the cervical spinal cord, from the time of initial contact by phrenic axons (Figs. 4.3A, 4.7A,B). Fig. 4.7 shows the descent of the liver, with the primordial diaphragm 'piggy-backing' on the dorsal and rostral extent of the liver during late E13 into E14.5. Prodigious growth of the heart and embryonic straightening likely account for the expansion of the thorax and drop of the liver to the lower thoracic level. Comparison of Fig 4.3A-C (E13) with Fig. 4.7E,F (E14.5) shows that as the liver and PPFs descend, the trailing phrenic nerve curves over the ventral extent of the lung. Within the PPF, the phrenic nerve can be observed to elaborate into distinct branches by E14.5 (compare close-up images in fig 4.7). Chapter 5 examines this branching pattern in detail. Thus, between initial contact at E13, consolidation of innervation by E13.5, and the elaboration of branching by E14.5, a one day waiting period is evident. This waiting period encompasses a period of great axonal elongation for the phrenic nerve as the thorax expands. Thus, branching may be limited until axonal resources can be diverted from medial, to distal tip, extension.

As the liver and PPFs descend, a number of important developmental features unfold. Most notably; 1) the elaboration of the pleuropericardial membrane (PCM), 2) the separation of the left common cardinal vein from the left PPF, and 3) the elaboration of the right inferior vena cava from the right common cardinal vein. Bilaterally, on their way to the PPFs, phrenic axons had passed through the lateral body wall along the lateral and caudal extent of the common cardinal veins. These veins are large bilateral branches from the anterior cardinal veins which extend ventrally and medially to fuse with the vitelline veins at the sinus venosus caudal to the heart. At E13.5, both left and right common cardinal veins are in contact with the rostral extent of the PPFs. Asymmetric differentiation of these veins results in a different fate for the elongation of the phrenic nerve within the thorax as the PPFs drop. On the right, the superior vena cava forms directly from the right common cardinal vein anterior to the heart. Posterior to the heart, the right common cardinal vein fuses with hepatic

venous vasculature, laid down initially by the vitelline vein. This results in the formation and elaboration of the inferior vena cava which penetrates the liver medially of the developing right hemi-diaphragm (see Fig. 4.5C,D). Thus, continuity of the common cardinal vein (vena cava) from the upper thorax to the diaphragm provides a platform along which the medial extent of the phrenic nerve can elongate towards the descending PPF, caudally. On the left, the common cardinal vein does not elaborate to connect with hepatic vasculature. Thus, connection to the PPF is lost as the latter descends within the thorax. The phrenic nerve maintains its contact with this vein anterior to the heart, but then posterior to the heart, it extends through the pleuropericardial membrane.

As the thorax expands, the PPFs essentially draw down a curtain of membranous tissue (the PCM) in their wake. As can be observed in Fig. 4.5C, the PPFs at E13.5 are fused laterally with the body wall, and medially with one another at the junction of the eosophageal mesentery. Thus, as the PPFs descend caudally, they can pull down a PCM which likewise spans the mediolateral breadth of the thorax, fused laterally at the body wall and running across the thorax along the ventral extent of the PPFs. Thus the PCM appears to have its origin with the PPF, as shall be elaborated upon below. This curtain is drawn dorsal to the heart, thereby separating it from the lung. The medial portion of the phrenic nerve is contained within this expanding PCM, and thus the position of the PCM within the thorax can be ascertained from the extent of the phrenic nerve in Fig 4.7.

Fig. 4.7: Descent and initial innervation of the developing diaphragm.
GAP-43 labelling of sagittal sections (70 μm) of whole fetal rats illustrating the phrenic nerve (arrow) at E13.5 (A,B); E14 (C,D) and E14.5 (E,F). At E13.5, the phrenic nerve had reached the pleuroperitoneal fold (PF) which is situated dorsal to the liver. 3B is a close-up from 3A showing the structures surrounding the point of initial contact between the phrenic nerve and the PF. By E14, the primordial diaphragm and the phrenic nerve had begun to descend caudally and the first sign of phrenic nerve defasciculation within the PF was observed (D is taken from a different animal at a similar stage of development as C). The descent of the phrenic nerve and PF had continued to E14.5 and intramuscular branching of the phrenic nerve within the primordial diaphragm had commenced. Abbreviations: Ph (phrenic), Li (Liver), ST (septum transversum), H (heart), Lu (lung), S (stomach), R (rostral), V (ventral). Scale bars = 500 μm (A,C,E), 200 μm (B,D,F).

Intradiaphragmatic branching and myotube formation.

Fig. 4.8 shows GAP-43 and desmin double immunolabelling in comparison to p75 immunolabelling within the developing diaphragm at E15.5 and E17. A more detailed examination of initial phrenic branching and muscle formation has been presented in chapter 5 in relation to PSA-NCAM expression (excluded here to avoid repetition). We postulated that myoblasts would either fuse in a sequential fashion which parallelled the extent of outgrowth of primary phrenic intramuscular branching (Bennett & Pettigrew, 1974), or synchronously throughout the diaphragmatic muscle mass to become subsequently innervated (Harris, 1981). GAP-43 and desmin labelling of wholemount diaphragms illustrates the intimate relationship between axonal growth and the fusion of myotubes, seen as striations running transversely across the axonal branches (fig 4.8A-C). Further, myotubes elongate as a function of the length of time of axonal contact. This relationship was established from the very onset of axonal branching and myotube formation at E14.5, and persisted throughout fetal development. See chapter 5 for further data regarding this intimate relationship in light of PSA-NCAM immunolabelling from E14.5 up to E18.

Immunolabelling for the p75 receptor differed from that for desmin in that p75 labelling revealed stellate shaped cells in the vicinity of the forming musculature, more consistent with their being mononucleated myoblasts and/or mesodermal cells. Throughout muscle development, these were limited to the region throughout and surrounding fused myotubes (compare Figs. 4.8F and 4.8E). Confirmation of the proximity of p75 labelling with the advancing axons can be observed in Fig. 4.8F, where p75-labelled axons can be discerned through mesodermal/(myoblast?) labelling. This trend continues up to E17 when the full neuromusculature of the diaphragm has been approximated (Figs. 4.8B,E). Such a relationship can also be observed for NCAM (myoblasts and myotubes) vs PSA-NCAM (myotubes only) labelling seen in Fig. 5.7. Such p75 labelling may be consistent with *in situ* hybridisation studies which have demonstrated that p75 receptor transcripts are expressed in developing and fusing myoblasts but not in myotubes (Wheeler & Bothwell, 1992). However, the apparent mesodermal identity of p75 labelled cells, as described above, may suggest that the diaphragmatic nerve and muscle migrrates with the deposition of the underlying mesoderm. This does not preclude the possibility that diaphragmatic myoblasts

express p75.

In following the advancement of p75, GAP-43 and desmin immunolabelling, we find that all labels appear to migrate over time around a central membranous tissue from E15.5 to E17 (Fig. 4.8). At E15.5, this unlabelled tissue is fused to the body wall ventrally, and to the neuromusculature laterally. By E17, the unlabelled tissue has become fully separated from the body wall and enclosed by the neuromusculature. This tissue does not become innervated or muscularised and does not express p75. In chapter 5, labelling for nerve and muscle shows that this tissue extends across the entire liver surface and fuses laterally with the body wall and dorsally with the pleuroperitoneal fold containing the nerve and muscle at E14.5 (Fig 5.6). This tissue appears to be the septum transversum. As the nerve and muscle advance up to E18, they appear to separate this membrane from the body wall in a progressively ventral course (Fig. 4.8). Two observations not shown but that are pertinent are: 1) During dissection of these tissues, the diaphragmatic neuromusculature (as delineated here by p75, GAP-43 and desmin expression) is never actually attached to the liver throughout development. On the other hand, the unlabelled tissue medial to (all ages) and ventral to (all ages up to E17) the advancing neuromusculature is strongly attached to the liver, both rostrally and via a tendinous extension into the liver parenchyma, principally observed at the sternum. Given that the liver develops from the caudal aspect of the septum transversum and that the central tendon of the diaphragm retains a thin tendinous connection which extends into the liver parenchyma, we propose that this tissue is the septum transversum. 2) During dissection, the advance of the pleuropericardial membrane precisely matches the progressive ventral advance of the neuromusculature. It is fused to the lateral wall ventral to the advancing musculature, and to the medial extent of the musculature as it advances ventrally. Thus, at E14.5, it is attached to the body wall adjacent to the pleuroperitoneal fold, whereas by E17, it is only attached to the body wall at the sternum. Given the common origin for the pleuroperitoneal and pleuropericardial tissues, discussed above, this provides further evidence for the progressive advance of the PPF around the septum transversum. Otherwise, the lower extent of the pleuropericardial membrane fused to the diaphragm would have to migrate across the face of the septum transversum towards the diaphragm. Intuitively, this would be unlikely.

These observations, taken together, provide compelling evidence that the neuromusculature of the diaphragm forms from the progressive advance of the pleuroperitoneal fold in between the septum transversum and the body wall to enclose the septum transversum completely by E17. Expansion of the body wall during fetal growth likely accommodates the advancing tissue. Thus, the phrenic track tissue appears to differentiate into the mesodermal substrate for the diaphragmatic neuromusculature. Taken together, we propose that the diaphragmatic neuromusculature derives solely from the PPF and that it is distinguishable from the septum transversum. Thus, at no time did we see any evidence supporting the standard explanation for diaphragmatic formation that implicates multiple embryological origins for mesodermal, neuronal and myogenic components of the diaphragmatic musculature (see Skandalakis et al., 1994).

Fig. 4.8: Correlation between the extent of phrenic nerve intramuscular branching and myotube formation. Whole-mounts of diaphragms isolated from fetal rats aged E15.5 (A,D,C,F) and E17 (B,E). A,B,C) Double immunolabelling for GAP-43 and desmin to illustrate the developing phrenic nerve and diaphragmatic myotubes, respectively. E is a close up of the advancing nerve and muscle development on the right side of A. Note that primary myotube formation (arrowhead in C), as indicated by striations running perpendicular to phrenic axons, was restricted to regions within the vicinity of phrenic nerve branches (arrow). By E15.5, the three characteristic primary branches of the phrenic nerve are observed, the sternal (St), dorsolateral (Do) and crural (Cr) branches. D,E,F) Immunolabelling for p75 in diaphragms age-matched to those in A,B,C illustrating that the developing neuromusculature is limited to regions expressing p75. F) The visualisation of axons in this close up of D (arrow) allows further confirmation for the proximity of the advancing p75 labelling with that for GAP-43 and desmin. Arrowhead in F shows extent of labelling ahead of axons, equivalent to that for desmin in C. Abbreviations: E (eosophagus), VC (vena cava), ST (septum transversum), S (sternum), V (ventral), R (right). Scale bars: A, B, D, E = 500μm; E, F = 250μm.

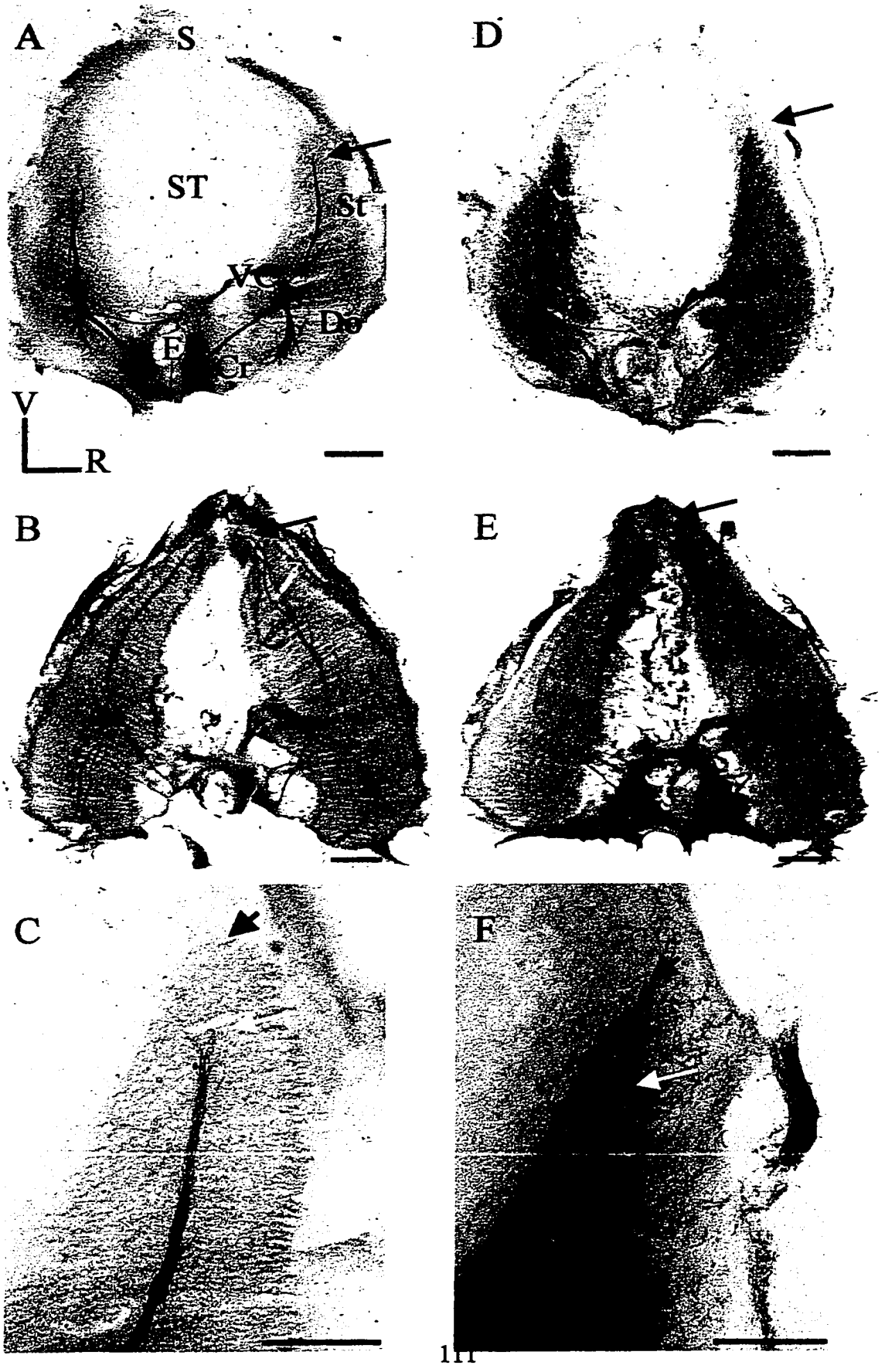

DISCUSSION

The following points are demonstrated in this study. 1) A subpopulation of pioneering phrenic axons migrate towards the primordial diaphragm, ahead of the majority of phrenic axons. 2) Phrenic axon migration towards the primordial diaphragm is restricted to a well-defined track of cells that express both p75 and NCAM that extend within the medial extent of the lateral body wall. 3) The diaphragmatic musculature originates from tissues located within the pleuroperitoneal fold. 4) The primordial diaphragm is located at the level of the cervical spinal cord at the time of initial contact by the phrenic nerve. 5) As the heart and lungs enlarge within the thoracic cavity, the primordial diaphragm and phrenic nerve descend together, caudally to a position within the lower thoracic cavity. 6) Myotube formation within the diaphragm proceeds in a sequential fashion which parallels the growth of primary phrenic intramuscular branches.

Pioneering axons

Our data clearly demonstrate the presence of a subpopulation of pioneering axons which preceded the bulk of growing phrenic axons towards the diaphragm pre-muscle mass. A similar situation, where a small number of pioneer axons migrate ahead of the remainder of the axon population, has been observed in a number of developing invertebrate and vertebrate systems. They are postulated to guide the axons following behind (Stainier & Gilbert, 1990; Eisen, 1991; Kim et al., 1991; Grenningloh & Goodman, 1992; Nagashima, 1994). Our observation contradicts a previous study of phrenic nerve outgrowth which suggested that developing axons grew *en masse* without any indication of pioneer axons advancing independently (Noakes et al., 1983). However, that previous study relied on difficult serial reconstructions of electron microscopic sections of nerve trunks to detect phrenic outgrowth, whereas we had the advantage of visualising the nerve directly via immunolabelling for GAP-43 in transverse and sagittal sections. This methodology is particularly well-suited for detecting the precise distribution of growing axons and monitoring the extent of growth cone progression in particular.

Migratory track to the primordial diaphragm: identification of p75 receptor-expressing cells

At the rat brachial plexus, cervical axons segregate into dorsal and ventral brachial branches and the phrenic nerve. When phrenic axons leave the brachial plexus, they migrate along a path, or track, of NCAM- and p75-immunopositive tissue located along the medial aspect of the lateral body wall. Phrenic axons were not seen to stray from this track in any sample examined. This track led directly into the pleuroperitoneal fold (PPF), which then appeared to differentiate into the primordial diaphragm. This study does not address the potential functional roles for NCAM and p75 receptor molecules in phrenic axon guidance, but simply uses the immunolabelling as a means of identifying the relative positions of nerve and migratory track. With regards to the identity of cells within the track, it has been previously demonstrated that both immature Schwann cells and muscle precursor cells express NCAM and p75 receptors (Wheeler & Bothwell, 1992). Both of these cellular populations have been postulated to guide motor axons, but both have been discounted as a primary guidance substrate (Phelan and Hollyday, 1990; Grim et al., 1992). In this study, the spatiotemporal pattern of p75 receptor expression is more consistent with the largest majority of cells being of somatic mesodermal identity. This does not discount the possibility that at least a sub-population of these cells are composed of muscle precursors and immature Schwann cells. Recent data shows that myoD labelling (which labels differentiating myoblasts) in the PPF is far more restricted than that of the p75 labelling (Babiuk and Greer, unpublished). Further, met-positive migrating muscle precursor cells are more restrictively distributed than the p75 labelling (Allan and Greer, 1997). Also, attempts to label neural crest cells with antibodies to the HNK-1 epitope labelled a population of migratory cells which were likewise more restricted (Allan et al, 1997). Ongoing work is aimed at identifying the p75-expressing cells. This is being performed with *HGF/SF* and *met* null mutant mice, which do not have a migrating population of muscle precursor cells (see Bladt et al.,1995), and *splotch* mutant mice, which have retarded neural crest and myogenic cell migration (see Serbedzija and McMahon, 1997; Kothary et al., 1993; Bober et al., 1994). The somatopleure-derived mesenchyme shall be implicated as the p75-expressing track-forming population if p75 labelling in such mutant mice reflects that described here.

Discriminating which cellular population(s) contribute to the phrenic track and which

may be required for phrenic axonal guidance would be of great interest, particularly due to its putative role in selective motor axon guidance. The somatopleure-derived mesenchyme is proposed to be the principal guidance substrate for motor axons in the chick hindlimb (Lance-Jones and Dias, 1991). Ebens et al. (1996) found evidence that hepatocyte growth factor/scatter factor (HGF/SF) expressed by somatopleural mesenchyme may form a permissive and trophic substrate for met-expressing motor axons (reviewed in Maina and Klein, 1999). However, general HGF/SF expression along the majority of motor pathways, including brachial and phrenic, would appear to preclude this particular molecular mechanism in generating selective pathfinding. As yet, no selective guidance mechanism at such a plexus has been uncovered. The fact that the phrenic nerve segregates as a single population at the plexus makes it an attractively simple model to examine factors postulated to promote selective guidance. On the other hand, individual limb muscle nerves form by sequential subtractive segregation of common nerve trunks, complicating interpretation of selective guidance of individual populations.

The nature of the guidance mechanism, whether it be specifically adhesive, chemotropic, trophic or facilitatory is unknown. The intriguing pattern of p75 immunolabelling in relation to phrenic axon outgrowth suggests that the primary guidance substrate for phrenic axons may be the somatopleure-derived mesenchyme. This would be consistent with previous reports that limb bud mesenchyme provides guidance for limb motor axons. If this is the case, then this would, at least theoretically, position a known guidance substrate at a spatiotemporally significant location to satisfy the guidance requirements of phrenic axons. Further, it would imply that long range signalling from the septum transversum, as standard theories would suggest, may not be the principal mechanism for phrenic guidance. The projection of the dorsal ramus from the ventral root is prevented by surgical deletion of the dermomyotome, implicating chemotropic signalling in the guidance of this motor axon population (Tosney, 1987). As yet, neither long range signalling nor contact-mediated signalling for phrenic axons has been proven or disproven. It is tempting to speculate that the immunologically-defined distinction of this pathway from alternative pathways exiting the brachial plexus may reflect molecular differences which promote population-specific guidance. At the very least, it implies that this population is distinct from

those implicated in axonal guidance within the limb bud. As yet, there is no particular reason to propose that either NCAM or p75 form the selective guidance substrate themselves. Any proposal for their function would be purely speculative at this point.

The pleuroperitoneal fold is the primordial target for phrenic axons

During E13, the phrenic nerve reaches a triangular shaped structure which spans, unilaterally, the lateral body wall and the eosophageal mesentery. The phrenic nerve migrates directly to the medial region of this tissue. This diaphragmatic pre-muscle mass has been referred to in the past as the post-hepatic mesenchymal plate (Iritani, 1984) and the dorsal extent of the septum transversum (Wells, 1954). In this study, p75 immunolabelling of this tissue immunologically discriminates it from surrounding tissues. Further, tracing the developmental history of this tissue with the aid of immunological discrimination shows that, 1) it apparently derives from a lateral mesodermal origin, 2) it coalesces as a fold of tissue on the dorsal and rostral extent of the liver, 3) it expands to close the pleuroperitoneal canals. Thus, by standard embryological criteria, this tissue corresponds to the pleuroperitoneal fold.

The growing phrenic nerve reached the PPF approximately one and a half days before any indication of intramuscular branching. During initial contact, the primordial diaphragm was located at the same level as the phrenic motor axons leaving the brachial plexus. The phrenic nerve and diaphragm pre-muscle mass then descended together to the lower thorax. These observations are, in part, consistent with aspects of the classical view of phrenic nerve-diaphragm development (Lewis, 1910), but are in direct contrast to later studies by Noakes et al (1983). This report claimed that the phrenic nerve migrates caudally through the thoracic cavity in close apposition to the cardinal vein (which differentiates into the inferior vena cava) to reach the descending primordial diaphragm by E14. As shown in this study, the phrenic nerve actually passes by the anterior cardinal vein and then migrates via the medial body wall to the PPF. Bilaterally, the phrenic axons migrate adjacent to the lateral and caudal extent of the common cardinal veins. Once axons contact the PPF by E13.5, they descend caudally within the thorax, 'piggy-backing' on the liver. On the right, the medial extent of the phrenic nerve maintains its contact with the right common cardinal vein as it differentiates into the vena cava. Thus, as the PPF descends, the medial extent of phrenic

nerve elongates along the vena cava into the developing, and subsequently adult, diaphragm. On the left side, the left common cardinal vein does not extend through the diaphragm and thus, as the PPF descends, contact between the two is lost. Thus, as the PPF descends, the medial extent of the left phrenic nerve elongates within the pleuropericardial membrane towards the descending PPF. This membrane is drawn down in the wake of the descending PPFs.

Growing phrenic motor axons first began to branch within the PPF at E14.5, which is in agreement with previous studies (Bennett & Pettigrew, 1974; Noakes et al., 1983). It is not clear whether the waiting period between initial contact with the diaphragm pre-muscle mass at E13 and branching at E14.5 is a function of limitations with the nerve and/or target which prevent initial synapse and myotube formation. One simple explanation would be that the considerable axonal elongation that occurs during the period of descent may delay growth at the axonal tips until sufficient resources can be directed towards branching. Interestingly, previous electrophysiological studies have demonstrated that phrenic motoneurons are electrically excitable and their axons are capable of transmitting action potentials by E14 (Greer et al., 1992). Thus, the potential for the induction and localisation of acetylcholine receptor expression in the diaphragm by presynaptic electrical activity in the phrenic nerve exists from the onset of branching and muscle formation (for review see Hall & Sanes, 1993). It would also appear that from the very onset of branching there are precise, but as yet unidentified, guidance mechanisms within the diaphragm for establishing the primary intramuscular branching pattern (Laskowski and Owens, 1994).

The pleuroperitoneal fold differentiates into the neuromuscular substrate for the diaphragm

Following p75 immunolabelling from E12.5 to E15.5 allows us to trace the development of the pleuroperitoneal fold and show that there is a continuity in labelling and morphological progression that strongly suggests that the PPF derives from the somatic mesoderm and goes on to form the substrate for the diaphragmatic neuromusculature. Further, tracking p75, GAP-43 and desmin (this chapter) as well as NCAM and PSA-NCAM immunolabelling (chapter 5) throughout diaphragmatic development demonstrates that all of the neural and muscular components of the diaphragm emanate from the pleuroperitoneal

fold. From E13 to E15, the PPF expands both sternally around the septum transversum, and dorsolaterally and caudally over the dorsal extent of the liver to fuse with the body wall and seal the PPCs caudal to the lung. Dorsolateral migration of the diaphragmatic tissue has also been described in light of scanning electron micrographs (Kluth et al., 1996). These issues shall be discussed further in the following chapters.

Discrimination of the primordial diaphragm is not only interesting from the perspective of respiratory system development, but also from that of the clinical importance of uncovering the pathogenic mechanism of congenital diaphragmatic hernia (CDH). Chapters 7 and 8 shall demonstrate the relevance of these findings to our current understanding of how an incomplete diaphragm forms in the instance of CDH. In short, those studies demonstrate that abnormal diaphragmatic development in the instance of CDH can be traced back to abnormal formation of the p75-immunopositive PPF. This lends further support to our contention that the PPF is the substrate for the diaphragmatic neuromusculature.

Relationship between intramuscular branching of the phrenic nerve and myotome development.

Whole-mount diaphragms immunolabelled for GAP-43 and desmin allowed for a clear delineation of the topographic distribution of intramuscular branching and myotube formation throughout the developing diaphragm. As demonstrated in this, and the following chapter, the development of diaphragmatic neuromusculature occurs in a rather unique geometry. Many muscles develop within a cable-like geometry where the addition of muscle fibres would be equivalent to adding more wires to the cable. The diaphragm, on the other hand, initially develops like a train track, the addition of new muscle equivalent to laying new railroad ties. Innervation deriving from a central insertion point then migrates at a short distance behind the newly laid fibres. This makes the initial innervation pattern remarkably simple to determine. Throughout initial diaphragm development, myoblasts a short distance ahead of the nerve began to fuse to form myotubes. As the nerve migrated through the various sectors of the diaphragm, muscle tissue along the nerve's path began to form additional myotubes. Initially, we perceived that myoblasts would be distributed throughout

the premuscle mass and myotube fusion would progress throughout this population. However, this study would suggest that myoblasts, and perhaps even the diaphragmatic mesoderm, migrate around the septum transversum within the expanding pleuroperitoneal fold a short distance ahead of the fusing myotubes and the advancing phrenic branches. Current examination of MyoD expression patterns in the diaphragm are being performed in an attempt to understand the migration of myoblasts during diaphragm development.

These data are in agreement with the general idea that motor axons impose regulatory influences on muscle from the time of initial contact which modulate and facilitate myotube formation via electrically mediated effects and/or diffusible substances (Kelly, 1983; Wakelam, 1985; Hall and Sanes, 1993). Studies performed in chapter 6, however, demonstrate that muscle fibres in the diaphragm are formed in the normal spatiotemporal pattern in the absence of innervation. Therefore it may be that the muscle and or the advancing mesoderm may be guiding/permissive for the phrenic axons, and not the other way around. Examination of axonal growth into the amuscular diaphragm of *HGF/SF* null mutant mice may prove instructive in this matter (see chapter 7). There was also a radiation of myotube formation from the point of nerve innervation at the centre of the fibres laterally towards the central tendon/septum transversum and the lateral edge of the diaphragm. This is likely due to the addition of new myoblasts which are preferentially absorbed at the ends of myotubes (Zhang & McLennan, 1995). Thus, the correlation of myotube formation with nerve outgrowth which we observed favours the earlier interpretation of Bennett & Pettigrew (1974) rather than that of Harris (1981). The following chapters discuss primary and secondary myogenesis more fully and thus are not discussed here.

Summary

How the phrenic nerve and diaphragm develops is a long-standing question in embryology and an understanding of these processes will be necessary for determining the pathogenesis of the often fatal developmental anomaly, congenital diaphragmatic hernia. This study utilises immunohistochemical markers for a number of tissues to demonstrate the initial migratory path and primordial diaphragmatic target for phrenic nerve outgrowth and the morphogenesis of the phrenic nerve and diaphragmatic musculature. The growth cones

of pioneering phrenic axons follow a well-defined track of cells of unknown identity (although they are most likely diaphragmatic mesodermal cells) to reach and make contact with the pre-muscle mass of the diaphragm within the pleuroperitoneal fold (PPF) by E13. By E14.5, the primordial diaphragm and the phrenic axons have translocated from the region of C5-C6 spinal cord to the lower thorax. As the PPF expands, intramuscular branching of the phrenic nerve commences, concomitant with the formation of diaphragmatic myotubes. Expansion of the PPF around the septum transversum ventrally, and over the dorsal aspect of the liver dorsally, results in the formation of the diaphragmatic substrate for neuromuscular formation. There is a tightly-regulated coordination between the outgrowth of phrenic nerve intramuscular branches and the fusion of myoblasts during primary myogenesis. The diaphragmatic neuromusculature reaches the sternum by E17, and thus approximates the full extent of the adult diaphragmatic surface area in time for the inception of respiratory movements at E17.

REFERENCES

Allan DW, Babiuk RP, Parsons BA, Greer JJ. (1997) Immunologically-defined tracks along the pathways taken by phrenic and brachial axons during fetal rat development. *27th Soc Neurosci Abstr.* 254.14.

Andersson A, Olsen M, Zhernosekov D, Gaardsvoll H, Krog L, Linnemann D, and Bock E (1993) Age-related changes in expression of the neural cell adhesion molecule in skeletal muscle: a comparative study of newborn, adult and aged rats. *Biochem J* 290:641-648.

Bennett MR and Pedigree AG (1974) The formation of synapses in striated muscle during development. *J. Physiol. (London)* 241:515-545.

Bladt F, Riethmacher D, Isenmann S, Aguzzi A and Birchmeier C (1995). Essential role for the c-Met receptor in the migration of myogenic precursor cells into the limb bud. *Nature.* 376: 768-771.

Bober E, Franz T, Arnold H-H, Gruss P and Tremblay P 91994) Pax-3 is required for the development of limb muscles: a possible role for the migration of dermomyotomal muscle progenitor cells. *Development.* 120: 603-612.

Capetanaki Y, Milner DJ and Weitzer G (1997) Desmin in muscle formation and maintenance: knockouts and consequences. *Cell Struct. & Funct.* 22: 103-116.

Ebens A, Brose K, Leonardo ED, Hanson MG Jr, Bladt F, Birchmeier C, Barres, BA, Tessier-Lavigne M (1996) Hepatocyte growth factor/scatter factor is an axonal chemoattractant and a neurotrophic factor for spinal motor neurons. *Neuron.* 17: 1157-1172.

Eisen JS. (1991) Motoneuronal development in the embryonic zebrafish. *Development Suppl.* 2:141-7, 1991.

Greer JJ, Smith JC and Feldman JL (1992) Respiratory and locomotor patterns generated in the fetal rat brain-stem spinal cord in vitro. *J. Neurophysiol.* 67:996-999.

Grenningloh G and Goodman CS (1992) Pathway recognition by neuronal growth cones: genetic analysis of neural cell adhesion molecules in Drosophila. *Curr. Op. Neurobiol.* 2:42-47.

Grim M, Halata Z and Franz T (1992) Schwann cells are not required for guidance of motor nerves in the hindlimb in splotch mutant mouse embryos. *Anat. Embryol.* 186: 311-318.

Hall ZW. and Sanes JR (1993) Synaptic structure and development: the neuromuscular junction. *Cell* 10 *(Suppl.)*: 99-121.

Harris AJ. (1981) Embryonic growth and innervation of rat skeletal muscles. III. Neural

regulation of junctional and extra-junctional acetylcholine receptor clusters. *Phil. Trans. R. Soc. London B* 293:287-314.

Iritani I. (1984) Experimental study on embryogenesis of congenital diaphragmatic hernia. *Anat. Embryol.* 169:133-139.

Kelly AM (1983) Emergence of specialization of skeletal muscle. In *"Handbook of Physiology"* Edited by LD Peachey: Section 10, pp. 507-537.

Kim GJ, Shatz CJ and McConnel SK. (1991) Morphology of pioneer and follower growth cones in the developing cerebral cortex. *J. Neurobiol.* 22:629-42.

Kluth D, Losty PD, Schnitzer JJ, Lambrecht W and Donahoe PK (1996) Toward understanding the developmental anatomy of congenital diaphragmatic hernia. *Clinics in Perinatology*. Congenital Diaphragmatic Hernia. Vol. 23: 655-669.

Kothary FT, Surani MA, Halata Z and Grim M (1993) The splotch mutation interferes with muscle development in the limbs. *Anat. Embryol.* 187: 153-160.

Lance-Jones C and Dias M (1991) The influence of presumptive limb connective tissue on motoneuron axon guidance. *Dev. Biol.* 143: 93-110.

Laskowski MB and Owens JL (1994) Embryonic expression of motoneuron topography in the rat diaphragm muscle. *Dev Biol* 166:502-508.

Lewis WH. (1910) The development of the muscular system. In *"Manual of Human Embryology"* Edited by Keibel F and Mall F: Vol. 1:454-522.

Maina F and Klein R (1999) Hepatocyte growth factor, a versatile signal for developing neurons. *Nature Neuroscience.* 2: 213-217.

Nagashima M. (1994) Postnatal development of the rat corticospinal tract, with special reference to confocal laser scanning microscopy of growing axons. *Neurosci. Res.* 19:81-92.

Noakes PG, Bennett MR and Davey DF (1983) Growth of segmental nerves to the developing rat diaphragm: absence of pioneer axons. *J. Comp. Neurol.* 218:365-377.

Phelan KA and Hollyday M (1990) Axon guidance in muscleless chick wings: the role of muscle cells in motoneuronal pathway selection and muscle nerve formation. *J. Neurosci.* 10: 2699-2716.

Reynolds ML, Fitzgerald M and Benowitz LI (1991) GAP-43 expression in developing cutaneous and muscle nerves in the rat hindlimb. *Neuroscience.* 41: 201-211.

Serbedzija GN and McMahon AP (1997) Analysis of neural crest migration in splotch mice

using a neural crest-specific lacZ reporter. *Dev. Biol.* 182: 139-147.

Skandalakis JE, Gray SW and Ricketts RR. (1994) The diaphragm. In *Embryology for Surgeons* Edited by Skandalakis JE and Gray SW: Ch.15.

Stainier DY and Gilbert W. (1990) Pioneer neurons in the mouse trigeminal sensory system. *Proc. Nat. Acad. Sci.* 87:923-927.

Strittmatter SM, Fankhauser C, Huang PL, Mashimo H, Fishman MC (1995) Neuronal pathfinding is abnormal in mice lacking the neuronal growth cone protein GAP-43. *Cell.* 80: 445-452.

Tosney KW (1987) Proximal tissues and patterned neurite outgrowth at the lumbosacral level of the chick embryo: deletion of the dermamyotome. *Dev. Biol.* 122: 540-588.

Wakelam MJ. (1985) The fusion of myoblasts. *Biochem. J.* 228:1-12.

Wells LJ. (1954) Development of the human diaphragm and pleural sacs. *Cont. Embryol.* 35:107-134.

Wheeler EF. and Bothwell M (1992) Spatiotemporal patterns of NGF and the low-affinity NGF receptor in rat embryos suggest functional roles in tissue morphogenesis and myogenesis. *J. Neurosci.* 12:930-945.

Zhang M and McLennan IS. (1995) During secondary myotube formation, primary myotubes preferentially absorb new nuclei at their ends. Dev. Dyn. 204:168-177.

Chapter 5

POLYSIALYLATED NCAM EXPRESSION DURING MOTOR AXON OUTGROWTH AND MYOGENESIS IN THE FETAL RAT

Adapted from the original publication:
Douglas W. Allan and John J. Greer
J. Comp. Neurol. 391: 275-292 (1998)

INTRODUCTION

Modulation of cellular adhesion and repulsion is an important mechanism by which developing axons and muscle cells regulate cellular interactions during motor axon pathfinding and muscle morphogenesis. During segregation of motor nerve trunks, adherent axons must defasciculate to allow for differential growth into muscle-specific nerve fascicles. Global and preferential adhesive and repulsive factors have been demonstrated to influence axonal migration at such decision points (reviewed in Tessier-Lavigne and Goodman, 1996). Once migrating motor axons reach the target musculature, a reduction in interaxonal adhesion promotes intramuscular axonal defasciculation and preferential growth over developing muscle fibres (reviewed in Rutishauser and Landmesser, 1996). Similarly, during muscle morphogenesis, the fusion of myoblasts forms tightly adherent pools of myotubes which subsequently must separate during two discrete phases of muscle formation associated with primary and secondary myogenesis (Kelly, 1983).

Cell adhesion molecules (CAMs), postulated to act primarily via homophilic binding, are integral to intercellular adhesion. These CAMs include members of the immunoglobulin family, such as the neural cell adhesion molecule (NCAM) and L1, and the cadherin family. NCAM is perhaps the most ubiquitously expressed adhesion molecule in nerve and muscle within the developing vertebrate embryo. It has been implicated in multiple aspects of neuromuscular development, including promotion of axonal adhesion, fasciculation and outgrowth (Rutishauser et al., 1982; Landmesser et al., 1988; reviewed in Hall et al., 1996), nerve-muscle adhesion (Rutishauser et al., 1983), and adhesion and fusion of myoblasts and myotubes (reviewed in McDonald et al., 1995).

The balance between intercellular adhesion and repulsion can be modulated by simply altering the ratio in expression of molecules that promote either adhesion or repulsion. For example, modulation of the expression levels of invertebrate NCAM homologues, *Drosophila* fasciclin II and *Aplysia* apCAM, correlates with the degree of interneuronal and neuromuscular adhesion (Lin et al., 1994; Lin and Goodman, 1994; Zhu et al., 1995; Schuster et al., 1996a,b). An alternative mechanism available to vertebrates is to modulate the adhesivity of NCAM itself, via modification of its molecular structure. Thus, although

NCAM is expressed by the majority of growing vertebrate axons and developing muscle, developmentally-regulated functional variations may be generated by the multiplicity of distinct isoforms which result from both alternate mRNA splicing and differential post-translational processing (reviewed in Barthels et al., 1992; Daniloff et al., 1994; Doherty et al., 1995; Rutishauser and Landmesser, 1996). A particularly striking modification of NCAM adhesiveness occurs via the post-translational addition of long polymers of sialyl residues to the extracellular domain of NCAM (Hoffman and Edelman, 1983; reviewed in Seki and Arai, 1993a; Rutishauser and Landmesser, 1996). In direct contrast to NCAM, polysialylated NCAM (PSA-NCAM) is postulated to sterically and electrostatically attenuate intercellular interactions, resulting in the "spacing" of apposed membranes (Yang et al., 1992, 1994). A functional role for PSA-NCAM-induced attenuation of membrane adhesion has been demonstrated in the developing chick hindlimb where its promotion of interaxonal defasciculation is required for axonal branching and the differential guidance of axonal populations from a common nerve trunk. Enzymatic removal of PSA from NCAM shifts the balance of adhesion and repulsion to primarily L1-mediated adhesion, causing excessive axonal fasciculation, thereby inhibiting branching and differential guidance (Landmesser et al., 1990; Zhang et al., 1992; Tang et al., 1992, 1994).

Previous studies of PSA-NCAM in developing mammalian motor systems have been limited to the determination that PSA-NCAM is expressed within the embryonic spinal cord and by spinal motoneurons (Boisseau et al., 1991; Seki and Arai, 1993b). In the present study, we expand upon these observations by examining PSA-NCAM expression in developing rat motoneurons and how it correlates with the segregation of distinct mammalian motor axon populations and nerve branching. Further, we provide the first clear demonstration of the spatiotemporal correlation between myotube separation and PSA-NCAM expression during primary and secondary myogenesis. These data are necessary to clarify the proposed role of PSA-NCAM in the repulsion of myotube membranes necessary for normal myogenesis (Fredette et al., 1993).

Towards these objectives, we have examined the spatiotemporal expression of PSA-NCAM throughout motoneuron and myotube development (embryonic days E11-E19) within a simple mammalian neuromuscular system, the rat phrenic nerve and diaphragm.

METHODS

The following numbers of embryos (E), taken from a specified numbers of dams (D), were used for this study. i) Whole embryo sections - E11.5 (10E, 4D); E12.5 (19E, 9D); E13 (38E, 15D); E14 (12E, 7D). ii) Diaphragm whole mounts - E14.5-E15 (22E, 8D); E15.5-E16 (39E, 14D); E16.5 (34E, 14D); E17-E17.5 (29E, 9D); E18-E18.5 (16E, 4D); E19 (11E, 1D). iii) Diaphragm cross-sections - E15.5-E16 (16E, 4D); E16.5 (6E, 2D); E17-E17.5 (8E, 2D); E18-E18.5 (6E, 2D); E19 (6E, 2D).

Whole embryo cross sections: Transverse and sagittal sections performed as described for vibratome sections. However, for more direct comparison of PSA-NCAM and total-NCAM expression on cervical axons within a given animal, serial sections from E12.5 fetuses were alternately processed for the two immunolabels.

Diaphragm cross-sections: The following two procedures were followed. 1) Isolated diaphragms were embedded and cut as described for vibratome sectioning. Sections were oriented for either mediolateral or dorsoventral vibratome sectioning at 30-40 μm. This produced sections which demonstrated the longitudinal and transverse axes of myotubes, respectively. Serial sections were washed in PBS and alternately immunoreacted free floating for PSA-NCAM and total-NCAM, mounted and coverslipped so that the sections were kept moist until examination. 2) Whole diaphragms were immunostained free floating, and embedded for microtome sectioning as described previously. Sections were cut in the dorsoventral (transverse) plane at 8 μm. All diaphragm cross-sections from both methods were examined with Nomarski optics.

Antibodies

GAP-43 was detected using the mouse anti-GAP-43 IgG monoclonal antibody (MAb) (Sigma) at a dilution of 1:500. This antibody recognises an epitope on both phosphorylated and dephosphorylated forms of GAP-43 (Meiri et al., 1991) Polysialylated NCAM was detected using the mouse anti-PSA IgM MAb, termed 12E3 (a generous gift from T. Seki; Juntendo University). 12E3-containing ascities fluid was diluted to 1:5,000-1:10,000. This MAb detects PSA-NCAM when a polymer of 6 or more α2,8-linked sialic acid residues are present and does not cross react with other sialylated species, such as gangliosides (Seki and

Arai, 1991; Sato et al., 1995). Total-NCAM was detected using a rabbit polyclonal antisera (a generous gift from E. Bock; University of Copenhagen) used at a dilution of 1:2,000-1:3,000. The antibody detects the three major isoforms of rat NCAM (120, 140, 180 kD; Andersson et al., 1993). L1 was detected using a rabbit polyclonal antisera to rat L1 (a generous gift from V. Lemmon; Case Western University) at a dilution of 1:1000. Secondary antibodies used for GAP-43 and PSA-NCAM labelling were peroxidase-conjugated goat anti-mouse IgG (Sigma; whole molecule) and biotinylated goat anti-mouse IgM (Sigma; μ-chain specific) respectively. For both total-NCAM and L1, peroxidase-conjugated goat anti-rabbit IgG (Sigma; whole molecule) was used. Immunohistochemistry was performed as previously described.

RESULTS

GAP-43 immunolabelling was used to provide a clear visualisation of the full extent of axonal outgrowth amongst cervical motoneurons at various stages of development beyond E12. To determine the spatiotemporal pattern of NCAM sialylation on axonal membranes, immunolabelling for total-NCAM and PSA-NCAM were compared. Immunolabelling for the functionally interrelated adhesion molecule L1 was also performed during times of brachial and phrenic axon separation. Finally, immunolabelling of the developing diaphragm for PSA-NCAM provided information regarding PSA-NCAM expression on phrenic axons during the time of intramuscular branching and on myotubes during primary and secondary myogenesis. The patterns of phrenic axon outgrowth, diaphragmatic myotube formation and immunolabelling for PSA-NCAM, total-NCAM, GAP-43 and L1 were remarkably consistent amongst embryonic rats of a given age and thus the results are presented as a series of representative figures at several important developmental stages.

Formation of cervical ventral roots (E11.5).

We began our studies at age E11.5, immediately after choline acetyltransferase- and neurofilament-positive motoneurons are first observed within the cervical spinal cord (Phelps et al., 1988; Chen and Chiu, 1992). Fig. 5.1 illustrates the comparison between total-NCAM and PSA-NCAM immunolabelling at cervical segment C5 from two different fetuses of the same age. At this age, cervical ventral roots were first emerging from the spinal cord and had extended as far as the positively labelled myotome. Small numbers of axons had penetrated the myotome, whereas others had begun to turn ventrally. Total-NCAM labelling (Fig. 5.1A) was primarily detected within the ventricular zone, commissural somata and their axons, ventral motoneuron populations and their axons, the floorplate and myotome. In contrast, PSA-NCAM labelling (Fig. 5.1B) was restricted to the myotome and a subpopulation of motoneurons within the ventrolateral spinal cord and their axons within the ventral root.

Fig. 5.1: Early formation of the cervical ventral root and phrenic nerve. Photos show A) total-neural cell adhesion molecule (NCAM) and B) polysialylated (PSA)-NCAM immunolabelling in transverse sections (40 μm) from the same level of the cervical spinal cord isolated from two fetal rats aged E11.5. Both total-NCAM and PSA-NCAM label motoneurons and the myotome. However, in contrast to total-NCAM, PSA-NCAM labelling does not appear in the floorplate, ventricular zone or commissural somata and their short axons. Further, PSA-NCAM labelling is restricted to a subpopulation of somata within the ventral motoneuron populations and axons within the ventral root. Abbreviations: Com (commissural somata) VR (ventral root), FP (floor plate), My (myotome). Scale bar = 100 μm.

Formation of the brachial plexus and axonal divergence (E12.5-E13)

E12.5 - Initiation of axonal segregation and differential growth at the brachial plexus

The maturational changes in the cervical spinal cord and surrounding tissues during the next day were visualised via immunolabelling for GAP-43, L1, total-NCAM and PSA-NCAM (Fig. 5.2). The motoneuron population within the ventral horn had increased in size, dorsal root ganglia (DRG) had formed and commissural axons had begun to cross the floorplate. Phrenic and brachial motor axons now extended towards an area lateral of the anterior cardinal vein at the base of the forelimb buds. There, the brachial plexi had formed and the earliest projections of the phrenic (continuing ventrally) and brachial nerves (turning laterally) could be observed. PSA-NCAM labelling (Fig. 5.2D) had increased in a number of spinal cord regions, including the floor plate and commissural somata and axons. PSA-NCAM labelling had also increased among motoneurons, although it was restricted to a subpopulation of motoneurons within the ventral horn and a subpopulation of axons extending within the cervical ventral roots. In particular, only regions within the ventromedial motoneuron populations (i.e. region of the phrenic and dorsal ramus motoneuron nuclei) and the axons which extended within the phrenic nerve and dorsal ramus consistently showed high levels of PSA-NCAM labelling. In contrast, PSA-NCAM labelling was barely detectable or totally absent along brachial motor axons distal to the plexus. Recently generated dorsal root ganglion (DRG) neurons were also largely PSA-NCAM negative whereas they labelled strongly for total-NCAM, GAP-43 and L1. Interestingly, the paucity of PSA labelling within the DRG was maintained throughout embryonic development and, once formed, sensory projections within the dermis were absent of PSA-NCAM immunoreactivity (Allan and Greer, unpublished observations).

Further demonstration of the differential labelling between total-NCAM and PSA-NCAM is provided in Fig. 5.3 which shows three consecutive serial sections taken from the same fetus that were alternately labelled for total-NCAM and PSA-NCAM. It is clear that PSA-NCAM labelling was localised to phrenic axons at the brachial plexus and to ventromedial motoneuron populations within the ventral horn.

Fig. 5.2: Restricted PSA-NCAM expression during initiation of axonal segregation at the brachial plexus. Transverse sections (40μm) from four fetal rats aged E12.5 comparing immunolabelling for GAP-43 (A), L1 (B), total-NCAM (C) and PSA-NCAM (D) at the same segmental level. Phrenic and brachial axons have begun to segregate at the brachial plexus. Phrenics continue ventrally as brachials turn laterally into the limb bud. GAP-43 delineates axonal processes of the dorsal ramus, commissurals, dorsal root ganglion (DRG), phrenics (Ph) and brachials (Br). L1 and total-NCAM label these axons to approximately the same extent as GAP-43, although there appears less L1 within commissural axons. PSA-NCAM labelling is specifically absent from brachial axons and is concentrated within the ventromedial region of the ventral horn (arrow). Abbreviations: V (ventral horn). Scale bars = 100μm.

Fig: 5.3. Comparison of total-NCAM and PSA-NCAM labelling during axonal segregation at the brachial plexus. Serial sections (40μm, A most caudal) taken from a fetal rat aged E12.5 and alternately immunolabelled for total-NCAM (A,C) and PSA-NCAM (B). In comparison to total-NCAM, PSA-NCAM is absent from brachial axons, dorsal root ganglia and ventral horn somata outside the ventromedial region. Abbreviations: DRG (dorsal root ganglion), My (myotome), Br (brachial axons), Ph (phrenic axons), FL (forelimb bud), . Scale bar = 100μm.

E13: Growth of the phrenic nerve from the brachial plexus to the primordial diaphragm.

Maturational changes achieved by E13 were also visualised via immunolabelling for total-NCAM, GAP-43, L1 and PSA-NCAM (Fig. 5.4). By this age, dorsal and ventral brachial branches could be clearly defined and a greater number of phrenic axons had grown beyond the brachial plexus. Total-NCAM, GAP-43 and L1 similarly labelled all identifiable neuronal structures at equivalent intensities. PSA-NCAM labelling, however, was again more localised. The somata and axons of commissural, dorsal ramus and phrenic neurons labelled strongly for PSA-NCAM. However, ventral motoneuronal somata outside the ventromedial pool, axons projecting into the forelimb bud, and the dorsal root ganglion (DRG) were specifically absent or labelled weakly for PSA-NCAM. Brachial axons did not begin to express consistently high levels of PSA-NCAM until E14, when the emerging forelimb musculature began to form. (Allan and Greer, unpublished observations)

Fig. 5.5A shows GAP-43 labelling within a sagittal section of a whole decapitated fetal rat aged E13. Phrenic axons can clearly be seen to extend beyond the brachial plexus towards the diaphragmatic primordium, the pleuroperitoneal fold. A comparison between GAP-43 (Fig. 5.5B) and PSA-NCAM (Fig. 5.5C) labelling of axons within the region of the plexus further demonstrates that PSA-NCAM was preferentially expressed by a subset of axons within the brachial plexus. These lead into the phrenic nerve and are thus presumably phrenic. This figure also demonstrates that phrenic axons do not travel through the plexus as a tightly fasciculated group, but rather seem to be intermingled with brachial axons. It is also clear from figure 5.5C that PSA-NCAM expression within ventral roots C4-C6 (C7 also visible) is greater than that which can be accounted for by phrenic axons. However, as can be observed in Figs. 5.3 and 5.4, axons within the dorsal ramus are also PSA-NCAM-positive. In summary, although phrenic axons are not the only cervical axons to express PSA-NCAM, they are the only ones to do so within the brachial plexus during the period of phrenic and brachial axon separation.

Fig: 5.3. Comparison of total-NCAM and PSA-NCAM labelling during axonal segregation at the brachial plexus. Serial sections (40μm, A most caudal) taken from a fetal rat aged E12.5 and alternately immunolabelled for total-NCAM (A,C) and PSA-NCAM (B). In comparison to total-NCAM, PSA-NCAM is absent from brachial axons, dorsal root ganglia and ventral horn somata outside the ventromedial region. Abbreviations: DRG (dorsal root ganglion), My (myotome), Br (brachial axons), Ph (phrenic axons), FL (forelimb bud), . Scale bar = 100μm.

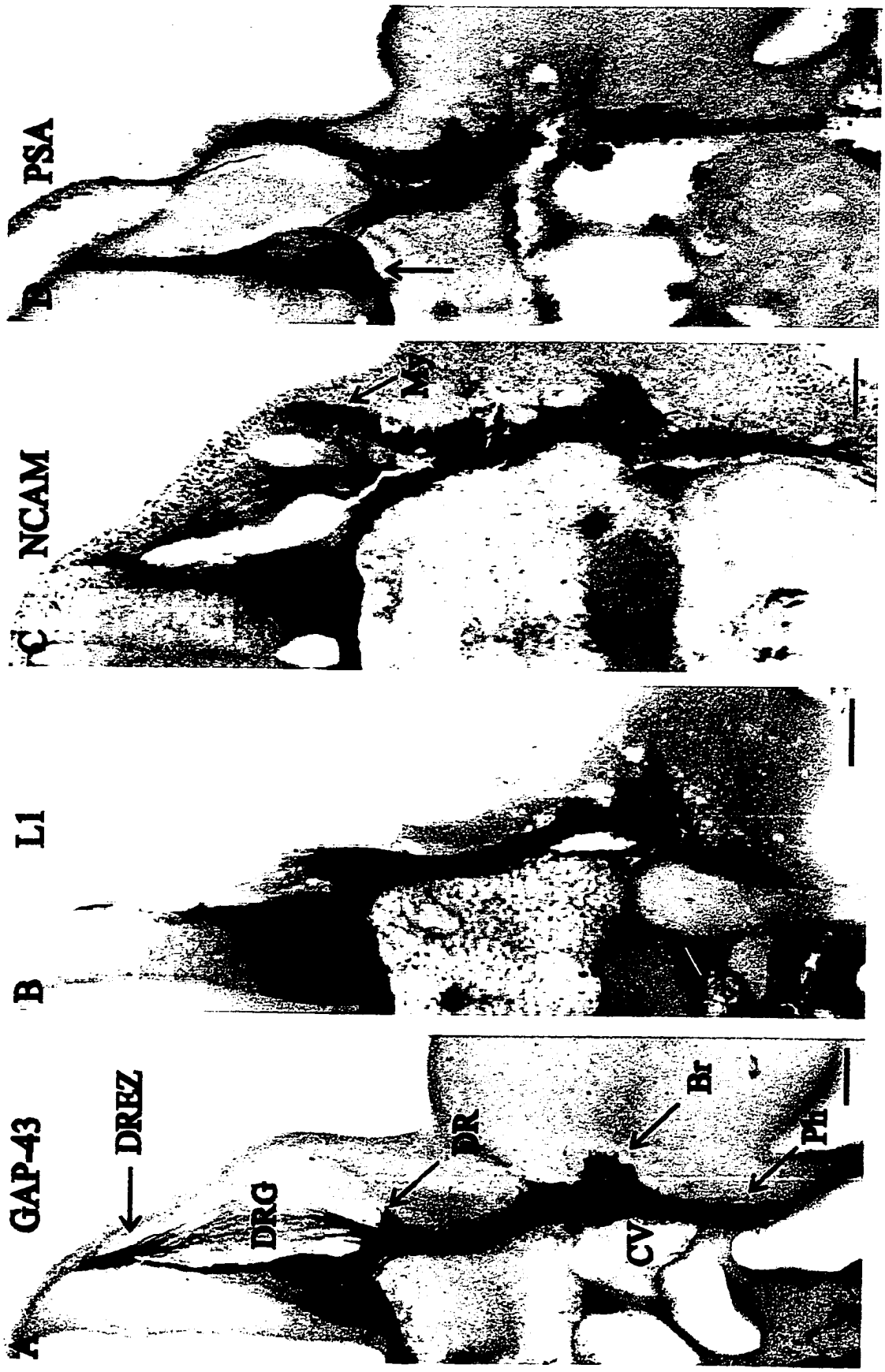

Fig. 5.5: Migration of phrenic axons towards the primordial diaphragm. (A) GAP-43 labelling of a sagittal section (60 μm) of whole fetal rat illustrates the extent of phrenic nerve (Ph) development at age E13. At this age, phrenic axons are approaching the primordial diaphragm, the pleuroperitoneal fold, at the dorsal extent of the liver (Li). (B and C) Close-up of the brachial plexus and the phrenic nerve shows GAP-43 (B) and PSA-NCAM (C) labelling of axons within the brachial plexus and within the growing phrenic nerve. PSA-NCAM was specifically expressed by phrenic axons within and beyond the brachial plexus. Abbreviations: Asterisk (anterior cardinal vein), H (heart), ST (septum transversum), S (stomach). Scale bars = 500 μm (A); 100 μm (B,C).

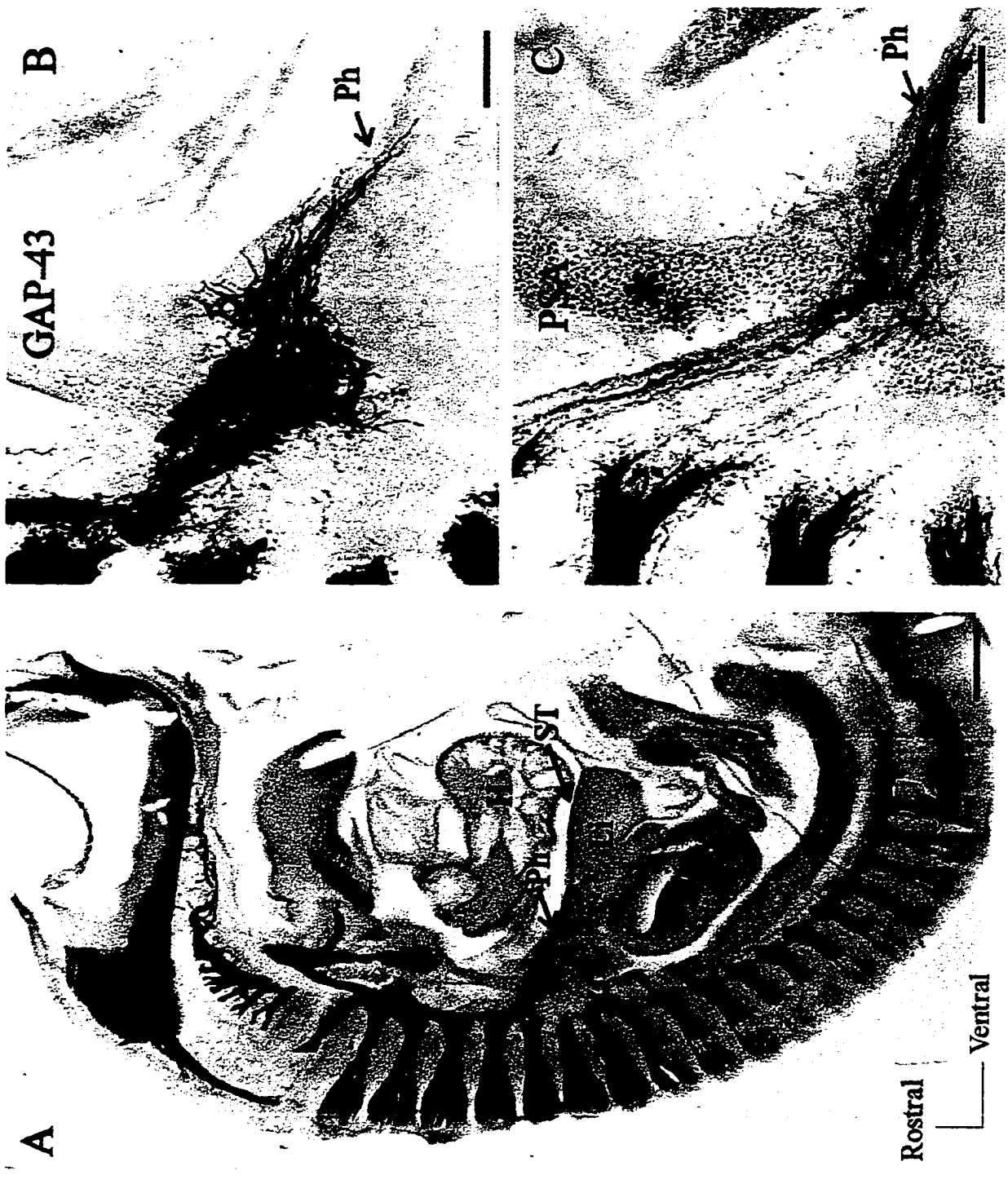

E14.5-E19: Development of intramuscular branches and myogenesis

E14.5: Initial stages of phrenic nerve trifurcation within the primordial diaphragm and the onset of primary myogenesis.

Whole-mount diaphragms taken from fetal rats aged between E14.5-E15 and labelled for GAP-43 illustrate the site at which the phrenic nerve commenced branching within the primordial diaphragm (Fig. 5.6A). A close-up view of the initial branching pattern on the right hemidiaphragm (Fig. 5.6B) shows the trifurcation of the nerve trunk into primary branches projecting towards crural, dorsal and sternal regions of the developing diaphragm. At the time of initial phrenic nerve trifurcation, PSA-NCAM labelling was very high within all three nerve branches (Figs. 5.6C,D). It was at this stage that a striated pattern of PSA-NCAM labelling was first observed running transversely across the dorsal and sternal branches of the phrenic nerve. The striated pattern corresponded to PSA-NCAM expression on recently fused primary myotubes. Primary myotube formation, as detected by PSA-NCAM labelling, was limited to regions immediately surrounding the dorsal and sternal branches,

Fig. 5.6: PSA-NCAM labelling is high on phrenic axons and myotubes during the onset of initial innervation. Whole-mounts of diaphragms isolated from two fetal rats aged E14.5. Top panels (A and B) show initial nerve branching as detected by GAP-43 immunolabelling. Bottom panels © and D) show corresponding labelling for PSA-NCAM in the phrenic nerve and on the first myotubes (arrow in D) to form within the diaphragm. The openings for the passage of the aorta (A), eosophagus (E) and inferior vena cava (VC) are illustrated in Fig. 6C. Abbreviations: S (sternal branch), D (dorsal branch) C (crural branch). Scale bars = 500 μm (A,C) 100 μm (B,D).

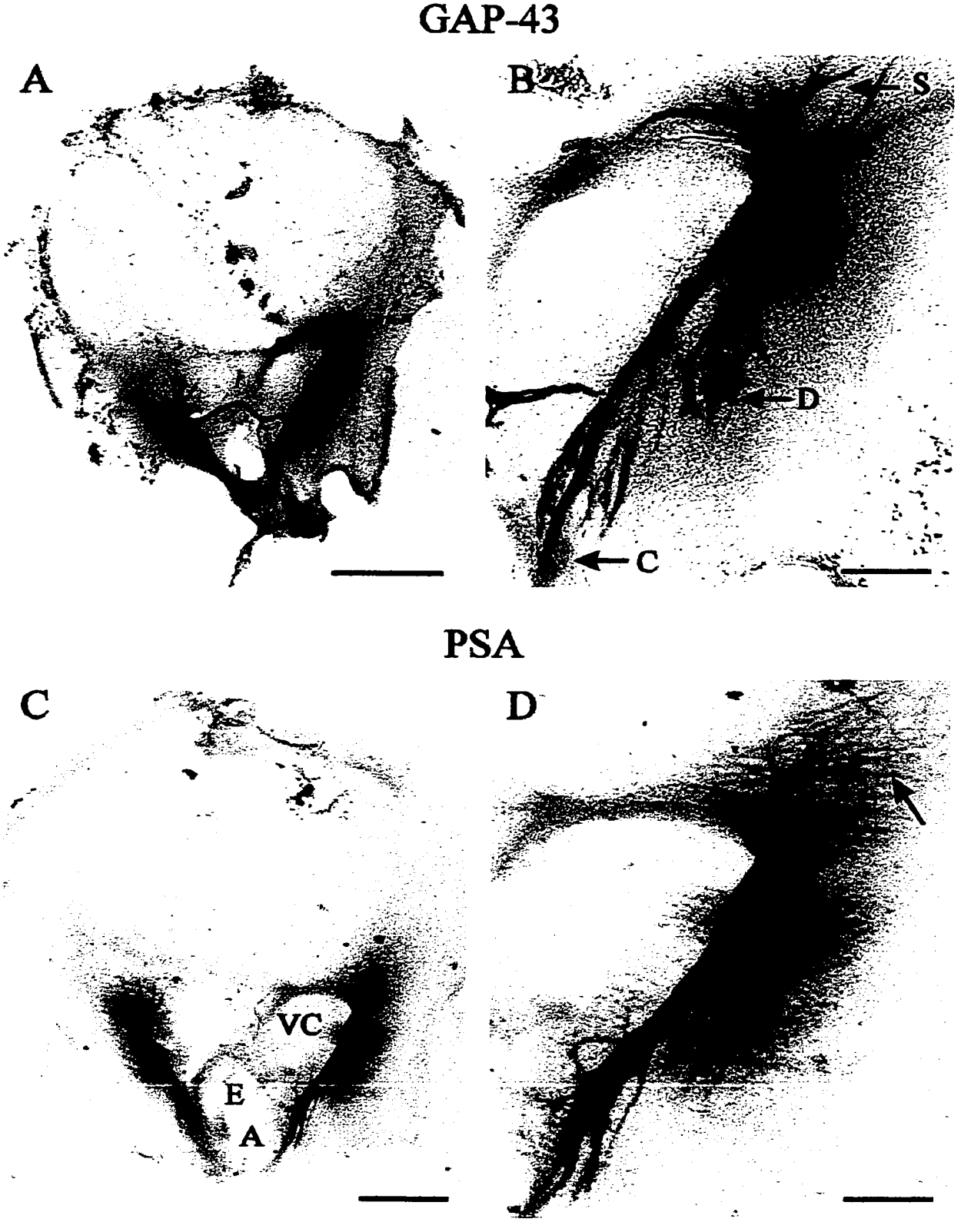

E15-E15.5: Elaboration of phrenic nerve intramuscular branching and primary myogenesis.

Fig. 5.7 illustrates the extent of phrenic nerve innervation within the developing diaphragm at age E15.5. The three major branches were well defined, and the crural branch had reached its target area. PSA-NCAM labelling remained high within the phrenic axons as higher order branching progressed (Figs. 5.7A-C). The formation, and subsequent PSA-NCAM labelling, of primary myotubes had progressed; 1) dorsoventrally in conjunction with the intramuscular growth of the primary phrenic intramuscular branches, and 2) mediolaterally from the site of initial axon-myotube contact as myotube elongation proceeded. A similar relationship between the extent of intramuscular branching of the phrenic nerve and myotube formation has been observed via combining immunolabelling for GAP-43 and desmin to delineate phrenic axons and myotubes, respectively (chapter 4). Fig. 5.7C demonstrates that primary myotubes began to form and express PSA-NCAM up to 150-200 μm distal to the tip of the growing phrenic axons.

A comparison between PSA-NCAM and total-NCAM (Figs. 5.7D-F) labelling showed that immunolabelling with these two antibodies overlapped. Moreover, it also became evident from comparing these two immunolabels, that total-NCAM was being expressed on cells beyond the subset which were expressing PSA-NCAM. Comparison of Figs. 5.7C and 5.7F, in particular, show that total-NCAM labelling was present between and beyond the boundaries of the striated PSA-NCAM immunoreactivity of primary myotubes. This pattern of total-NCAM labelling coincides well with the fact that unfused primary myoblasts within developing muscle express NCAM (Covault & Sanes, 1986). Further, the distribution (close proximity to myotubes) of the total-NCAM labelling that surrounds myotubes was similar to that of the p75 low-affinity nerve growth factor receptor (chapter 4), which we have postulated to label either mesoderm and possibly myoblasts in developing diaphragms. In serially sectioned and alternately labelled diaphragm sections (as in Figs. 5.9A versus B), there were no discernible differences between myotube length as determined by PSA-NCAM versus total-NCAM labelling. This indicates that PSA-NCAM expression commences shortly after, or coincidently with, the time when myoblasts fuse to form and/or elongate primary myotubes.

Fig. 5.7: Comparison between PSA-NCAM and total-NCAM labelling on developing nerve and muscle. Whole-mounts of diaphragms isolated from two fetal rats aged E15.5 showing the relative distribution of PSA-NCAM (A-C) compared with total-NCAM (D-F). PSA-NCAM labelling was limited to primary myotubes (arrow in C), whereas total-NCAM was more widely distributed (as at asterisk in F). Note that primary myotube formation, as demarcated by both PSA-NCAM and total-NCAM labelling, was similar for both immunolabels and was initiated within regions of intradiaphragmatic phrenic nerve branches. Abbreviations: S (sternal branch), D (dorsal branch), C (crural branch), CT (central tendon). Scale bars, 500 μm (A,D), 100 μm (B,C,E,F).

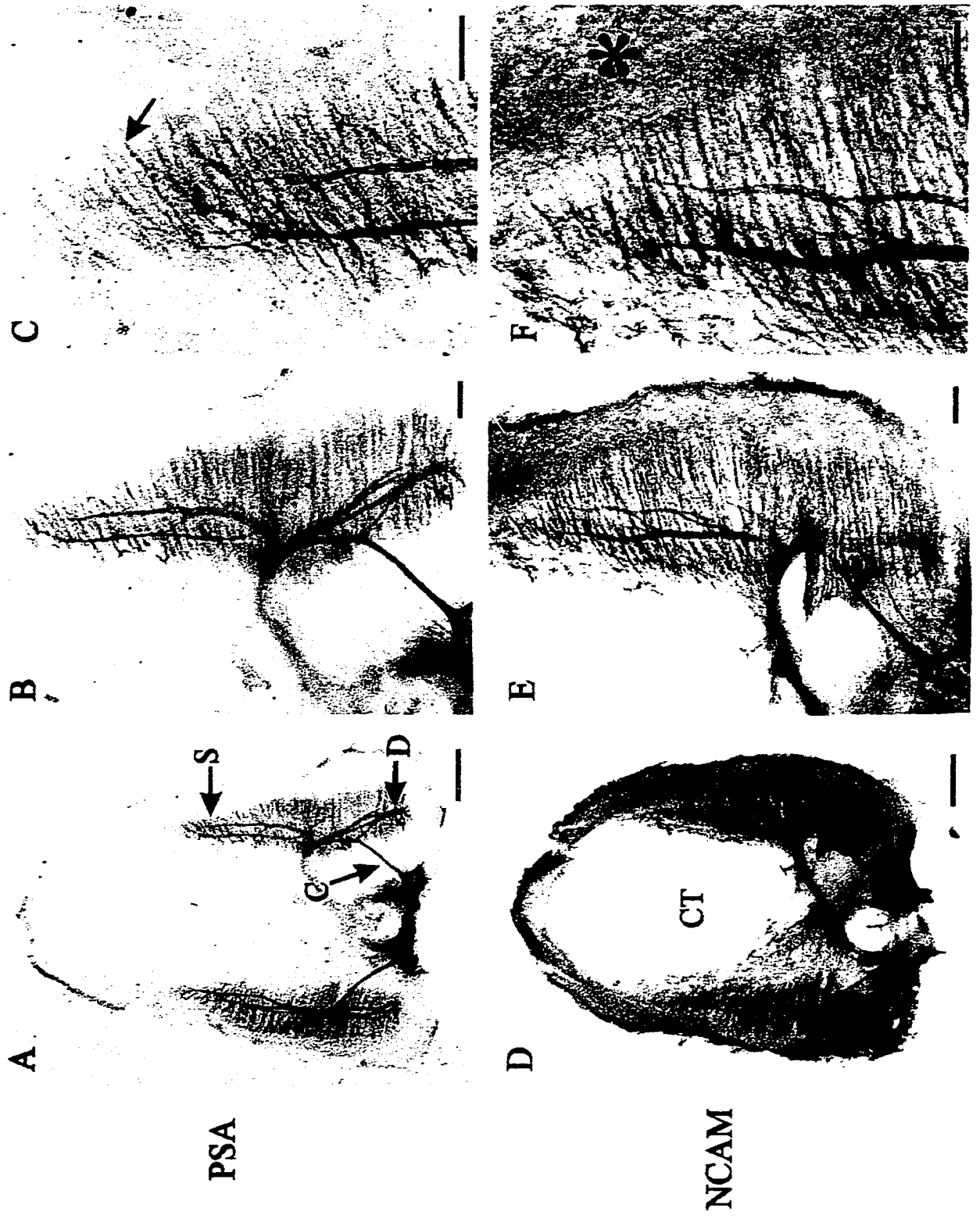

E16-E19: Maturation of axonal branching pattern and biphasic PSA-NCAM expression along myotubes

Intramuscular branching: Intramuscular branches of the phrenic nerve continued to elaborate from ages E16 (Fig. 5.8A) through to E18 (Fig. 5.8D), by which time the full extent of the diaphragm had become innervated. During E18, labelling for PSA-NCAM within the nerve started to decrease in a proximal-to-distal manner to a point where it was barely detectable by age E18.5 - E19, except within those diaphragm regions innervated at the latest stage (eg. the sternal region, Fig. 5.8D). This is demonstrated by an absence of phrenic branch PSA-NCAM immunolabelling in central diaphragmatic regions by E18 (Fig. 8D), which proceeds distally up to E19. The reduction in PSA-NCAM labelling consistently correlated with decreased expression of GAP-43 within phrenic axons, whereas total-NCAM labelling was maintained up to the latest age studied (E19) (data not shown).

Myogenesis - wholemount diaphragms: Heavy labelling for PSA-NCAM on developing primary myotubes persisted into age E16 (Fig. 5.8A). As with earlier ages, the spread of PSA-NCAM labelling in the dorsoventral direction coincided with the growth of phrenic axons, and in the mediolateral direction as a function of time since the centre of a myotube had formed and been initially innervated. However, it became apparent from immunolabelling for PSA-NCAM in diaphragms between ages E16 and E19 (Figs. 5.8A-D) that there was a striking bimodal expression of PSA-NCAM within the diaphragmatic musculature. At approximately age E16.5, there was a consistent down-regulation of PSA-NCAM expression within the majority of the diaphragmatic musculature (Fig. 5.8B). Down-regulation occurred in central muscle regions where primary myogenesis was essentially complete and primary myotubes have separated (Harris, 1981; Harris et al., 1989; Yiping et al., 1992). PSA-NCAM labelling had become limited to regions of most recent innervation (the more distal regions of sternal and dorsal muscle zones) and more recent myoblast addition (the most lateral extents of myotubes). Thus, PSA-NCAM expression along regions of myotubes formed during E14.5 had been maintained for approximately 1.5-2 days, and the labelling observed during E16.5 was limited to regions which had only become

PSA-NCAM-positive within the previous 1.5 days.

A second wave of PSA-NCAM expression spread throughout the diaphragm starting during early E17 (Fig. 5.8C). This corresponded with the onset of the majority of secondary myogenesis (Harris et al., 1989; Yiping et al., 1992). As during primary myogenesis, PSA-NCAM expression first appeared within the middle of myotubes, around the point of innervation, and progressed mediolaterally and dorsoventrally as secondary myogenesis proceeded into E18 (Fig. 5.8D). PSA-NCAM expression was again down-regulated coincident with the completion of the majority of secondary myogenesis (E19 for the majority of the diaphragm), following a comparable time course as during primary myogenesis. This pattern of PSA-NCAM expression is consistent with the notion that secondary myotubes extend longitudinally along the primary myotubes radiating from the point of nerve innervation (Duxson and Sheard, 1995). An exception to the bimodal pattern of PSA-NCAM expression in the developing diaphragm was observed in the crural region (Fig. 9). Both primary and secondary myogenesis were likely prolonged within this region as the crural area thickened considerably in relation to other regions of the diaphragm. PSA-NCAM expression in the crural region was subsequently maintained throughout to the last developmental stage that we systematically studied (E19).

Fig. 5.8. Two waves of PSA-NCAM labelling in developing diaphragm myotubes. Whole-mounts of diaphragms isolated from fetal rats aged E16 (A), E16.5 (B), E17.5 (C) and E18 (D) showing the relative distribution of PSA-NCAM in the nerve and muscle at various ages. PSA-NCAM labelling in the nerve decreased as the mature branching pattern was attained. PSA-NCAM labelling along myotubes appeared in two waves, separated by down-regulation during E16.5. The crural musculature (asterisk), however, maintained high levels of PSA-NCAM expression throughout all times examined. Abbreviations: CT (central tendon). Scale bars = 500 μm.

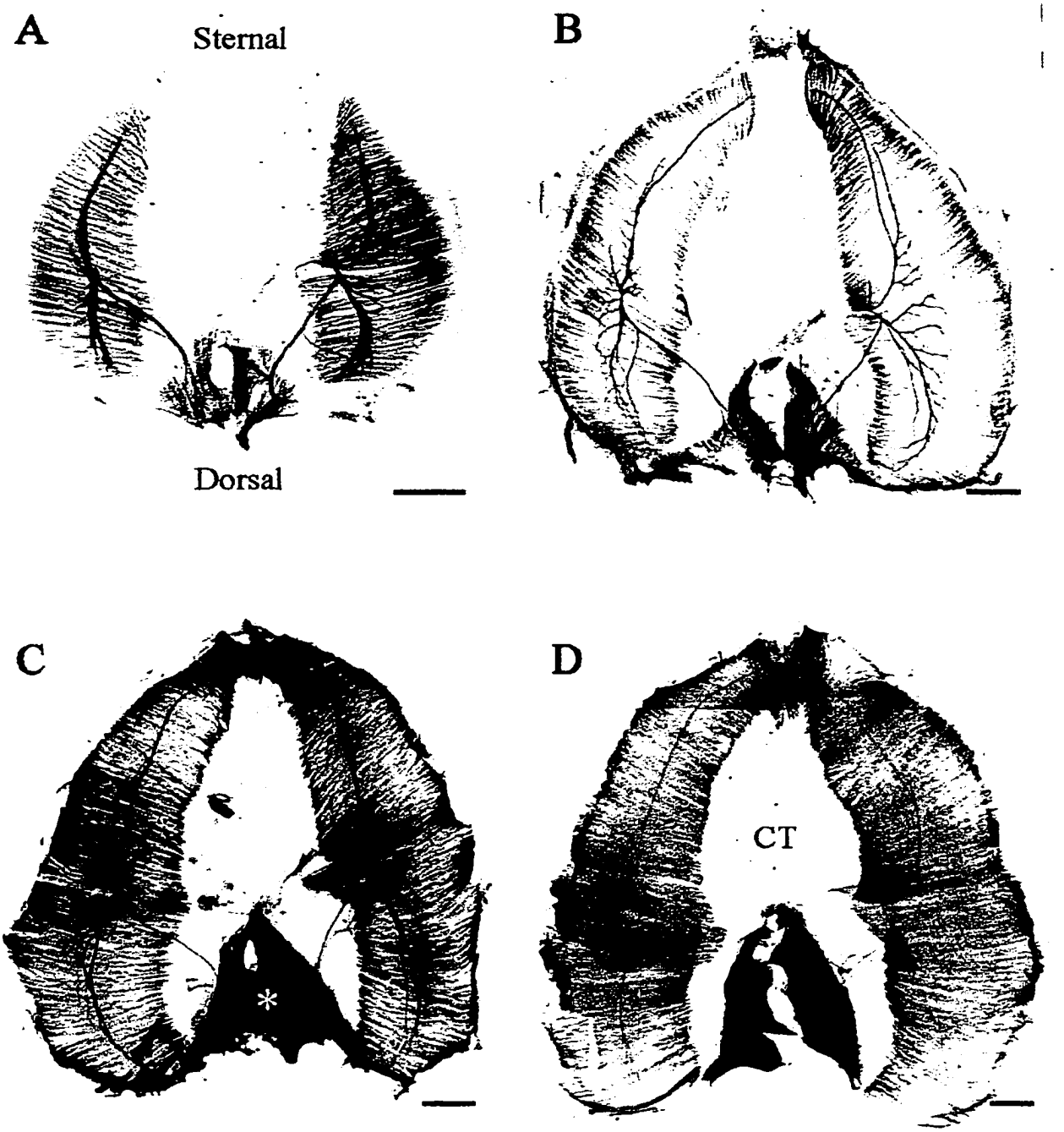

Myogenesis - diaphragm cross sections: In addition to immunolabelling of diaphragm whole mounts, a series of immunoreactions were performed on longitudinal (30-40 μm) and transverse (8-30 μm) cross-sections of embryonic diaphragms in order to illustrate the following two points: 1) The waves of PSA-NCAM expression observed in the whole-mounts were not merely an artifact due to variability in the efficacy of immunolabelling associated with age-related increased thickening of the developing diaphragm. 2) The two waves of PSA-NCAM expression correlated precisely with the two waves of myotube formation characteristic of muscle formation (primary and secondary myogenesis).

Fig. 5.9A shows examples of longitudinal sections from similar regions of immunolabelled diaphragm sections taken from fetuses of various ages. This profile shows the level of PSA-NCAM immunolabelling along the mediolateral aspect of the diaphragm and myotubes. At age E15, PSA-NCAM labelling was restricted to the centre of the hemidiaphragm where the phrenic nerve branch had entered. An adjacent section labelled for total-NCAM is shown to demonstrate that NCAM labelling extended to tissue beyond the developing myotubes throughout early development. By age E16.5, PSA-NCAM labelling was restricted to the medial and lateral ends of myotubes (note that the nerve located at the centre of the myotubes labelled for PSA-NCAM). Total-NCAM immunoreactivity was maintained throughout the whole extent of the myotubes in these diaphragms, although a slight decrease in labelling was often observed in PSA-NCAM-negative regions. The maintenance of PSA-NCAM expression on the medial and lateral extents of myotubes is likely due to ongoing primary myogenesis as primary myotubes preferentially absorb new mononucleated myoblasts at their ends as muscle elongates (Zhang & McLennan, 1995). By age E17, PSA-NCAM expression on myotubes was upregulated within the central portions of the diaphragm, to proceed as it had during primary myogenesis, and then decrease again by E19.

Fig. 5.9B addresses the same issue of the two waves of PSA-NCAM expression by illustrating PSA-NCAM labelling of transverse cross-sections of diaphragm. This profile shows PSA-NCAM immunolabelling on the surface of myotubes along the dorsoventral aspect of the diaphragm, transversely to the myotubes. The arrangement of primary myotubes from cross-sections of diaphragms taken from animals during age E15 was similar to that

described by Yiping et al. (1992), being tightly apposed and arranged in rows (palisades). The majority of the myotubes expressed PSA-NCAM. However, by age E16.5, only the nerve was expressing detectable levels of PSA-NCAM within the central portions of myotubes. By age E17, PSA-NCAM expression continued to be evident in the nerve and also reappeared on the surface of myotubes within the centre of the diaphragm. It is noteworthy that at this stage of secondary myogenesis, there was a dramatic increase in the number and density of myotubes within the diaphragm. By age E19, no labelling for PSA-NCAM in the nerve or myotubes could be detected within diaphragmatic cross-sections.

Fig. 5.9: Immunolabelling of thin sections of diaphragm illustrating the biphasic expression of PSA-NCAM on myotubes. A) Longitudinal sections (30 to 40 μm) of diaphragm muscle taken from fetal rats aged E15, E16.5 and E17 showing the waves of PSA-NCAM labelling along the mediolateral axis of the myotubes. Top two photos also illustrate the restricted localisation of PSA-NCAM labelling within the early developing diaphragm in relation to total-NCAM labelling. PSA expression was high within the central regions of primary myotubes at E15. PSA-NCAM labelling was subsequently down-regulated in the central portion of myotubes at age E16.5, and reappeared within the central portion during secondary myogenesis at age E17. B) Transverse cross-sections (8 to 30 μm) showing the distribution of myotubes and PSA-NCAM labelling in diaphragms from fetal rats aged E15 to E19. Further evidence that PSA-NCAM expression appeared in two waves, during primary (E15) and secondary (E17) myogenesis. At stages between primary and secondary myogenesis (E16.5) and upon completion of secondary myogenesis (E19), PSA-NCAM expression was down-regulated. Arrows point to phrenic axons, showing that PSA-NCAM labelling was constant on the nerve up to E17. Scale bars = 100 μm.

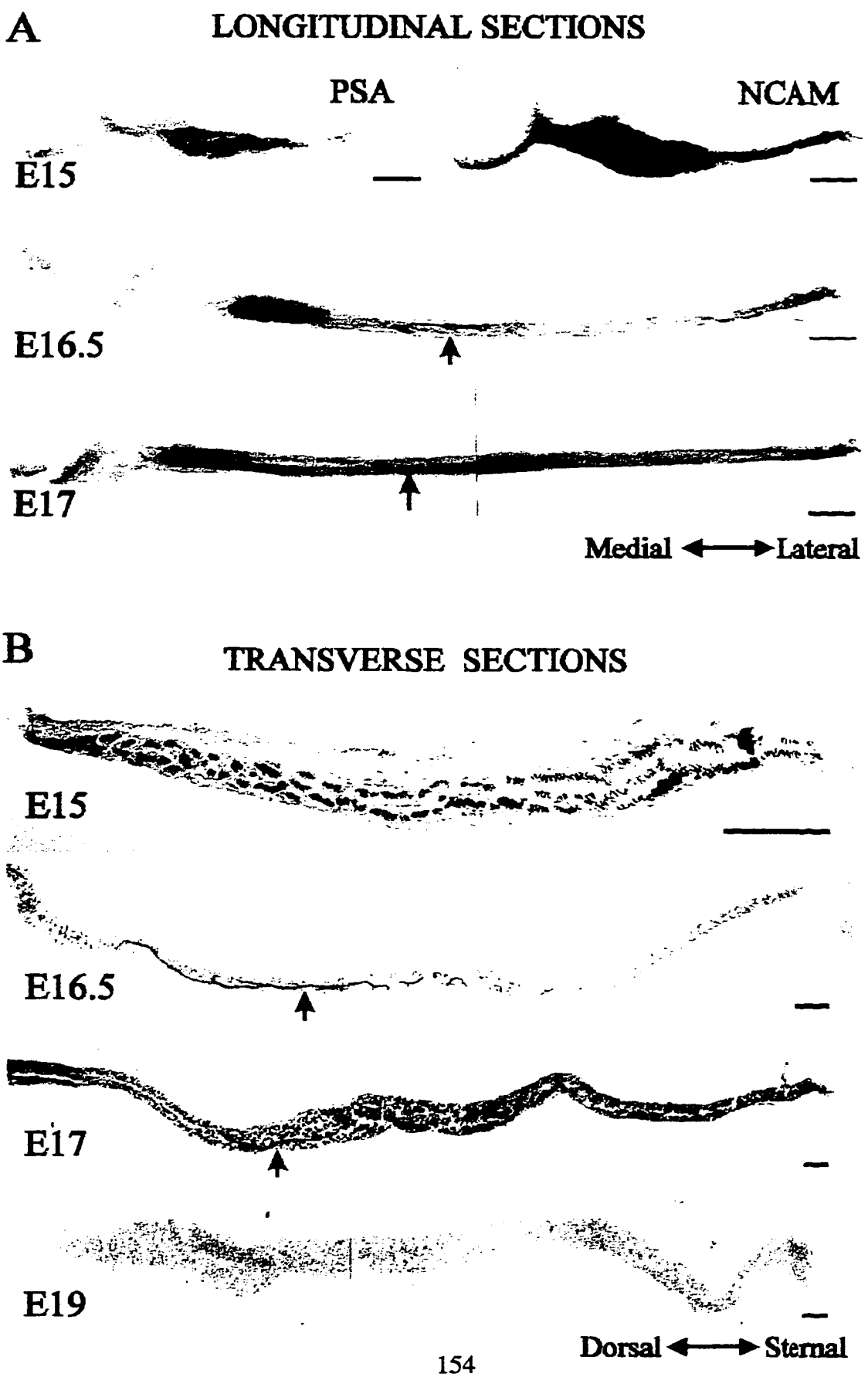

PSA-NCAM expression between developing myotubes: Figs. 5.10B-C show highly magnified views of PSA-NCAM on primary myotubes during age E15. PSA-NCAM labelling was discretely limited to regions of the primary myotube membranes which were in very close contact with their neighbours. This is in contrast to total-NCAM expression which is present on the full extent of the myotube membrane surface through to birth (Covault and Sanes, 1986; Fredette et al., 1993).

Figs. 5.10D-F show a highly magnified view of PSA-NCAM on primary and secondary myotubes at age E17.5. The density of myotubes had increased and two distinct sizes of myotubes were obvious. PSA-NCAM labelling was discretely localised on apposed membranes between adjacent secondary myotubes and between adjacent primary and secondary myotubes. Labelling often appeared as two apposed lines, which were frequently intermittent, indicative of PSA-NCAM expression by both apposed myotubes.

Fig. 5.11 is an illustration which summarises our interpretation of the timing and role of PSA-NCAM expression on primary and secondary myotubes. Specifically, it shows the utilisation of non-polysialylated NCAM in initial myoblast adhesion but the transient up-regulation of PSA-NCAM upon myoblast fusion to enable separation of myotubes (see Discussion below).

Fig. 5.10: Discrete expression of PSA-NCAM on membranes of adjacent primary and secondary myotubes. (A-C) PSA-NCAM labelling of transverse cross-sections (8 μm) of diaphragm (taken during E15) showing the relative localisation of PSA-NCAM expression on developing primary myotubes. (A) is a low magnification view of the muscle cross-section showing the groupings of developing myotubes into distinct clusters throughout the belly of the muscle. Figs. B and C are higher magnifications illustrating that PSA-NCAM labelling was discretely located on portions of primary myotube membranes which are juxtaposed and presumably ready to separate. (D-F) Low (D) and high magnification views (E and F) of diaphragm transverse sections (30 μm) from fetal rats aged E17.5. PSA-NCAM labelling was located on apposing membranes of primary and secondary myotubes. Scale bars = 50 μm (A) 5 μm (B,C) 200 μm (D) 7 μm (E,F).

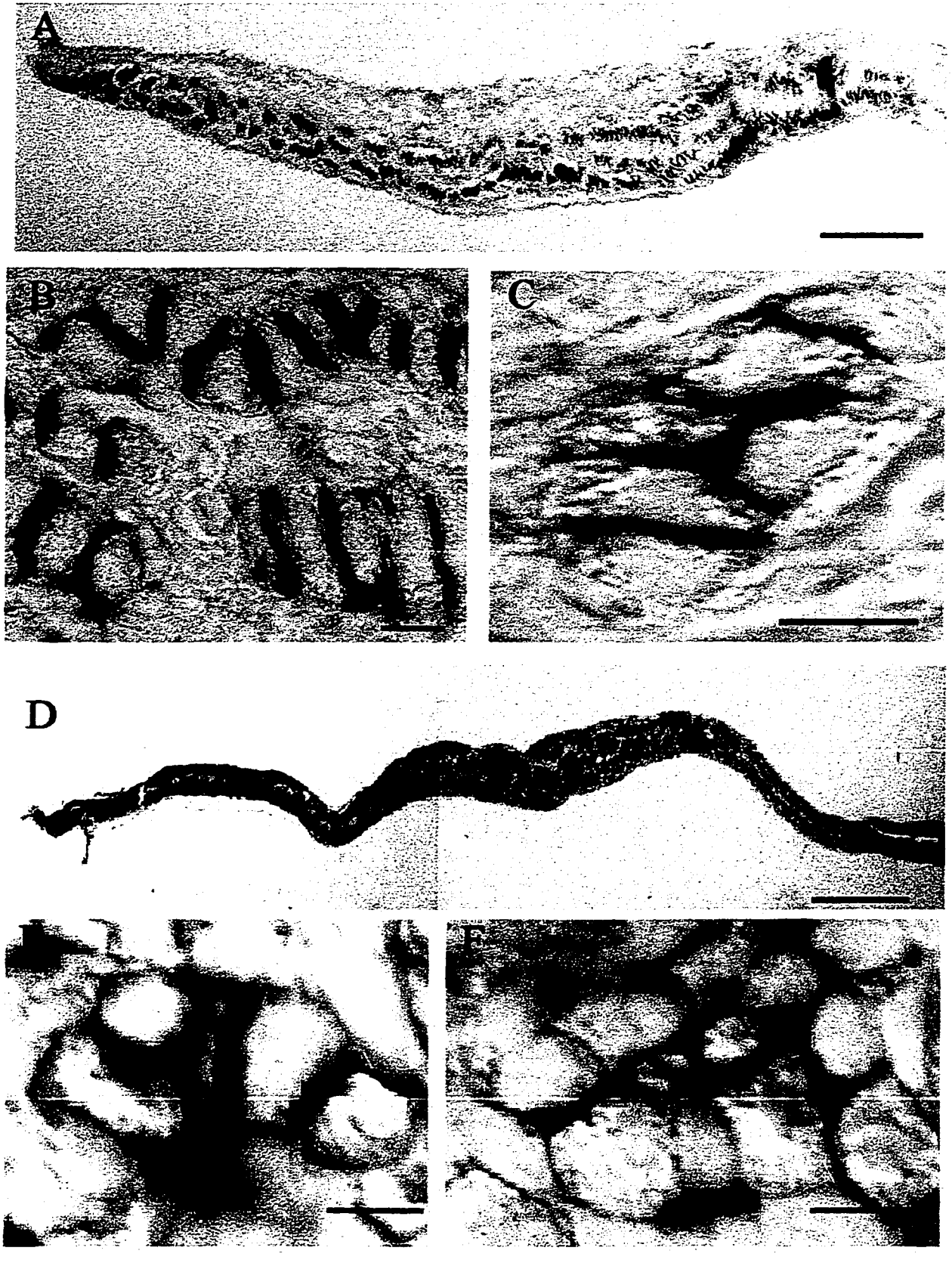

Fig. 5.11: Summary of the expression of PSA-NCAM during primary and secondary myogenesis within the developing diaphragm. Primary myogenesis commences with the fusion of myoblasts. NCAM is likely one of the adhesion molecules involved in this process. Primary myotubes are initially aligned and attached with neighbouring membranes, in part, via NCAM mediated adhesion. Upon fusion, up-regulation of PSA-NCAM on myotube membranes facilitates the separation of primary myotubes. Subsequently, PSA-NCAM is down-regulated along regions where myotubes have separated. Secondary myogenesis proceeds from the central, innervated portion of separated primary myotubes. Increased expression of PSA-NCAM on the membranes of primary and secondary myotubes facilitates separation of primary and secondary myotubes, followed rapidly by down-regulation upon separated regions of myotubes. See Discussion for further details.

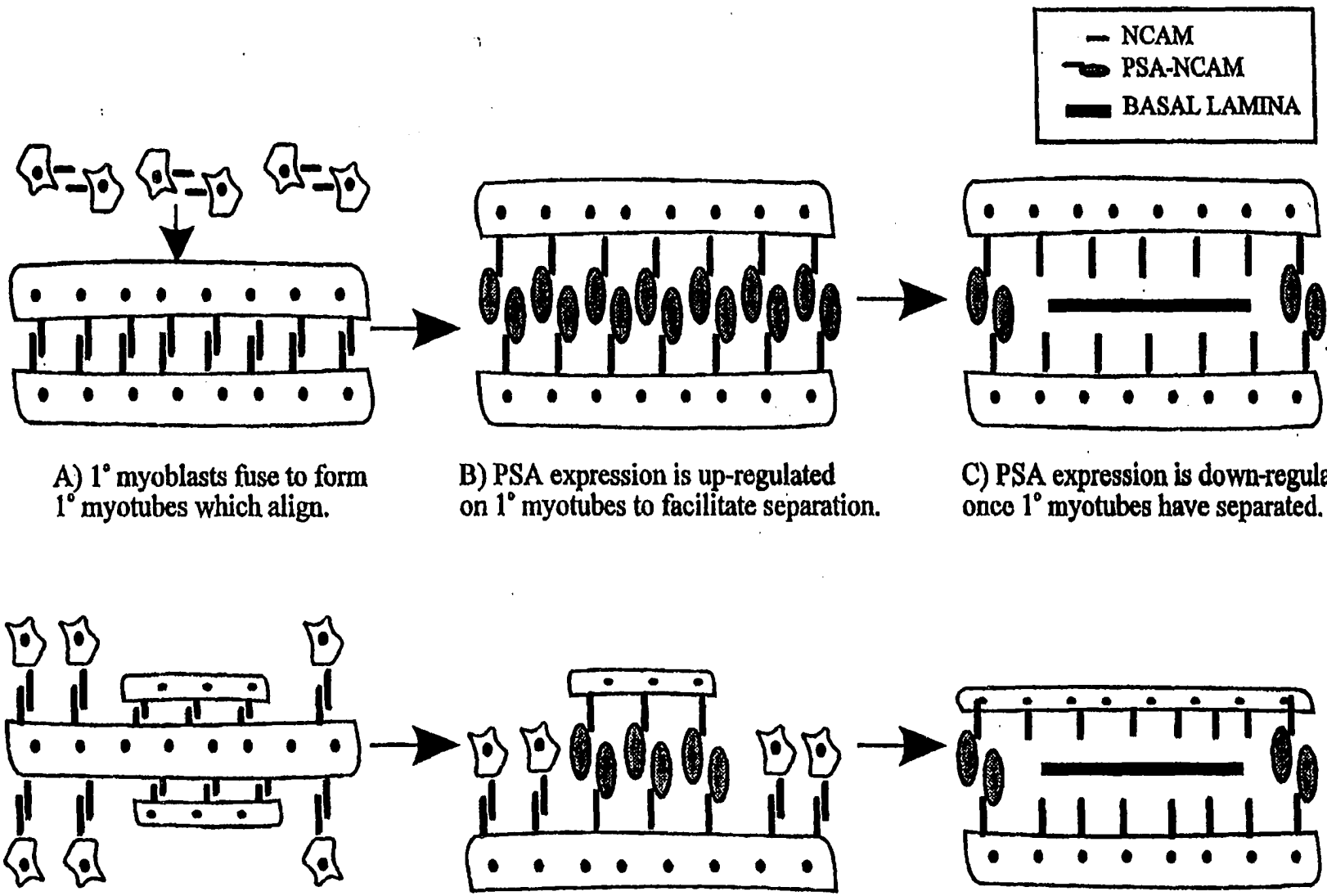

DISCUSSION

PSA-NCAM expression and phrenic nerve guidance.

Guidance of phrenic axon growth and branching is likely controlled by the combined influences of a number of developmentally-regulated molecules expressed by the nerve, muscle and surrounding tissue. In the current study, we examined the expression of one such candidate, PSA-NCAM, which induces membrane separation and thereby, axonal defasciculation. We demonstrate that specific expression of PSA-NCAM by phrenic axons correlates well with a proposed role in phrenic axon guidance at the brachial plexus and intramuscular branching. Further, our data suggest that the segregation of two motor axon populations may be achieved by PSA-NCAM expression of only one population.

PSA-NCAM and phrenic-brachial axon separation

During E12-E13, phrenic and brachial axons from multiple lower cervical segments merge at the brachial plexi. Subsequently, the two populations diverge as phrenic axons continue to grow ventrally towards the diaphragm primordium and brachial axons turn laterally to grow into the limb bud. From the onset of ventral root formation through to the completion of axonal segregation at the brachial plexi, PSA-NCAM expression was high within phrenic and dorsal ramus populations but extremely low or absent in brachial axonal populations. Brachial axons did not start to express regularly high levels of PSA-NCAM until approximately E14, approaching the onset of innervation of the forelimb musculature. Such spatiotemporally restricted PSA-NCAM expression is in contrast to the expression of total-NCAM, L1 and GAP-43, as immunolabelling for these molecules was equivalent for axons in all motor populations at each stage of outgrowth. During motor axon growth into the chick hindlimb, NCAM sialylation occurs coincidentally, and is perhaps triggered by, axonal growth into the plexus region (Tang et al., 1992). However, in the present study, PSA-NCAM expression was expressed at higher levels on a subset of motoneurons from the very initiation of motor axonal outgrowth, before interaction with either the plexus region or the target musculature. Thus, we postulate that during the initial stages of motor axon outgrowth in the rat, levels of NCAM sialylation may be directly governed by groups of

genes, possibly related to population identity (reviewed in Tanabe and Jessell, 1996). Differences in the expression of the LIM homeodomain family of transcription factors have been demonstrated between different populations of spinal motoneurons (Tsuchida et al., 1994; Appel et al., 1995). Such putative differences in the combination of genes transcribed are postulated to drive the expression of unique combinations of molecules by each motoneuron population which contribute to differential axonal pathfinding. Further studies characterising the promoter region of the sialyltransferase(s) responsible for polysialylation of NCAM may shed light on the regulatory mechanism underlying differential levels of PSA-NCAM expression between motoneuron populations (see Yoshida et al., 1996).

At later stages of axonal outgrowth, there were correlations between changes in the polysialylation levels of cervical motor axons and the timing of functional recruitment and target interactions. This agrees with the data illustrating that motoneuron polysialyltranferase activity and concomitant levels of NCAM polysialylation can be modulated by target interaction, synaptogenesis and neuromuscular electrical activity (Brusés et al., 1995). However, the mechanism by which any of these factors might modify polysialylation levels within axons remains undetermined.

From a functional perspective, the distinct expression of PSA-NCAM by phrenic axons at the brachial plexus raises a number of questions with regards to the potential role of PSA-NCAM in promoting the separation of brachial and phrenic axonal populations. The most insightful work to date regarding the actions of PSA-NCAM on the segregation of axonal populations comes from the studies of the developing chick hindlimb by Tang et al. (1992, 1994). In those series of experiments, a combination of PSA removal from NCAM with the enzyme α2,8-linked sialic acid endoneuraminidase (endoN) and the use of function blocking antibodies demonstrated that PSA-NCAM decreased interaxonal adhesion primarily by attenuating L1-mediated adhesion. Specifically, PSA-NCAM acted to interfere with the adhesive interactions of L1 and thus allowed for the necessary axonal defasciculation required for segregation and accurate pathfinding into dorsal and ventral nerve trunks. The data provided in the present study raises the possibility that PSA-NCAM could act similarly in the fetal rat via interference with L1-mediated adhesion between phrenic and brachial axonal populations, both of which express similarly high levels of L1. It is interesting in the

case of phrenic and brachial axons that only one population expressed high levels of PSA-NCAM. In the chick hindlimb, while the absolute levels of PSA-NCAM differs amongst the separating population of axons, there is not the extreme situation where only one axonal population expresses regularly detectable levels of PSA-NCAM. Thus, the current data could be interpreted as; 1) providing evidence suggesting that functionally relevant defasciculation may occur when only one population of axons expresses PSA-NCAM, or 2) PSA-NCAM may be playing a more selective role at the rat brachial plexus than at the chick crural plexus, providing a specific defasciculatory ability to phrenic axons which may be necessary for their differential guidance at the plexus. This raises the intriguing question as to what mediates defasciculation of brachial axons.

Alternatively to the passive role of hindering L1-mediated adhesion, PSA-NCAM may be playing a more instructive role in selective phrenic axon guidance. In this regard, it is interesting that the effect of PSA-NCAM expression on the adhesion of growing axons depends upon the substrate tested (Acheson et al., 1991; Boisseau et al., 1991; Zhang et al., 1992). PSA-NCAM on phrenic axons therefore may be acting to prevent interaction with a putative cue utilised by brachial axons for guidance, or alter the response of phrenic axons to cues common to both phrenics and brachials. Further, the spatial separation of surfaces induced by PSA may promote certain molecular interactions not favoured across closely apposed surfaces, as postulated by Yang et al (1992). See general discussion for information regarding the functional testing of these hypotheses.

Intramuscular branching

At approximately age E14.5, phrenic axons defasciculate to form three characteristic intramuscular branches. The axons which make up the three branches are not compartmentalised into branch-specific fascicles prior to this time (Laskowski & Sanes, 1987). Thus, at the initial point of trifurcation individual axons must separate from their neighbouring axons and reorganise so as to become associated with other axons destined for the same branch (Laskowski & Owens, 1994). The high levels of PSA-NCAM immunoreactivity associated with the primary branching site is consistent with the idea that it is involved in the axonal defasciculation necessary for this re-ordering process

(Landmesser et al., 1990). PSA-NCAM expression remained high in primary and higher order branches of intradiaphragmatic phrenic axons through to age E17.5, at which time the mature pattern of innervation was approximated, the majority of secondary myotubes had formed and respiratory-related rhythmic electrical activity of the phrenic nerve had commenced. Subsequently, from age E17.5 through to E19, PSA-NCAM expression decreased within the nerve in a spatiotemporal manner which parallelled the regional termination of further axonal growth and branching. Total-NCAM expression remained high on phrenic axons up to birth, suggesting that PSA down-regulation is achieved by either specific removal of PSA from NCAM or non-specific turn-over of NCAM coincident with specific down-regulation of NCAM sialylation. The regulatory mechanism controlling PSA-NCAM expression in the nerve is unknown, but there have been suggestions that increased neural activity and/or the interaction between nerve and target is playing a key role in the down-regulation, likely through the modification of polysialyltransferase activity (Landmesser et al., 1990; Brusés et al., 1995). Our results are in general agreement with, and provide a functional correlate, for these proposals, as PSA-NCAM expression within axons of the phrenic nerve starts to decrease when respiratory drive transmission commences (Greer et al., 1992) and when axonal branching has ceased and synaptic maturation is underway within the region innervated by the axon.

PSA-NCAM Expression on Developing Myotubes.

A number of cell adhesion molecules, including several forms of NCAM, integrins and cadherins are developmentally-regulated during myogenesis, and are believed to mediate phases of cell adhesion and separation (Covault et al., 1986; Rosen et al., 1992; Fredette et al., 1993; reviewed in McDonald et al., 1995). As PSA-NCAM functions as an anti-adhesive molecule and is expressed by developing myotubes, it is a prime candidate for involvement in myotube separation. A previous study reported that PSA-NCAM levels within developing chick musculature increased progressively throughout myogenesis, peaking during secondary myogenesis (Fredette et al., 1993). However, it was unclear as to whether PSA-NCAM was associated with separation of primary myotubes, and limitation of its immunoreactivity to free surfaces of myotubes during secondary myogenesis would appear counter-intuitive to

a role in separation.

Past studies have shown that NCAM is expressed on myoblasts and upon all surfaces of developing myotubes during myogenesis (Covault and Sanes, 1986). Our data demonstrates that the NCAM expressed between very closely apposed regions of myotube membranes is highly polysialylated at the time of myotube separation during both primary and secondary myogenesis. Upon myotube separation, more distantly apposed membranes were no longer immunoreactive for PSA-NCAM. Functionally, such localised distribution is consistent with the proposed role for PSA-NCAM as attenuating adhesion at points of cell separation. Further, the absence of PSA-NCAM from free surfaces would allow non-polysialylated NCAM to mediate axon-myotube adhesion. During corticospinal tract development in the spinal cord, a similar cellular restriction of PSA-NCAM over total-NCAM has been observed (Daston et al., 1996), which correlates to the localised ability of those axons to branch. However, the mechanisms(s) responsible for precisely targeting PSA-NCAM over total-NCAM to specific regions of the cell are currently unknown.

It was interesting to note that between myotubes, PSA immunoreactivity seemed to appear on both apposed myotubes transiently during primary and secondary myogenesis. Therefore, primary myotubes may undergo two discrete periods of NCAM sialylation. The intrinsic cellular mechanisms regulating the transient expression of PSA-NCAM on developing myotube membranes are not known, but likely result from precise temporal regulation of either polysialyltransferase activity or alternate splicing of NCAM in isoforms which differ in their ability to be polysialylated. The levels of PSA-NCAM expression by ciliary ganglion neurons is closely regulated by polysialyltransferase activity (Brusés et al., 1995). Further, a temporally-regulated switch of NCAM isoform expression was observed to coincide with polysialylation of NCAM in chick myotubes (Fredette et al., 1993) which may alter affinity for PSA addition (see Small et al., 1988 and Nelson et al., 1995).

The underlying regulator of temporally-regulated change in PSA-NCAM expression on myotubes is not well understood. However, within the diaphragm, PSA-NCAM expression commenced from the onset of primary myotube formation at E14.5, very soon after initial myoblast fusion. The close proximity of axons to newly forming myotubes in the diaphragm implicates axon-myotube communication in triggering myotube formation and

PSA-NCAM expression. At this early stage, phrenic axons are electrically excitable and can induce contraction of diaphragmatic myotubes (Greer et al., 1992; Laskowski and Owens, 1994). The idea of phrenic nerve-induced PSA expression within the diaphragm is further supported by the demonstration that neuromuscular electrical activity and myotube contractility positively regulate myotube expression of PSA-NCAM in a mechanism involving an influx of calcium and activation of protein kinase C (Fredette et al., 1993; Rafuse and Landmesser, 1996). Alternatively, physical contact between developing myotubes was also intimately correlated with PSA-NCAM labelling, with the expression on primary and secondary myotubes commencing upon initial contact and declining after separation. This putative contact-related control may be mediated by any of a combination of inter-myotube gap junctional communication, contact-stimulated myotube surface receptor activity and/or nerve-induced contractile activity.

Summary

The aim of the present study was to examine PSA-NCAM expression during various developmental stages of a model mammalian neuromuscular system, the phrenic nerve-diaphragm axis in fetal rats. PSA-NCAM was highly expressed by phrenic axons throughout nerve outgrowth up to its down-regulation once the mature intramuscular branching pattern had been attained, secondary myogenesis was complete and functional recruitment had commenced. Its pattern of expression suggests a specific role for PSA-NCAM in phrenic axon guidance at the brachial plexus and during intramuscular branching. In relation to muscle development, PSA-NCAM expression was discretely limited, spatially and temporally, to myotubes which were undergoing separation during both primary and secondary myogenesis.

REFERENCES

Acheson A, Sunshine JL, and Rutishauser U (1991) NCAM polysialic acid can regulate both cell-cell and cell-substrate interactions. *J. Cell. Biol.* 114:143-153

Andersson A, Olsen M, Zhernosekov D, Gaardsvoll H, Krog L, Linnemann H and Bock E (1993) Age-related changes in expression of the neural cell adhesion molecule in skeletal muscle: a comparative study of newborn, adult and aged rats. *Biochem. J.* 290: 641-648.

Appel B, Korzh V, Glasgow E, Thor S, Edlund T, Dawid IB and Eisen JS (1995) Motoneuron fate specification revealed by patterned LIM homeobox gene expression in embryonic zebrafish. *Development.* 121: 4117-4125.

Barthels D, Vopper G, Boned A, Cremer H and Wille H (1992) High degree of NCAM diversity generated by alternative RNA splicing in brain and muscle. *Eur. J. Neurosci.* 4: 327-337

Bennett MR and Pettigrew AG (1974) The formation of synapses in striated muscle during development. *J. Physiol. (Lond)* 241: 515-545.

Boisseau S, Nedelec J, Poirier V, Rougon G and Simonneau M (1991) Analysis of high PSA N-CAM expression during mammalian spinal cord and peripheral nervous system development. *Development* 112: 69-82

Brusés JL, Oka S and Rutishauser U (1995) NCAM-associated polysialic acid on ciliary ganglion neurons is regulated by polysialyltransferase levels and interaction with muscle. *J. Neurosci.* 15: 8310-8319.

Chen EW and Chiu AY (1992) Early stages in the development of spinal motor neurons. *J. Comp. Neurol.* 320: 291-303.

Covault J and Sanes JR (1986) Distribution of NCAM in synaptic and extrasynaptic portions of developing and adult skeletal muscle. *J. Cell. Biol.* 102: 716-730.

Covault J, Merlie JP, Goridis C and Sanes JR (1986) Molecular forms of N-CAM and its RNA in developing and denervated skeletal muscle. *J. Cell. Biol.* 102: 731-739

Daniloff JK, Moore V and Oliver EH (1994) Activity of neural cell adhesion molecule (NCAM) components: a review. *Cytobios.* 79: 97-106

Daston MM, Bastmeyer M, Rutishauser U and O'Leary DD (1996) Spatially restricted increase in polysialic acid enhances corticospinal axon branching related to target recognition and innervation. *J. Neurosci.* 16:5488-5497.

Doherty P, Fazeli MS and Walsh FS (1995) The neural cell adhesion molecule and synaptic plasticity. *J. Neurobiol.* 26: 437-446.

Duxson MJ and Sheard PW (1995) Formation of new myotubes occurs exclusively at the multiple innervation zones of an embryonic large muscle. *Dev. Dyn.* 204: 391-405.

Fredette BJ, Rutishauser U and Landmesser L (1993) Regulation and activity-dependence of N-cadherin, NCAM isoforms and polysialic acid on chick myotubes during development. *J. Cell. Biol.* 6: 1867-1888

Greer JJ, Smith JC and Feldman JL (1992) Respiratory and locomotor patterns generated in the fetal rat brain-stem spinal cord in vitro. *J. Neurophysiol.* 67:996-999.

Hall H, Walsh FS and Doherty P (1996) Review: a role for the FGF receptor in the axonal growth response stimulated by cell adhesion molecules? *Cell Adh. & Comm.* 3: 441-450

Harris AJ. (1981) Embryonic growth and innervation of rat skeletal muscles. I. Neural regulation of muscle fiber numbers. *Phil. Trans. R. Soc. Lond. B* 293: 257-277.

Harris AJ, Fitzsimons RB and McEwan JC (1989) Neural control of the sequence of expression of myosin heavy chain isoforms in foetal mammalian muscles. *Development* 107: 751-769.

Hoffman S and Edelman GM (1983) Kinetics of homophilic binding by embryonic and adult forms of the neural cell adhesion molecule. *Proc. Natl. Acad. Sci. USA.* 80: 5761-5766

Kelly AM (1983) Emergence of specialization of skeletal muscle. In *Handbook of Physiology* (L.D. Peachey, Ed.) Section 10, pp. 507-537.

Landmesser L, Dahm L, Schultz K and Rutishauser U (1988) Distinct roles for adhesion molecules during innervation of embryonic chick muscle. *Dev. Biol.* 130: 645-670

Landmesser L, Dahm L, Tang J and Rutishauser U (1990) Polysialic acid as a regulator of intramuscular nerve branching during embryonic development. *Neuron* 4: 655-667.

Laskowski MB and Sanes JR (1987) Topographic mapping of motor pools onto skeletal muscles. *J. Neurosci.* 7: 252-260.

Laskowski MB and Owens JL (1994) Embryonic expression of motoneuron topography in the rat diaphragm muscle. *Dev. Biol.* 166: 502-508.

Lin DM and Goodman CS (1994) Ectopic and increased expression of Fasciclin II alters motoneuron growth cone guidance. *Neuron.* 13: 507-523

Lin DM, Fetter RD, Kopczynski C, Grenninloh G and Goodman CS (1994) Genetic analysis of Fasciclin II in Drosophila: defasciculation, refasciculation, and altered fasciculation. *Neuron* 13: 1055-1069

McDonald KA, Horwitz AF and Knudsen KA (1995) Adhesion molecules and skeletal myogenesis. Semin. *Dev. Biol.* 6: 105-116

Meiri KF, Bickerstaff LE and Schwob JE (1991) Monoclonal antibodies show that kinase C phosphorylation of GAP-43 during axonogenesis is both spatially and temporally restricted in vivo. *J. Cell. Biol.* 112: 991-1007.

Nelson RW, Bates PA and Rutishauser U (1995) Protein determinants for specific polysialylation of the neural cell adhesion molecule. *J. Biol. Chem.* 270: 17171-17179

Phelps PE, Barber RP and Vaughn JE (1988) Generation patterns of four groups of cholinergic neurons in rat cervical spinal cord: A combined tritiated thymidine autoradiographic and choline acetyltransferase immunocytochemical study. *J. Comp. Neurol.* 229: 459-472.

Rafuse VF and Landmesser L (1996) Contractile activity regulates isoform expression and polysialylation of NCAM in cultured myotubes: involvement of Ca^{2+} and protein kinase C. *J. Cell. Biol.* 132: 969-983.

Rosen GD, Sanes JR, LaChance R, Cunningham JM, Roman J and Dean DC (1992) Role for the integrin VLA-4 and its counter receptor VCAM-1 in myogenesis. *Cell* 69: 1107-19.

Rutishauser U, Hoffman S and Edelman GM (1982) Binding properties of a cell adhesion molecule from neural tissue. *Proc. Natl. Acad. Sci. USA.* 79: 685-689

Rutishauser U, Grumet M and Edelman G (1983) Neural cell adhesion molecule mediates initial interactions between spinal cord neurons and muscle cells in culture. *J. Cell. Biol.* 97: 145-150

Rutishauser U and Landmesser L (1996) Polysialic acid in the vertebrate nervous system: a promoter of plasticity in cell-cell interactions. *TINS.* 19: 422-427

Sato C, Kitajima K, Inoue S, Seki T, Troy FA and Inoue Y (1995) Characterization of the antigenic specificity of four different anti-(α2→8-linked polysialic acid) antibodies using lipid-conjugated oligo/polysialic acids. *J. Biol. Chem.* 270:18923-18928.

Schuster CM, Davis GW, Fetter RD and Goodman CS (1996a) Genetic dissection of structural and functional components of synaptic plasticity: I. Fasciclin II controls synaptic stabilization and growth. *Neuron* 17: 641-654

Schuster C.M, Davis GW, Fetter RD and Goodman CS (1996b) Genetic dissection of structural and functional components of synaptic plasticity: II. Fasciclin II controls presynaptic structural plasticity. *Neuron* 17: 655-667

Seki T and Arai Y (1991) Expression of highly polysialated NCAM in the neocortex and piriform cortex of the developing and adult rat. *Anat. Embryol.* 184: 395-401.

Seki T and Arai Y (1993a) Distribution and possible roles of the highly polysialylated neural cell adhesion molecule (NCAM-H) in the developing and adult central nervous system. *Neurosci. Res.* 17: 265-290.

Seki T and Arai Y (1993b) Highly polysialylated NCAM expression in the developing and adult rat spinal cord. *Dev. Brain. Res.* 73: 141-145.

Small SJ, Haines SL and Akeson RA (1988) Polypeptide variation in an N-CAM extracellular immunoglobulin-like fold is developmentally regulated through alternative splicing. *Neuron.* 1: 1007-1017.

Tanabe Y and Jessell TM (1996) Diversity and pattern in the developing spinal cord. *Science.* 274: 1115-1123

Tang J, Landmesser L and Rutishauser U (1992) Polysialic acid influences specific pathfinding by avian motoneurons. *Neuron* 8:1031-1044.

Tang J, Rutishauser U and Landmesser L (1994) Polysialic acid regulates growth cone ehaviour during the sorting of motor axons in the plexus region. *Neuron* 13:405-414.

Tessier-Lavigne M and Goodman CS (1996) The molecular biology of axon guidance. *TINS* 274:1123-1133

Tsuchida T, Ensini M, Morton SB, Baldassare M, Edlund T, Jessell TM and Pfaff SL (1994) Topographic organization of embryonic motor neurons defined by expression of LIM homeobox genes. *Cell* 79: 957-970

Yang P, Yin X and Rutishauser U (1992) Intercellular space is affected by the polysialic acid content of NCAM. *J. Cell. Biol.* 116:1487-1496.

Yang P, Major D and Rutishauser U (1994) Role of charge and hydration in effects of polysialic acid on molecular interactions on and between cell membranes. *J. Biol. Chem.* 269: 23039-23044.

Yiping L, Appelt D, Kelly AM and Franzini-Armstrong C (1992) Differences in the rat histogenesis of EDL and diaphragm in rat. *Dev. Dyn.* 193: 359-369.

Yoshida Y, Kurosawa N, Kanematsu T, Kojima N and Tsuji S (1996) Genomic structure and promoter activity of the mouse polysialic acid synthase gene (mST8Sia II). *J. Biol. Chem.* 271: 30167-30173.

Zhang H, Miller RH and Rutishauser U (1992) Polysialic acid is required for optimal growth of axons on a neuronal substrate. *J. Neurosci.* 12: 3107-3114

Zhang M and McLennan IS (1995) During secondary myotube formation, primary myotubes preferentially absorb new nuclei at their ends. *Dev. Dyn.* 204: 168-177.

Zhu H, Wu F and Sketcher S (1995) Changes in expression and distribution of *Aplysia* cell adhesion molecules can influence synapse formation and elimination *in vitro*. *J. Neurosci.* 15: 4173-4183.

Chapter 6

THE ROLE OF PSA-NCAM EXPRESSION IN EMBRYONIC MAMMALIAN AND AVIAN MYOGENESIS

Upon completion, to be submitted under the following authorship:

Douglas W. Allan, Wei Zhang and John J. Greer

INTRODUCTION

This chapter presents data regarding the functional testing of the role and regulation of PSA-NCAM expression in the fetal diaphragm. This study is not yet complete and a number of key aspects are awaiting confirmation and testing, but sufficient work has been performed to elucidate certain trends.

During muscle morphogenesis, phases of muscle cell fusion and separation associated with both primary and secondary myogenesis are postulated to be mediated by the relative balance of repulsion and adhesion, as dictated by the relative contribution of cell adhesion molecules expressed on the surfaces of apposed muscle cells (Kelly, 1983; eg. Covault et al., 1986; Rosen et al., 1992; Fredette et al., 1993; reviewed in McDonald et al., 1995). Studies presented in chapter 5 have demonstrated that the expression of PSA-NCAM is concentrated on the apposed surfaces of myotubes undergoing separation during both primary and secondary myogenesis. The PSA form of NCAM appears to be discretely targeted to apposed membranes on myotubes, indicating a high degree of selectivity in targeting. Immunoreactivity for total NCAM is observed on all myoblast and myotube surfaces throughout both chick and rat embryonic development (Covault and Sanes, 1986, Fredette et al., 1993, chapter 5). Functionally, such localised distribution is consistent with the proposed role for PSA-NCAM as attenuating adhesion at points of cell separation. However, functional testing for the role of PSA-NCAM in myotube separation has not been reported.

Ongoing work presented here is aimed at testing the effects of removing PSA from NCAM on the separation of myotubes in both rodent and chick muscle. This is being performed in two ways: 1) enzymatic removal of PSA from NCAM utilising α-2,8 endoneuraminidase N (endoN), and 2) examination of muscle development in mice null mutant for NCAM. Unfortunately, a colony of NCAM null mutant mice has only just been established and thus our studies of these animals shall commence after thesis submission. To date, PSA-NCAM removal from the rat diaphragm has been successful in only one trial, most likely due to the difficulty in obtaining the required level of endoN activity in the diaphragm (which is too thin the inject directly). In any case, endoN had a dramatic effect on the development of the diaphragm in this trial. Phrenic intramuscular branching was reduced (as

would be predicted, Landmesser et al., 1990) and separation of primary myotubes was severely retarded, as would be predicted from the proposed role of PSA-NCAM in muscle morphogenesis (Fredette et al., 1993; chapter 5). In direct contrast to this, injection of endoN into the hindlimb of the chick does not appear to affect the ability of muscle cells to separate during either primary or secondary myogenesis. This implies that subtle differences in the molecular regulation of muscle morphogenesis may exist between rat and chick muscle, or between the diaphragm and other muscles.

Currently, the mechanisms regulating the expression of PSA-NCAM are poorly understood. One important regulator of PSA-NCAM expression is electrical activity. Blockade of neuromuscular transmission decreases muscle PSA-NCAM expression (Fredette et al., 1993). *In vitro*, spontaneous activity and electrical excitation of muscle cells upregulates PSA-NCAM expression (Rafuse and Landmesser, 1996), in a Ca^{2+}-dependent manner. Ultimately, the transient expression of PSA-NCAM on developing myotube membranes is likely regulated by the modulation of polysialyltransferase expression and its activity (see Brusés et al., 1995; Brusés and Rutishauser, 1998; reviewed by Nakayama et al., 1998). In this regard, it is interesting that polysialyltransferase activity is positively regulated by Ca^{2+} (Brusés and Rutishauser, 1998). Within the rat diaphragm, PSA-NCAM expression commenced from the onset of primary myotube formation at E14.5, very soon after initial myoblast fusion. The close proximity of axons to newly forming myotubes in the rat diaphragm (see chapters 4 and 5) implicates axon-myotube communication in triggering PSA-NCAM expression. At this early stage, phrenic axons are electrically excitable and can induce contraction of diaphragmatic myotubes (Greer et al., 1992; Laskowski and Owens, 1994). This raises the question as to whether the onset and regulation of PSA-NCAM expression by embryonic muscle is regulated by innervation. We chose to examine the effects of removal of innervation on the diaphragmatic expression of PSA-NCAM and resultant muscle morphogenesis.

Previous studies have examined muscle development in the absence of innervation. Several main strategies have been utilised, including neural tube removal prior to muscle formation in chick (Fredette and Landmesser, 1991), neuronal destruction prior to and during muscle formation using the presynaptic neurotoxin β-bungarotoxin which kills embryonic

neurons in chick (Hirokawa, 1978) and rat (Harris, 1981; McCaig et al., 1987; Condon et al., 1990), and examination of myogenesis in mouse mutants, such as *peroneal muscular atrophy* (*pma*) in which certain muscles of the lower limb receive neither motor nor sensory innervation (Ashby et al., 1992), and in *Wnt-1* null mutants where extraocular muscles develop in the complete absence of oculomotor and trochlear motoneurons (Porter and Baker, 1997) All paradigms demonstrate that prevention of innervation results in the development of severely atrophied muscles. With regards to morphogenesis, myotube separation in chick hindlimb muscles is retarded when the neural tube has been removed (Fredette and Landmesser, 1991), but PSA-NCAM levels have not been reported for denervated muscle. Given that reduction of PSA-NCAM in muscle after blockade of neuromuscular transmission may cause inhibition of myotube separation in these muscles (Fredette and Landmesser, 1993), one would anticipate that an equivalent mechanism results in lack of myotube separation in denervated muscles.

We have examined PSA-NCAM expression in diaphragms that developed in the absence of innervation, by injecting the neurotoxin, β-bungarotoxin, into E13.5 fetuses. In contrast to what we had expected, muscle PSA-NCAM expression is maintained (and perhaps even enhanced) in aneural diaphragms. Further, down-regulation of expression by E20 proceeds approximately as in innervated diaphragms, although the transient down-regulation observed at E16.5 does not occur. Evidence that the aneural diaphragm is spontaneously electrically active provides a possible explanation for PSA-NCAM expression in the aneural diaphragm. Similar denervation of chick hindlimb musculature confirms previous reports that denervation inhibits myotube separation in these muscles. Preliminary evidence implies that PSA-NCAM levels are reduced in denervated chick hindlimb muscles. Ongoing work is aimed at further characterising these early results.

METHODS

Purification of endoneuraminidaseN

This was performed in the laboratory of Dr. W. Gallin (Department of Zoology, University of Alberta), utilising materials provided by his laboratory. Purification of Endoneuraminidase N (endoN), a soluble bacteriophage-induced endo N-acetylneuraminidase, specifically hydrolyses poly-α-2,8-linked sialosyl residues with a minimum polymeric size of 5 and above. This widely used enzyme has a high specificity for the α-2-8-linked PSA present on NCAM in vertebrates. Purification of this enzyme followed the original protocol of Hallenbeck et al. (1987), with slight modifications.

Briefly, 12L of LB broth containing EV36 bacteria was infected by addition of KIF bacteriophage and cultured until bacterial lysis occurred. This was saturated to 50% with ammonium sulphate and protein and debris was pelleted with centrifugation at 18,000g. Pellets were resuspended into 10mM Tris.HCl (pH 7.6) and subsequently centrifuged at 18,000g to remove cellular debris from suspended protein. Pooled supernatants were ultracentrifuged at 150,000g for 60mins to remove further contaminating debris, particularly phage particles. Supernatant was dialysed exhaustively against 10mM Tris.HCl (pH 7.6) utilising 25kDa dialysis tubing. The remaining dialysate was loaded on a DEAE cellulose ion exchange column and fractionated across a 0 to 0.4M NaCl linear gradient. Fraction spectrophotometer readings at OD_{280} were taken and chosen fractions were assayed for endoN activity. EndoN activity within these fractions was assayed by their ability to digest poly-α2,8-linked sialic acid of colominic acid. Incubation of 100μg colominic acid with 10μl of each fraction for 1 hour was followed by assay of colominic acid digestion by its mobility on silica gel G TLC plates, as revealed by reduction of Bial reagent, producing a purple colour. Thirteen fractions demonstrated strong endoN activity. Pooled active fractions were precipitated with 50% ammonium sulphate and centrifuged at 16,000g. Pellets were resuspended in a sodium phosphate buffer (pH 6.8) and dialysed exhaustively against the same buffer. EndoN was extracted from the dialysate using an equal volume of hydroxyapatite and supernatant was precipitated by saturation to 50% with ammonium sulphate. Pellets were spun at 16,000g, resuspended in 10mM Tris (pH 7.6), dialysed

exhaustively against this same buffer, and stored as a 50% glycerol solution at -20°C. Specific endoN activity was assayed by incubation of serial two fold dilutions of the purified endoN solution with 100μg colominic acid, followed by assay of colominic acid digestion products by running incubates on TLC plates and chromogenic exposure of reducing sugars to Bial reagent. The purified endoN demonstrated a specific activity of approximately 12,800U/ml (Fig 1A). This solution was aliquoted and sterilised by centrifugal filtration through 0.22μm centrifugal Utrafree-MC filters (Millipore, Bedford, MA). SDS-PAGE on a 7% gel, transfer to a nitrocellulose membrane (as described below) and Ponceau S protein staining revealed that the purified endoN solution migrated as a single band at approximately 105kDa, as previously described (Hallenbeck et al., 1987).

Determination of endoN activity on PSA-NCAM by SDS-PAGE and Western blotting

The activity of the enzyme on vertebrate PSA-NCAM was confirmed by SDS-PAGE and Western blot analysis. Pooled E18 rat diaphragm (during secondary myogenesis) was utilised as the test tissue (Fig. 1B). Tissues were homogenised, sonicated and centrifuged in a 0.05M Tris buffer with 1% Triton X-100 and 1% protease inhibitor cocktail (Cocktail #3, Calbiochem), and adjusted to 1.5mg/ml using the BCA total protein assay method (Pierce). 100μl aliquots of each homogenate was incubated at 37°C for 1hour with either 1μl of endoN or boiled endoN. 30μg of each sample was resolved by SDS-PAGE on a 6% gel and transferred to nitrocellulose membranes. Western blot analysis (Fig 1B) was performed using a rabbit anti-NCAM polyclonal antiserum (a generous gift from E. Bock, U. Copenhagen). This was followed by appropriate biotinylated secondary antibodies (Sigma, St Louis), followed by 1% avidin biotinylated-peroxidase complex (ABC) (Vectastain, ABC Kit PK-4000). Antibody binding was visualised using the ECL method (Santa Cruz) and exposed films were developed in an automated film developer.

In utero rat fetus drug treatment

1-1.5μl of purified endoN or 1μl of β-Bungarotoxin (1mg/ml) in sterile 0.9% saline was injected via a sterile pulled microelectrode into individual E13-E13.5 rat fetuses. Previous studies (Harris, 1981; McCaig et al., 1987) have demonstrated that this dose of β-

Bungarotoxin at this age results in total denervation of the diaphragm within 24 hours. In this study, GAP-43 immunodetection of intradiaphragmatic axons revealed total denervation within 24 hours (earliest time tested), and elimination of all motoneurons from the C3-C5 cervical spinal cord segments, as detected by haematoxylin and eosin histochemistry (not shown). At E13-E13.5, it is only possible to discern the fetal forelimb and head through the uterus with strong trans-illumination, primarily due to the thickness of the decidual layer. Both drugs were injected into the brachial region of the fetus, in the approximate area of the phrenic nerve and diaphragm at this age. Injections into this site provided approximately 75-80% fetal survival and proved successful for the desired drug action on the phrenic nerve and diaphragm. A maximum of three fetuses were injected within each litter as increasing the number of injected fetuses reduced the number of surviving fetuses, both injected and non-injected. Controls for β-bungarotoxin injections consisted of saline injected into another fetus of the same litter and of boiled endoN into another fetus for endoN controls. It was an exception, rather than the rule that both control injected and drug injected fetuses survived within any one litter over the treatment period. For this reason, we compared control injected and drug injected fetuses with fetuses which had not been injected. In all cases where control injected fetuses could be compared with non-injected fetuses, no differences in any of the parameters tested were observed.

Drug treatment of chick fetuses

1-1.5μl purified endoN or 1mg/ml β-Bungarotoxin in sterile 0.9% saline was injected via a sterile pulled microelectrode into chick right thighs at St 29 and St 34 to analyse primary and secondary myotube development after either PSA removal or denervation, respectively. Controls for β-Bungarotoxin consisted of 0.9% NaCl injection and for EndoN, boiled endoN was injected. As with the rat injections, no differences were observed when all tested parameters were compared between control injections and fetuses which had not been injected. Denervation of chick thighs could be visualised by the complete absence of nerves within the hindlimb (most notably the sciatic nerve), as determined histologically. 2mg (+)-tubocurarine (Sigma) in 100μl sterile 0.9% NaCl was injected daily through a small window placed in the egg shell onto the chorioallantoic membrane of embryos age-matched

to controls. Treatments commenced at St 29 and St 34 to analyse primary and secondary myotube development after paralysis, respectively. This treatment has previously been shown to block nerve induced contraction of skeletal muscle of embryos over the treatment period (Fredette and Landmesser, 1991; Fredette et al., 1993). Only embryos which remained paralysed throughout the experimental period were further examined. Controls consisted of similarly treated embryos with vehicle-only.

Tissue Preparation

Rat Embryos treated with EndoN

Injected fetuses were removed during late E16, after the completion of primary myogenesis in the region adjacent to the vena cava, PSA-NCAM expression had been reduced and the onset of secondary myogenesis was apparent. Diaphragms were isolated and further dissected to obtain: 1) whole left hemidiaphragm, 2) whole crus and 3) the region adjacent to the vena cava on the right hemidiaphragm, dissected in such a way that the region of innervation was identifiable in serial sections. The crus was immunostained freefloating for PSA-NCAM to test the efficacy of the endoN injection. This tissue maintains the highest level of PSA-NCAM expression and thus was a satisfactory rapid assay. The left hemidiaphragm was immunostained free floating for GAP-43 to visualise the full extent of the intramuscular phrenic branches. The dissected right hemidiaphragm was processed and cut for paraffin embedded microtome sectioning at 5μm. Serial ribbons were alternately processed for haematoxylin and eosin staining to visualise the morphology (see below) and anti-laminin immunohistochemistry to visualise the basal lamina to functionally test for myotube separation. Only diaphragms in which PSA-NCAM removal was complete were further analysed. Generally, we found that every injection resulted in a reduction (often dramatic) in PSA-NCAM levels. No effect on muscle morphogenesis was observed in these fetuses. However, only one fetus thus far (out of approximately 26 injected), has had PSA-NCAM levels totally abolished. The data from this fetus is presented.

Rat Embryos treated with β-Bungarotoxin

Injected fetuses were removed at all ages subsequent to injection. A number of these were processed to ascertain PSA-NCAM immunolabelling by standard techniques. In order

to visualise the distribution of PSA-NCAM expression on aneural myotubes, immunolabelled diaphragms were microtome sectioned (5μm) and eosin stained. A number of fetuses were processed to visualise the morphology of developing myotubes in aneural muscle by haematoxylin and eosin staining. These were processed as described below.

Chick Embryos

Chick embryos were raised from fertilised white leghorn chicken eggs in an incubator at 37°C. Embryos were staged according to the Hamburger-Hamilton staging series (1951), hindlimbs were removed and fixed in an extended position in 4% paraformaldehyde for 2 hrs. The thigh was then embedded in paraffin wax and sectioned transversely to the developing muscle fibres at 3-5μm and placed on Superfrost Plus slides. Chosen sections were processed as described below. In all cases, the exact same methodology was rigorously followed to standardise tissues taken at different times.

Histology

Slides of sections chosen for comparison between control and drug-exposed tissues were serially rehydrated and placed in Gill's Haematoxylin (Formulation #1: Fisher Scientific) for 1 to 2 minutes, washed in water and placed in eosin (in 95% ethanol) for 10 secs. Slides were washed in 95% ethanol, dehydrated, cleared in xylene and mounted in entellan mounting medium.

Rat diaphragm section immunohistology

All sections were serially rehydrated and washed in PBS. Antigenic retrieval by proteinase K treatment was followed by washing, incubation in 10% goat serum for 30mins and incubation in 1:50 anti-laminin (Sigma polyclonal antisera) for 2 hours. After washing and appropriate secondary antibody labelling for 30mins, labelling was visualised using 1% Streptavidin-Alexa 546 (Molecular Probes, Eugene, Or). Nuclei were further visualised by a 10min DAPI nuclear stain, and the sections were mounted in Cytoseal and examined under appropriate fluorescent light on a Leitz Diaplan microscope. Controls were provided by primary antibody omission. In all cases when the staining profile was compared, all sections were processed concurrently using a common stock solution during each step.

Chick hindlimb section immunohistology

All sections were serially rehydrated and washed in PBS. For PSA-NCAM immunostaining, sections were processed as above for PSA-NCAM, except that incubation times were shortened, 10 minutes for the methanol/hydrogen peroxide, 2 hours for the primary antibody, and 30mins for all other steps. Sections were lightly counter-stained with a brief eosin exposure and mounted in entellan.

Assessment of apoptosis in the rat diaphragm

Paraffin-embedded and microtome-sectioned rat diaphragms were analysed for the extent of apoptosis using an In Situ Cell Death Detection Kit (Boehringer Mannheim, #1 684 809). Methods were performed as per the manufacturer's instructions. Ribbons containing control and aneural diaphragm sections were mounted onto a single slide. These were serially rehydrated, exposed to proteinase K (20μg/ml) for 15mins and washed in PBS. One half of each ribbon was used for controls, the other half for tests of apoptosis levels. Essentially, terminal deoxynucleotidyl transferase catalyses the addition of fluorescein coupled nucleotides to segments of single stranded DNA. An anti-fluorescein antibody conjugated to alkaline phosphatase recognises fluorescein on the DNA. Catalytic conversion of an alkaline phosphatase substrate to a red deposit visualises the cells. Controls included the omission of the terminal transferase for negatives, and DNAse I (0.5mg/ml, 10mins) to break up the DNA for positives (not shown).

Measurement of embryonic rat diaphragm EMG

EMGs were recorded from control and aneural embryonic rat diaphragms. The diaphragm was pinned horizontally to a home-made Sylgard platform. The tissue was bathed in a modified Krebs-Ringer solution at 27±1°C during both the dissections and recordings. The solution contained (in mM): NaCl (117), KCl (6), Na_2HPO_4 (1.3), $CaCl_2$ (2.6), $MgSO_4$ (1.3), $NaHCO_3$ (24), glucose (10); pH 7.4 following bubbling with 95%O_2 and 5% CO_2. Embedded into the Sylgard platform were two rows of pins for recording electrical activity. Switching between different pins between the two rows allowed for recording of maximal response. Signals were amplified, low pass filtered and recorded on line with Axotape.

Spontaneous activity of aneural diaphragms was pharmacologically tested. We added (+)-tubocurarine to a final bath concentration of 40μM. We had previously determined that this concentration was adequate to block nerve-induced neuromuscular transmission and contraction of the control diaphragm (not shown). We then added tetrodotoxin to a final bath concentration of 1μM. This blocked all spontaneous activity.

RESULTS

Testing EndoN activity.

First, we examined the ability of our endoN to cleave purified colominic acid, and α-2,8-linked polysialic acid. Fig. 1A shows TLC analysis of endoN activity. 10μl of serially diluted endoN was incubated with 100μg colominic acid for 1hr at 37°C. These were then spotted onto TLC plates and chromatographic separation of cleaved colominic acid was observed as migratory activity from the point of origin. No migration was observed in controls (not shown). In dilutions of 1:256 and 1:512, a lack of complete colominic acid digestion results in a circle of sialic acid at the point of origin. As can be observed, complete digestion and migration of colominic acid can be observed up to a dilution of 1:128, giving a specific activity of 12,800U/ml.

Prior to testing the role of PSA-NCAM in vertebrate myogenesis, we first had to confirm that our endoN could completely remove PSA from NCAM. E18 rat diaphragms (during secondary myogenesis) were pooled. Immunolabelling for total NCAM is shown for immunoblots of endoN treated and boiled endoN treated rat tissue in Fig.1B. This shows that the smear of labelling (due to PSA on NCAM) in the control is removed to reveal three major bands as published by Andersson et al., 1993). Interestingly, the GPI-linked 120kD band appears to be the most heavily expressed during secondary myogenesis. This reflects the upregulation of this isoform during secondary myogenesis in the chick hindlimb (Fredette et al., 1993).

Fig 6.1: Testing efficacy of endoneuraminidase enzyme.

A) Results from TLC analysis of colominic acid digestion by endoN. 10μl aliquots of the serially diluted enzyme from 1:1 to 1:512 were incubated with 100μg of colominic acid. As can be observed in the 1:256 and 1:512 lane, undigested colominic acid can be observed as a circle of unmigrated poysialic acid at the point of origin. Up to 1:128, complete digestion of colominic acid had occurred. B) Western blot analysis of the effects of endoN on rat diaphragm homogenates. The same tissue homogenate was incubated with 1μl boiled endoN (lane 1) or 1μl endoN (Lane 2). After separation by 7% SDS-PAGE, the presence of NCAM was revealed by immunolabelling for total NCAM. EndoN had removed the PSA (smear) from NCAM to reveal the three major isoforms of NCAM, as previously published (see text).

A

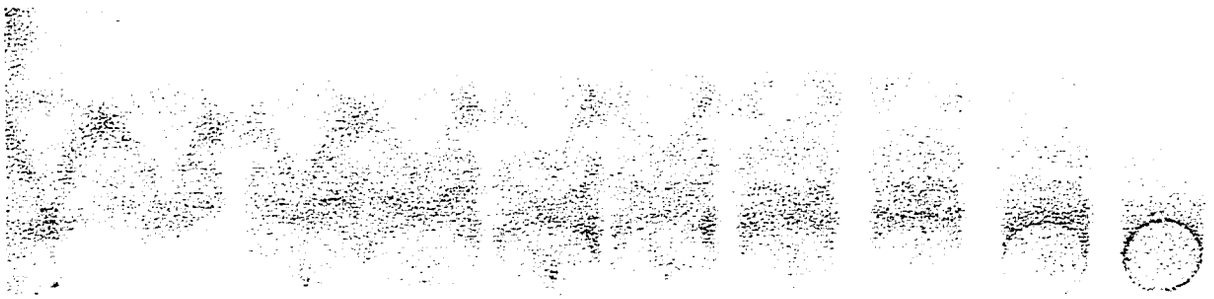

1 2 4 8 16 32 64 128 256 512

B

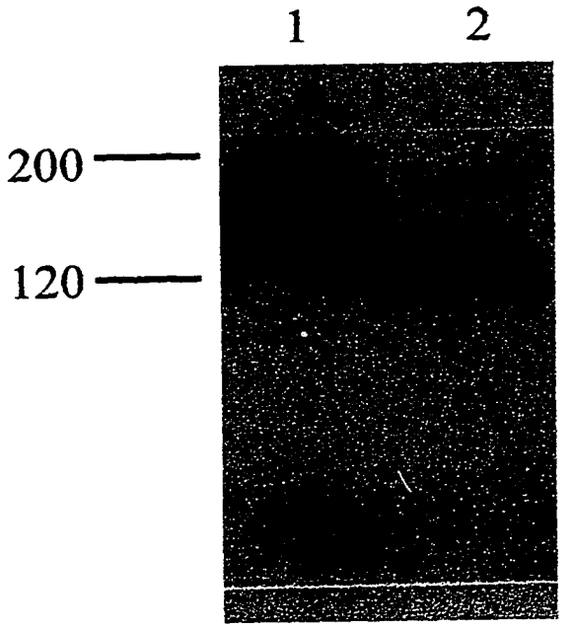

EndoN treatment of rat fetuses.

Our decision to focus on the role of PSA-NCAM during primary myogenesis reflected our success in the complete removal of PSA during primary, as opposed to secondary, myogenesis. As direct injection of the diaphragm is not possible at any age, we had to rely upon the diffusion of endoN from the injection site to the diaphragm. This would appear to be more successful in the smaller embryo at E13.5 (7mm, crown to rump) as opposed to E16 (14mm). At best, we could obtain dramatic reductions, but not abolition, of PSA levels throughout secondary myogenesis. Merely reducing, but not abolishing, PSA levels did not appear to alter the normal course of muscle morphogenesis in any obvious way during either primary or secondary myogenesis (not shown). In such cases, it is difficult to assess whether a reduced level of PSA is capable of maintaining normal function or whether PSA has no primary role in myotube separation. To avoid this ambiguity, we limited our analysis to diaphragms in which PSA had been totally removed. Thus far, we have obtained one diaphragm which demonstrated a total abolition of PSA immunoreactivity (as assessed by 12E3 MAb) by E16.5.

PSA removal retards primary myotube separation and phrenic intramuscular branching

From E13.5 to E16.5, primary myogenesis occurs across the majority of the diaphragm and a characteristic phrenic intramuscular branching pattern develops (see chapter 5). GAP-43 immunohistochemistry was utilised to determine the branching pattern of phrenic motor axons across the diaphragm after endoN treatment. Normal branching can be seen in Fig 6.2D. This is compared to that obtained after endoN treatment in Fig 6.2B. A reduction in higher order branching is observed, although the three primary branches are well formed and innervation covers the extent of the musculature. Further characterisation of this requires more samples.

Both morphological (haematoxylin and eosin (H&E) histology, Fig 6.3) and functional (laminin immunofluorescence, Fig 6.4, 6.5) criteria were utilised to assess the extent of myotube separation after primary myogenesis in control and the endoN treated fetus. By E16.5 in control muscles (Fig 6.3A), large cytoplasmic cells consistent with primary myotubes had separated and their surfaces had become intimately associated with

nuclear dense secondary myoblasts in tight clusters. In endoN treated muscles, equivalent large cytoplasmic primary myotubes were clustered into condensed pools, with the nuclear dense secondary myoblasts restricted to the outer surfaces of these pools (Fig 6.3B). Laminin immuofluorescence (Fig 6.4A) combined with nuclear staining with DAPI (Fig 6.5B) confirms that clusters containing only a few nuclei are contained within their own basal lamina in control tissue. In endoN treated fetuses, laminin immunofluorescence (Fig 6.4B) confirmed that the basal lamina had not fully penetrated these large clusters, with the observation that larger laminin profiles contained a greater number of nuclei than in controls (Fig 6.5B). These results clearly indicate an inhibition of myotube separation as a result of PSA removal.

It should be stressed that the differences between the control and endoN treated diaphragms occurred on a more probabilistic than absolute basis. EndoN treated diaphragms did not exclusively contain large primary myotube clusters, as isolated primary myotubes with associated secondary myoblasts were observed. Likewise, in control muscles, not all primary myotubes had become fully separated and a few small clusters of primary myotubes were observed. However, we have never found an example in control muscles where clusters of primary myotubes were either so frequent or so large as those common to this endoN treated muscle. Thus, we are confident that PSA removal has directly caused a dramatic retardation of primary myotube separation in this rat diaphragm. We are continuing our attempts to repeat this experiment at least two to three more times to confirm these results.

Fig. 6.2: EndoN injection removes PSA-NCAM from the developing diaphragm and reduces phrenic nerve intramuscular branching.

Control (C,D) and endoN-injected (A,B) litter mates at late E16. Panels A,C show the expression of PSA-NCAM in the crus of each diaphragm. In C, PSA-NCAM expression appears as intermittent lines of labelling running the length of each crural half. In A, PSA-NCAM was entirely missing. B,D) the left hemidiaphragm from the same diaphragm as in A,C. In D, the labelling for GAP-43 clearly shows the normal phrenic branching pattern at this age. B shows that the elaboration of higher order branches has been reduced after endoN injection, despite the normal elaboration of the typical branching pattern. Greater background in A is primarily due to higher density of tissue in the endoN treated diaphragm, see Fig. 6.3. Fetuses treated with boiled endoN have an appearance equivalent to controls in all respects and have not been shown here. Scale bars = 250μm.

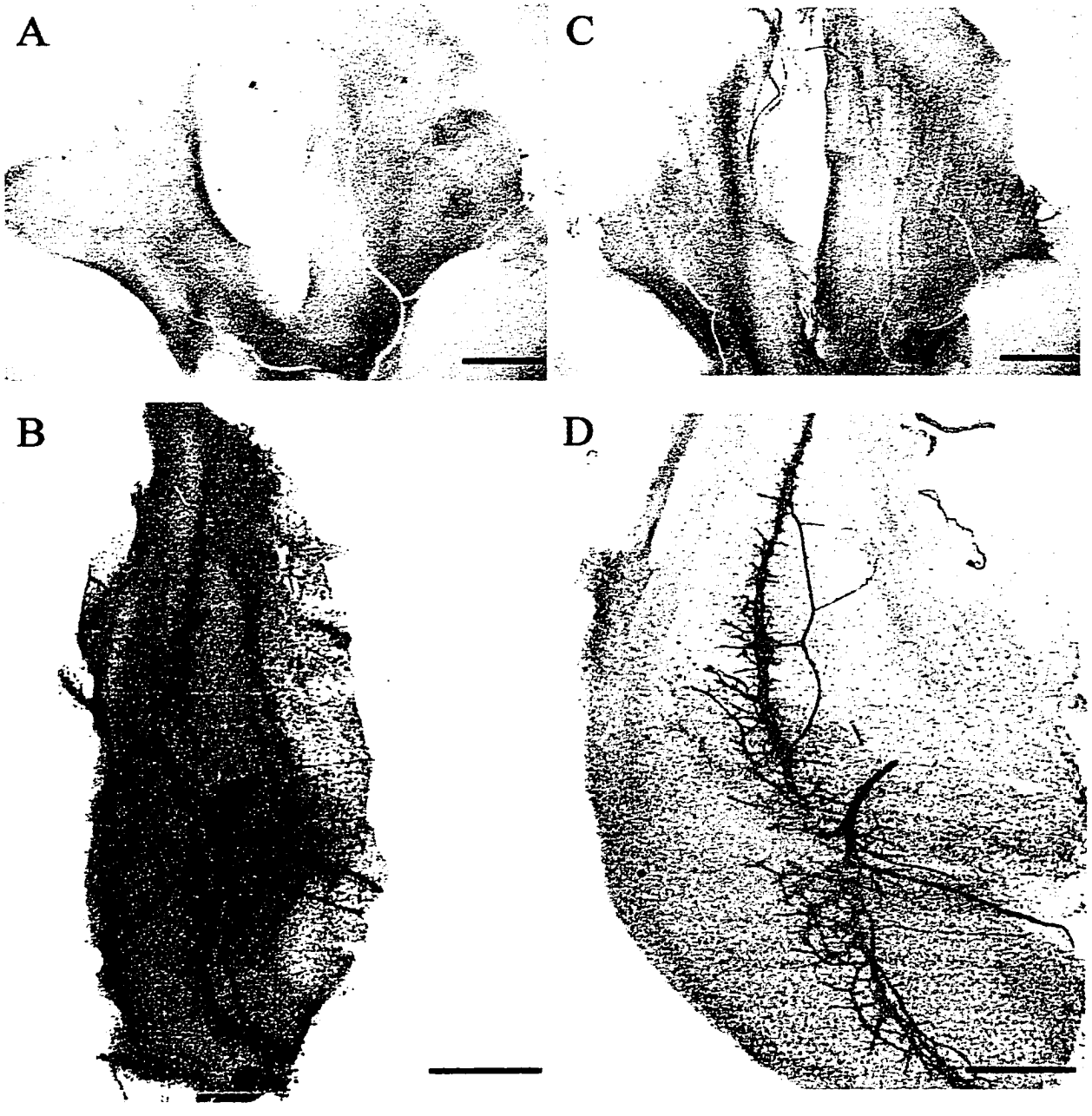

Fig. 6.3: EndoN treatment results in retardation of primary myotube separation. Comparison of haematoxylin (purple) and eosin (pink) histology of a control (A) and endoN diaphragm (B) cross sections taken from the right hemidiaphragm of the same fetuses as presented in Fig 6.2. Large cytoplasmic (eosin) primary myotubes are surrounded by smaller nuclear (haematoxylin) myoblasts during late E16. However, whereas in the control diaphragm, primary myotubes are well separated, in the endoN treated diaphragm, primary myotubes coalesce in large clusters which have not physically separated. Small secondary myoblasts are observed to fuse to the outer limits of these large clusters. Scale bars = 10μm.

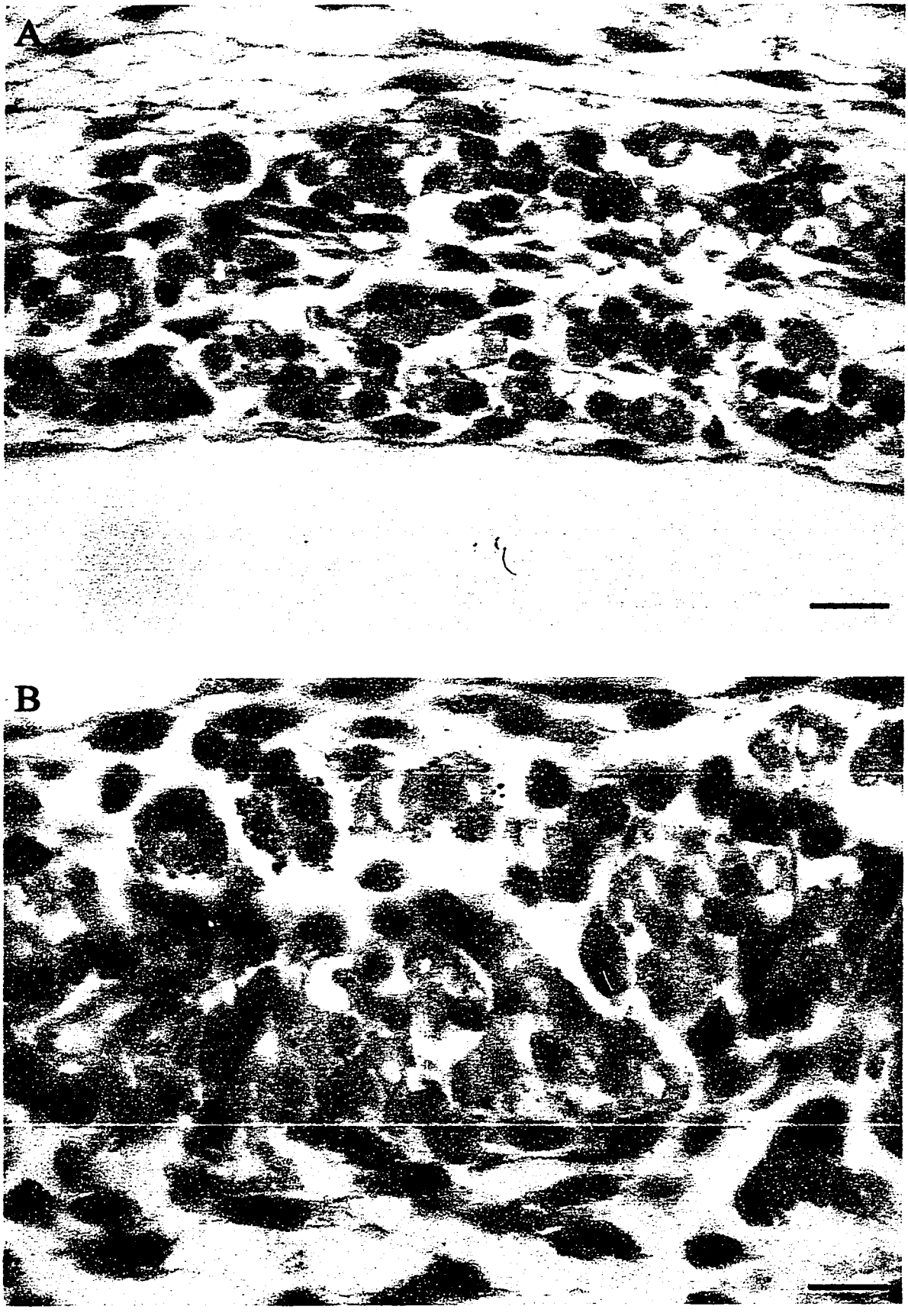

Fig. 6.4: Laminin immunofluorescence reveals larger basal lamina profiles in the endoN treated diaphragm.

Immunofluorescent labelling for the basal lamina component, laminin, of sections taken from the same region of the right hemidiaphragm as in Fig. 6.3. Basal lamina envelops myotubes as they become separated (Kelly, 1983). Basal lamina profiles of individual myotube clusters are larger in endoN treated fetuses (B) than in control (A) fetuses. This indicates that myotubes are still adherent, as opposed to merely being closer together, in endoN treated fetuses. Scale bars = 10μm.

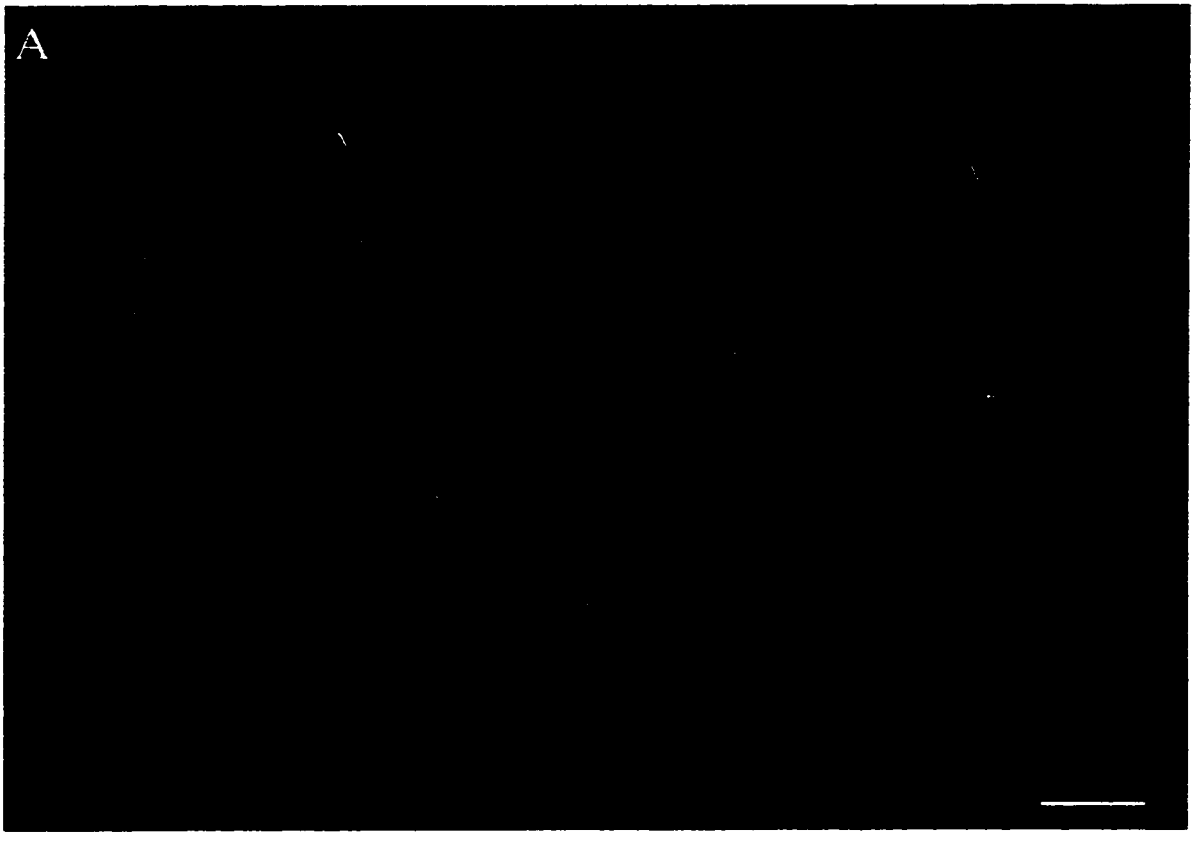

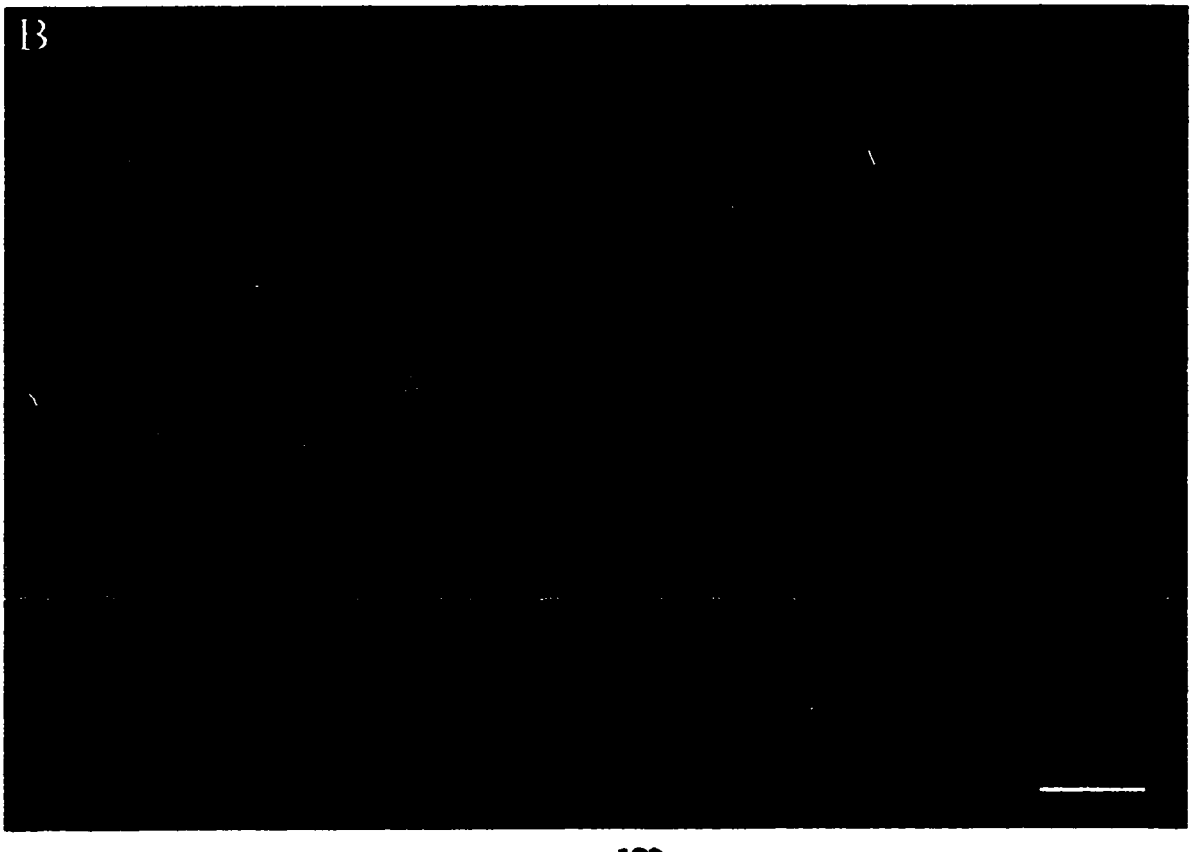

Fig. 6.5: Laminin immunofluorescent staining combined with nuclear staining. Sections from the same right hemidiaphragm as in Figs. 4.3, 4.4 immunolabelled for laminin (red) and the nuclear stain DAPI (blue). In the endoN treated diaphragm (B), laminin profiles are larger than in controls (A) and usually contain more nuclei. Counts have not been performed as of yet. It is important to note that we have never observed myotube clusters such as these in any control or boiled endoN control. Further, reduction, but not abolition, of PSA levels in the diaphragm does not appear to reduce myotube separation in any way. Scale bars = 10μm.

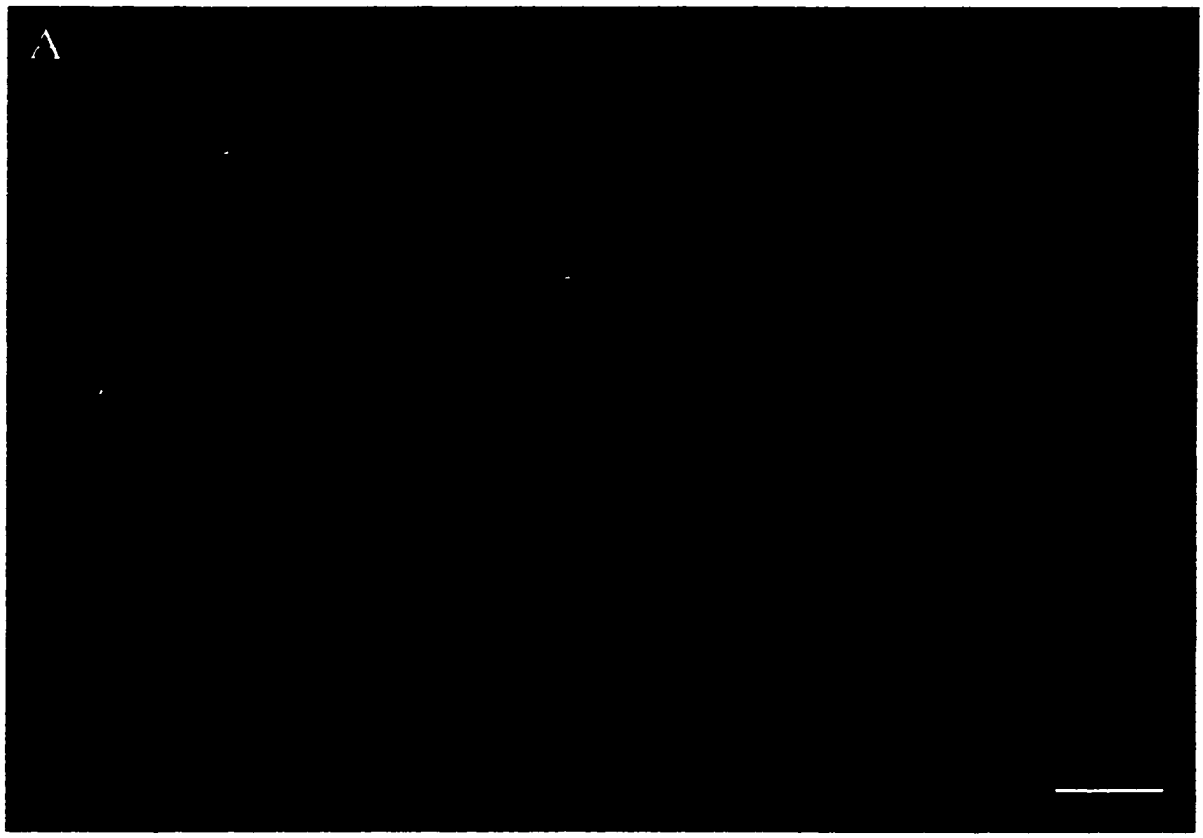

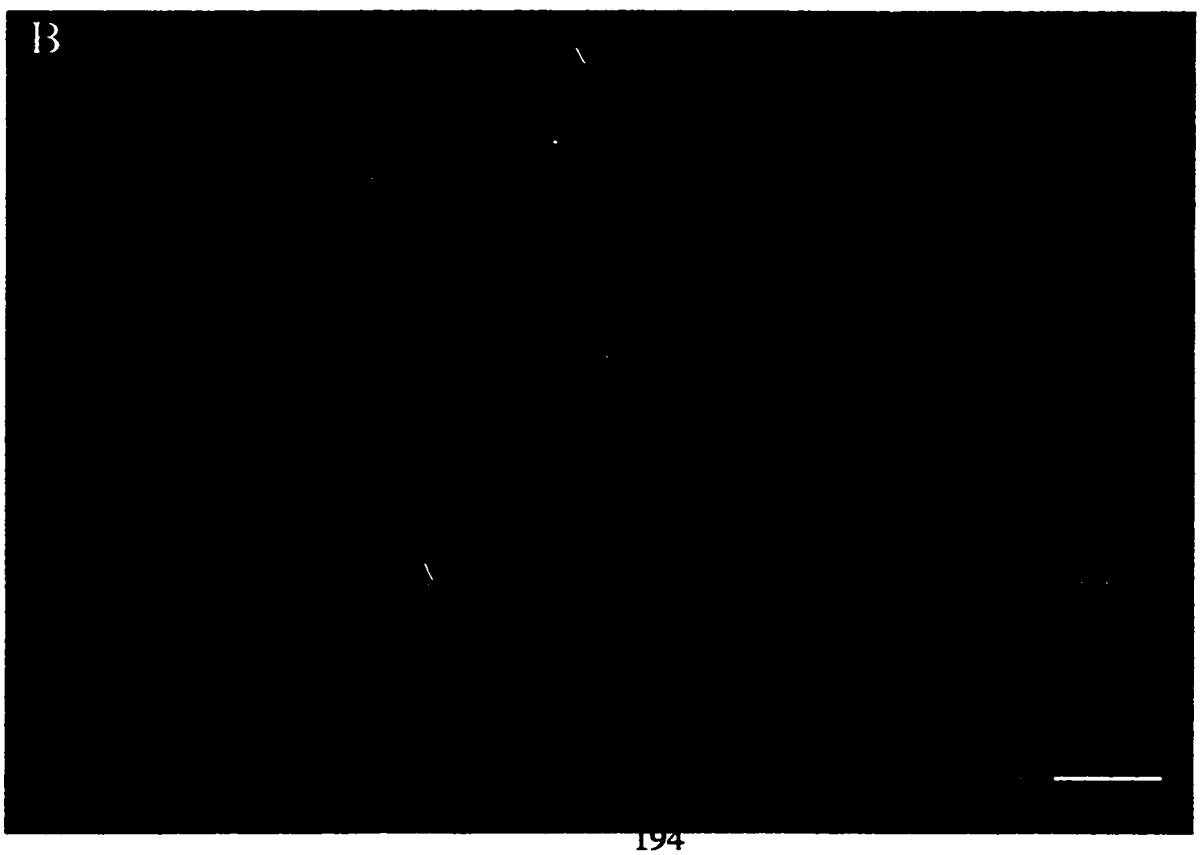

PSA-NCAM expression in denervated rat diaphragms.

Injection of 1μg β-bungarotoxin into rat fetuses at E13.5 completely denervated diaphragms from E14.5 up to the latest age examined, E21, as assessed by both GAP-43 (not shown) and PSA-NCAM immunoreactivity (Fig. 6.6). As described in chapter 5, immunoreactivity for PSA-NCAM can be used to follow the gross anatomical development of diaphragmatic myotubes. First, we were surprised to find that muscle PSA expression is high from E14.5 up to E20-21, when levels begin to fall after the major phase of secondary myogenesis (chapter 5). Further, the phasic reduction in PSA-NCAM levels normally observed at E16.5 is not observed in denervated diaphragms. Although we did not quantitatively compare PSA levels in denervated and control diaphragms, qualitatively, there actually appeared to be an upregulation of PSA expression on denervated myotubes, as denser reaction product was observed throughout the muscle and around myotubes viewed in section. However, we have not eliminated the possibility of this is artifactual due to better labelling in sparser tissue.

Following the progression of PSA-NCAM immunoreactivity, we found that the progression of muscle formation was remarkably normal in aneural diaphragms (Fig 6.6). However, several abnormal features can be discerned, suggesting that the nerve normally imposes regulatory influences on developing muscle which is required for appropriate morphogenesis. For example, myotubes did not extend up to the ribcage, and individual mis-aligned myotubes were frequently observed extending tangentially across the general myotube population.

Aneural diaphragms were compared to controls after sectioning to examine the development of the muscle (Fig. 6.7, 6.8, 6.9). Both the onset and major morphogenetic events of primary and secondary myogenesis proceed as normal in aneural diaphragms. Fig. 6.7 compares typical H&E histology of sections through the aneural diaphragm and control diaphragms during secondary myogenesis. Aneural diaphragms (Fig 6.7B) underwent a dramatic reduction in myotube density at all ages post-injection compared to controls (Fig 6.7A). However, as can be observed, myotube separation had proceeding as in controls. In this figure, larger profile primary myotubes are well separated and are surrounded by smaller eosin-dense secondary myotubes and haematoxylin-dense myoblasts. This confirms previous

reports in the chick that the basic myogenic program proceeds as normal in aneural muscle (Fredette and Landmesser, 1991) but argues against a report by Harris (1981) that secondary myogenesis does not occur in aneural diaphragms. Because muscular atrophy in aneural muscles has been widely reported in the past, we have not attempted to quantify the reduction in myotube numbers. However, using a standard nicked-end DNA labelling method for visualising the presence of apoptotic nuclei, we found that denervation had indeed enhanced the incidence of apoptotic myotube nuclei from E16 up to birth (Fig 6.9 shows typical labelling for apoptotic nuclei at E20 in control vs aneural diaphragms). This implies an inter-dependance of both nerve and muscle for their mutual survival in the embryo.

Fig 6.8 presents typical PSA-NCAM immunoreactivity in aneural diaphragms during secondary myogenesis. It is clear that the distribution of PSA-NCAM immunoreactivity in aneural diaphragms was consistent with that obtained in normal tissues (see chapter 5), being limited to the apposed surfaces of myotubes during both primary and secondary myogenesis. The normal expression pattern of PSA-NCAM corresponds to the findings that PSA promotes myotube separation and denervated diaphragms exhibit high levels of PSA expression.

Fig. 6.6: Expression of PSA-NCAM labelling in aneural diaphragms.

Comparison of PSA-NCAM immunolabelling of β-bungarotoxin treated (A-C) and control (D-F) fetuses throughout fetal development. A,D) During the onset of primary myogenesis at E14.5, PSA-NCAM expression reveals the formation of myotubes adjacent to the phrenic nerve (D). However, the absence of the phrenic nerve in aneural diaphragms does not prevent the timely expression of PSA-NCAM in the aneural diaphragm (A). B,E) By E16.5, downregulation of PSA-NCAM expression has occurred in the medial region of the musculature in controls, whereas the nerve maintains high levels of expression (E). In aneural diaphragms, the usual down-regulation of PSA-NCAM expression does not occur (B). Note that the musculature is considerably thinner in aneural diaphragms but that the extent of muscle formation is comparable to that in controls. C, F) By E20, PSA-NCAM expression is being downregulated throughout the diaphragm and expression within the nerve is lost in all but the most sternal regions (F). In the aneural diaphragm, equivalent downregulation of expression has occurred (C). Note that although the extent of muscle formation is similar, the gross morphology of the muscle is retarded in the aneural diaphragm. In particular, the mesodermal substrate for the diaphragm extends beyond the muscle. During dissection, the muscle of these diaphragms does not reach the ribcage. Scale bars = 1mm.

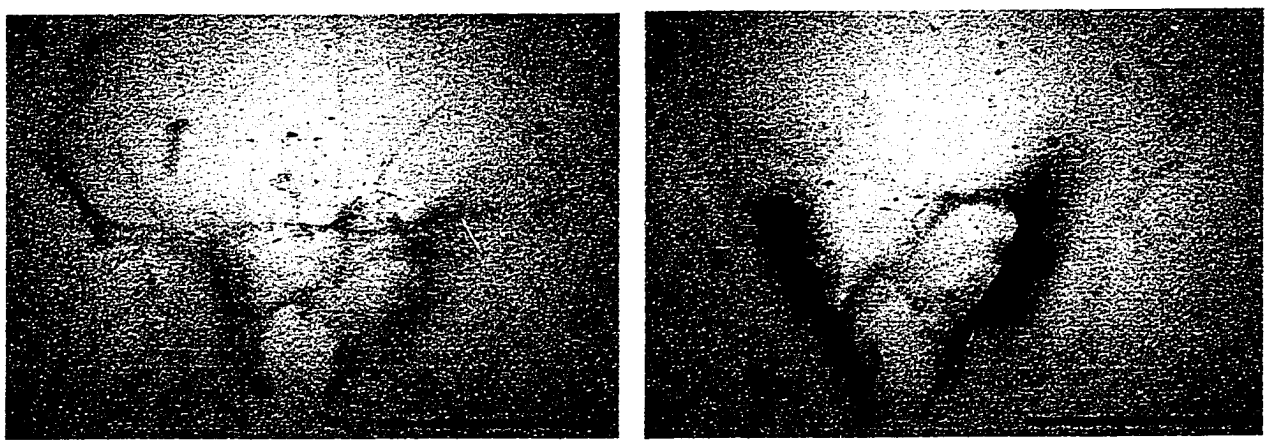

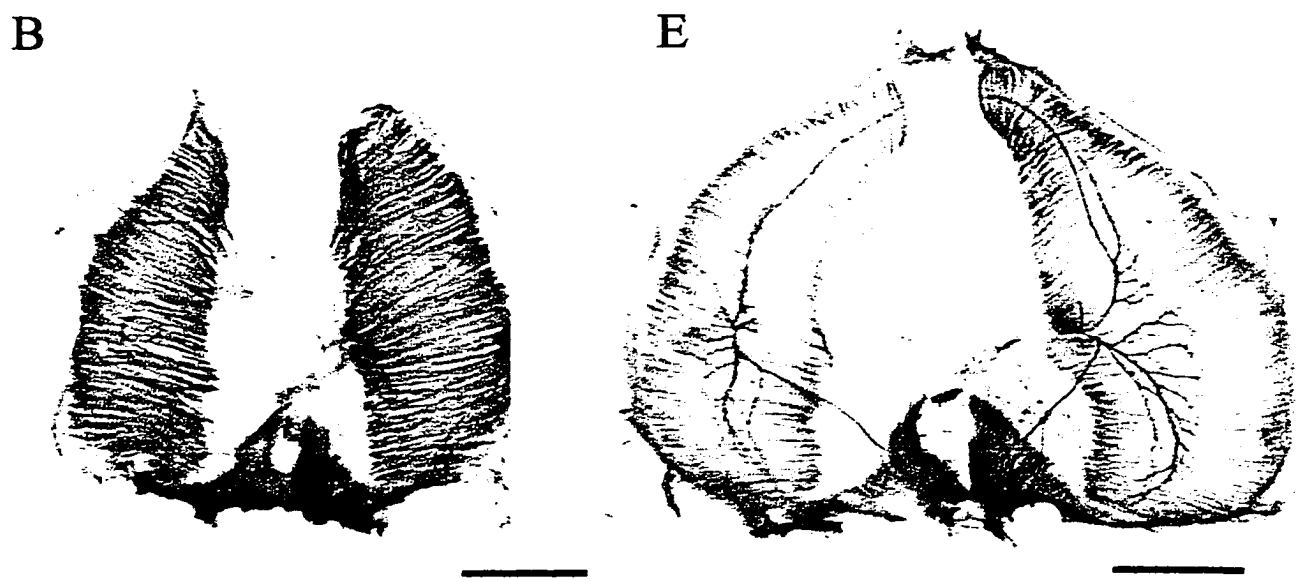

Fig. 6.7: Myogenesis proceeds as normal in aneural diaphragms.

Comparison of haematoxylin (purple) and eosin (pink) histology of a control (A) and aneural diaphragm (B) at E20. The control diaphragm is thicker and has a considerably higher density of muscle cells than the aneural diaphragm. In both cases, large cytoplasmic (eosin) primary myotubes are surrounded by smaller cytoplasmic secondary myotubes and small nuclear (haematoxylin) myoblasts. Examining the distribution of larger profile myotubes in both diaphragms, it is clear that myotube separation is unaffected by denervation. Further, the presence of smaller secondary myoblasts that are still adherent to the larger myotubes in both control and aneural diaphragms indicates that myogenesis is proceeding as normal in denervated diaphragms. Also note that large central nuclei are evident in aneural myotubes, whereas nuclei have largely migrated to the periphery of the cell in controls. Scale bars = 10μm.

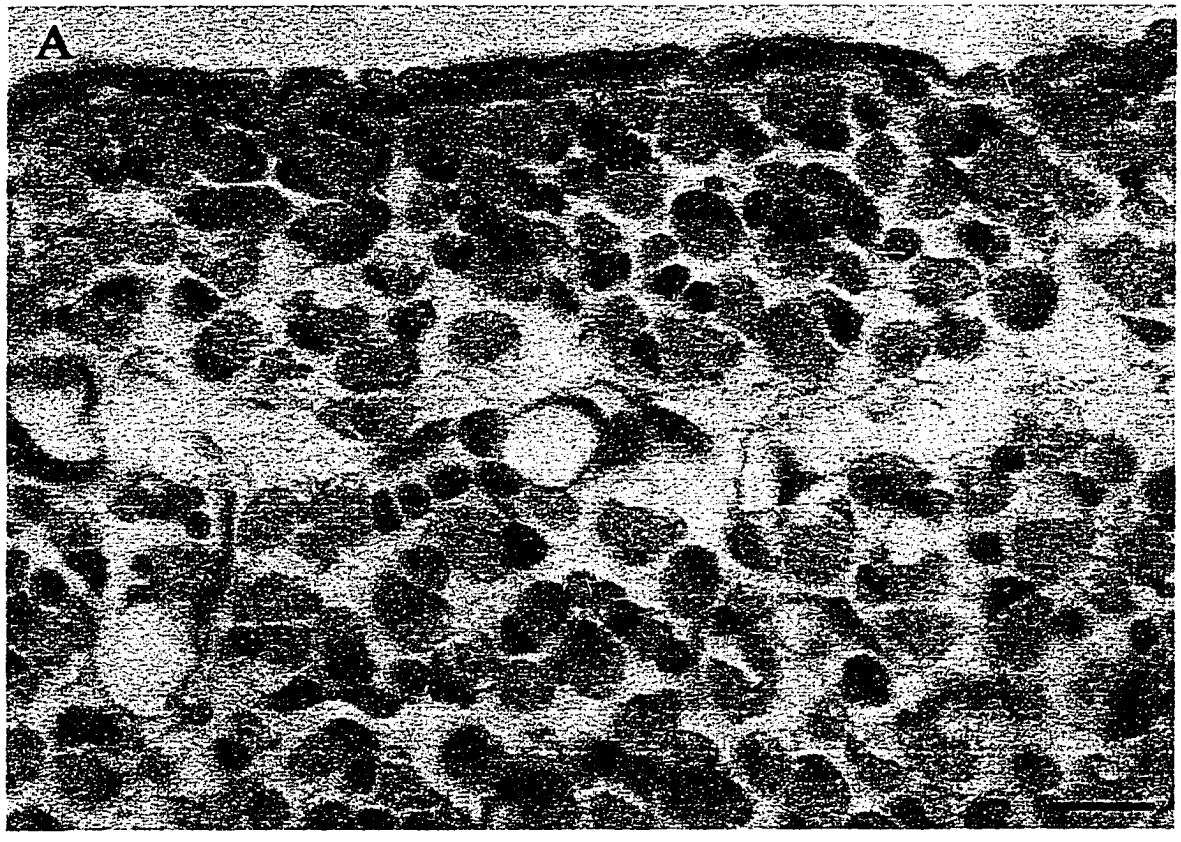

Fig. 6.8: PSA-NCAM expression is normal in aneural diaphragms.

Two examples of PSA-NCAM expression in two aneural diaphragms during secondary myogenesis. Eosin staining indicates the distribution of the muscle cells. Haematoxylin staining has been omitted to emphasise the immunohistochemical staining for PSA-NCAM. In all cells present, PSA-NCAM is limited to the apposed membranes of primary and secondary myotubes, as in controls (see chapter 5). Equivalent immunolabelling is obtained during primary myogenesis (not shown). Arrows indicate classical examples of apposed primary and secondary myotubes in which the PSA-NCAM immunolabel can be observed to be limited to the juxtaposed membranes. Scale bars = 10μm.

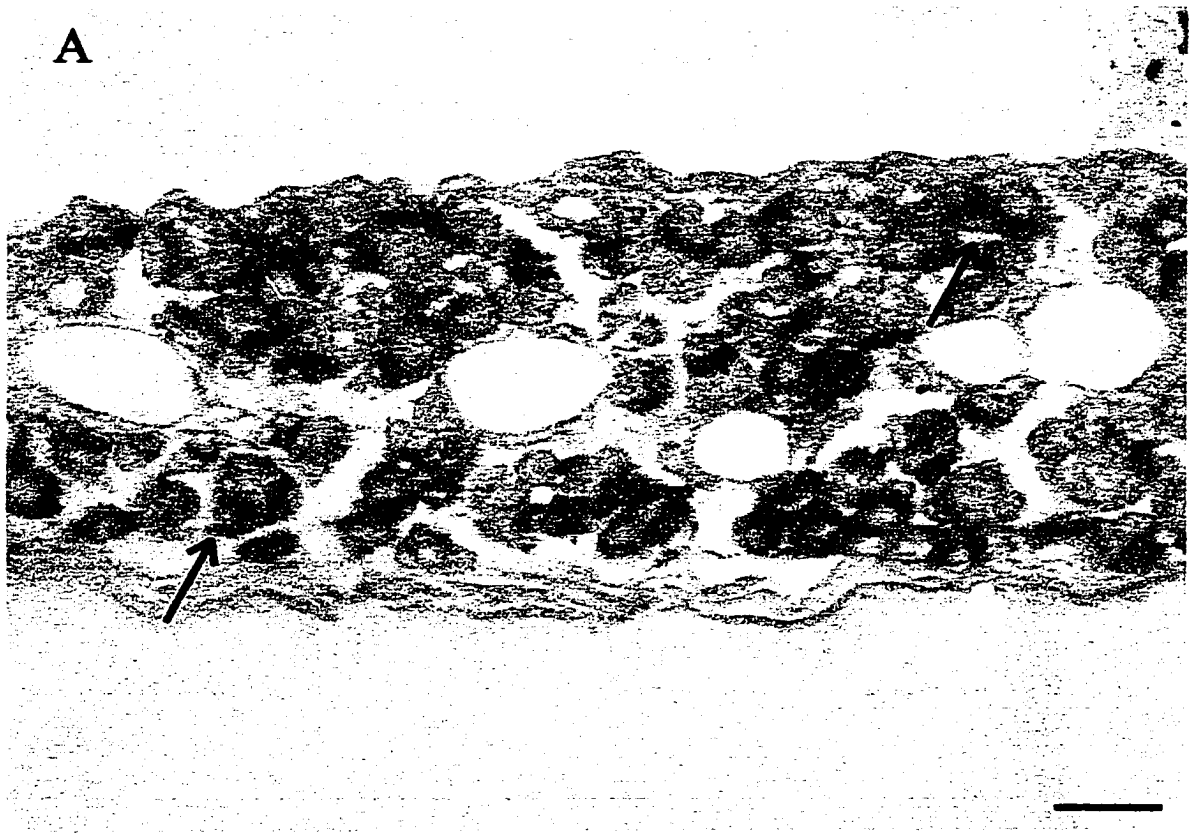

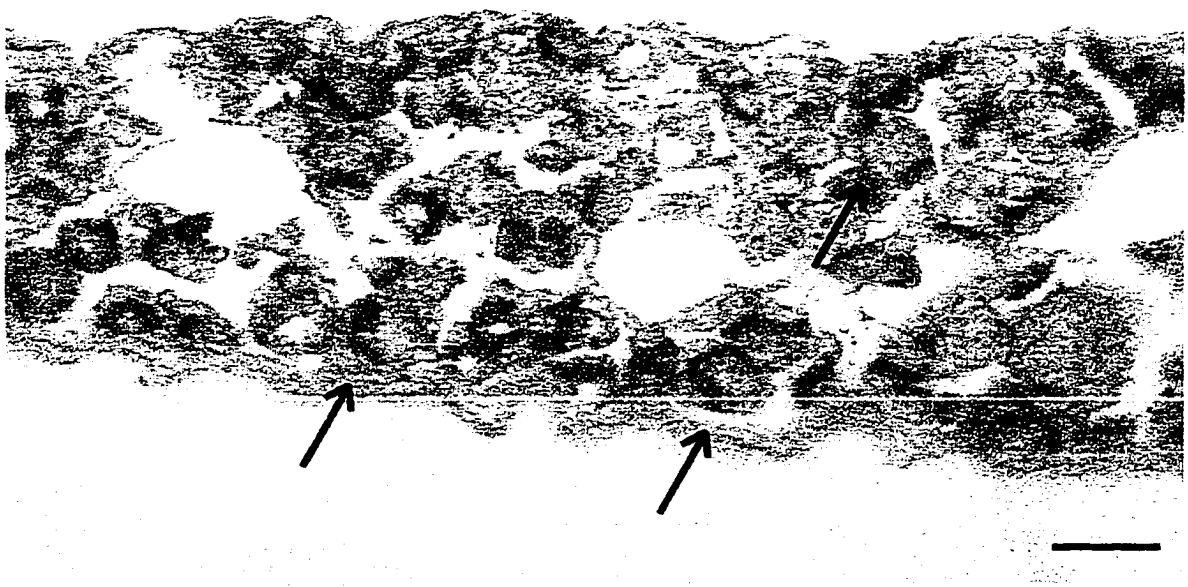

Fig. 6.9: Enhanced apoptosis in aneural diaphragms.

Nicked-end labelling of DNA in apoptotic muscle cells in E21 innervated (A,B) and aneural (C,D) diaphragms. Control sections (A,C), where the nucleotide mixture but no terminal transferase added, are shown adjacent to test sections (B,D), where the terminal transferase added. Apoptotic nuclei appear red, surviving nuclei appear. By E21, apoptosis within diaphragmatic myotubes is limited. However, in aneural diaphragms, a significant proportion of nuclei are apoptotic. Arrowheads point to red apoptotic profiles, whereas arrows in D point to blue surviving profiles. Counts have not been performed as yet, but an increase in apoptosis is clearly evident in aneural diaphragms. Note the aberrant central location of the nucleus in aneural diaphragms. Scale bars = 10μm.

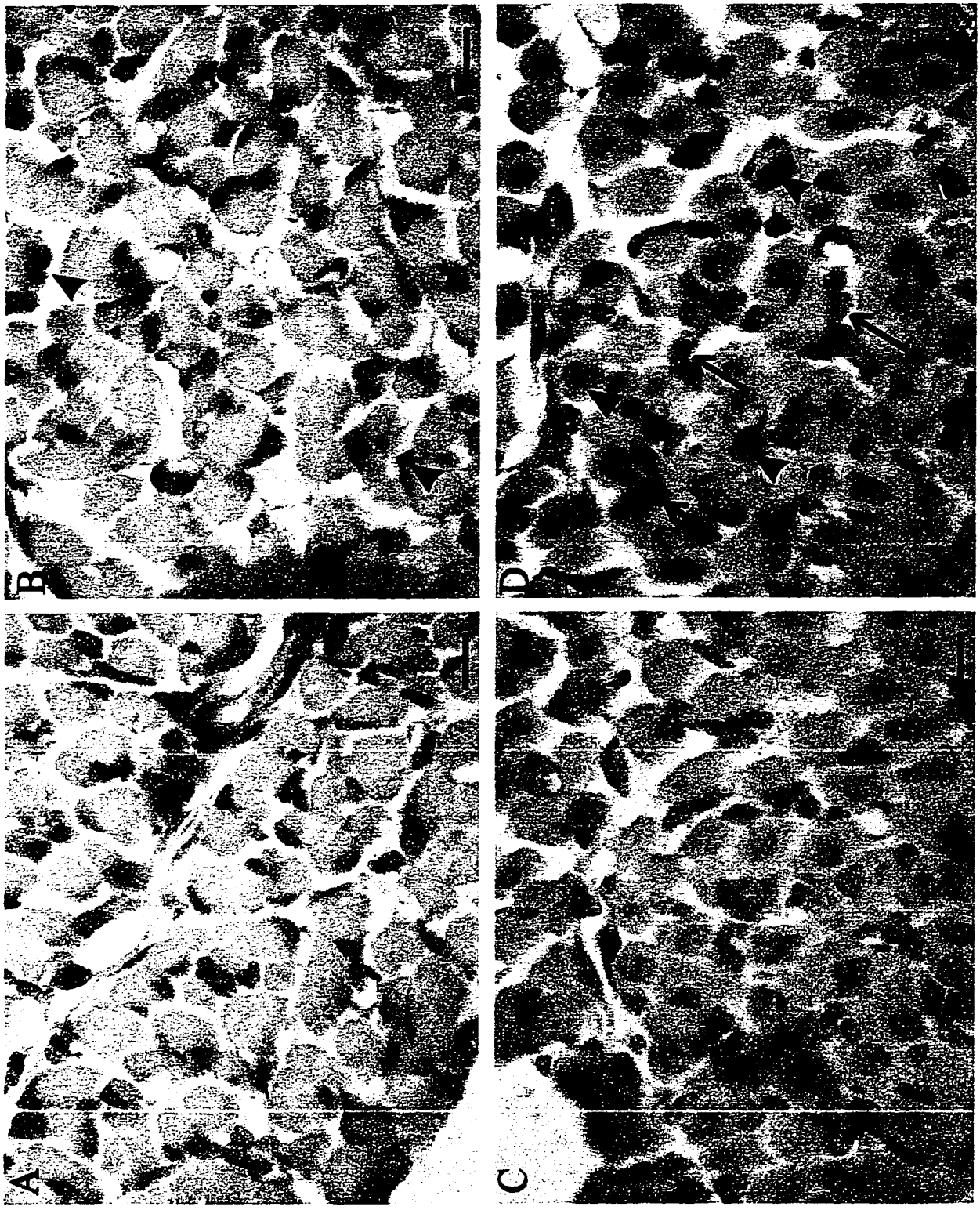

Spontaneous contractility in denervated diaphragms

We wished to determine whether the expression of PSA-NCAM in denervated diaphragms could be due to spontaneous contractility of the muscle, as occurs *in vitro* (Rafuse and Landmesser, 1996). Thus far, we have recorded from control (Fig. 6.10A) and aneural diaphragms (Fig. 6.10B-C) at age E21. Several attempts to record from E16.5 diaphragms (a time of high PSA-NCAM expression in denervated diaphragms) have not been successful as of yet, but this is being pursued. Hemidiaphragms were removed and pinned out over a microarray of electrodes which recorded electrical activity across the muscle surface. Spontaneous electromyographic measurements of muscle electrical activity were compared in control and denervated diaphragms from E21 fetuses.

By E21, the control diaphragm demonstrated no spontaneous activity over a long period of recording (Fig 6.10A). We verified that the control diaphragms tested responded appropriately to stimulation of the nerve (not shown). In E21 aneural diaphragms, spontaneous activity was observed of varying amplitude and frequency (Fig. 6.10B). This was characterised by quiescent periods of up to 50 seconds interspersed by periodic low amplitude bursting. This form of activity was not seen in any controls. This spontaneous activity was unaffected by addition of tubocurarine to the bath (to a final concentration of 40μM) (Fig. 6.10C). This concentration blocks neuromuscular transmission in control diaphragms (not shown). This demonstrates that spontaneous activity was not due to any remaining axonal drive. However, addition of tetrodotoxin to the bath (to a final concentration of 1μM) (Fig. 6.10D) completely abolished the activity. This indicates that spontaneously-generated Na^+-dependant currents are responsible for EMG activity in the denervated diaphragm. Thus far, we have examined 2 diaphragms from each group and obtained similar results.

Fig 6.10: Aneural diaphragms generate spontaneous Na^+-dependent activity

Comparison of spontaneous electromyographic activity in isolated control (A) and aneural diaphragms (B-C) at E21 from the same litter. (A) No spontaneous was observed in an innervated diaphragm. (B) Aneural diaphragms were spontaneously active, as observed from intermittent episodes of electrical activity. (C) Addition of tubocurarine at a known effective concentration did alter spontaneous activity. Larger burst in C is likely derived from multiple myotubes and emphasises that activity is not inhibited. Similar larger bursts were observed prior to drug treatment. (D) Tetrodotoxin completely blocks all activity, indicating that spontaneous activity is likely Na^+-dependent. Scale bars indicate voltage (V) and time in seconds (s).

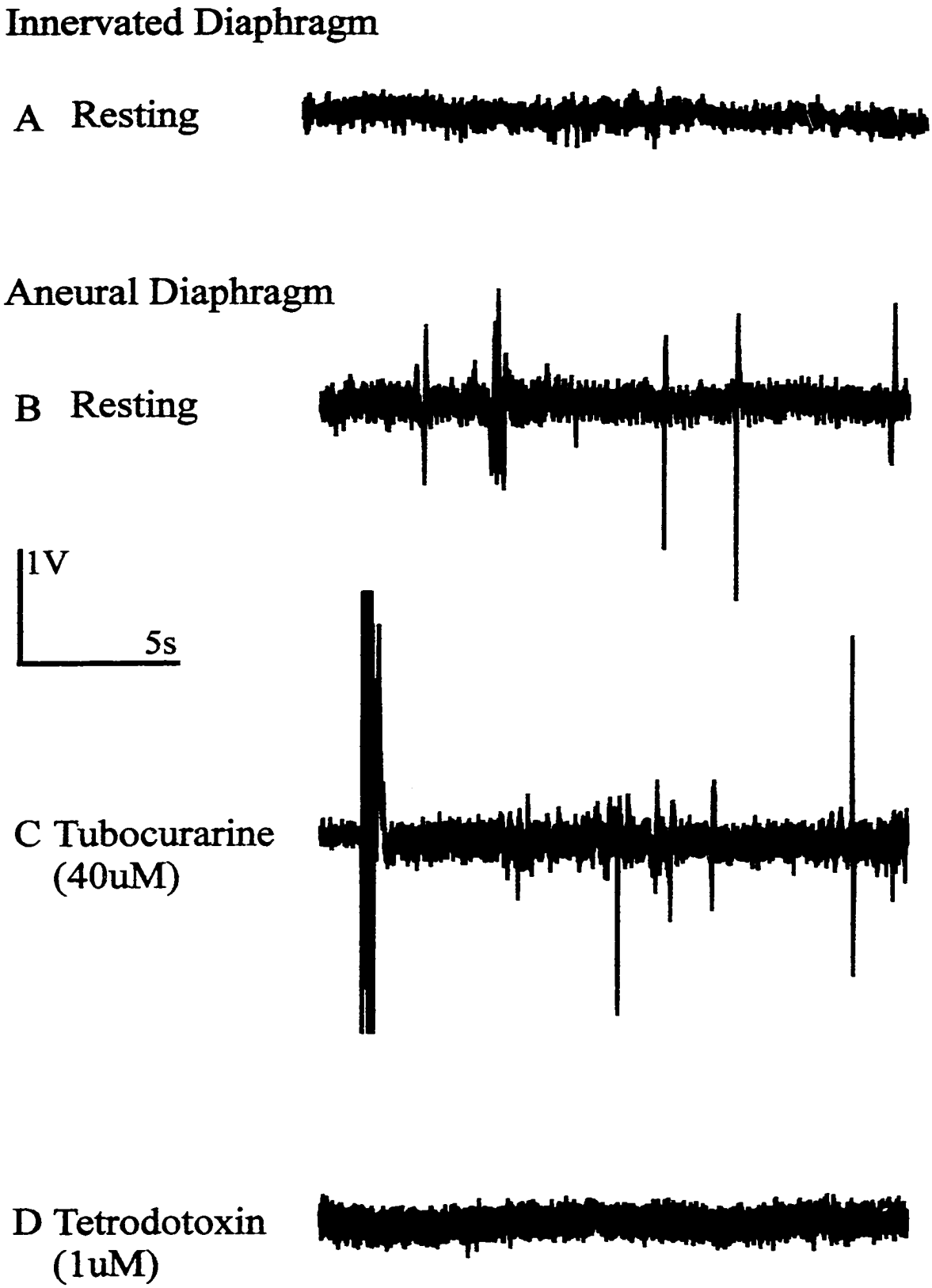

PSA-NCAM expression in the chick hindlimb

A previous study examined the timing and pattern of expression of PSA-NCAM in the chick hindlimb musculature throughout primary and secondary myogenesis using the 5A5 monoclonal antibody (Fredette et al., 1993). However, the precise distribution of PSA-NCAM during secondary myogenesis appeared counter-intuitive to its postulated role. We have begun to examine PSA-NCAM expression during chick hindlimb development using the 12E3 monoclonal antibody (Seki and Arai, 1991). This study is ongoing and recent complications with our antibody labelling has prevented satisfactory detailed study of PSA-NCAM labelling in these tissues in time for submission of this thesis. However, I shall present what we have found to date.

The 5A5 antibody utilised in the study by Fredette et al. (1993) is sensitive to paraffin wax embedding and thus cryostat and electron microscopy of immunolabelled thick (100μm) vibratome sections were examined for PSA-NCAM immunoreactivity during chick myogenesis. Determining precise antibody label distribution around myotubes is very difficult in cryostat sections due to a loss in tissue integrity at higher resolutions. Staining patterns obtained at the electron microscopic resolution demonstrated PSA immunoreactivity around, but not between, myotubes. Use of the 12E3 antibody permits immunolabelling of 4% paraformaldehyde or Carnoy's B fixed paraffin-embedded microtome sectioned (5μm) chick thigh musculature. Further, tissue integrity is maintained to a level sufficient for determination of labelling pattern. The PSA-NCAM immunoreactivity obtained in chapter 5 suggested that PSA-NCAM was concentrated along the juxtaposed membranes of adherent myotubes. As can be observed in the single micrograph in Fig 6.11, PSA-NCAM immunoreactivity was limited to the apposed membranes of adherent primary and secondary muscle cells at St 38. Labelling was apparent between both primaries and secondaries and between adjacent secondaries. No consistent labelling can be observed upon the free surfaces of muscle cells. This labelling pattern corresponds precisely to that obtained in our rat diaphragm studies.

Fig. 6.11: PSA-NCAM immunoreactivity of developing chick muscle

12E3 immunolabelling of chick hindlimb muscle cells at St 38. Equivalent labelling was obtained throughout the musculature from St 36 to St 38 (the two ages successfully labelled to date). The Carnoy's B fixation allows visualisation of nuclei in many cells in these eosin stained sections. As can be clearly observed, labelling is limited to the juxtaposed membranes of adjacent cells. Labelling is observed between primaries and secondaries, as well as between two secondaries. Asterisk in a few selected primary myotubes draws attention to certain excellent examples of a large primary myotube surrounded by smaller secondary myotubes and myoblasts. Scale bar = 10μm.

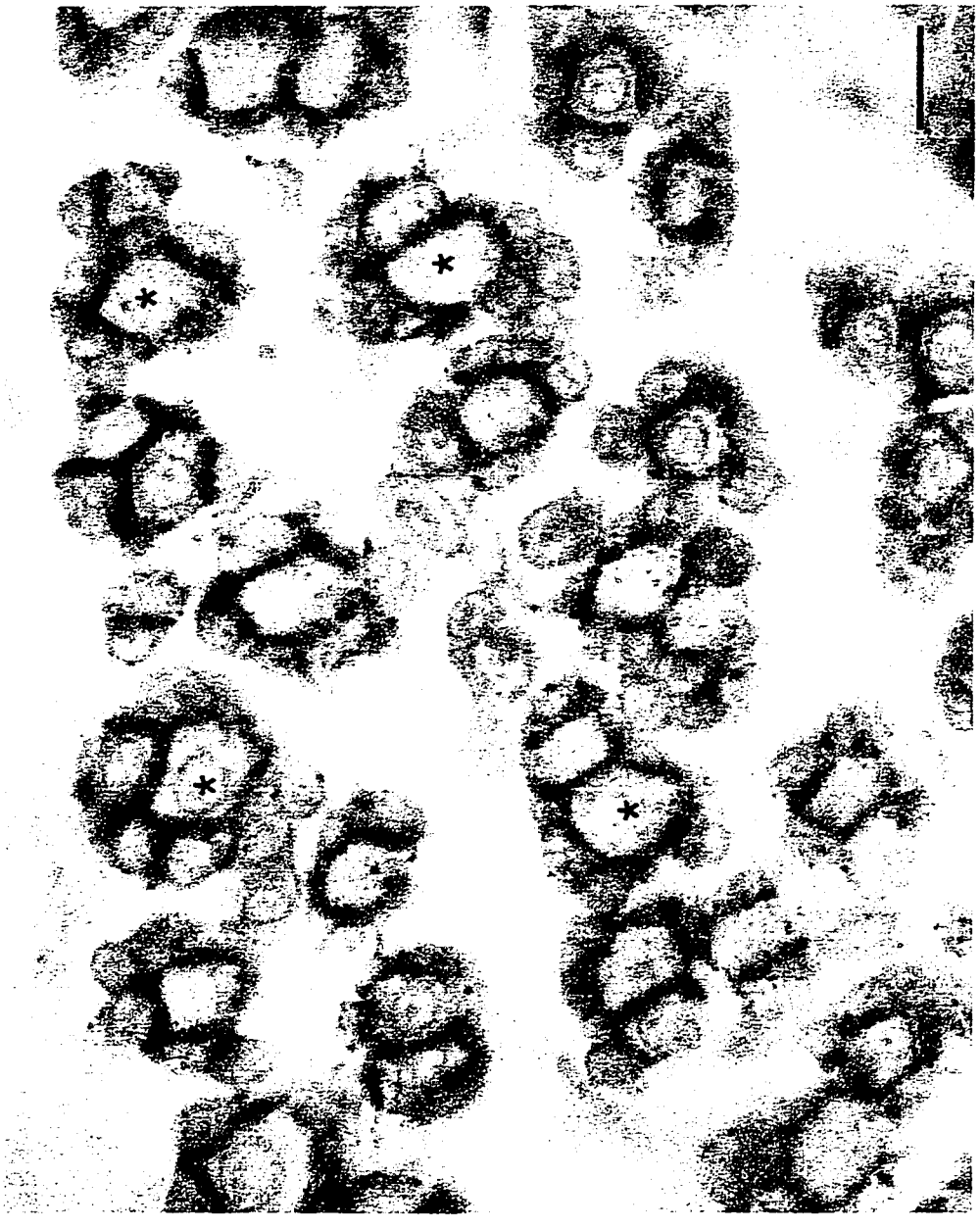

Chick hindlimb myotube separation is not affected by absence of PSA during primary myogenesis

A previous report showed that both tubocurarine-induced paralysis and neural tube removal (denervation) increased myotube cluster size by St 37½ and St38. Differential immunolabelling of primary (slow myosin heavy chain, MHC) and secondary (fast MHC) muscle cells in the slow region of the iliofibularis showed that both cell types were included within clusters (Fredette and Landmesser, 1991). Fredette et al. (1993) showed that the increase in cluster size was correlated with a reduction in PSA-NCAM immunoreactivity throughout development. Thus, separation of primary and secondary myotubes during both phases of myogenesis were postulated to be mediated by PSA-NCAM-induced cellular separation.

We have directly tested the role of PSA-NCAM in muscle morphogenesis in the chick hindlimb during primary and secondary myogenesis by injecting EndoN into the thigh at St 27-29, at the start of primary myogenesis, and at St 34-36, at the start of secondary myogenesis. Lower density of myotubes at St 36 has allowed a simple visual inspection of muscle cell separation after primary myogenesis. Laminin immunofluorescence is currently being used to assess myotube separation after secondary myogenesis. Thighs were removed at St36 to examine the profile of developing myotubes after primary myogenesis was complete and secondary myogenesis had begun. Comparison of control and endoN injected thigh musculature shows that absence of PSA-NCAM immunoreactivity does not interfere with myotube separation in the chick hindlimb (Fig. 6.12). Similar results have been obtained in numerous trials. We have confirmed the abolition of PSA-NCAM immunoreactivity by endoN injection by St 36 (Fig. 6.13). However, previous studies have determined that endoN removes PSA from the chick hindlimb within a few hours and it does not reappear for up to 3 or 4 days (Landmesser et al.,1990). We are analysing injected fetuses to ensure that PSA has been removed throughout primary myogenesis.

Sections taken from tubocurarine-paralysed and β-bungarotoxin-denervated chick hindlimb muscles have been included to emphasise that the inhibition of primary myotube separation observed in these muscles is considerable in comparison. Preliminary evidence suggests that tubocurarine (as previously determined; Fredette et al., 1993) and β-

bungarotoxin induced denervation of chick hindlimbs reduces PSA-NCAM expression in chick hindlimb muscle. However, with regards to the effects of denervation, we obtained one reliable result prior to our antibody complications and thus this issue has not been resolved to our satisfaction (not shown).

Fig. 6.12: Comparison of myotube separation after removal of PSA, paralysis or denervation.

Injections were performed at St29, during the onset of primary myogenesis within the chick hindlimb. Thighs were removed at St36 and were stained with haematoxylin and eosin to visualise the morphology of developing myotubes. The iliofibularis muscle was chosen for this study due to previous focus on this muscle (Fredette and Landmesser, 1991; Fredette et al., 1993). (A) Control fetus injected with 0.9% NaCl to demonstrate the normal distribution of primary myotubes (large cytoplasmic cells) and secondary myotubes and myoblasts (smaller with largely nuclear appearance). Individual primary myotubes can be observed to have separated and become surrounded by secondary myotubes and myoblasts into well separated clusters. (B) EndoN injected fetus with no observable difference in muscle cell distribution, cluster size or cluster density. The exact same result has been obtained in repeated trials. (C) Tubocurarine-induced paralysis of the chick results in inhibited primary myotube separation, as described in Fredette et al. (1993). Note the larger cluster profiles in comparison to those in A and B. Close inspection reveals the greater number of nuclei within clusters. (D) β-bungarotoxin denervation of the chick hindlimb muscle dramatically reduces the number of myotubes, but reduced separation of primary myotubes is represented by larger cluster size. Plates A,B and C are taken from the slow region of the iliofibularis. D is taken from the fast region of this muscle. Due to a significantly greater cell death in the slow region over that in the fast region (confirming previous reports (Fredette and Landmesser, 1993)), the slow region is frequently devoid of muscle. Retention of greater numbers in the fast region permits better visualisation of the reduction of myotube separation in these fetuses. Scale bars = 10μm.

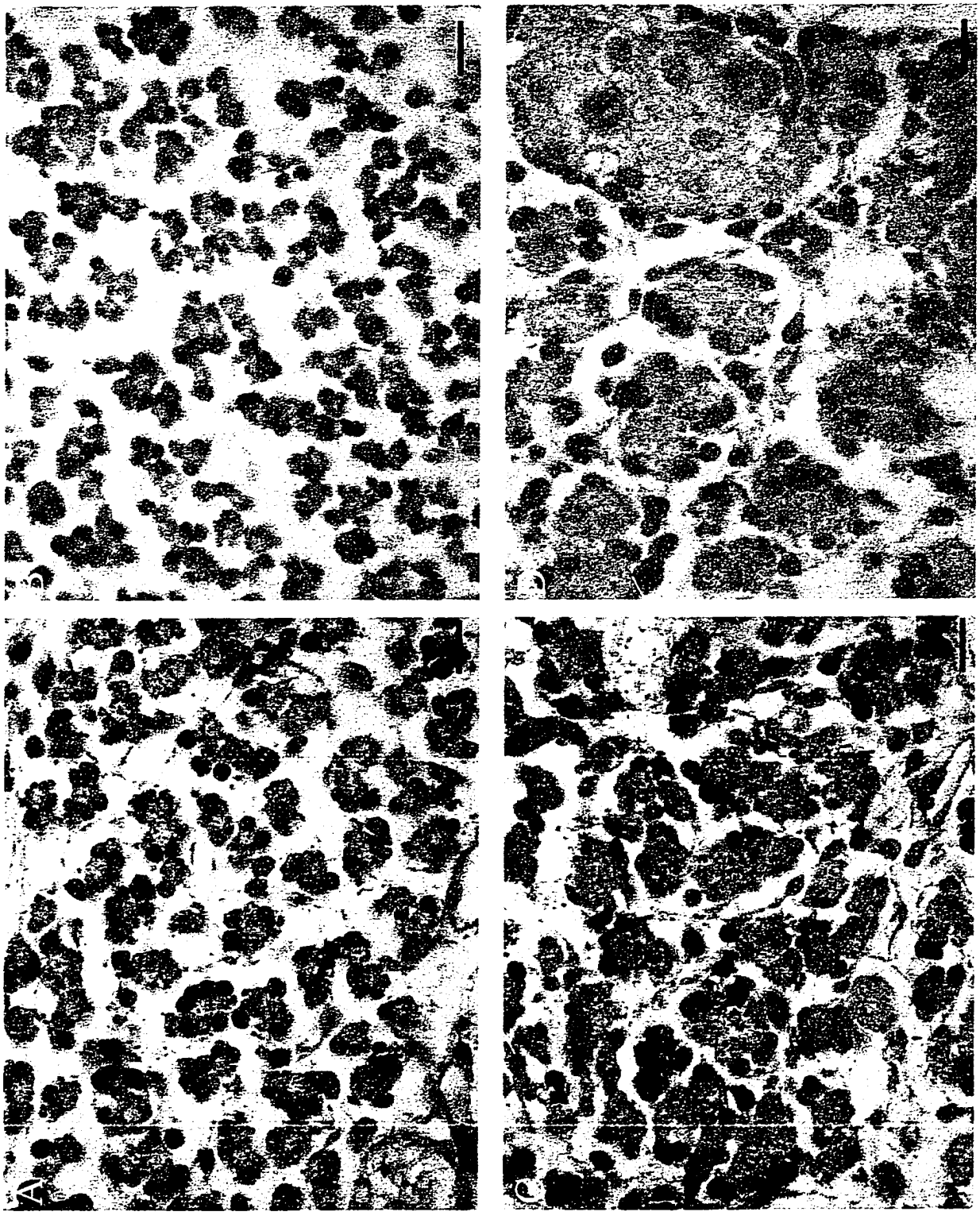

Fig. 6.13: Reduction of PSA-NCAM by endoN in the chick thigh

Immunohistochemistry for PSA-NCAM in control (A,B) and endoN treated (C,D) chick hindlimb musculature at St 36. B and C and magnified views of A and D, respectively. Black immunoreactive deposits are evident in the sciatic nerve (SN), intramuscular branches within the iliofibularis muscle (IFIB) and in other nerves (arrows) in control sections. (B) Myotubes adjacent to immunopositive intramuscular branches are also immunopositive for PSA-NCAM. C,D) At no time did we observe any positive immunoreactivity for PSA-NCAM in the injected thigh of endoN treated fetuses. Arrows denote immunonegative nerve branches in these plates and no labelling is observed amongst developing myotubes. Scale bars in A,C = 100μm; B,D = 10μm.

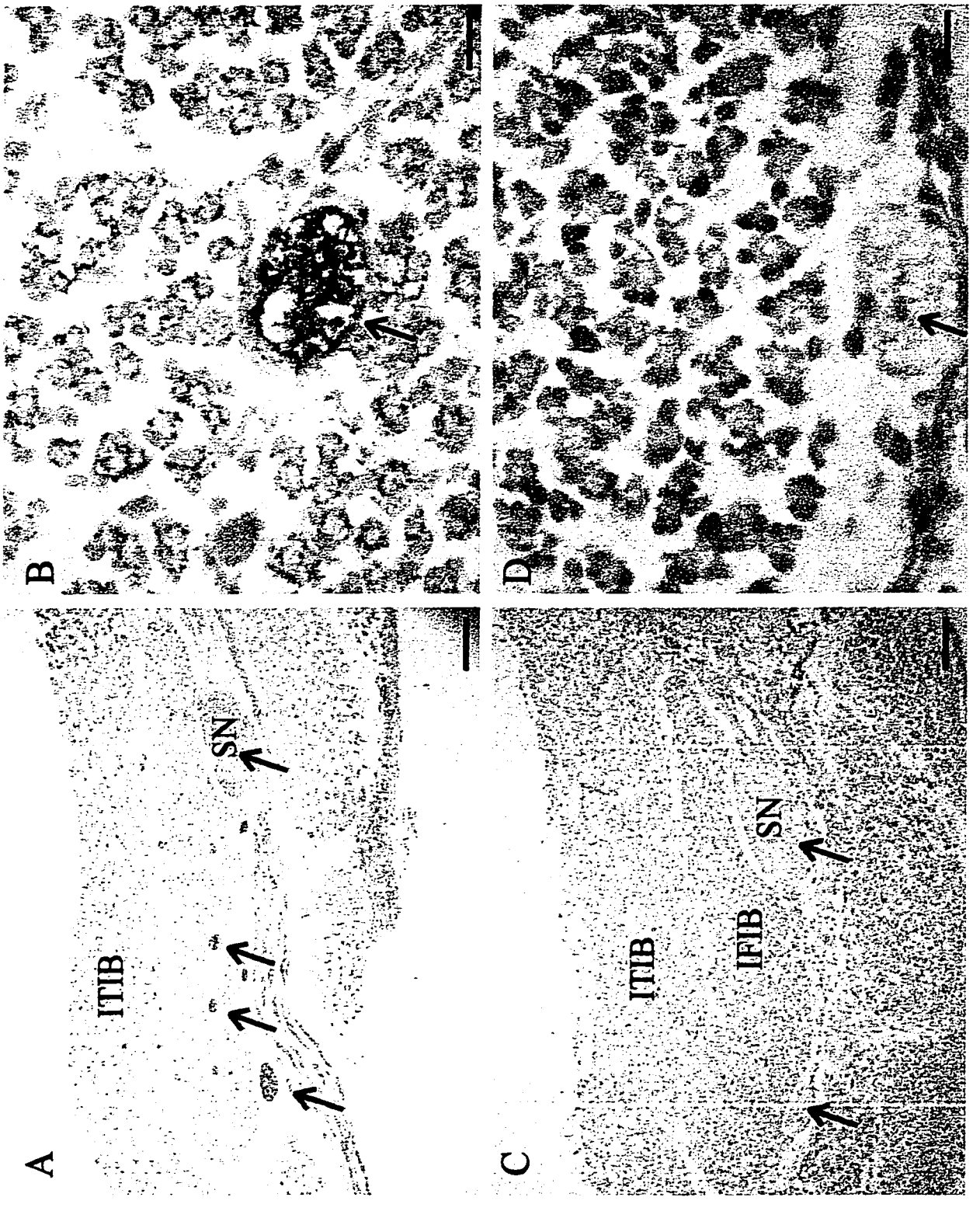

DISCUSSION

Previously, we had determined that PSA-NCAM expression in the embryonic rat diaphragm is discretely limited, both spatially and temporally, to myotubes which were undergoing separation during both primary and secondary myogenesis (chapter 5). In this study, we have extended upon these observations to obtain data regarding the functional role of PSA-NCAM in muscle development and to further our understanding of how its expression is regulated. We have extended this study in the rat to incorporate experiments in the chick. Certain differences between the role of PSA-NCAM in myotube separation in these two species may prove illuminating in understanding the molecular control of muscle morphogenesis.

PSA-NCAM Expression on Developing Myotubes.

We have found that expression of PSA-NCAM on chick myotubes reflects that found in the rat diaphragm during secondary myogenesis. Ongoing work is determining the distribution of PSA-NCAM labelling during primary myogenesis. A previous study (Fredette et al., 1993) determined that PSA-NCAM was expressed by muscle cells throughout myogenesis. However, attempts to define the precise distribution of the PSA-NCAM immunolabel relied upon the use of the 5A5 monoclonal antibody on thick (100μm) vibratome sections of glutaraldehyde and paraformaldehyde fixed chick thigh. Electron-dense reaction product was observed on all free surfaces, but not inbetween, separating myotubes, counter-intuitive to the role proposed for PSA-NCAM during muscle development. Clearly, when antibody labelling with the 12E3 monoclonal is applied to thin paraffin-embedded microtome sectioned chick thighs, labelling is found to penetrate myotube clusters. Labelling extends between the apposed membrane surfaces of primary and secondary muscle cells, and between two secondary muscle cells. No separated myotubes were found to express PSA-NCAM on their free surfaces, except in occasional cases where myotubes were physically separated but were still very close, perhaps indicative of very recently separation. The current data suggests that limitations of the antibody within the methodology utilised in the study of Fredette et al. (1993) likely resulted in poor tissue penetration, and thus, imprecise labelling

patterns in that study.

Removal of PSA-NCAM may inhibit primary myotube separation in the rat diaphragm

We have achieved successful injection of endoN in one fetus, in that it had abolished PSA-NCAM immunoreactivity in the rat diaphragm up to three days post-injection. This is unlikely a limitation of the enzyme, as it removes PSA from NCAM in rat diaphragm homogenates, it fully digests 100μg of colominic acid up to a dilution of 1:128 and it successfully removes PSA-NCAM from the chick hindlimb as determined immunohistologically. Frequent experimental trials have resulted in regularly dramatically-reduced levels of PSA-NCAM in the rat diaphragm, but not abolition. In these cases, examination of phrenic intramuscular branching pattern and myotube separation have shown that neither parameter has been affected. Instead, this problem appears related to the diffusion of the enzyme into the diaphragm. The diaphragm is not directly injectable at any age, particularly in fetuses. Thus, we have had to inject as close to the developing diaphragm as possible. Nevertheless, the one successful injection indicates that persistence may pay off, and trials are ongoing.

In the successful experiment, we obtained results strikingly consistent with that proposed for PSA-NCAM function in neuromuscular development. Determination of myotube separation by morphological and functional criteria demonstrated that myotubes had not separated as they normally would by the end of primary myogenesis (late E16). As histological examination does not discount the possibility that myotubes are simply not as well separated, we used laminin immunohistology to provide an assessment of functional myotube separation. As described in Kelly (1983) and Harris (1981), deposition of basal lamina between separated myotubes occurs after separation of both primary and secondary myotubes. After PSA removal, larger laminin profiles containing greater numbers of nuclei were observed throughout the muscle. In controls, one large primary myotube and several secondary myoblasts/tubes were enclosed within a basal lamina. After removal of PSA, larger clusters apparently containing numerous larger primary myotubes surrounded by smaller secondaries were enclosed within these larger clusters. Hence, it appears that primary myotube separation has been inhibited by removal of PSA-NCAM.

We had intended to examine muscle morphogenesis in NCAM null mutant mice which do not express PSA-NCAM throughout life (Cremer et al., 1994). We have obtained breeding pairs of mice and a colony is now established, which we are about to start examining. Ono et al (1994) found evidence that aspects of neuronal development are perturbed in NCAM null mutant mice that may be entirely due to disruption of PSA function. NCAM null mutant mice are surprisingly normal in motor behaviour and the development of neuromuscular synapses (although slightly delayed) (Cremer et al., 1994, Ono et al., 1994, Moscoso et al., 1998). The lack of motor deficits in these mutants may reflect normal muscle development. However, muscle morphogenesis has not, to our knowledge, been rigorously examined in mice null mutant for NCAM.

Removal of PSA-NCAM may not inhibit primary myotube separation in the chick hindlimb

Previous studies have indicated that either paralysis or denervation of the hindlimb prior to axonal outgrowth inhibits myotube separation (Fredette and Landmesser, 1991; Fredette et al.,1993). In the case of paralysis, PSA-NCAM levels were found to have been dramatically reduced in muscle. However, they also showed that the adhesion molecule, N-cadherin, had become mis-expressed between the apposed membranes of myotubes which had not separated (also see Hahn and Covault, 1992). N-cadherin is normally expressed between developing myoblasts, and between myotubes and myoblasts. Its role appears to include promotion of terminal differentiation (George-Weinstein et al., 1997), muscle cell fusion (Mege et al., 1992) and myotube adhesion (Hahn and Covault, 1992; Fredette et al., 1993). Muscle N-cadherin expression is negatively regulated by synaptic activity (Hahn and Covault, 1992; Fredette et al., 1993), whereas muscle PSA-NCAM is positively regulated by synaptic activity in the fetus (Fredette et al., 1993). Thus, in paralysed muscle, prevention of N-cadherin down-regulation as well as loss of PSA-NCAM expression could either combinatorially or individually explain the enhanced adherence between myotubes in these paralysed muscles. We examined the effects of removing PSA-NCAM levels independent of neuromuscular inactivity in an attempt to find if increased anti-adhesion could account for inhibited myotube separation alone. No apparent alteration in muscle morphogenesis was observed after PSA-NCAM removal in the chick. Thus, our trials to date suggest that PSA-

NCAM is not necessary for the promotion of myotube separation in the chick hindlimb. It appears that downregulation of N-cadherin (Fredette et al., 1993), and possibly also M-cadherin (Donalies et al., 1991), may provide the principle drive for myotube separation in the chick hindlimb. The role for PSA-NCAM would therefore appear facilitatory. Testing of this hypothesis with function blocking antibodies to these cadherins with or without removal of PSA-NCAM may resolve this issue.

The role of PSA-NCAM in rat and chick muscle

Does PSA-NCAM act to attenuate adhesion to the point where the probability of separation is increased, does it actually push cells apart, or does it merely facilitate separation? Perhaps subtle differences in the precise role of PSA-NCAM between the chick and rat muscle may result in the differences observed after endoN injection. One molecule which seems to be functionally related to PSA during muscle separation is N-cadherin (Fredette et al., 1993), and possibly also M-cadherin. The functional relationship between cadherins and PSA-NCAM may hold the key to differences in PSA-NCAM function in the rat and chick. Conceivably, the downregulation of the adhesive cadherin concomitant with the upregulation of the anti-adhesive PSA-NCAM may function together to promote myotube separation. Throughout our studies, we have observed PSA-NCAM expression along the apposed membranes of apparently very young myoblasts and myotubes (as determined by histological criteria; very large nucleus to cytoplasm ratio). This would be in contrast to N-cadherin expression, which is gradually lost prior to separation (Hahn and Covault, 1992; Fredette et al., 1993). Such early expression may imply that PSA-NCAM is expressed in anticipation of its acting to facilitate separation once intermyotube adhesion had been lost, perhaps by down-regulation of cadherins. However, subtle differences in such a mechanism between rat and chick may result in differences in the effect of removing PSA-NCAM from developing myotubes. For example, shifting the balance of the relative importance of adhesion vs repulsion during myotube separation may account for the observed differences. Thus, perhaps cadherin mediated adhesion predominates in the chick, whereas PSA-NCAM mediated repulsion predominates in the rat. Further, one factor that cannot be discounted is that removal of PSA may render NCAM capable of promoting myotube adhesion. How this

may translate into increased adhesion in rat, but not chick muscle, however, is uncertain. We must, however, obtain more solid data before we can form any firm conclusions.

Previous reports would suggest that both N– and M-cadherin are important regulators of primary myogenesis in the rodent, equivalent to their role in the chick (eg Moore and Walsh, 1993, Cifuentes-Diaz et al., 1995). Preliminary evidence in the rat diaphragm indicates that, similar to the situation in the chick, cadherin expression is limited to the apposed membranes of primary myotubes and secondary myoblasts, but is lost when these myoblasts differentiate into secondary myotubes (unpublished observations). Further analysis of the precise relationship of cadherin and PSA-NCAM expression in the rodent diaphragm is necessary.

Regulation of PSA-NCAM expression in developing muscle.

Given the lack of myotube separation within denervated chick muscle previously described (Fredette and Landmesser, 1991), and supported here, it is perhaps surprising that myotube separation within the aneural rodent diaphragm was essentially normal. However, examination of developing rodent muscles in the absence of innervation consistently demonstrate normal myotube separation in toxin-induced, spinal cord ablation, and natural mutant paradigms (eg Harris, 1981; Hughes et al., 1992, Ashby et al., 1993). This shows that there are likely species-based differences in the effect of denervation on muscle morphogenesis. Examination of PSA-NCAM levels show that diaphragmatic muscle expresses high levels of normally distributed PSA-NCAM throughout diaphragmatic development. Given the putative role for PSA-NCAM in diaphragmatic muscle development, this would suggest that the expression of PSA-NCAM in aneural diaphragms drives myotube separation. We intend to co-inject β-bungarotoxin and endoN in an attempt to test this hypothesis directly. Further, it would be interesting to examine PSA-NCAM expression and the effects of endoN injection in the mouse mutant, *peroneal muscular atrophy*, in which certain hindlimb muscles receive no innervation, but undergo apparently normal myotube separation (Ashby et al., 1993).

Evidence that aneural diaphragms spontaneously generate Na^{2+}-dependent electrical activity, at least by E21, may provide a mechanistic explanation for PSA-NCAM expression

in aneural diaphragmatic myotubes, given that such activity would be postulated to promote PSA-NCAM expression. Two important experiments pertinent to these questions are: 1) Does abolition of neuromuscular activity (eg tubocurarine) and/or electrical activity (eg tetrodotoxin) reduce PSA-NCAM levels in the rat? Tetrodotoxin-induced paralysis in the rodent fetus has been performed successfully (eg Houenou et al., 1990), but we are uncertain as to whether myotubes separate normally or whether PSA-NCAM expression would be affected. 2) Would a tetrodotoxin-paralysed aneural diaphragm which did not generate spontaneous electrical activity express PSA-NCAM and how would muscle morphogenesis be affected? This would directly answer whether aneural diaphragm myotube spontaneous electrical activity contributes to PSA-NCAM expression, and subsequential myotube separation.

Another method that could be employed would be to examine muscle morphogenesis in relation to PSA-NCAM expression in the muscular dysgenesis (*mdg*) mutant mouse, which has a defect in excitation-contraction coupling and does not exhibit any spontaneously or induced muscle activity (see Houenou et al., for a comparison of development between TTX-induced inactivity and that observed in the *mdg* mutant). Despite the fact that electrical activity along the myotube surface would not be prevented by defects in excitation-contraction coupling, intracellular release of Ca^{2+} would be prevented. As discussed above, PSA-NCAM expression is coupled to levels of intracellular Ca^{2+} and may therefore be affected within these mutants (Rafuse and Landmesser, 1996; Brusés and Rutishauser, 1998).

Before we arrive at satisfactory answers, a number of factors must be determined. First, how do cadherin and PSA expression patterns relate to one another during myotube separation in the chick and rat muscle? Second, how is expression of PSA-NCAM and cadherins affected by denervation in the chick hindlimb? Spontaneously contractile chick myotubes express PSA-NCAM *in vitro*. However, we have not obtained reliable results concerning the expression of PSA-NCAM in aneural chick muscle and we are unsure as to whether any spontaneous activity in aneural chick myotubes would likewise promote PSA-NCAM expression. Third, are cadherin levels high or low along the membranes of separating rat aneural myotubes? Fourth, would function blocking antibodies or peptides to cadherins affect myotube separation in tubocurarine-paralysed muscles? In other words, is PSA even

required for separation, or is absence of cadherin sufficient. Fifth, how might paralysis affect rat myotube PSA and cadherin expression and, subsequently the separation of myotubes? Would PSA removal from aneural rat myotubes affect their separation? Finding answers to such questions may put us in a better position to design experiments to modulate the relative balance of cadherins and PSA-NCAM in order to examine the precise functional role of each molecule during muscle morphogenesis in both rat and chick.

REFERENCES

Ashby PR, Wilson SJ and Harris AJ (1993) Fomation of primary and secondary myotubes in aneural muscles in the mouse mutant *peroneal muscular atrophy. Dev. Biol.* 156: 519-528.

Brusés JL, Oka S and Rutishauser U (1995) NCAM-associated polysialic acid on ciliary ganglion neurons is regulated by polysialyltransferase levels and interaction with muscle. J. Neurosci. *15*:8310-8319.

Brusés JL and Rutishauser U (1998) Regulation of neural cell adhesion molecule polysialylation: Evidence for nontranscriptional control and sensitivity to an intracellular pool of calcium. *J. Cell Biol.* 140: 1177-1186.

Cifuentes-Diaz C, Nicolet M, Alameddine H, Goudou D, Dehaupas M, Rieger F and Mege RM (1995) M-cadherin localisation in developing adult and regenerating mouse skeletal muscle: possible involvement in secondary myogenesis. *Mech. Dev.* 50: 85-97.

Condon K, Silberstein L, Blau HM and Thompson WJ (1990) Differentiation of fiber types in aneural musculature of the prenatal rat hindlimb. *Dev. Biol.* 138: 275-295.

Covault J and Sanes JR (1986) Distribution of NCAM in synaptic and extrasynaptic portions of developing and adult skeletal muscle. J. Cell. Biol. *102*:716-730.

Covault J, Merlie JP, Goridis C and Sanes JR (1986) Molecular forms of N-CAM and its RNA in developing and denervated skeletal muscle. J. Cell. Biol. *102*:731-739

Cremer H, Lange R, Christoph A, Plomann M, Vopper G, Roes J, Brown R, Baldwin P, Kraemer P, Scheff S, Bathels D, Rajewsky K and Wille. (1994) Inactivation of the N-CAM gene in mice results in size reduction of the olfactory bulb and deficits in spatial learning. *Nature.* 367: 455-459.

Donalies M, Cramer M, Ringwald M, Starzinski-Powitz A (1991) Expression of M-cadherin, a member of of the cadherin multigene family correlates with differentiation of skeltal muscle cells. *Proc. Natl. Acad. Sci. USA*. 88: 8024-8028.

Fredette BJ and Landmesser LT (1991) A reevaluation of the role of innervation in primary and secondary myogenesis in developing chick muscle. *Dev. Biol.* 143: 19-35.

Fredette BJ, Rutishauser U and Landmesser L (1993) Regulation and activity-dependence of N-cadherin, NCAM isoforms and polysialic acid on chick myotubes during development. J. Cell. Biol. *6*:1867-1888

George-Weinstein M, Gerhart J, Blitz, J, Simak E, Knudsen KA (1997) N-cadherin promotes the commitment and differentiation of skeletal muscle precursor cells. *Dev. Biol.* 185: 14-24.

Greer JJ, Smith JC and Feldman JL (1992) Respiratory and locomotor patterns generated in the fetal rat brain-stem spinal cord in vitro. J. Neurophysiol. *67*:996-999.

Hahn C-G and Covault J (1992) Neural regulation of N-Cadherin gene expression in developing and adult skeletal muscle. *J. Neurosci.* 12: 4677-4687.

Hallenbeck PC, Vimr ER, Yu F, Bassler B and Troy FA (1987) Purification and properties of a bacteriophage-induced endo-N-acetylneuraminidase specific for poly-α-2,8-sialosyl carbohydrate units. *J. Biol. Chem.* 262: 3553-3561.

Harris AJ. (1981) Embryonic growth and innervation of rat skeletal muscles. I. Neural regulation of muscle fiber numbers. Phil. Trans. R. Soc. Lond. B *293*:257-277.

Hirokawa N (1978) Characterisation of various nervous tissues of the chick embryos through responses to chronic application and immunocytochemistry of β-bungarotoxin. *J. Comp. Neurol.* 180: 449-466.

Houenou LJ, Pinçon-Raymond M, Garcia L, Harris AJ, Rieger F (1990) Neuromuscular development following tetrodotoxin-induced inactivity in mouse embryos. *J. Neurobiol.* 21: 1249-1261.

Hughes DS, Schade RR, Ontell M (1992) Ablation of the fetal mouse spinal cord: The effect on soleus muscle cytoarchitecture. *Dev. Dyn.* 193: 164-174.

Kelly AM (1983) Emergence of specialization of skeletal muscle. In "Handbook of Physiology" (L.D. Peachey, Ed.) Section 10, pp. 507-537.

Landmesser L, Dahm L, Tang J and Rutishauser U (1990) Polysialic acid as a regulator of intramuscular nerve branching during embryonic development. Neuron *4*:655-667.

Laskowski MB and Owens JL (1994) Embryonic expression of motoneuron topography in the rat diaphragm muscle. Dev. Biol. *166*:502-508.

McCaig CD, Ross JJ and Harris AJ (1987) Embryonic somatic nerve destruction with β-bungarotoxin. *Cell Tiss. Res.* 247: 41-50

McDonald KA, Horwitz AF and Knudsen KA (1995) Adhesion molecules and skeletal myogenesis. Semin. Dev. Biol. *6*: 105-116

Mege RM, Goudou D, Diaz C, Nicolet M, Garcia L, Geraud G and Rieger F (1992) N-cadherin and N-CAM in myoblast fusion: compared localisation and effect of blockade by peptides and antibodies. *J. Cell Sci.* 103: 897-906.

Moore R and Walsh FS (1993) The cell adhesion molecule M-cadherin is specifically expressed in developing and regenerating, but not denervated skeletal muscle. *Development.*

117: 1409-1420.

Moscoso LM, Cremer H and Sanes JR (1998) Organization and reorganization of neuromuyscular junctions in mice lacking neural cell adhesion molecule, tenasci-C, or fibroblast growth factor-5. *J. Neurosci.* 18: 1465-1477.

Nakayama J, Angata K, Ong, Katsuyama T and Fukada M (1998) Polysialic acid, a unique glycan that is developmentally regulated by two polysialyltransferases, PST and STX, in the central nervous system: From biosynthesis to function. *Pathology International.* 48: 665-677.

Ono K, Tomasiewicz H, Magnuson and Rutishauser U (1994) N-CAM mutation inhibits tangential neuronal migration and is phenocopied by enzymatic removal of polysialic acid. *Neuron.* 13: 595-609.

Porter JD and Baker RS (1997) Absence of oculomotor and trochlear motoneurons leads to altered extraocular muscle development in the *Wnt-1* null mutant mouse. *Dev. Brain Res.* 100: 121-126.

Rafuse VF and Landmesser L (1996) Contractile activity regulates isoform expression and polysialylation of NCAM in cultured myotubes: involvement of Ca^{2+} and protein kinase C. J. Cell. Biol. *132*:969-983.

Rosen GD, Sanes JR, LaChance R, Cunningham JM, Roman J and Dean DC (1992) Role for the integrin VLA-4 and its counter receptor VCAM-1 in myogenesis. Cell *69*:1107-19.

Seki T and Arai Y (1991) Expression of highly polysialated NCAM in the neocortex and piriform cortex of the developing and adult rat. Anat. Embryol. *184*:395-401.

Seki T and Arai Y (1993) Distribution and possible roles of the highly polysialylated neural cell adhesion molecule (NCAM-H) in the developing and adult central nervous system. Neurosci. Res. *17*:265-290.

Chapter 7

PATHOGENESIS OF NITROFEN-INDUCED CONGENITAL DIAPHRAGMATIC HERNIA IN FETAL RATS

Adapted from the original publication:
Douglas W. Allan and John J. Greer
J. Appl. Physiol. 83(2): 338-347 (1997)

INTRODUCTION

Congenital diaphragmatic hernia (CDH) is a developmental anomaly characterised by the malformation of the diaphragm. Normally, during *in utero* development, the diaphragm develops to form a continuous sheet which completely separates the thoracic and abdominal cavities. However, in the instance of CDH, regions of the diaphragm are missing. Consequently, the developing viscera has access through an opening in the diaphragm to the thoracic cavity which it invades, occupying space normally reserved to accommodate the growing lungs. As a result, newborns with CDH (~1:3000 births) suffer from a combination of pulmonary hypoplasia, pulmonary hypertension and surfactant deficiency (Karamanoukian et al., 1995; Torfs et al., 1992). The mortality rate of infants suffering from CDH is approximately 50% (Harrison et al., 1994). Moreover, it has been estimated that a further 1 in 2000 conceptions fail to reach term due to complications associated with CDH (Harding, 1994).

While the mechanisms underlying the aetiology of CDH remain obscure, there are a number of theories pertaining to the pathogenesis of the condition. First, a theory which has persisted states that the diaphragmatic malformation is merely a secondary defect due the maldevelopment of the adjacent lung tissue (Iritani, 1984). Second, Iritani (1984) has also suggested that there is a perturbation of the normal innervation of the diaphragm by the phrenic nerve, which may subsequently arrest proper diaphragmatic muscle development. A third and the most commonly cited explanation for CDH, states that there is an abnormality with the closure of the pleuroperitoneal canal (Skandalakis et al., 1994). Fourth, it has been suggested that the developing muscle fibres (myotubes) within the region of herniation may fail to form or are weak and prone to rupturing in the presence of underlying forces produced by the expanding abdominal contents (Skandalakis et al., 1994). However, there is very little scientific data supporting any of these theories and a basic understanding of how the normal, let alone the pathological diaphragm, develops is lacking (Kluth et al., 1989; Skandalakis et al., 1994). Towards such an understanding, we have examined the normal ontogenesis of the phrenic nerve and diaphragm in fetal rats (chapter 4 and 5) and, in the present study, we systematically test each of the above mentioned hypotheses

regarding the pathogenesis of CDH (see also Greer et al., 2000).

We have utilised the nitrofen-induced CDH rat model to examine lung growth, phrenic nerve innervation and the formation of the diaphragmatic musculature in instances of CDH. We determined if abnormalities in their development were either primary or secondary to herniation of the diaphragm. Nitrofen (2,4-dichloro-phenyl-p-nitrophenyl ether) is a toxic herbicide which produces, when given as a single oral dose to a pregnant dam, a condition in fetal rats remarkably similar to that associated with CDH observed in human infants (Alles et al., 1995; Kluth et al., 1989, 1990, 1993; Puri, 1989: Wickman et al., 1993). The weight, and the protein and DNA content of lungs (Zamenhof et al., 1964) were compared in CDH and control animals before and after invasion of visceral organs into the thoracic cavity. Immunohistochemical labelling for growth associated protein (GAP-43) and the polysialylated form of the neural cell adhesion molecule (PSA-NCAM), both expressed within growing phrenic axons (chapters 4 and 5), was performed to determine the pattern of phrenic axon intramuscular branching from its onset at embryonic day (E)14.5 up to near its completion at E18. In conjunction with GAP-43 and PSA-NCAM immunolabelling, electron microscopy of phrenic nerve cross sections provided information regarding nerve diameter and axonal number before and after programmed neuronal cell death in instances of CDH. Further, we retrogradely labelled phrenic motoneuron cell bodies with the lipophilic dye DiI to examine the distribution of motoneurons in normal versus CDH fetuses. Finally, the formation of the primordial diaphragmatic anlage, the pleuroperitoneal fold, and the onset of myotube formation within the diaphragm was examined via immunolabelling for low affinity nerve growth factor receptor (p75) and the polysialylated form of the neural cell adhesion molecule (PSA-NCAM). As shown in the present study, the primordial diaphragm expresses the p75 receptor, while as previously reported, developing diaphragmatic myotubes express PSA-NCAM (chapter 4).

METHODS

Delivery of nitrofen

It was noted during initial routine toxicological studies of the herbicide nitrofen, that while it was relatively non-toxic to adult animals, it produced a number of lethal abnormalities associated with pulmonary and cardiovascular malfunction in fetuses exposed prenatally (Ambrose et al., 1971; Costlow et al., 1983; Gray et al., 1983). Further, when given as a single dose on gestation day E9 or E11, the major abnormality produced by nitrofen was a maldevelopment of the diaphragm which was strikingly similar to the developmental anomaly, CDH. In order to specifically produce diaphragmatic malformations, the timing of the nitrofen delivery to the dam is critical. Administration of a single dose on E9 produces hernias on the left and/or right side of the diaphragm. Delivery of nitrofen on E11 produces solely right-sided hernias. The number of fetuses within a dam affected by the nitrofen is dose-dependant and may also vary with the efficacy of teratogen transfer to each of the respective fetuses in a litter.

In the present study, nitrofen was obtained from the U.S. Environmental Protection Agency and prepared as a solution of 100 mg/ml in olive oil. The timing of pregnancies was determined from the appearance of sperm plugs in the breeding cages (designated as E0). Pregnant dams on the ninth day of gestation (E9) were temporarily (~10 min) anaesthetised with halothane (1.25% in 95% 0_2-5% CO_2) and given 100 mg of nitrofen via a gavage tube to produce either left, right or bilateral hernias (Table 7.1). In two animals, nitrofen was administered on E11 to produce solely right-sided hernias.

Embryo sections, wholemount diaphragms, immunohistology, DiI retrograde labelling:

These were all performed as previously described.

Electron microscopy of phrenic axons

Axons from control and nitrofen-exposed rats were examined in phrenic nerve sections taken ~500 μm rostral to the point of innervation of the diaphragm. Nerves were immersed in a mixture of 2% paraformaldehyde and 2.5% glutaraldehyde in 0.1 M sodium cacodylate

buffer (pH 7.4) for 2-4 hours. After three washes of 5 minutes each in 0.1M cacodylate (pH=7.4), the nerves were post-fixed for 15 minutes in a mixture of 1% OsO_4 and 0.1 M phosphate buffer (pH=7.4). The tissue was then washed 3 times in distilled water, dehydrated in graded ethanol and embedded in TAAB 812 resin. Sections were cut with a microtome, stained with uranyl acetate and lead citrate, and observed with a Philips 410 electron microscope. Photomicrographs were taken (x4300) and measurements of nerve area were made using an image analysis system (JAVA; Jandel Inc.). Axon numbers were counted be viewing the photograph negatives with a stereo microscope at 10 times magnification.

Measurements of lung weight, protein and DNA content.

Preparation of the lungs: Lungs were removed, weighed and quickly frozen in liquid nitrogen and stored at -80°C until analysed when they were defrosted and kept on ice. Each lung was homogenised in 1 ml distilled water in an ice bath with a polytron homogeniser at setting number 5 for 30 seconds (Brinkman Instruments, Westbury, NY). The homogenate was divided into two 500 ml aliquots for measuring protein and DNA content.

Protein assay: Protein was determined using an array spectrophotometer (Hewlett Packard model 8452A; Palo Alto, CA) with a Bradford microassay (Bio-Rad Laboratories, Hercules, CA; 6). Bovine serum albumin (Sigma; St. Louis) was used for the standard.

DNA assay: The DNA quantitation technique was adapted from Downs and Wilfinger (1983). Homogenate and DNA extraction solution (1 M NH_4OH, 10 mM EDTA) were incubated at 37°C in a shaking water bath for 30 minutes. After centrifugation at 2500 rpm for 3 minutes, 25 µl of supernatant was added to 35 µl of distilled water and further centrifuged in an evaporator centrifuge for ten minutes. Distilled water was added to make a final volume of 500 µl. Fifty µl was then removed and added to 1.5 ml dye solution. The dye solution was prepared by mixing 50 µl Hoechts 33538 and 100 ml DNA assay buffer (100 mM NaCl, 10 mM EDTA, 10 mM TRIS, pH=7.0). Samples to be measured were then vortexed and left at room temperature for 30 minutes before DNA concentration was determined using fluorescence spectrophotometer (Hitachi F-2000; Tokyo).Graded known concentrations of calf thymus DNA (Sigma; St. Louis) were used as a reference.

Results are expressed as mean ± S.E.M. and any differences were tested using an unpaired student's *t* test; significance was accepted at P values less than 0.05.

RESULTS

Hernias induced by nitrofen

Administration of a single dose of nitrofen on day E9 resulted in CDH in 52% of fetuses. Diaphragmatic holes were limited to regions of the costal neuromusculature (and crural ipsilateral to the costal defect if it were large) on the right (25%), left (21%) and bilaterally (6%) (Table 7.1). Administration of nitrofen on E11 resulted in the formation of right-sided hernias only. The range of hernia sizes and locations are illustrated in Fig. 7.1. The range of defects included: 1) mild to very severe left-sided malformations where approximately 50-90% of the muscle is missing, 2) mild to medium right-sided malformations where approximately 5-50% of the muscle is missing, and 3) bilateral malformations of equivalent asymmetric sizes. All malformations emanated from the posteromedial area referred to as the 'region of Bochdalek'. Defects found in nitrofen-induced rodents are identical in both size and location, and in the variability of size, as found in human infants with CDH (Skandalakis et al., 1994).

TABLE 7.1 INCIDENCE OF DIAPHRAGMATIC HERNIAS INDUCED BY NITROFEN (ADMINISTERED E9)

TOTAL#	NORMAL	LEFT HERNIA	RIGHT HERNIA	BILATERAL HERNIA
181 (17 dams)	86 (48%)	39 (21%)	45 (25%)	11 (6%)

Note that there were several occasions where fetal reabsorptions had occurred. There were also 3 experiments where all of the fetuses present at the time of inspection were normal despite the administration of nitrofen. On two further occasions, nitrofen was administered on E11; a total of zero left and 9 right hernias were produced compared to 21 normals. None of the above mentioned data has been included in the table.

Fig. 7.1: Range of diaphragmatic malformations within one litter induced by the administration of nitrofen on E9. Diaphragms were removed from a single dam at E21 and stained for eosin to visualise the neuromusculature. (A) Control diaphragm demonstrating the normal extent of neuromusculature of the E21 diaphragm. (B,C) Left hernias. Over 50% of muscle surface is always missing. Note that in these two severe cases, the left crus is absent. The left crus is maintained in smaller left hernias (not shown here). (D,E) Right hernias. Typical range for right hernias, ranging up to 50% missing. (F) Bilateral hernia demonstrating the relative size of left vs right malformations. Abbreviations: S (sternum), CT (central tendon), VC (vena cava), Cr (crural region), Co (costal region), V (ventral), R (right). Scale bar same for all = 5mm.

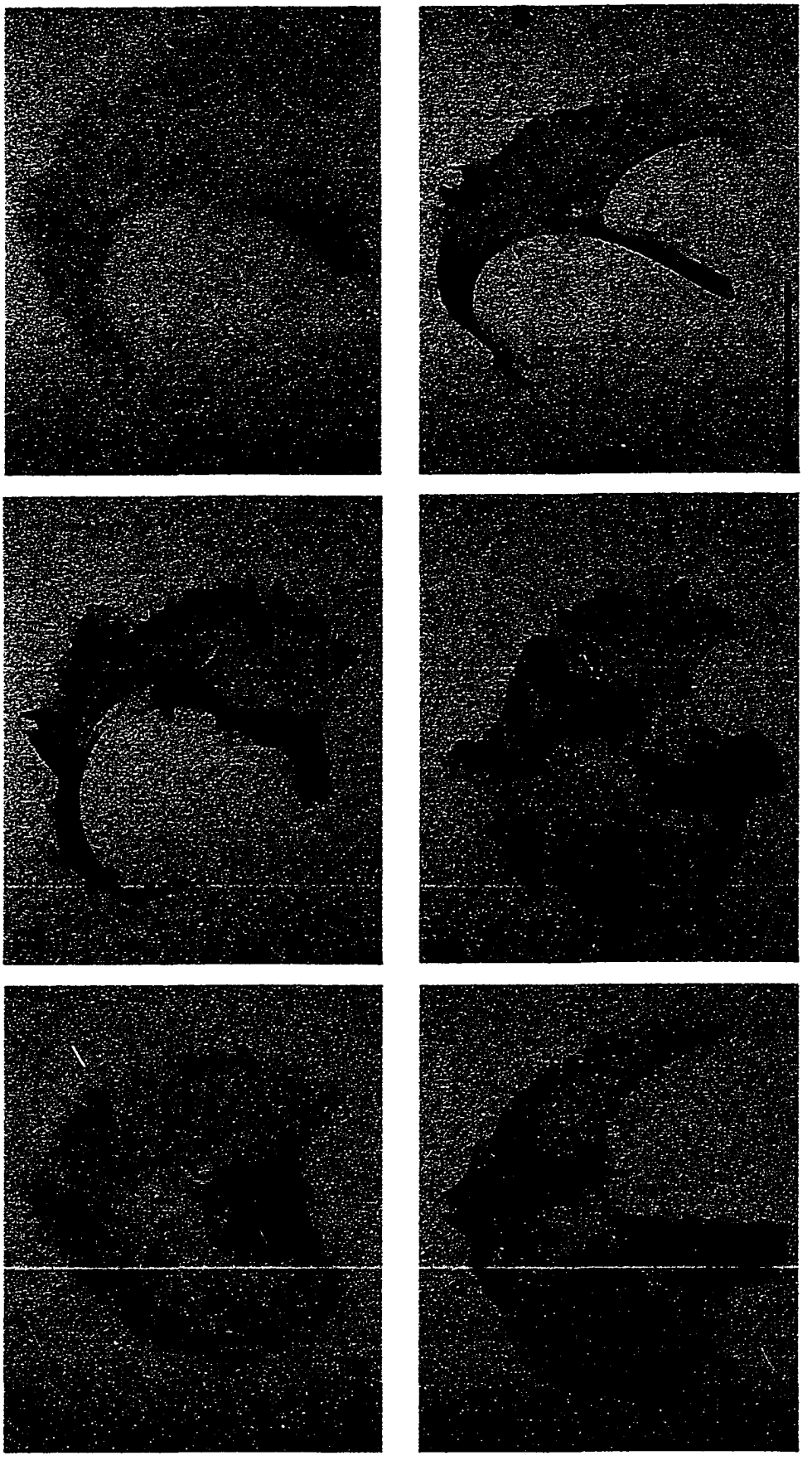

Lung growth

Measurements of lung growth were made to determine whether the lung hypoplasia associated with CDH occurred pre-(E15) or post-invasion (E18) of the abdominal contents into the thoracic space. For the lung measurements, only medium to severe hernias were used. By E15, abdominal contents had not grown sufficiently to enter the thoracic space through herniated diaphragms. By E18 on the other hand, significant invasion of the thoracic cavity by abdominal contents had occurred in herniated fetuses. Thus, we compared lung development in normal and herniated fetuses pre-and post-invasion of abdominal contents in animals from the same litter. Body weight, lung weight, lung protein and DNA content were measured in control and CDH rats at ages E15 and E18.

As illustrated in Table 7.2, there were no significant differences in the body weight, lung weight, lung protein and lung DNA content between controls and animals with extensive diaphragmatic malformations at age E15. At age E18, there was a significant reduction in overall lung weight, as well as protein and DNA contents of the lungs in herniated animals compared with control; all suggesting a decreased cell content within the lung. Thus, collectively, these data illustrate that lung hypoplasia is a secondary effect resulting from the restricted thoracic space associated with the misplacement of abdominal contents, rather than a primary defect which precedes diaphragm malformation.

TABLE 7.2 EFFECTS OF DIAPHRAGMATIC HERNIAS ON LUNG GROWTH AT AGES E15 AND E18

Group	Body weight (g)	Lung weight (mg)	Lung/body weight (mg/g)	Total lung protein (mg)	Protein/lung weight (mg/g)	Total lung DNA (ug)	DNA/lung weight (mg/g)
E15 control (n=12)	0.36±0.01	3.3±0.2	9.2±0.4	.08±.01	26.0±2.6	10.2±1.2	3.3±0.3
E15 hernia (n=11)	0.35±0.01	2.6±0.3	7.4±0.9	.08±0.01	33.3±3.0	9.1±1.0	3.5±0.4
E18 control (n=14)	1.4±0.04	41.6±1.3	29.2±1.0	1.6±0.06	38.3±1.7	215.3±12.7	5.2±0.3
E18 hernia (n=13)	1.4±0.03	33.2±1.3*	24.9±0.8*	0.9±0.1*	29.3±3.1*	136.7±13.9*	4.1±0.5

Values are mean ± SD. n = number of fetuses. * Indicates a significant difference from control value ($p<0.05$).

The Phrenic Nerve

These measurements were made to assay whether or not the phrenic nerve was malformed in instances of CDH, and if so, to determine whether or not phrenic nerve atrophy occurred prior or secondarily to the diaphragmatic herniation. To quantify the diameter of phrenic nerves in normal and herniated animals, transmission electron micrographs of nerve cross sections were examined. Fig. 7.2 shows the left and right nerves from three animals, one aged E15 (left hernia) and two E18 (left and right hernias). There was no significant difference in the areas of the nerve ipsilateral (589±31 μm^2; n=3) and contralateral (550±41 μm^2; n=3) to the hernia at E15. However at E18, the phrenic nerve ipsilateral to the abnormality had atrophied. Measurements of nerve area confirmed that the nerve ipsilateral to the hernia was significantly smaller (814±6 μm^2; n=6) than the contralateral nerve (1348±8 μm^2; n=9). Counts of axonal number at E15 were not significantly different on the side innervating the ipsi- or contra-lateral to the herniated hemidiaphragm (not shown). Counts of axon number in phrenic nerves from two fetal rats aged E18 with large left-sided hernias demonstrated that the reduced nerve area resulted from a decrease in the total number of axons; 582 and 695 axons in the ipsilateral versus 1078 and 1061 axons in the contralateral phrenic nerves were counted in the two animals, respectively. These observations can be explained by the fact that the majority of phrenic motoneuron cell death occurs between E15 and E16 and thus, the degree of motoneuron survival within the ipsilateral motoneuron pool would be compromised by the reduced musculature and its associated target-derived neurotrophic factors (Hamburger, 1975).

Fig. 7.2: Assessment of phrenic nerve size in animals with CDH. Shown are a series of photos from transmission electron microscopic images of phrenic nerve cross sections taken from animals with either left or right-sided hernias at ages E15 or E18. The top two panels contrast the size of the phrenic nerve area (demarcated by the dashed line) on the left and right side from an E15 animal with a large left-sided hernia. The nerve ipsilateral to the diaphragmatic malformation is similar in size to the contralateral side. In contrast, as shown in the middle and bottom panels, the phrenic nerve ipsilateral to the diaphragmatic malformation is smaller than the contralateral nerve in large left and right-sided hernias at age E18. This atrophy of the phrenic nerve at the older age can be explained by increased apoptosis which occurs secondarily to removal of a portion of the muscle target during the period of naturally occurring cell death. Magnification = x4300.

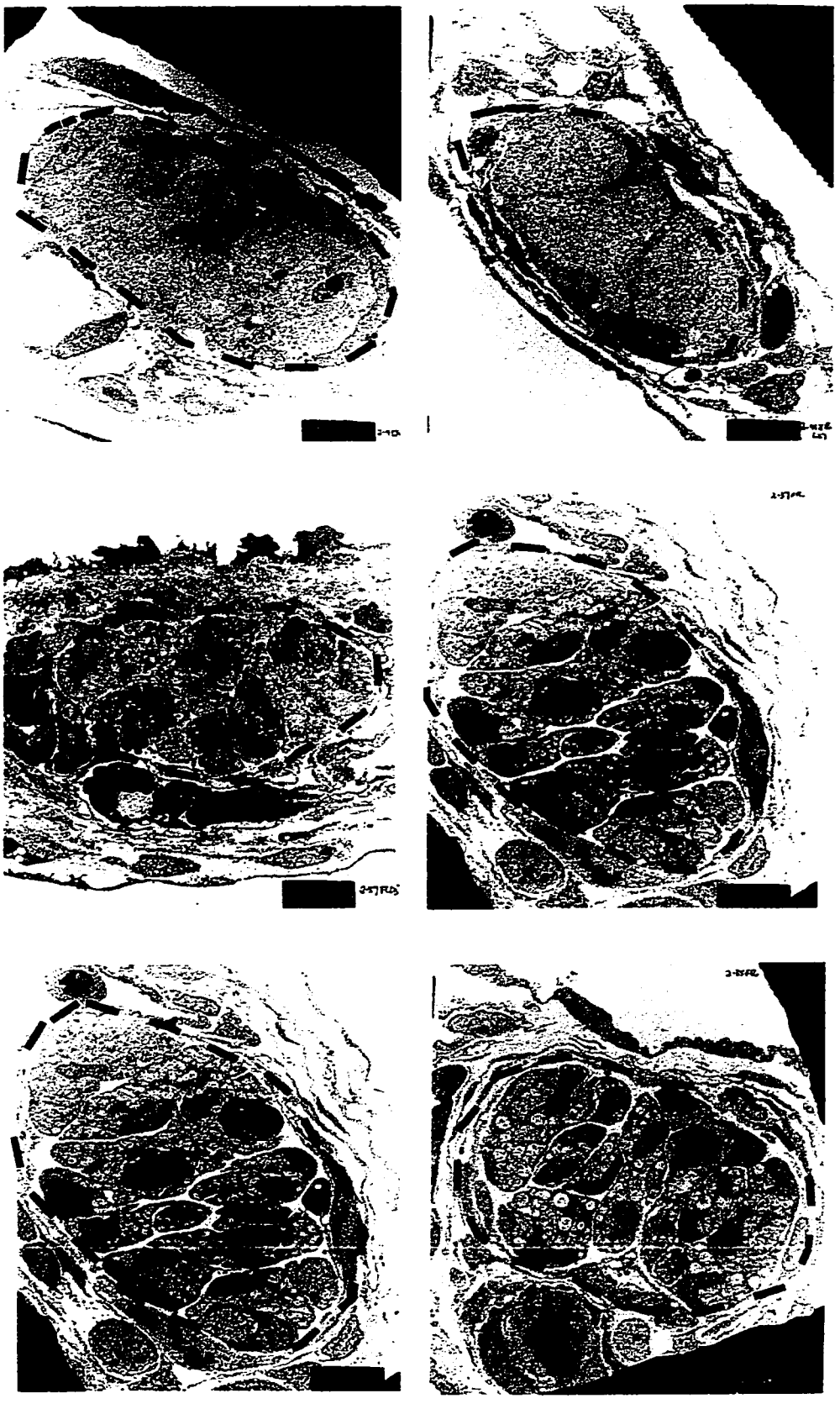

LEFT **RIGHT**

The decrease in the normal number of phrenic motoneurons ipsilateral to the hernia after naturally occurring cell death was also evident from retrograde fills with DiI at age E18 (Fig. 7.3). The number of somata counted within the phrenic motoneuron pool ipsilateral to large left-sided hernias was 67±8% of the contralateral side ($n=6$; $p< 0.05$). Note, there is normally a well defined topographical innervation of the diaphragm with the dorsal regions of the musculature innervated primarily by phrenic motoneurons within the C5-C6 cervical segments of the motoneuron pool (Laskowski and Sanes, 1987). The sternal region is primarily innervated by motoneurons located at the level of the third and fourth cervical segments. Thus, without a compensatory mechanism whereby phrenic axons re-establish an essentially normal topographic projection within the remaining musculature, one would expect a massive die off of neurons caudal to C4 regions. Clearly, this is not the case, as decreased access of phrenic axons to the normal amount of musculature results in a loss of survival which, while slightly heavier within caudal regions, is shared by the remainder of the phrenic motoneuron column.

Fig. 7.3: DiI retrograde fills of phrenic motoneurons at E18: This figure demonstrates that fewer motoneurons survive within the phrenic motoneuron pool on the side ipsilateral to the diaphragmatic malformation. Photos A-D show the rostrocaudal extent of the phrenic motoneuron pool in a series of adjacent ventral (A) to dorsal (D) sections (sections were cut at 70 μm). Note that there are fewer motoneurons labelled throughout the rostrocaudal distribution of the phrenic motor pool on the side ipsilateral (left) to the hernia (3/4 of the diaphragm was missing from the left side) as compared to the contralateral (right) side. Further, note that the rostrocaudal extent of the phrenic pool was maintained. Scale bar = 200 μm.

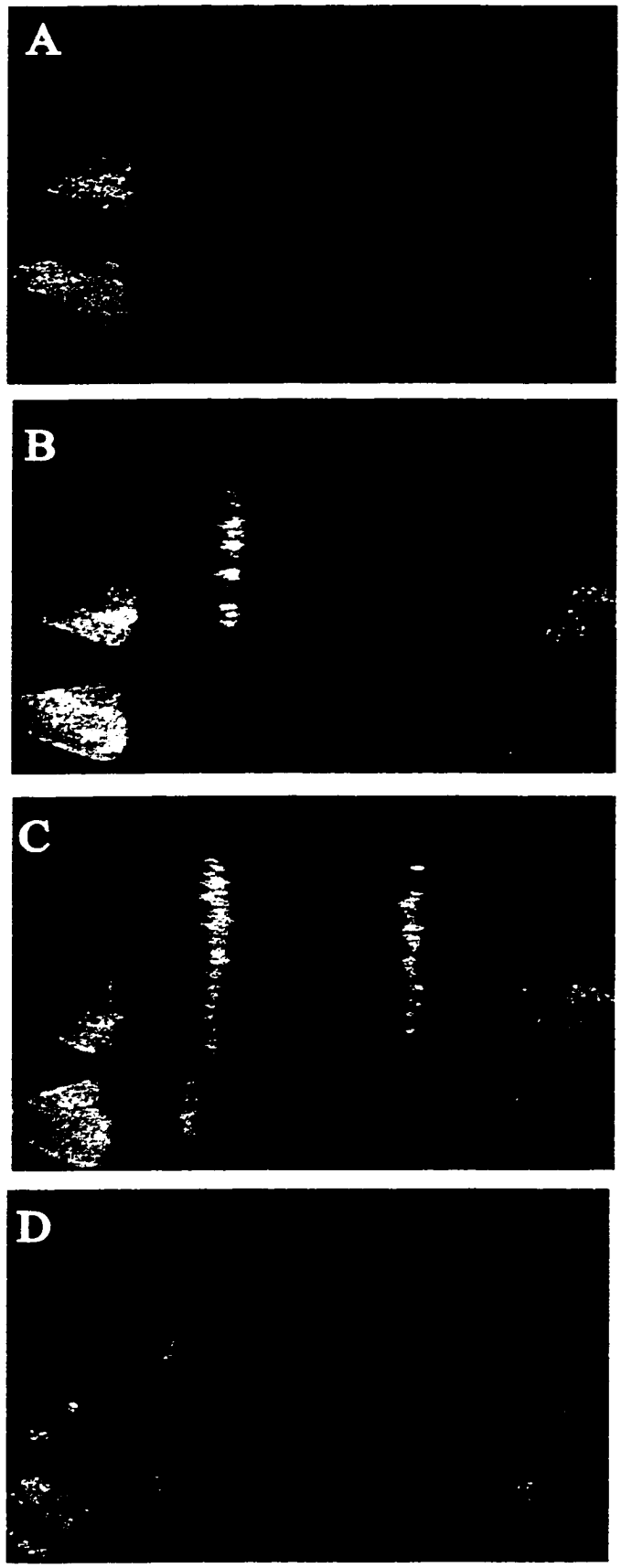

Neuromuscular formation

We examined the pattern of innervation and myotube formation in herniated diaphragms through fetal development. Fig. 7.4 demonstrates the pattern of nerve and muscle development at E14.5 (GAP-43), E15.5 and E17.5 (PSA-NCAM) in left hernias. In all cases, a normal right hemidiaphragm serve as internal controls. The phrenic nerve appears capable of compensation for the defect (missing region) in that, although translocated ventrally, the characteristic trifurcation at the primary branching site is retained at all ages. Even in the severe hernia shown in Fig 7.4D, closer examination shows that three characteristic branches form (not shown). Further, axons were often observed projecting around the herniated region, being diverted laterally or medially in search of its normal, but displaced target. At E14.5 (Fig. 7.4A), the crural branch of the nerve extends a considerably greater distance to reach the crural musculature medially. Further, the dorsolateral branch which would normally project immediately dorsal, close to the crural branch (see Fig. 5.6), now reaches more laterally. Likewise, by E15.5 (Fig 7.4B) the crural and dorsolateral branches follow considerably detoured paths to innervate their appropriate muscular region. In Fig 7.4C, the crural branch reaches and innervates a displaced crural musculature.

Likewise, the muscle appears to attempt compensation for the defect. PSA-NCAM labelling of muscle fibres shows that muscle fibres form around the defect as normal, but that the remaining is thickened, suggesting that muscle normally destined for the defective region has been displaced (Fig. 7.5). In Fig 7.4B, innervated muscle can be observed to fill the extreme lateral edge of the diaphragm around the defect. In dissecting these diaphragms, such extension of long thin strips of neuromusculature were commonly observed at the lateral edge of the defect. The severe defect in Fig 7.4D was dissected from the body wall to which it was attached. Fig. 7.5 shows examples of whole-diaphragms taken from two animals aged E17, one with a large left hernia labelled for PSA-NCAM and the other a medium sized hernia labelled for GAP-43. Cross sections taken from diaphragms identical to those presented as wholemounts and immunolabelled for PSA-NCAM show that the density of labelling, reflecting myotube number, was highest in regions adjacent to the hernia. Thus, myotube formation within the herniated diaphragms is only abnormal in that myotubes normally destined to span the region of herniation have accumulated adjacent to

it. We did not, however, count the number of myotubes in control vs CDH diaphragms, thus the possibility of the formation of fewer myotubes has not been addressed. Reduced axonal number in electron microscopic axonal counts ipsilateral to the defect at E18 would implicate a reduction in the number of myotubes, however.

Fig. 7.4: Development of diaphragmatic neuromusculature in left herniated diaphragm.
Progression of neuronal and muscular development in herniated diaphragms from E14.5 to E17.5. (A) GAP-43 immunolabelled diaphragm showing compensation of nerve around the large dorso-medial defect. Muscle labelling (not shown due to difficulty in discerning axons) parallels that of neuronal labelling. (B) E15.5 immunolabelled for PSA-NCAM showing that the nerve and muscle compensate medially and laterally of the defect. (C,D) Two diaphragms at E17.5 immunolabelled for PSA-NCAM to show variation in size of herniation. In C, particularly, normal, but displaced trifurcation and higher order branching can be observed on the left herniated side. Further, a higher density of PSA-NCAM immunolabel on the herniated side in C and D imply a greater density of fibres on the herniated side (see next figure). Scale bars = 500μm.

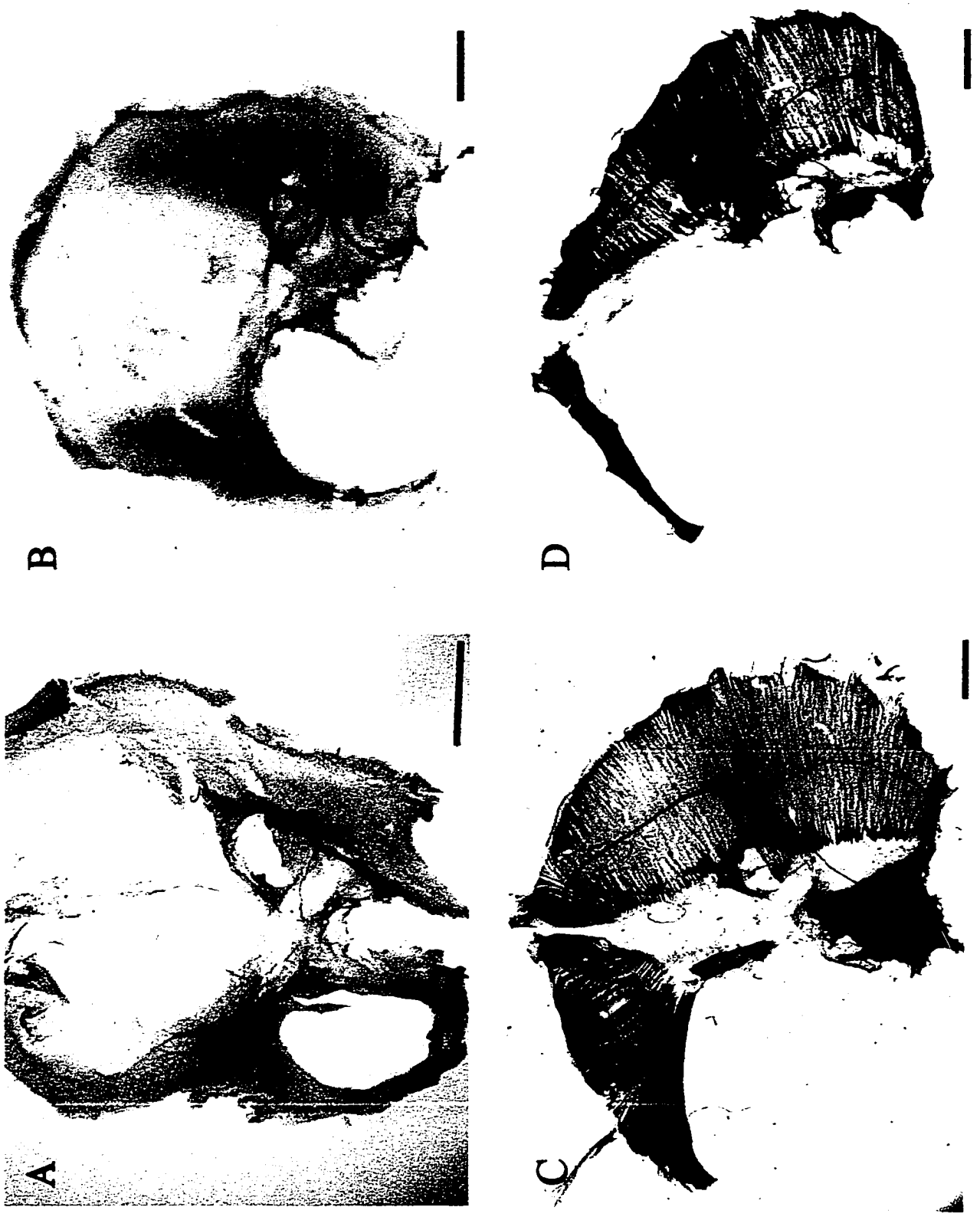

Fig. 7.5: Assessment of myotube formation in the region of herniation. The top panel (A) shows a large left-sided hernia with cross-sections taken from the left and right side of an identical diaphragm, both labelled for PSA-NCAM. The bottom panel (B) shows a right-sided hernia labelled for GAP-43 with cross sections of the musculature from the right side of an identical diaphragm labelled for PSA-NCAM. Dashed lines in both photos demarcate the approximate location from which muscle cross-sections were taken. It is apparent from the PSA-NCAM labelling of the myotubes in (A), that there is a more condensed distribution of myotubes on the herniated side and the initial branching site is translocated ventrally (position of phrenic nerve insertion point is indicated by arrow). Cross-sections from both sides of the diaphragm indicate that the muscle is approximately three times as thick on the side ipsilateral to the malformation as compared with the contralateral side. (B) further illustrates the thickening of the musculature in the periphery of the hernia (arrow), but in this case of a right-sided hernia. Scale bars (μm) = whole mount diaphragms, 500; cross sections, 200.

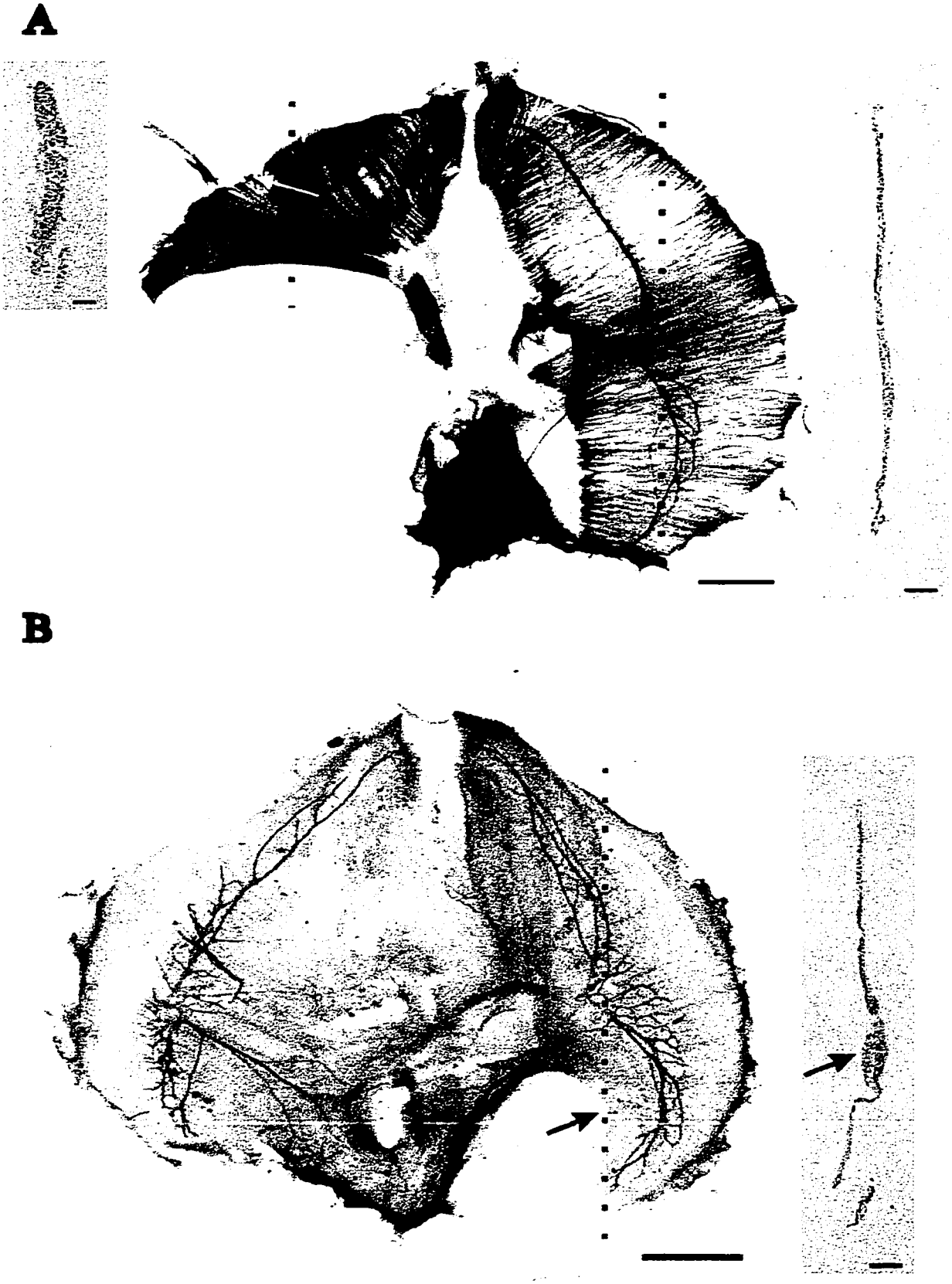

Closure of the pleuroperitoneal canal

We examined fetal diaphragms for defects at E14.5, prior to pleuroperitoneal canal closure. Our rationale was that if the hernia occurred as a result of the failure of pleuroperitoneal canal closure, then no defects would be observed prior to E15. The left and right pleuroperitoneal canals (PPC) in fetal rats typically close at ages E14.75 and E15.25, respectively (Gattone and Morse, 1984). The location of the pleuroperitoneal canals in a normal diaphragm from an animal aged E14.5 is illustrated in Fig. 7.6A. Two diaphragms from animals aged E14.5 which have been exposed to nitrofen on E9 are shown beside the control diaphragm (Figs. 7.6B,C). There are clear defects which appear prior to canal closure on both left (B) and right sides (B,C). Further, the region of herniation clearly occurs medially of the canal. This is particularly evident in small right hernias where the PPC is observed lateral, the defect medially, and a small strip of developing neuromusculature between the two (C). It is also clear that the defect is observed to precede canal closure, and thus temporally, can not be due to a failure of the canal to close. Thus, the abnormality must occur independently from a simple failure of pleuroperitoneal canal closure.

Fig. 7.6: Pleuroperitoneal canal in normal and CDH diaphragms. (A) illustrates a normal diaphragm taken from an animal aged E14.5 immunolabelled for PSA-NCAM. The pleuroperitoneal canals (marked with an asterisk) in the control animal have not yet completely closed. Panels B and C show diaphragms from a similar age immunolabelled for PSA-NCAM which have been affected by the exposure to nitrofen on E9. It is clear that there are gross malformations on the left (B) and right (B,C) sides of these diaphragms which are spatially distinct from the pleuroperitoneal canals. Further, defects can be observed prior to canal closure. This indicates that the malformations associated with nitrofen-induced hernias occur prior to and independently from closure of the pleuroperitoneal canal. Abbreviations: D (defect). Scale bars = 500 μm.

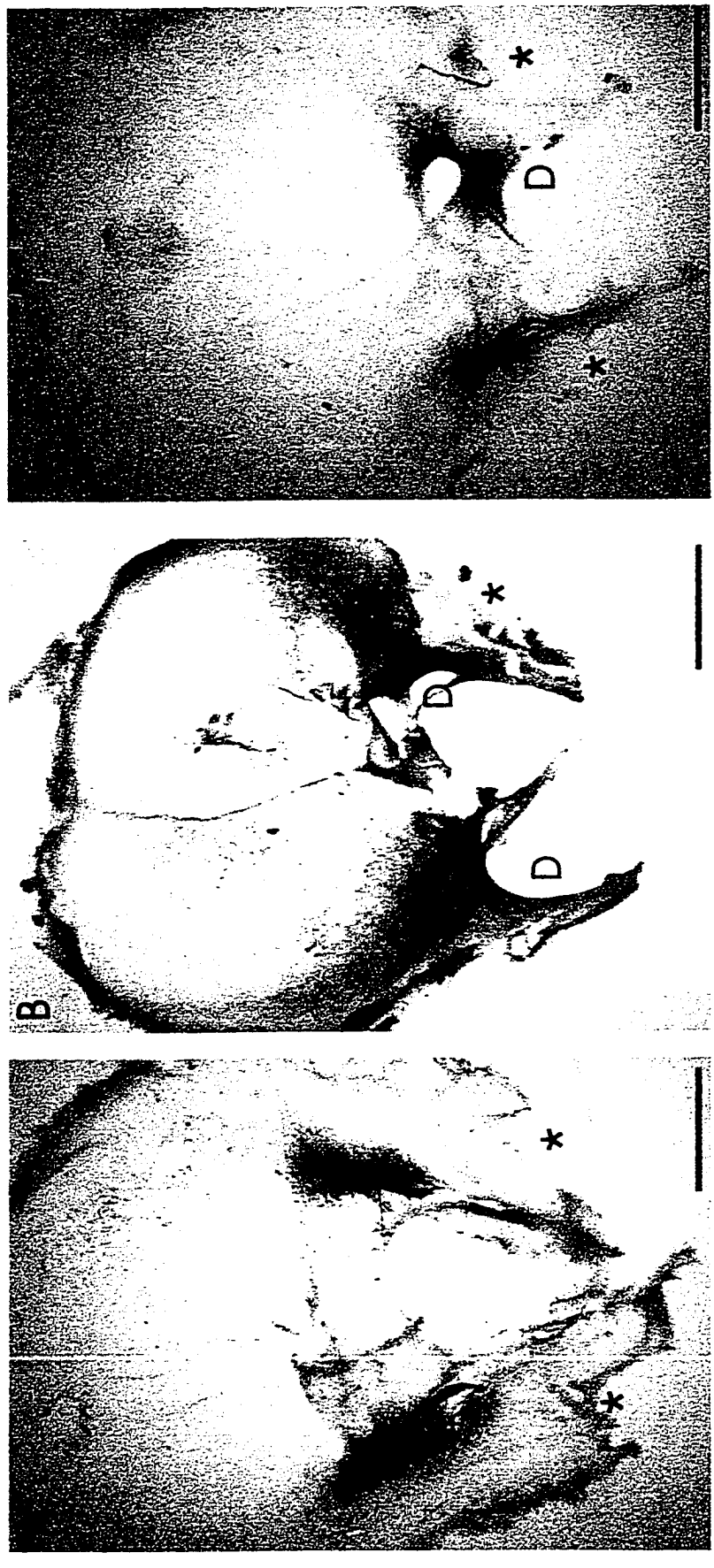

Formation of the primordial diaphragm, the pleuroperitoneal fold

The primordial diaphragmatic muscle tissue is located within the pleuroperitoneal fold. This fold of tissue is shown in Fig. 6A. We knew from earlier observations that a track of cells expressing NCAM and the low affinity nerve growth factor (p75) receptor proceeds phrenic nerve outgrowth (chapter 4). Although we have not yet identified the population, we took advantage of the characteristic immunolabelling for p75 receptors in control and nitrofen-exposed animals aged E13.5 to determine if the pleuroperitoneal fold was malformed in the instance of CDH. We observed defects of the left and right pleuroperitoneal fold amongst nitrofen-exposed animals. Fig. 6B shows a large defect within the left pleuroperitoneal fold of one such fetus at age E13.5. More rostral sections demonstrate that the nerve reached the displaced pleuroperitoneal fold by its projection through the pleuropericardial membrane (as in normal fetuses), which is fused with the diminished pleuroperitoneal fold.

Fig. 7.7: Deformation of the pleuroperitoneal fold in herniated fetuses. The primordial diaphragmatic tissue within the pleuroperitoneal fold (marked by an asterisk) at age E13.5. Shown are transverse cross sections from two E13.5 fetal rats immunolabelled for p75 receptor, one from an animal affected by exposure to nitrofen (A) and a control animal (B). It is clear from photo (A), that the animal affected by nitrofen has a large component of the laterally located pleuroperitoneal fold missing (outlined by the dashed line). The arrows point to where the phrenic nerve enters the control and abnormal pleuroperitoneal folds. We propose that the pathogenesis of CDH is associated with a malformation of the early stages of primordial diaphragm development. Abbreviations: Lu (lung), Fl (forelimb), A (aorta) L (lateral), D (dorsal). Scale bars = 100 μm.

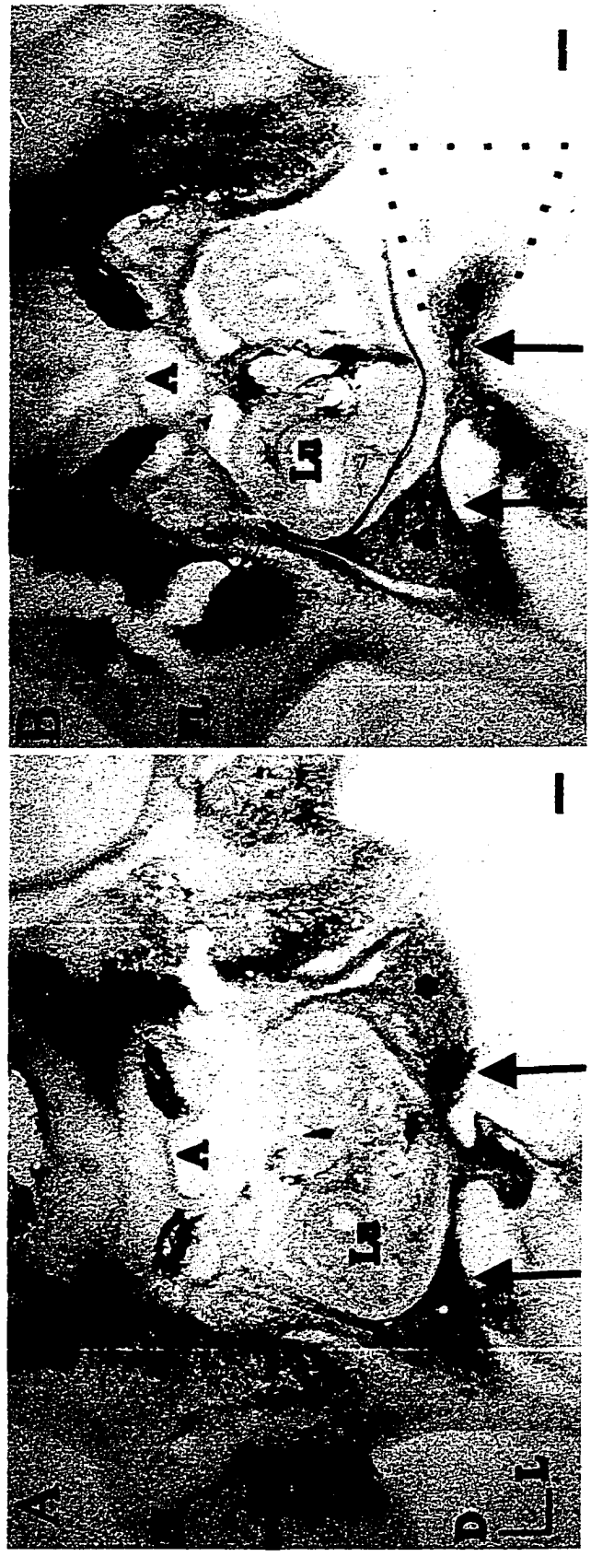

DISCUSSION

This systematic study evaluated the status of the lung, the phrenic nerve and diaphragmatic muscle formation at various stages during the course of the abnormal development of the diaphragm associated with nitrofen-induced CDH. We demonstrate that previously proposed theories regarding the primary role of the lung, phrenic nerve, myotube formation and the closure of pleuroperitoneal canal in the pathogenesis of CDH are incorrect. Rather, the primary defect associated with nitrofen-induced rodent CDH occurs at an early stage with the formation of the primordial diaphragm within the pleuroperitoneal fold.

General comments on the nitrofen model for CDH

Nitrofen is a diphenyl ether herbicide which acts by an unknown mechanism for the control of broad-leaved weeds. Initial toxicological studies revealed that while nitrofen was relatively non-toxic to adult animals, it did produce a number of lethal abnormalities associated with pulmonary and cardiovascular malfunction in fetuses exposed prenatally (Ambrose et al., 1971; Costlow and Manson, 1981, 1983; Gray et al., 1983; Ostby et al., 1985). When given as a single dose on gestation day E9 or E11 in the rat, the major abnormality produced by nitrofen was the maldevelopment of the diaphragm. As illustrated in Fig. 1, the range and location of hernias produced by nitrofen in the rat are remarkably similar to that observed in the human congenital anomaly. In the rat CDH model, the extent of the invasion of abdominal contents into the thoracic cavity varied according to the size of the defect within the diaphragmatic musculature. In humans, the extent of herniation also varies and is a critical determinant of the subsequent degree for pulmonary hypoplasia and the eventual prognosis (Adzick et al., 1985). Further, it is interesting to note that the rate of fetal reabsorptions increases in rats after administration of nitrofen on gestational age E9. In this context, it has been estimated that approximately 1:1000-2000 human fetuses do not make it to term due to complications associated with CDH and accompanying defects (Harding, 1994). Thus, while there is no concrete data associating environmental toxins with the aetiology of CDH, there does seem to be a remarkable similarity between the nitrofen model and the majority of human CDH anomalies. However, differences between the rat

nitrofen model and the human condition include the fact that multiple congenital anomalies are associated with CDH in ~30% of infants (Dillon and Renwick, 1993; Philip et al., 1991). Typically, associated anomalies (e.g. cardiac malformations, hydrocephalus, skeletal malformations) only occur in the rat model when the dam has been exposed to higher doses of nitrofen than those used in the present study. Further, approximately 10% of the cases where CDH is associated with MCA in infants can be linked to specific genetic abnormalities (i.e. trisomy 13 and 18 as well as Fryn's Syndrome; Dillon and Renwick, 1993; Philip et al., 1991).

Lung development

Previous reports have suggested that the lung is malformed independently, and perhaps as a cause, of the diaphragmatic anomalies. There have been two sources for this thinking that have persisted in the literature. First, was the report of Iritani (1984), which showed a photograph of an abnormal lung and adjacent tissue which they referred to as the post hepatic mesenchymal plate (PHMP). In that experimental paradigm, nitrofen was fed *ad libitum* to pregnant rats from days E5 to E11 and as a result a number of developmental anomalies arose. It may have been that massive doses of nitrofen administered at very early stages for long periods disrupted a number of tissues, including the lungs. However, Kluth et al. (1993) reexamined the issue of whether the lung was atrophied at an early stage (E14) of diaphragmatic malformation and concluded, also from visual inspection (utilising scanning electron microscopy), that the lungs were normal prior to the invasion of the abdominal contents into the thoracic cavity. The quantitative analysis of lung size and cell content in the present study demonstrates that lung hypoplasia is indeed a secondary effect rather than a primary cause of the diaphragm malformation.

The second line of evidence which has been presented for implicating the lung as a source of the anomaly has been the fact that the lung contralateral to the herniation is sometimes hypoplastic in newborns with CDH. However, the contralateral hypoplasia, which is often minor compared to the ipsilateral hypoplasia, can be explained by the fact that the mediastinum, and subsequently the contralateral lung, is compressed by the presence of the invading viscera. Thus, considering the evidence presented when nitrofen is administered in

a manner to minimise associated anomalies, lung development is normal at the early stages of CDH progression and is only compromised as a secondary result of the subsequent migration of viscera through the diaphragmatic opening.

Status of the phrenic nerve

The phrenic nerve innervating the herniated side of a diaphragm in older fetal rats (post E16) often appears smaller in diameter compared with the unaffected side. The electron micrographs of the phrenic nerve and the retrograde fills of phrenic motoneurons in the present study provides quantitative evidence for this observation. However, these abnormalities are also a result, rather than a cause for CDH. Before naturally occurring neuronal cell death (E15; Harris and McCaig, 1984), the numbers of phrenic motoneurons and axons in CDH fetuses were similar to control animals on both ipsi- and contralateral sides to the herniation. This apparent discrepancy can be explained by the fact that the number of neuronal cell bodies and axons which remain after the period of apoptosis is critically determined by the target tissue (Hamburger, 1975). In the instance of severely herniated diaphragms, a significant proportion of the target is missing and the remaining musculature is arranged abnormally, thereby explaining the increased phrenic motoneuron cell death. Data regarding the development of the diaphragm in the absence of innervation (chapter 6) shows that herniation does not occur in these diaphragms. Thus, it is most unlikely that any defect in innervation results in CDH.

Diaphragm formation

The notion that myotubes in the region of the herniation form in a weak fashion and then rupture due to the pressure induced by the underlying viscera does not hold up with the nitrofen model. Rather, it is clear that myotube formation is enhanced adjacent to the hernia, with some of the myotubes normally destined for the herniated region aligning next to the diaphragmatic opening. Further, diaphragms which develop in the absence of innervation have a severely atrophied musculature. Also, in mice null mutant for hepatocyte growth factor/scatter factor, diaphragms which are completely devoid of muscle do not rupture (Babiuk, Allan, Greer, unpublished observations). Thus, rupturing of weak regions of muscle

does not appear to be a potential mechanism for CDH.

Similarly, our data does not support the idea that the herniation results from a failure of pleuroperitoneal canal closure. First, herniation often occurs medially of the pleuroperitoneal canals. Secondly, it was obvious that well-defined holes in the diaphragm were present on either the right or left side at E14.5, approximately 0.25 and 0.75 days before the closure of the right and left pleuroperitoneal canals, respectively (Gattone and Morse, 1984). Kluth et al. (1993) also noted malformations on the right side of diaphragms at E14 in response to nitrofen administration at E11, which is consistent with the defects in the diaphragm occurring prior to closure of the pleuroperitoneal canal.

The malformation of the diaphragmatic musculature clearly occurs at an earlier stage of development than myotube formation and pleuroperitoneal canal closure. In the present study, the primordial diaphragmatic tissue, the pleuroperitoneal fold, was found to be grossly malformed in the nitrofen model of CDH. As a result, the nerve migrates past its normal point of innervation, which is missing in left hernias, and innervates tissue ventrally. It is interesting that the phrenic nerve branches in a pattern similar to normal, even when its primordial target is either missing or misplaced in the instances of CDH. It would be interesting to study potential topographically organised cues in normal and herniated diaphragms to better understand this adjustment phenomena. Post E13.5, herniated diaphragms then develop without the normal substrate for the medial and dorsal regions.

The tissue classified by Iritani (1984) as the post-hepatic mesenchymal plate (PHMP), is likely the pleuroperitoneal fold. As far as we have been able to discern, there has not been a single anatomical description of a tissue anomalous to the PHMP described independently from that proposed by Iritani (1984). Moreover, others have raised doubts regarding the identity of the PHMP, suggesting that it is a part of the dorsal mesenchyme of the septum transversum. With the clearer visualisation of the tissue with the presently available immunohistochemical markers, we can clearly observe the defect in the pleuroperitoneal fold.

The present data clearly shows that the diaphragmatic defect associated with maternal nitrofen exposure occurs with the initial, rather that the latter stages of diaphragm development. It will now be important to determine if it is a matter of improper muscle

precursor cell migration from somites or a malformation of the mesenchymal tissue which provides the supporting structure for diaphragm formation. The fact that left-sided hernias only occur when nitrofen is administered at E9, suggests that the primary insult must be occurring during a well defined time-frame. A past study of the distribution and metabolism of orally administered nitrofen in rats has shown that nitrofen reaches the fetus within 2 hours after administration, with the level peaking at 4-6 hours and declining to half the initial value by 24 hours (Costlow and Manson, 1981). One proposal regarding the pathogenesis of CDH suggests that there is an increased amount of cell death in the cervical somites associated with nitrofen administration (Alles et al., 1995). However, the correlation was not quite so clear as the increased cell death was bilateral in instances of presumptive left-sided herniation and totally absent in instances of presumptive right-sided hernia. A further complication arose in that study as it was assumed that all herniations would be left-sided in response to nitrofen administration at E9, which has been illustrated in this and past studies (Kluth et al., 1990) to be an over generalisation. Clearly, further studies regarding the source of diaphragmatic pre-muscle tissue in the normal and pathological states are needed to address this issue. We are now focussing on two potential features of pleuroperitoneal fold development which may be affected during CDH development, the migration of muscle precursors from somites and the deposition of the mesenchymal substructure on which the diaphragmatic anlage form. We are approaching this by examining the development of the diaphragm in mice null mutant for hepatocyte growth factor/scatter. These mice do not have limb bud, diaphragmatic or tongue musculature due to the inability of myogenic precursor cells to delaminate and migrate from the somite (see general introduction). Preliminary evidence demonstrates that the diaphragms of these mice do not show any defects consistent with CDH. We postulate that nitrofen exposure of the pregnant HGF/SF heterozygotic dam will result in defects equivalent to those described here. This will provide evidence that CDH results from defective development of the mesoderm of the pleuroperitoneal fold.

REFERENCES

Adzick HS, Harrison MR, Glick PL, Nakayama DK, Manning FA and deLorimier AA (1985) Diaphragmatic hernia in the fetus: prenatal diagnosis and outcome in 94 cases. *J. Ped. Surg.* 20:357-361

Alles AJ, Losty PD, Donahoe PK, Manganaro TF and Schnitzer JJ. (1995) Embryonic cell death patterns associated with nitrofen-induced congenital diaphragmatic hernia. *J. Ped. Surg.* 30:353-360

Ambrose AM, Larson PS, Borzellieca JF, Blackwell-Smith R and Hennigar GR (1971) Toxicologic studies on 2,4-dichlorophenyl-p-nitrophenyl ether. *Toxicol. App. Pharm.* 19:263-275

Costlow RD and Manson JM (1981) The heart and diaphragm: target organs in the neonatal death induced by nitrofen (2,4-dichlorophenyl-p-nitrophenyl ether). *Toxicology* 20:209-227.

Costlow RD and Manson JM (1983) Distribution and metabolism of the teratogen nitrofen (2,4-dichloro-4-nitro diphenyl ether) in pregnant rats. *Toxicology* 26:11-23.

Dillon E and Renwick M (1993) Antenatal detection of congenital diaphragmatic hernias: the norther region exposure. *Clin. Radiol.* 48(4):264-267.

Downs TR and Wilfinger WW (1983) Fluorometric quantification of DNA in cells and tissue. *Ann. Biochem.* 131:538-548.

Gattone VH and Morse DE (1984). Pleuroperitoneal canal closure in the rat. *Anat. Rec.* 208:445-460.

Gray LE, Kavlock RJ, Chernoff N, Ostby J and Ferrell J (1983) Postnatal developmental alterations following prenatal exposure to the herbicide 2,4-dichlorophenyl-p-nitrophenyl ether: a dose response evaluation in the mouse. *Teratol. App. Pharm.* 67:1-14.

Greer JJ, Allan DW, Babiuk RP, Lemke RP (2000) State of the Art Review: Recent advances towards un understanding of the pathogenesis of nitrofen-induced congenital diaphragmatic hernia. *Ped. Pulmon.* In press.

Hamburger V (1975) Cell death in the development of the lateral motor column of the chick embryo. *J. Comp. Neurol.* 160:535-546.

Harding R (1994). Development of the respiratory system. In *Textbook of Fetal Physiology Textbook of Fetal Physiology*. Edited by Thorburn, GD and Harding R: New York, Oxford pp. 140-167.

Harris, AJ and McCaig CD (1984). Motoneuron death and motor size during embryonic development of the rat. *J. Neurosci.* 4:13-24.

Harrison MR, Adzick NS, Estes JM and Howell LJ (1994) A prospective study of the outcome for fetuses with diaphragmatic hernia. *JAMA* 271:382-384.

Iritani I (1984) Experimental study on embryogenesis of congenital diaphragmatic hernia. *Anat. Embryol.* 169:133-139.

Karamanoukian HL, Glick PL, Wilcox DT, Rossman JE, Hom BA and Morin FC (1995) Pathophysiology of congenital diaphragmatic hernia. VIII: Inhaled nitric oxide requires exogenous surfactant therapy in the lamb model of congenital diaphragmatic hernia. *J. Ped. Surg.* 30:1-4.

Kluth D, Petersen C and Zimmermann HJ (1989) The embryology of congenital diaphragmatic hernia, in Puri P (ed): Congenital Diaphragmatic Hernia. Mod Probl Paediatr Vol 24. Basel, Switzerland, Karger pp 7-21.

Kluth D, Kangah R, Reich P, Tenbrinck R, Tibboel D and Lambrecht WN (1990) Nitrofen-induced diaphragmatic hernias in rats: an animal model. *J. Ped. Surg.* 25:850-854.

Kluth D, Tenbrinck R, Ekesparre M, Kangah R, Reich P, Brandsma A, Tibboel D and Lambrecht W (1993) The natural history of congenital diaphragmatic and pulmonary hypoplasia in the embryo. *J. Ped. Surg.* 28:456-463.

Laskowski MB and Sanes JR (1987). Topographic mapping of motor pools onto skeletal muscles. *J. Neurosci.* 7:252-260.

Ostby JS, Gray LE, Kavlock RJ and Ferrell JM (1985) The postnatal effects of prenatal exposure to low doses of nitrofen (2,4, dichlorophenyl-p-nitrophenyl ether) in Sprague-Dawley rats. *Toxicology* 34:285-297.

Philip N, Gambarelli D, Guys JM, Camboulives J, Ayme S (1991) Epidemiological study of congenital diaphragmatic defects with special reference to aetiology. *Eur. J. Pediat.* 150:726-729.

Puri P (1989) Epidemiology of congenital diaphragmatic hernia, in Puri P (ed): Congenital Diaphragmatic Hernia. Mod Probl Paediatr Vol 24. Basel, Switzerland, Karger pp 22-28.

Skandalakis JE, Gray SW and Ricketts RR. The diaphragm. In *Embryology for Surgeons.* Edited by Skandalakis & Gray. Ch. 15, 1994.

Torfs CP, Curry CJ, Bateson TF and Honore LH (1992) A population-based study of congenital diaphragmatic hernia. *Teratology* 46:555-565.

Wickman DS, Siebert JR and Benjamin DR (1993) Nitrofen-induced congenital diaphragmatic defects in CD1 mice. *Teratology* 47:119-125.

Zamenhof S, Bursztyn H, Rich K and Zamenhof PJ (1964) The determination of deoxyribonucleic acid and of cell number in brain. *J. Neurochem.* 11:505-509.

Chapter 8

STRUCTURE OF THE PRIMORDIAL DIAPHRAGM AND DEFECTS ASSOCIATED WITH NITROFEN-INDUCED DIAPHRAGMATIC HERNIA

Submitted to Pediatric Research under the following authorship:

John J. Greer, David Cote, Douglas W. Allan*, Wei Zhang, Randal P. Babiuk, Linh Li, Robert P. Lemke and Keith Bagnall

* Contribution to this work:

Involved in conception and design of project

Isolation of embryos

Involved in determination of pleuroperitoneal fold dimensions, verification that 3-D reconstruction and designing data presentation

Assisted in writing of manuscript

INTRODUCTION

The previous chapters had identified the pleuroperitoneal fold (PPF) as the primordial diaphragm and shown that a defect in the formation of this tissue likely results in nitrofen-induced congenital diaphragmatic hernia in rats (see also Greer et al, 2000, in press). The current study is an extension on these studies and focuses on two main objectives. First, to clearly elucidate the anatomical structure of the PPF at E13.5. Second, to determine which regions of this structure malform in the animal model of CDH. These aims were achieved by generating 3-D reconstructions of normal and defective PPFs from serial transverse sections of control and nitrofen-exposed rat embryos. The reconstructions were generated from tissue isolated at E13.5, the stage when the PPF has formed into a well-defined structure and defects are clearly discernible in the nitrofen model (see chapter 7).

METHODS

As previously described, E13.5 embryos from control and nitrofen exposed dams were processed for microtome sectioning (6 μm thickness). Sections were then stained for haematoxylin and eosin. Sections were then dehydrated and coverslipped with Entellan.

Image processing and 3-D reconstructions

It was not possible to ascertain which of the embryos had nitrofen-induced PPF defects by visual inspection of the whole embryo. Therefore, all of the embryos from the nitrofen-exposed rat were sectioned and defects within the PPF, as characterised in past work (chapter 7), were detected via microscopic examination of transverse tissue sections (see Fig. 8.2 for examples). Subsequently, serial transverse sections from representative embryos with and without PPF defects were chosen for 3-D reconstructions. To meet the criteria for reconstruction, the series of tissue sections from a given embryo had to be structurally complete throughout the rostrocaudal extent of the PPF. Photomicrographs of each transverse section were then captured in digital format using Image Pro software connected to a MCI 3CCD camera mounted on a Leitz Diaplan microscope (x10 objective). Digital images were imported into CorelDRAW 8.0 program where the drawing tool was used to outline the PPF (see Fig. 8.2 for an example). Images were transformed into gray-scale images and stored as 'TIFF' files. During our initial reconstructions, each 6 μm slice spanning the rostrocaudal extent of the PPF was captured and used for the 3-D reconstructions (36-41 sections per PPF; n=2). However, we found with later reconstructions that capturing every second section sufficed for generating renderings which faithfully depicted PPF structure (17-21 sections per PPF; n=6).

The TIFF formatted images were transferred to Adobe Photoshop 4.0 for preliminary cropping and alignment of the sections using the esophagus as a fiducial point. The esophagus was a prominent feature in each of the transverse sections and appeared in a consistent locale throughout the limited rostrocaudal extent of the PPF (i.e. < 250 μm thickness). The image sets were opened up as a series in the 3-D rendering program, SURFdriver 3.5 (see www.surfdriver.com). Data regarding the scaling and dimensions of the

tissue sections were entered into the software program. A calibrated micrometer incorporated into the microscope eyepiece was used to measure values in the X and Y dimensions. The values in the Z direction were derived from the settings on the cutting microtome. The final fine adjustments necessary to align the sections were performed in SURFdriver prior to the outlining of the PPF contours for the rendering of the 3-D image. Once generated, the 3-D images were rotated in the rendering window and captured at X,Y,Z coordinates which we considered optimum for visualising the overall shape of the PPF and the regions of nitrofen-induced defects. Perspective views of the PPFs from both the right and left side of the embryos were selected. The images were then exported from SURFdriver as bitmap files (BMP) to CorelDRAW software for the construction and labeling of final figures.

RESULTS

Nitrofen-induced defects

The nitrofen exposed dam used for this study carried 20 embryos aged ~E13.5. Examination of serial cross-sections from the 20 embryos revealed obvious PPF defects in 12 embryos (1 right- sided, 11 left-sided). Four of the defective (1 right- and 3 left-sided) and two normal PPFs from the nitrofen-exposed rat were selected for 3-D reconstructions. Serial sections from an embryo isolated from a control dam (i.e. not exposed to nitrofen) were also used for a 3-D reconstruction. No structural differences were found between the non-defective PPFs from nitrofen-exposed and control animals (not shown).

2-D PPF structure

The location of the PPF within a cervical section of an E13.5 rat is illustrated in Fig. 8.1A. The PPF tissue is clearly discernable from surrounding structures (e.g. lung, liver, body wall) based on differential cell density and size, as revealed by H&E staining (asterisk in Fig. 8.1). The adjacent photomicrograph (8.1B) shows a close-up of the PPF tissue labeled for the low-affinity nerve growth factor (p75) receptor. We used a combination of H&E staining and the immunolabeling profiles of developmentally-regulated molecules from previous studies to establish the boundaries for delineating the PPF (see previous chapters and Greer et al., 1999, 2000 in press). Fig 8.2 (middle panel) shows the PPF in a number of serial sections. The rostral border was estimated to be the first serial transverse section where the triangular shaped PPF tissue could be clearly seen protruding medially from the cervical lateral wall. The PPF thickens and extends caudally while maintaining close contact laterally with the body wall and medially with the primary oesophageal mesentery. The limit of the caudal boundary was estimated to be the point where the PPF was no longer clearly discernable from the underlying liver tissue. The extent of the boundaries of the PPF used for the 3-D reconstructions are outlined in Fig 8.2. Based on the defined boundaries chosen, the average rostrocaudal extents of the PPF at E13.5 were 206 ± 23 μm (n=18) and 229 ± 16 μm (n=18) for the left and right sides, respectively.

Fig. 8.2 illustrates cross sections of the PPF at E13.5 in control (middle panel) and

nitrofen-exposed rats (left and right panels). Sections are shown from the rostral, middle and caudal regions of the PPF. This figure illustrates the defects observed in CDH fetuses in comparison to a control. As can be observed in fetuses with defects, the dorsal and lateral extent of the PPF becomes progressively more retarded from its rostral to caudal extent. The extent to which the defect encompassed more medial areas of the PPF varied.. The right-sided defect was first noticeable at 110 μm from the rostral border of the PPF. The left-sided defects started at an average of 143 ± 24 μm (n=11) from the rostral border of the PPF. Thus, the nitrofen-induced defects of the PPF, whether on the right or left side, were consistently found in sections taken from the middle to caudal regions of the PPF. Interestingly, the space vacated by this missing region appears to be invaded by the liver. It should be stressed, however, that in most cases, the more rostral extent of the PPF spanned over the liver.

Fig 8.1: Photomicrographs from E13.5 rat embryos showing the location and 2-D shape of the pleuroperitoneal fold (PPF). A) Transverse section showing the location of the PPF (*) with respect to the surrounding tissue (H&E staining). B) Higher magnification of the PPF region from another E13.5 embryo in which immunohistochemical labeling for the low-affinity nerve growth factor (p75) receptor has labeled the phrenic nerve and primordial diaphragmatic tissue of the PPF. Abbreviations: SC (spinal cord), H (heart), FL (forelimb), Lu (lung), E (eosophagus), A (aorta), VC (vena cava).

Fig. 8.2: Serial transverse sections showing defective pleuroperitoneal fold:
A series of transverse sections taken from the rostral, middle and caudal regions of the PPF (*) are shown from three different E13.5 embryos (H&E staining). Normal tissue from a control animal is shown in the middle panel. The right (R) and left (L) sides of the fetus are shown. The left panel shows transverse sections from an embryo with a nitrofen-induced right (R)-sided PPF defect. The panel on the right shows tissue from a nitrofen-exposed rat with a left (L)-sided PPF defect. See the top-middle panel for an example of the outline drawn to define the extent of PPF boundaries for the purpose of generating 3-D reconstructions. Arrows point to the liver tissue which occupies regions where the PPF is missing in the nitrofen-exposed embryos. Abbreviations: A (aorta), Lu (lung), E (eosophagus).

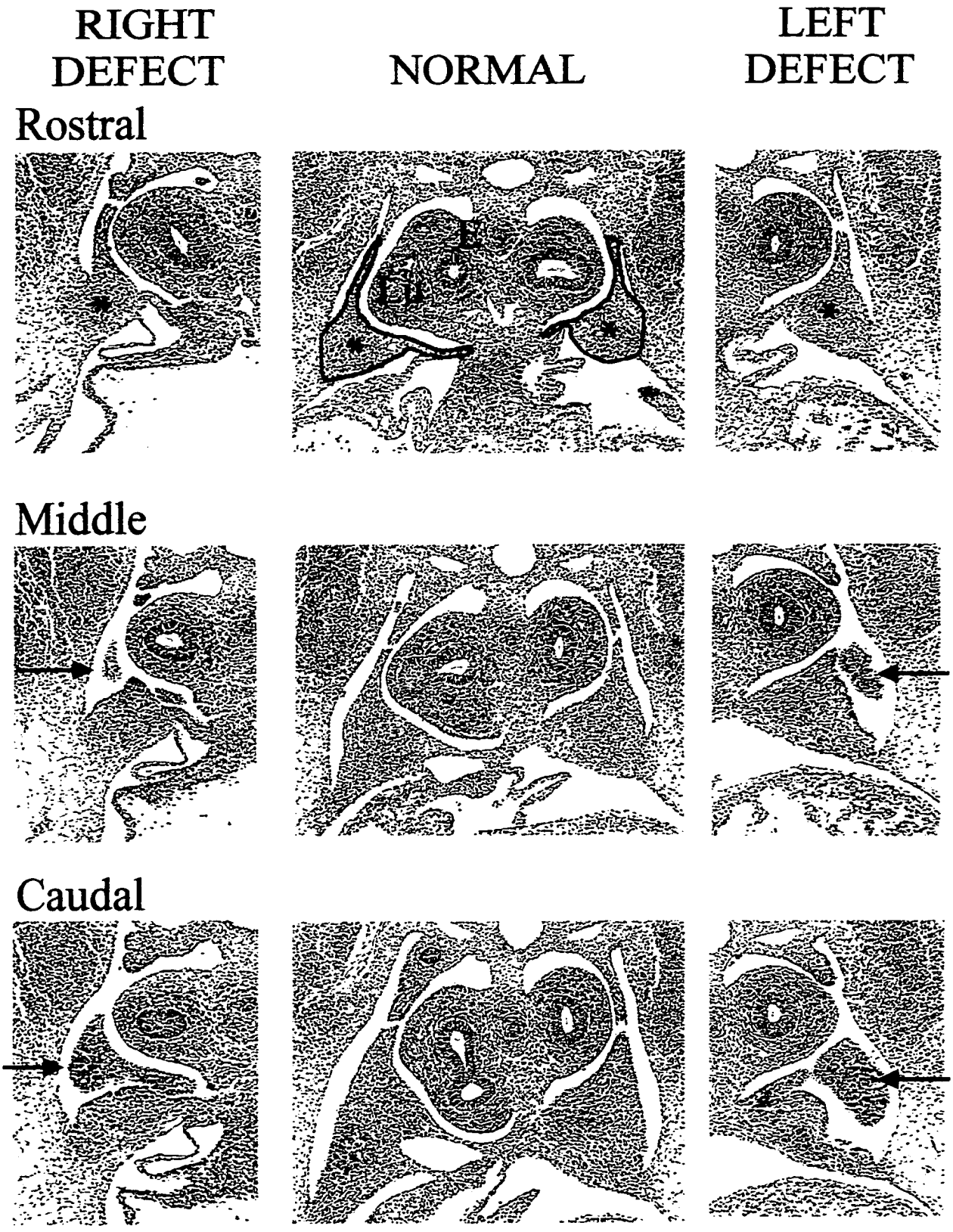

3-D PPF structure

Fig. 8.3 shows 3-D reconstructions from embryos taken from the nitrofen-exposed dam. PPFs from one normal (A,B) and three defective embryos (C-H) are shown. These reconstructions are built from outlining the PPF bilaterally (as in the top panel in Fig. 8.2), digitally removing this shape, and then stacking them in a 3-D computer graphics program. Thus, the images are the paired isolated PPFs taken from a real embryo. These 3-D reconstructions are orientated to provide views of the PPFs from each fetus from both the left and right lateral walls. This allows for a clear visualisation of medial and lateral perspectives of the bilateral PPFs. A comparison of the left PPF in control (Fig. 8.3A,B) and defective PPFs (Figs. 8.3B-H) illustrates that the malformed regions are located caudally and dorsolaterally. In contrast, the rostral, ventral and most medial regions of the defective and normal PPFs are similar. Further, PPF defects of varying magnitudes, ranging from mild (Fig. 8.3C,D) to moderate (Fig. 8.3E,F) to severe (Fig. 8.3G,H) were detected.

Fig. 8.4A shows defects in the right PPF in relation to a control. This control was not exposed to nitrofen. Its structure is similar to that of the nitrofen-exposed control PPF in Fig. 8.3A. Images of a defective right PPF from a nitrofen-exposed animal are shown Fig. 8.4B. As was the case for left-sided defects, the malformed PPF regions are those located caudally and dorsolaterally. Only the right PPF is shown from this embryo because the corresponding left PPF tissue sections were not of suitable quality for reconstruction.

Fig 8.3: Representative 3-D reconstructions of a normal PPF and left-sided defects. In each panel, the bilateral PPFs from one E13.5 fetus have been reconstructed from serial sections. A and B are the same reconstruction, viewed from the right (A) and left (B) sides. The defective PPFs below are presented in the same format, so (C) and (D) are the right and left views of the same reconstruction, respectively. Orientation axes show the rostral (R), Ventral (V), Right and Left directions. A,B) Normal bilateral PPFs, left (L) and right (R) PPFs viewed from the left and right sides of the reconstruction. Arrowhead denotes the region that is intact in control fetuses, but missing in left sided herniated fetuses. C-H) 3-D reconstructions of left-sided defects of varying degrees (arrow points to defective regions). In all cases, the defects are in the dorsolaterally located regions of the caudal PPF. C,D) A mild left hernia. E,F) A medium sized left hernia. G,H) A more severe left hernia. Scale bars = 100 μm

VIEW FROM RIGHT VIEW FROM LEFT

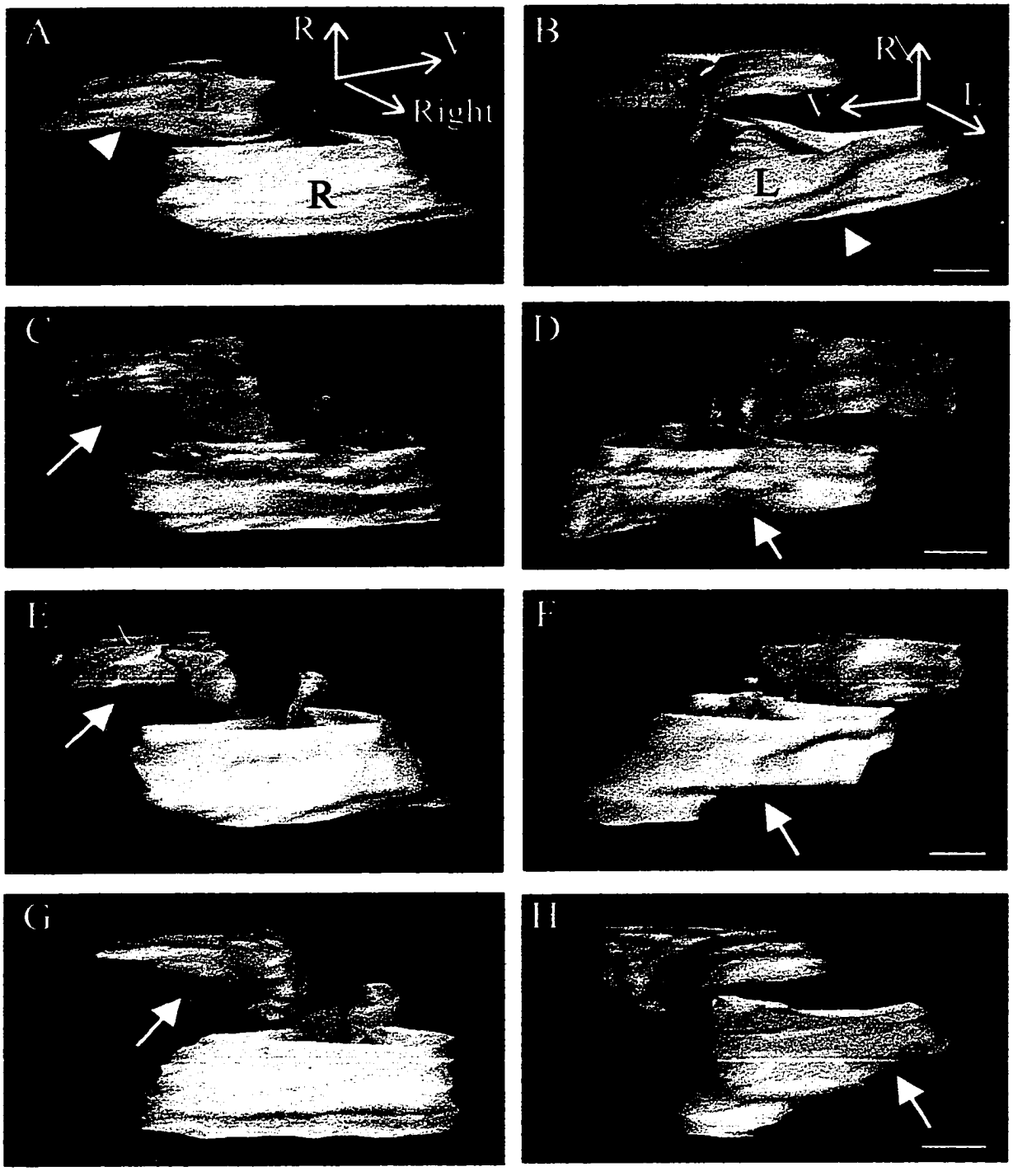

Fig 8.4: Representative 3-D reconstructions of a normal PPF and right-sided defect. In each panel, the bilateral PPFs from one E13.5 fetus have been reconstructed from serial sections. A and B are the same reconstruction, viewed from the right (A) and left (B) sides. The defective PPFs in C and D below are presented in the same format, so (C) is the view from the right side and (D) is the view from the left side. Orientation axes show the rostral (R), Ventral (V), Right and Left directions. A,B) Normal bilateral PPFs from a control animal not exposed to nitrofen. Left (L) and right (R) PPFs viewed from the left and right sides of the reconstruction. Arrowhead denotes the region that is intact in control fetuses, but missing in right sided herniated fetuses. C,D) Only the right PPF is shown, the left was unsuitable for reconstruction. A 3-D reconstruction of a right-sided defect (arrow points to defective regions). As was the case for left-sided defects (Fig. 8.3), the malformation is located in the dorsolaterally located regions of the caudal PPF. Scale bars = 100 μm

Correlation between PPF and diaphragm muscle defects

Fig.8.5 was constructed to assist the reader in envisioning how the regional defects of the PPF could translate into the lack of dorsolateral diaphragmatic musculature at later stages of development. The defect in the PPF at E13.5 (Fig 8.5A) is located in the typical dorsolateral portion. A representative moderately sized nitrofen-induced defect of diaphragm musculature at E15.5 is shown in Fig. 8.5B. Note that the area of diaphragm musculature missing is also located in the dorsolateral portions. Therefore, while we do not yet have a complete understanding of how the PPF expands to form the neuromuscular region of the diaphragm, the profiles of regional defects in the PPF and diaphragm correlate well.

Fig 8.5: Juxtaposed photomicrographs of a defective PPF (E13.5) and diaphragm (E15.5) to illustrate the correlation between regional defects at the two stages of development. The spinal cord (dorsal) and sternal (ventral) regions are towards the top and bottom, respectively, of both photomicrographs. A) Photomicrograph showing a close-up of the PPF in a transverse section from a nitrofen-exposed E13.5 embryo. There is a pronounced malformation (arrow) of the left PPF in the characteristic dorsolateral region. Note that the liver tissue has been removed from the photograph for increased clarity of the defective region (compare with Fig. 8.2). B) Photomicrograph of a diaphragm from an E15.5 embryo with a classical nitrofen-induced left-sided defect (arrow). The tissue has been immunolabeled for PSA-NCAM. By comparing the two images (A vs B), one can appreciate how the defect in the dorsolateral PPF would translate into a hole in the dorsolateral region of the diaphragm musculature at later stages of development. Further, the size of the defect in the diaphragm musculature would be dictated by the magnitude of the PPF malformation. Abbreviations: Lu (lung); E (eosophagus;), A (aorta). VC (vena cava).

DEFECTIVE PPF (E13.5) DEFECTIVE DIAPHRAGM (E15)

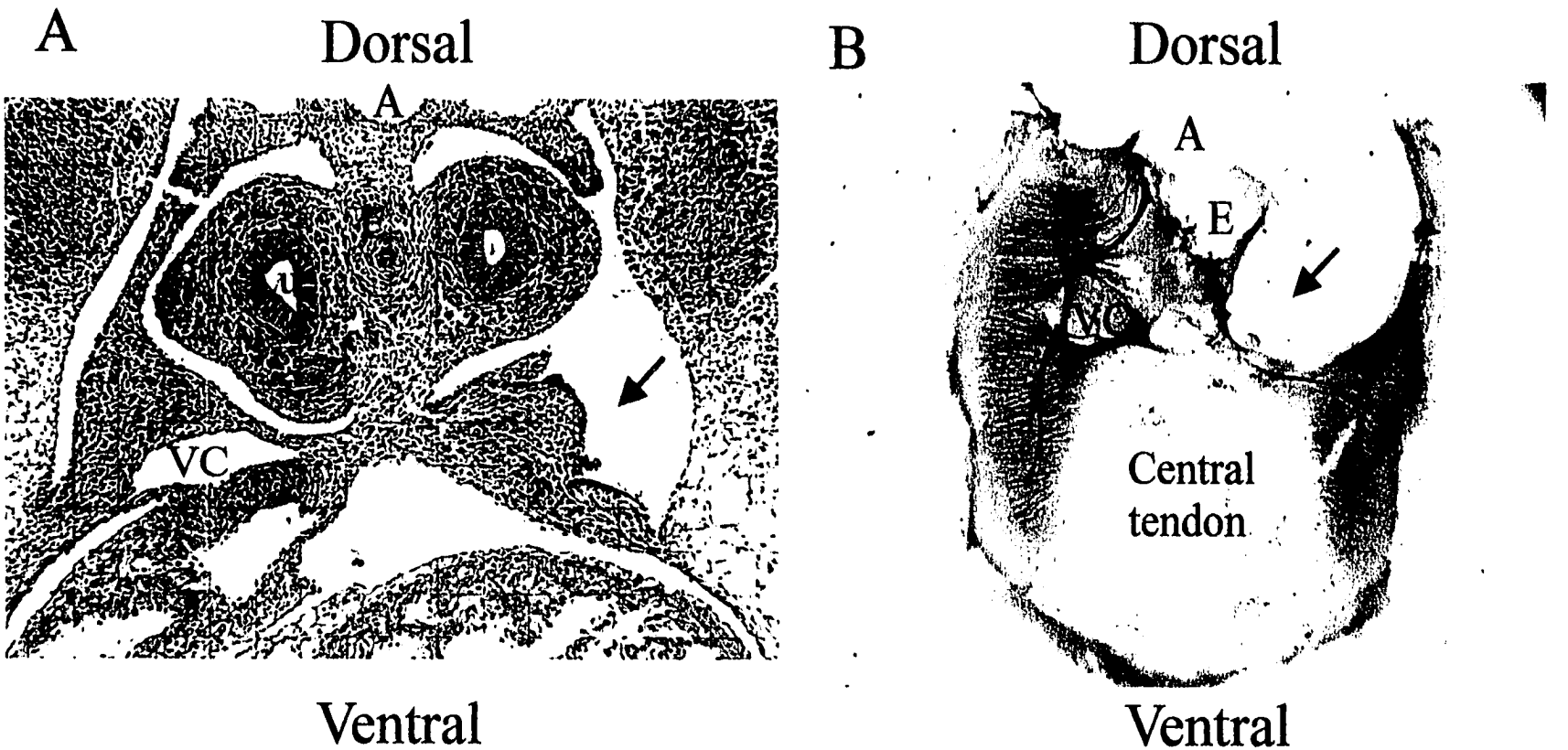

DISCUSSION

The 3-D images provide a clear visualisation of PPF morphology and dimensions. Further, the images of nitrofen-induced defective PPFs allow for an appreciation of precisely which areas of the PPF are malformed. The realisation that the dorsolateral region is defective provides a plausible explanation of why the holes in diaphragmatic muscle are typically found in the corresponding dorsolateral regions. Moreover, these data lend further support against the widely stated hypothesis that a failure of pleuroperitoneal canal closure underlies the pathogenesis of nitrofen-induced CDH.

Structure of the primordial diaphragm, the PPF

Textbooks typically provide a brief description of diaphragm embryogenesis which states the mesodermal substrate and musculature is derived from multiple sources (Skandalakis et al, 1994). However, those descriptions are largely based on speculations derived from the proximity of these potential sources, rather than actual tracking of muscle formation (Wells, 1954; Leak, 1979). While there remain unresolved issues pertaining to the formation of the diaphragm, recent data strongly suggests that the PPF is the primary structure from which the diaphragmatic neuromusculature derives (chapter 7). The 3-D reconstructions provided in this study allow for a clear visualisation of PPF morphology prior to the onset of diaphragm myotube formation. It could be argued that the rendered 3-D image of the PPF would differ somewhat if the boundaries chosen in the tissue sections were varied. However, unless the boundaries were chosen well outside those suggested by the staining profiles described, the general shape of the PPF and the identification of the defective regions in the nitrofen model would not differ significantly from those presented. Further, defects within the chosen region are the only defects observed in this region, they are contained within the putative diaphragm, and the developmental sequence leading to diaphragmatic defects can be clearly envisioned. Further, in examining numbers of fetuses at small age increments from E13.5, we have followed the progression of this defect into the diaphragmatic defect characteristic of CDH.

Defects of the PPF associated with the nitrofen model of CDH

As reported previously, the first sign of a nitrofen-induced defect in diaphragm tissue can be traced back to a mesenchymal plate at the dorsal aspect of the liver. Studies by Iritani (1984) and Kluth et al. (1989, 1990, 1993) also demonstrated nitrofen-induced defects in the region of the PPF as early as E13-14. They referred to the malformed tissue as the post hepatic mesenchymal plate (PHMP) or the dorsal plate of the septum transversum. However, upon comparing the data, it appears that the tissue being described in all of the studies is the PPF. The 3-D reconstructions provided in this study allow for a clear appreciation of the regional defects within the PPF. The malformed areas are consistently located in the dorsolateral region. Correspondingly, the dorsolateral region of the diaphragm musculature is precisely the area affected in CDH. Future studies involving monitoring the fate of dye-labeled cells within various regions of the PPF will be necessary to provide a definitive understanding of the regional sources of diaphragmatic tissue precursors. However, the available data is consistent with a causal relationship between a defect within the PPF and later diaphragmatic musculature malformations.

It should be stressed that the regions of the PPF missing are not merely the region of the somatic mesodermal tissue which expands to close the pleuroperitoneal canals (PPCs). The PPCs form dorsolaterally located channels linking the future abdominal and thoracic cavities. The failure of the PPCs to adequately close is often cited as the key pathogenetic factor associated with CDH (see chapter 7). However, if the defect was simply due to abnormal closure, we would not see any defect in the PPF. Simply put, all that would be observed would be a lack of PPF spreading across the PPC at the appropriate age. Further, large the defects are obvious prior to PPC closure and the regions of missing musculature extend well-beyond the PPCs (chapter 7). It is apparent from the 3-D reconstructions of defective PPFs that the degree to which more medially and ventrally located tissues are affected varies. It seems reasonable to hypothesise that the variability in the size of the holes in the diaphragmatic neuromusculature with CDH is dictated by the extent of the initial defect within the PPF.

There are a number of fundamental issues pertaining to the relationship between the PPF and CDH which remained unresolved. First, do PPF defects result from a problem with

muscle precursor migration, proliferation or differentiation? Alternatively, is there a problem with the formation of the underlying somatic mesodermal-derived connective tissue on which the muscle precursors develop? The fact that there is a thickening of muscle fibers around the hole in the diaphragm (chapter 7) is consistent with the hypothesis that at least some of the muscle precursors normally destined for the defective region of the primordial diaphragm migrate around the missing substratum to occupy adjacent PPF tissue. We are examining the diaphragmatic tissue derived from *HGF/SF* null mutant mice. Thus far, we have not detected any diaphragmatic defects, despite a lack of muscle in the developing diaphragm. This data argues against the influence of defective muscle development in the formation of the diaphragmatic defect. Ongoing work is aimed at resolving this clearly. One further aspect that requires resolution is the developmental events that lead to the formation of the defective PPF. We would anticipate that abnormality is associated with the expansion of the PPF, rather than its initial formation. Why? Clearly, no matter how large the defect is, the remaining tissue is innervated and muscularised (chapter 7). Thus, the migrating myogenic cells and the phrenic nerve have a substrate spanning from the lateral wall to the medial PPF. In all defective PPFs thus far, the rostral aspect of the PPF spans the entire mediolateral breadth of a normal PPF. The defect is caudal to this. However, the necessary studies examining the earlier stages of normal and pathological PPF formation are underway to directly observe the ingrowth of nerve and muscle into the defective PPF to test these hypotheses.

A second issue of uncertainty is the potential role of the liver in the pathogenesis of CDH. It is clear that the liver occupies space normally reserved for the PPF when there is a defect present. Whether or not the presence of the liver tissue in this area is causal of the defect or merely representing an early stage of liver displacement secondary to the PPF defect cannot be clearly elucidated with the current data.

Third, there is predominance of left-sided defects in infants with CDH (Skandalakis et al, 1994). The ratio of left versus right sided defects in the animal model varies depending on the day on which the nitrofen is administered to the dam (Ambrose et al., 1971; Costlow & Manson, 1981; Nakao et al., 1987, chapter 7). These data suggest an age-dependent variation in the susceptibility of left and right PPFs for malformations. However, without a

clear understanding of the aetiology of CDH, or the mechanism of nitrofen action, it is difficult to speculate on these trends. However, their elucidation would likely prove very insightful.

REFERENCES

Ambrose AM, Larson PS, Borzellieca JF, Smith RB, Hennigar GR (1971) Toxicologic studies on 2,4-dichlorophenyl-p-nitrophenyl ether. *Toxicol App Pharm* 19:263-275.

Costlow RD, Manson JM (1981) The heart and diaphragm: target organs in the neonatal death induced by nitrofen (2,4-dichlorophenyl-p-nitrophenyl ether). *Toxicol* 20:209-227.

Greer JJ, Allan DW, Martin-Caraballo M, Lemke RP (1999) Invited Review: An overview of phrenic nerve and diaphragm muscle development in the perinatal rat. J. Appl. Physiol. 86:779-786.

Greer JJ, Allan DW, Babiuk RP, Lemke RP (2000) State of the Art Review: Recent advances towards un understanding of the pathogenesis of nitrofen-induced congenital diaphragmatic hernia. *Ped. Pulmon.* In press.

Iritani I (1984) Experimental study on embryogenesis of congenital diaphragmatic hernia. *Anat Embryol* 169:133-139.

Kluth D, Petersen C, Zimmermann H J (1989) The embryology of congenital diaphragmatic hernia. In Puri P (ed) *Congenital Diaphragmatic Hernia.* Karger, Basel, Switzerland, pp 7-21.

Kluth D, Kangah R, Reich P, Tenbrinck R, Tibboel D, Lambrecht WN (1990) Nitrofen-induced diaphragmatic hernias in rats: an animal model. *J. Pediatr. Surg.* 25:850-854.

Kluth D, Tenbrinck R, Ekesparre M, Kangah R, Reich P, Brandsma A, Tibboel D, Lambrecht W (1993) The natural history of congenital diaphragmatic and pulmonary hypoplasia in the embryo. *J. Pediatr. Surg.* 28:456-463.

Leak LV (1979) Gross and ultrastructural morphologic features of the diaphragm. *Am. Rev. Respir. Dis.* 119:(supplement 3-21).

Nakao Y, Ueki R (1987) Congenital diaphragmatic hernia induced by nitrofen in mice and rats: characteristics as animal model and pathogenetic relationship between diaphragmatic hernia and lung hypoplasia. *Cong. Anom.* 27:397-416.

Skandalakis JE, Gray SW, Symbas P (1994) The trachea and lungs. In Skandalakis JE and Gray SW (eds) *Embryology for Surgeons.* Williams and Wilkins, Baltimore MD pp 414-450

Wells L J (1954) Development of the human diaphragm and pleural sacs. *Contr. Embryol. Carnegie Inst.* 35:107-134.

Chapter 9

WHOLE EMBRYO CULTURE

INTRODUCTION

We needed to develop a model where many of the hypotheses raised within the previous chapters could be tested directly. Initially, we attempted slice cultures of the rat cervical region. However, the pleuroperitoneal fold did not develop and necrotic cell death deep within the slice implied that nutrients were not penetrating the tissue. Further, *in utero* perturbations at these early ages is not possible, fetal death is very high and the density of the decidua up to E14 is too dense to clearly visualise the embryo. Thus we turned to the whole embryo technique. The original technique of whole rodent embryo culture was developed by Denis New in the late 60's (reviewed by New, 1990). This methodology has become a almost commonplace in teratology laboratories as, within known limits, embryonic development is remarkably normal (Cockroft, 1990). We have modified these techniques to suit our purposes. Adoption of this methodology is expected to allow us to test hypotheses regarding early stages of diaphragm development *in vitro*. Pharmacological agents, function blocking antibodies, dye injections and surgical deletions/modifications are possible in these cultures.

METHODS

A timed-pregnant dam is anaesthetised and caesarean section is performed under near-aseptic conditions. Sterilised instruments are used throughout. Individual fetuses are removed within their decidual tissue, so that the placenta and all embryonic membranes are undamaged. They are briefly dipped in a 70% ethanol solution and then placed, in a laminar flow hood, in a gas sterilised home made dissecting dish which contains a bubbled sterilised mock cerebrospinal fluid (CSF) (containing (in mM): NaCl (128), KCl (3), $NaHPO_4$ (0.5), $CaCl_2$ (1.5), $MgCl_2$ (1), $NaHCO_3$ (23.5), glucose (30); pH 7.4 when bubbling with 95%O_2, 5% CO_2). The dissecting dish has an in-built bubbling stone, solution inlet and air inlet. Solution in maintained in an upturned sterilised syringe containing bubbled mock sterilised CSF which is plugged into the solution inlet of the dish, regulated by a flow regulator. Air is filter sterilised at the point of the dish air inlet with a Millex-FG_{50} 0.2μm air filter.

Under a cleaned dissecting microscope (Leica M3C), E9 to E11.5 embryos are dissected so as to leave their yolk sac and placenta intact. Thus, only the Reicherdt's membrane is carefully removed. In embryos older than E11.5, a small incision is cut into the yolk sac, avoiding any major blood vessels, and the embryo is carefully pushed through the opening. The amnionic sac is also carefully cut.

These are placed in the culture set-up. Embryos are placed into 5ml of culture medium in sterile 50ml centrifuge tubes (Fisherbrand Disposables). The caps of these have been modified to accommodate an air inlet attached to a short length of polyethylene tubing running into the centrifuge tube. The basic constituents are filter sterilised whole adult rat serum (taken from adult male rats in the laboratory and frozen until use) and filter sterilised Waymouth's MB 752/1 Medium (Sigma) containing 100μg/ml streptomycin and 100IU/ml penicillin. The ratio of rat serum to Waymouth's medium varies depending upon the age of the embryo: E9 (90% serum, 10% medium), E10 (75% serum, 25% medium), >E11 (50% serum, 50% medium). The capped 50ml centrifuge tube containing the embryo and culture medium is clipped onto on a home made plate sitting on a Roto-Torgue heavy duty rotator (Cole Palmer). Tubes are rotated at 25rpm in a humidified 5% CO_2 incubator at 37°C (Forma Scientific #3029). An air inlet running through the rotator is split to each culture tube

(usually 4-6 per experiment) at a regulator on the rotator plate. Each line is individually regulated by flow regulators. Air is fed into each culture tube so as to bubble the culture medium. The percentage of O_2 in the gas varies from 5 to 95%, in E9 to >E11 fetuses. The gas is regulated by a solenoid valve controlled by a timer set with a 15 minute duty cycle. As fetuses grow, the culture conditions are altered to suit their new age, as above.

Embryonic growth is assessed by multiple embryological criteria and their crown-rump length. Embryos are assessed for the growth of axons at the fore- and hind-limbs by standard immunohistochemical procedures. These parameters are compared to age-matched control fetuses.

RESULTS

These can be seen in Fig 9.1. In the top panel, the growth of fetuses from E9 to E12, and then from E12.5 to E13.75 results in an apparently normal development. It should be stressed that these are the usual limits of embryonic growth *in vitro*. So, we can maintain normal growth from E9 to E12 and after E12 we can maintain normal development for one and a half days maximum. However, as shown in the lower panels, these times encompass key phases of axonal pathfinding at both the brachial (A to B) and hindlimb (C to D) plexi. Generally, when culturing from E9 to E12, there is an approximately half day delay in overall development, whereas after E12, development proceeds at a roughly quarter day lag over a day and a half development. Success rate was initially very low, but once we had established the optimal conditions we obtained approximately 50% survival. This would likely be increased with continued use and experience during experimental periods. Applications for this technology are detailed in the general discussion.

Fig. 9.1: Culture of rat embryos

The top two panels demonstrate the extent of fetal development in the *in vitro* system developed. The top left panel shows a control E9 fetus maintained prior to culture from the same litter as the adjacent cultured embryo, now aged E12. Inset is shown a ~E10 rat fetus that was grown in culture from the E9 stage to show that normal cephalocaudal flexion and foregut formation is underway. These fetuses are normal by a number of criteria (most importantly axonal growth) after the culture period. Scale bars at side are 1mm increments to show that the fetuses are the normal length for their post-culture age. Bottom four panels (A-D) demonstrate that plexus axonal segregation proceeds normally under culture conditions. A and C are sectioned and labelled littermates of the cultured fetuses in B and D, respectively. These controls were fixed at the onset of the culture period. Comparison of pre- and post-culture periods demonstrates that the three nerve trunks at the brachial plexus and the two nerve trunks of the hindlimb plexus develop normally and on schedule during the culture period. Also note that development of surrounding tissues is apparently normal (see previous chapters for comparisons. Abbreviations: DRG (dorsal root ganglion), FL (forelimb), Ph (phrenic nerve).

GROWTH OF EMBRYONIC RATS IN CULTURE

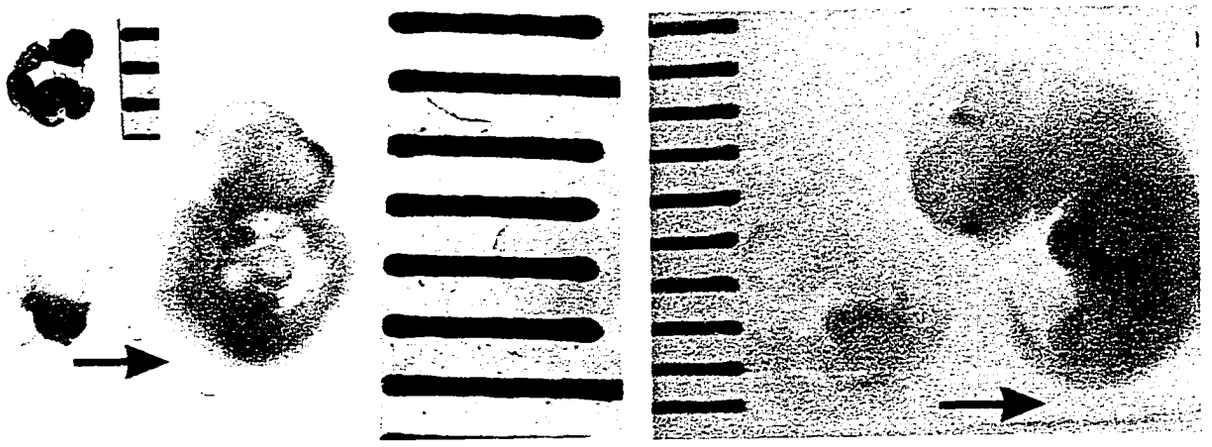

AXON OUTGROWTH IN CULTURE

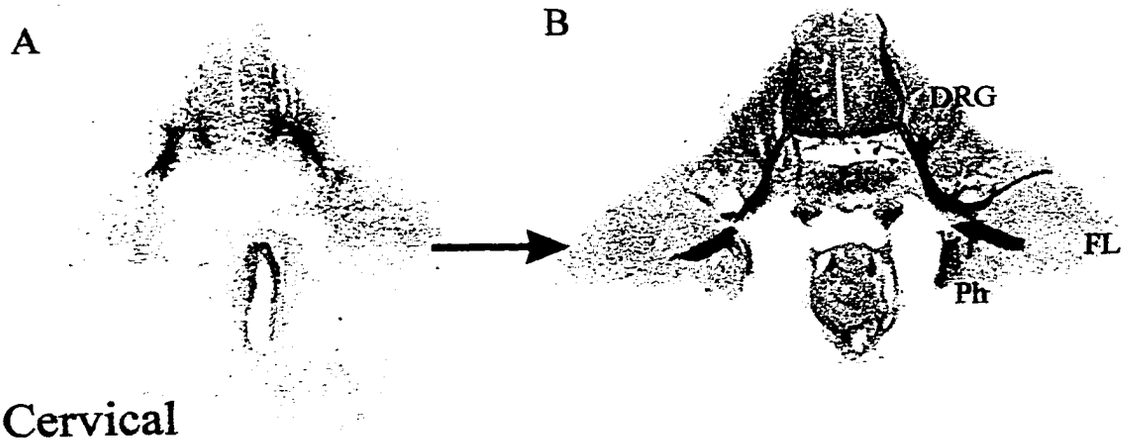

Cervical

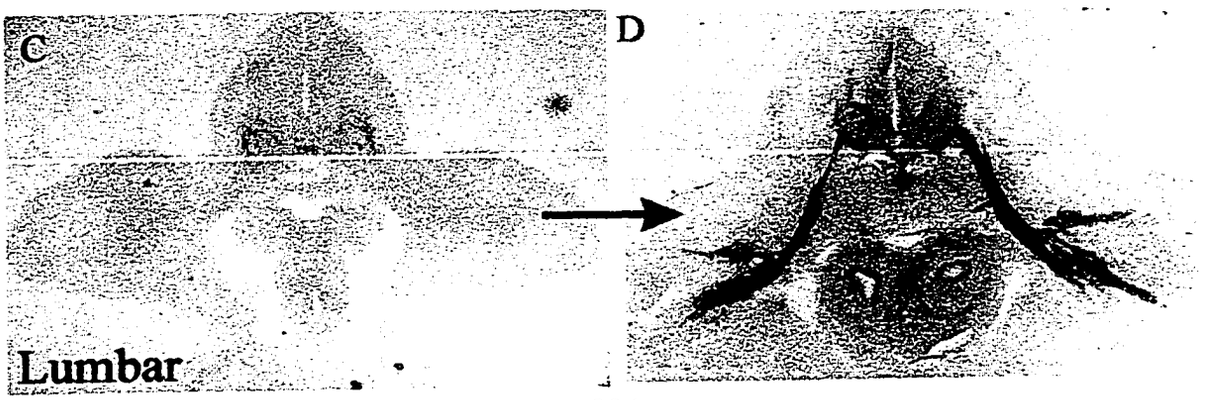

DISCUSSION

As can be observed, we obtain segregation of axons at both the forelimb and hindlimb plexi of rat fetuses in culture conditions at a reasonable success rate. These data show that we could experimentally test a number of the hypotheses developed during these studies. These would include dye injection into various tissues and directly tracking the progression of the tissue. Also, endoN injection into the brachial plexus would directly test the role of PSA-NCAM in phrenic axon selective guidance. See the general discussion for more details of potential uses.

REFERENCES

Cockroft DL (1990) Dissection and culture of postimplantation embryos. *Postimplantation mammalian embryos: a practical approach.* Edited by Copp AJ and Cockroft DL. Oxford press, pp 15-40.

New DA (1990) Introduction. *Postimplantation mammalian embryos: a practical approach.* In Edited by Copp AJ and Cockroft DL. Oxford press, pp 1-13

Chapter 10

SUMMARY AND GENERAL DISCUSSION

Summary

In all mammals, including humans, every breath taken throughout life is generated by phrenic nerve-induced contraction of the diaphragm. Thus, the developmental formation of a phrenic-diaphragm motor system that is fully functional by birth is critical to postnatal life. Previous work on the development of this motor system has focused on its postnatal maturation. Essentially, those studies demonstrate that it has attained many of its adult characteristics by birth. Thus, in order to define the fundamentally important steps in the developmental formation of the phrenic nerve and diaphragm, one has to examine events occurring prenatally. Such studies would not only be pertinent towards furthering our understanding of phrenic-diaphragm motor system development, and of mammalian motor systems in general, but they would also be crucial towards providing a substantive foundation for researching the pathogenesis of relevant congenital disorders. One major concern in this regard is the high incidence (1:2000-3000 newborns) congenital disorder, congenital diaphragmatic hernia, whereupon a large region of the diaphragm is entirely missing. As a result, abdominal organs, including the liver, stomach and intestines, protrude into the thorax of the developing fetus, occupying space normally reserved for the growing lungs. Subsequently, lung development is retarded to the extent that the lungs of newborns are severely hypoplastic (small), hypertensive (poor blood flow) and immature (incapable of adequate gaseous exchange). Despite modern intervention and ongoing advances in pre- and post-natal care, the lungs of these infants are often simply incapable of supporting life and mortality remains high at approximately 50%. Furthermore, the majority of survivors suffer from persistent sequalae, largely related to cardio-pulmonary compromise.

However, despite the importance of this neuromuscular system beyond birth, and the profound clinical implications of abnormal development, very little is known concerning the developmental formation of this motor system. The prevalent literature regarding phrenic nerve and diaphragm embryogenesis consists of a patchwork of untested, and often conflicting, assumptions that suffer from a lack of coherence and any solid scientific support. Thus, there has been no substantive basis for a rigorous analysis of the pathogenesis of relevant congenital abnormalities. This thesis describes a body of work which has rectified

these issues by:

i) Providing the first coherent, detailed description of the prenatal development of phrenic nerve and diaphragm in the rat. My findings establish a new standard in this field and as such are anticipated to contribute significantly to future accounts of the embryogenesis of the phrenic nerve and diaphragm in medical, embryological and respiratory texts.

ii) Performing the first systematic examination of the prevalent theories regarding the pathogenesis underlying congenital diaphragmatic hernia (CDH) in a well established rodent model. My findings directly show that these theories are incorrect and refocus the investigative effort of this field to the earliest stages of diaphragm formation.

iii) Initiating studies of the molecular control of certain key aspects of phrenic-diaphragm development. These studies have focused on the role of the anti-adhesive cell surface molecule, polysialylated neural cell adhesion molecule (PSA-NCAM). Importantly, these data provide novel information regarding the roles that PSA-NCAM plays in developing neuromuscular systems, as well as providing data pertinent to the guidance of growing phrenic motor axons and the morphogenesis of the muscle of the diaphragm.

1) Developmental Formation of the Rat Phrenic Nerve and Diaphragm.

The developing rat offers an amenable and relevant model for studying phrenic-diaphragm development. First, the rat has become the standard model for studies of respiratory function and its development. Thus, the studies performed herein can benefit from, and contribute to, the broader context provided from ongoing studies of rat respiratory system development. Second, the availability of large numbers of rat fetuses of all ages provides adequate tissue to confidently detail each step of the formation of the phrenic nerve and diaphragm. Third, published images of human fetal tissues bear the same hallmark features of the developing phrenic and diaphragm as herein identified in the rat. This enables the interpretation of these features in human fetal tissues and confirms the validity of the rat studies. In these studies, the utilisation of immunological markers selective for particular cell types has enabled the visualisation of the developmental formation of the rat phrenic nerve and diaphragm. A number of contentious issues have been clarified:

The timing and pathway of phrenic motor axon growth from the spinal cord to the primordial diaphragm. Antibodies to GAP-43 (a selective marker for growing axons) were used to track the growth of phrenic motor axons throughout prenatal development. Axons destined for the phrenic and brachial nerves exit the cervical spinal cord at E11.5 and co-mingle at the brachial plexus during E12. By E12.5, a small number of phrenic axons 'pioneer' a uniquely phrenic path from the brachial axons towards the primordial diaphragm. These are followed by the majority of phrenic axons. During E13, phrenic axons first establish contact with the primordial diaphragm. Comparison of neuronal labelling with the use of antibodies that mark muscle fibres (PSA-NCAM and the muscle-specific intermediate filament, desmin) allowed us to delineate subsequent neuromuscular development within the diaphragm. By E14.5, the phrenic nerve begins to branch, extending axons to establish synaptic contact with the newly forming muscle fibres of the diaphragm. This close relationship between the formation of new muscle fibres and innervation by phrenic axons is maintained throughout subsequent development. By E17, when fetal breathing movements commence, the diaphragmatic musculature and its phrenic innervation have established the basic morphology of the adult diaphragm.

Discovery of a cellular track that likely provides the guidance substrate for phrenic axons to the primordial diaphragm. A major question in developmental neuroscience concerns how growing axons are guided to their target location within the embryo. The use of antibodies to NCAM and to the low affinity nerve growth factor receptor, p75, clearly defined a mesodermal cellular 'track' that was ideally positioned, both spatially and temporally, to perform a guidance role for phrenic axons. Phrenic axons never stray from this 'track' as they grow from the brachial plexus to the primordial diaphragm. Based upon our general understanding of axonal guidance, as gleaned from numerous animal models, this track is an ideal candidate for a selectively attractive and/or permissive substrate for growing phrenic axons. This finding provides the first indication that phrenic axon guidance is likely mediated by signalling from mesodermal cells, as is the case for limb motor axons. The identification of this mesodermal track is not only important from the standpoint of providing a target for future investigation into the molecular mechanisms of selective phrenic axon guidance, but

also significantly narrows the search for what those molecular mechanisms might be.

Identification of the primordial diaphragm. The available literature holds that the diaphragm is composed of tissues derived from a number of embryological sources, most notably the septum transversum, of anterior endodermal origin. Following our discovery of a mesodermal phrenic guidance track, we found that this cellular track subsequently differentiates into the pleuroperitoneal fold (PPF). Importantly, this study has determined that the PPF is the embryological precursor to the diaphragm. All of the mesoderm, muscle and nerve required for diaphragm formation is localised to the PPF during E13. Subsequent expansion of the mesoderm of the PPF provides the substructure for the addition of new muscle fibres within the expanding boundaries of the PPF. Phrenic axons follow closely behind this advancing wave to innervate the muscle fibres as they form. By E17, this process is completed when the basic morphology of the adult diaphragmatic neuromusculature has been attained, just in time for the onset of fetal breathing movements.

Phrenic motor neuron somatodendritic morphology. It is widely believed that the characteristic morphology of phrenic motor neurons within the spinal cord is intimately related to their function. Previous studies had determined that this characteristic morphology was essentially fully developed by birth. By retrogradely back-labelling the phrenic nerve (from E13.5 to birth) with the lipophilic neuronal tracer dye, DiI, phrenic cell bodies and their dendritic arbors were visualised within the spinal cord throughout development. Importantly, the characteristic morphology of adult phrenics did not become apparent until after E17, during a major period of phrenic dendritic restructuring that spans E18-E21. This immediately follows the onset of brainstem-mediated fetal breathing movements at E17. Thus, we postulate that the onset of respiratory drive likely provides the stimulus, and perhaps the co-ordination, for the major morphological changes that result in the characteristic phrenic motor neuron morphology. Parallel studies in the laboratory confirm that this time span correlates with the major period of maturation of phrenic electrophysiological properties. Thus, the emergence of mature phrenic motor neuron properties occurs between E17 and E21, making the events occurring during this period a

major focus of future studies. Further, studies aimed at understanding the pathogenesis of certain respiratory distress-related disorders in perinates (such as those related to maternal smoking) now have a target for investigation of the potential role of abnormal phrenic nerve development.

The Role of PSA-NCAM in Phrenic Pathfinding and Muscle Morphogenesis

PSA-NCAM is a post-translationally modified form of the neural cell adhesion molecule (NCAM). A long chain of up to 200 α-2,8-linked sialosyl residues are added to the extracellular portion of NCAM, forming a large, negatively charged carbohydrate moiety termed polysialic acid (PSA). PSA-NCAM is postulated to attenuate cell-cell adhesion by virtue of stearic hinderance and electrostatic repulsion.

Phrenic Axon Pathfinding: Studies in the chick have shown that PSA-NCAM attenuates adhesion between populations of PSA-NCAM-expressing axons. This is postulated to facilitate the separation of those axonal populations at points of segregation. This process is termed global defasciculation. Studies performed herein have shown that PSA-NCAM is uniquely expressed by phrenic axons as they grow through and beyond the brachial plexus. This strongly suggests that phrenic axons utilise this molecule to selectively separate them from brachial axons at the plexus, enabling them to respond to phrenic-specific guidance cues, such as those from the phrenic 'track'. Thus, PSA-NCAM may be acting in a previously unsuspected role as a selective defasciculator of certain axonal populations. Although time limitations prevented my direct testing of this proposal, I have established the experimental paradigms required for such testing. I have manufactured a viral α-2,8-specific endosialidase, termed endoneuraminidase N (endoN), which selectively removes the PSA from NCAM. The effects of endoN-induced PSA removal on phrenic axon guidance at the brachial plexus shall be examined by use of two techniques that I have established within the laboratory; i) direct injection *in utero*, and ii) direct injection into whole rat fetuses that have been removed from the uterus and are maintained in culture throughout the period of testing. We are also currently breeding NCAM null mutant mice which do not express PSA-NCAM. Once a suitably large colony has been established, phrenic axon guidance at the brachial

plexus shall be compared in wild-type versus null mutant mice.

PSA-NCAM in muscle morphogenesis: Previous work had established that PSA-NCAM was expressed by developing chick hindlimb muscle, but nothing was known regarding its role. Analysis of PSA-NCAM expression in the developing diaphragm has established that it is expressed between the apposed membranes of juxtaposed adherent muscle fibres prior to, and during, their major phases of separation. Thus, we postulated that PSA-NCAM was required to separate muscle fibres. Preliminary results from studies where endoN had been injected *in utero* indicate that muscle fibre separation is inhibited in the absence of PSA-NCAM, establishing a causal link between expression of PSA-NCAM and the separation of muscle cells. As above, NCAM null mutant mice shall also be utilised to provide further evidence, and strengthen our contention, that PSA-NCAM regulates the interaction of muscle cells. In further studies, removal of the phrenic nerve throughout muscle formation in the diaphragm (by injection of the neurotoxin, β-bungarotoxin), established that the expression of muscle PSA-NCAM occurs in the absence of the nerve. This demonstrates that the commonly held belief that PSA-NCAM expression by muscle is induced by nerve-induced activity is not entirely correct. Instead, our finding that the denervated diaphragm is spontaneously-electrically active implies that it is the electrical activity of the muscle that induces PSA-NCAM expression.

Pathogenesis of Congenital Diaphragmatic Hernia (CDH)

Our new understanding of phrenic-diaphragm development has provided the background to permit the first systematic study of the pathogenesis of CDH in a rodent model. CDH is characterised by the formation of a diaphragm which does not completely separate the thoracic and abdominal cavities. Instead, a hole, of varying size, becomes apparent in the emerging diaphragm. Previous theories proposed that this diaphragmatic defect was due to any one of a number of mechanisms (see below). Despite a lack of any scientific support, these hypotheses form the basis of our understanding of the pathogenesis of CDH and persist within the modern literature. This study provides the first direct testing of each of these hypotheses in a well established rodent model of CDH. A herbicide, nitrofen,

is administered to pregnant female rats (dams) at day 9 of embryonic gestation (E9). This results in defects in rat diaphragm formation that are remarkably similar to those observed in human perinates.

Malformation of the growing lung which, by an unclear mechanism, induces the diaphragmatic defect. The lungs of both human and rat (nitrofen-induced) perinates with CDH are severely hypoplastic, hypertensive and immature. This observation has led to the commonly cited hypothesis that an initial perturbation in lung formation induces the diaphragmatic defect. By measuring lung protein and DNA content at key times, it was established that lung malformation occurred as a result of the invasion of abdominal organs into the thorax, long after the diaphragmatic defect had emerged. In other words, lung malformation was due to the herniation of viscera through the diaphragmatic defect.

Lack of proper innervation from the phrenic nerve induces the diaphragmatic malformation. The phrenic nerve that innervates the defective side of the diaphragm in both human and rat perinates with CDH contains fewer axons than that innervating the unaffected side. This observation has led to the hypothesis that insufficient or aberrant innervation of the diaphragm results in the diaphragmatic defect. By electron microscopic analysis and DiI retrograde labelling of the phrenic nerve, it was observed that phrenic motor neuron number was dependent upon the size of the defect. The process of programmed neuronal cell death (E15-E16 for phrenics) reduced the number of phrenics to match the size of the reduced musculature long after the defect had formed. Further, immunological tracking of the nerve in CDH-defective diaphragms showed that the phrenic nerve always attempts to compensate for the defect by growing around it. Finally, toxin-induced removal of the phrenic nerve, which prevents innervation of the diaphragm, did not result in the characteristic CDH diaphragmatic defects. Thus, the diaphragmatic defect does not occur as a result of either insufficient or aberrant innervation. Instead, the fate of the phrenic nerve is secondary to the diaphragmatic defect.

Formation of weak regions in the diaphragmatic musculature which then rupture, resulting

in the diaphragmatic defect. In both human and rat perinates with CDH, the diaphragmatic defect always appears as a region of missing musculature. This led to the hypothesis that the defect is due to the formation of weak regions of muscle, which subsequently rupture under the pressure of growing abdominal organs. Diaphragms which developed in the total absence of innervation (by injection of a neurotoxin *in utero*) had severely reduced, 'weak' musculature. However, these diaphragms were never observed to rupture. Moreover, examination of diaphragms that are completely devoid of any muscle (as is the case in hepatocyte growth factor/scatter factor null mutant mice) confirmed that even in this extreme case, the diaphragm never ruptures. Thus, it is unlikely that localised rupture of a weak diaphragm results in CDH. Instead, by following the formation of muscle in CDH-defective rat diaphragms, I have found that muscle never actually forms in the missing, defective region. Interestingly, the region of muscle that remains in CDH-defective diaphragms is greatly thickened. Taken together, these data imply that the muscle normally destined to form in the missing region is displaced into the remaining musculature, causing hypertrophy of that region. This shows that the muscle is compensating for the missing region, making abnormal muscle formation secondary to the diaphragmatic defect.

Improper closure of the pleuroperitoneal canals. This is the most commonly cited hypothesis. The pleuroperitoneal canals are bilateral channels connecting the thoracic and abdominal cavities at the dorsal aspect of the diaphragm. They close as a result of diaphragm (PPF) expansion during E15. If these canals were not to close normally, it is conceivable that abdominal organs may herniate through them into the thorax. If this were the case, it would be unlikely that we would observe any defect prior to canal closure. However, examination of defective diaphragms prior to canal closure indicates that the defect is apparent as a region of missing tissue prior to, and actually spatially distinct from, the pleuroperitoneal canals. Thus the defect arises independently of, and actually prior to, pleuroperitoneal canal closure.

Defective formation of an uncharacterised mesenchymal tissue which resides upon the dorsal aspect of the liver. Previous studies had identified a mesenchymal tissue which appeared to be related to early diaphragm formation and seemed to be perturbed in the instance of

nitrofen-induced CDH. Analysis performed herein has identified this tissue as the pleuroperitoneal fold and has provided the first indication that this tissue differentiates into the entire diaphragmatic neuromusculature. 2-D and 3-D computer reconstructions of the pleuroperitoneal fold in nitrofen-exposed and normal embryos has established that this tissue develops abnormally in nitrofen-exposed fetuses. Essentially, regions of this tissue fail to form normally in the instance of nitrofen-induced CDH in rats. Further, the region missing in the PPF is entirely consistent with the region missing in CDH defective diaphragms. The lack of formation of this region of the PPF, and subsequently the diaphragm, not only provides an explanation for the defect observed in CDH diaphragms, but also explains all of the associated defects in the nerve, muscle and lung.

Previously, if one were to attempt to develop a preventative treatment or cure for congenital diaphragmatic hernia, one would have had to base that research upon whichever of the prevalent hypotheses your bias favoured. Based upon the information contained within medical texts, one would actually have been led down one of a number of wrong paths. It is perhaps surprising that this should be the case, particularly in light of the prevalence and mortality associated with CDH. However, this situation arises from a simple lack of understanding of the normal development of the diaphragm, as well as an unfortunate acceptance of prevalent hypotheses and a lack of their rigorous assessment. This study provides: i) The understanding of diaphragm embryogenesis that has been required to identify the malformation of the pleuroperitoneal fold as the principal defect associated with CDH. ii) The first systematic attempt to evaluate the validity of the commonly cited hypotheses. This study re-focuses the investigative effort of the field to events occurring during the early embryogenesis of the diaphragm that lead to the malformation of the pleuroperitoneal fold. It is anticipated that this work shall form the basis of a major revision of the literature regarding the pathogenesis of congenital diaphragmatic hernia.

General Discussion

From the outset, the principal aim of this work has been to understand the embryonic development of the phrenic nerve and diaphragm. Previous work in the field has focused on the postnatal development of the phrenic nerve and diaphragm. Essentially, these studies demonstrate that this motor system has attained many of the characteristics of the adult by birth. Thus, one has to examine events occurring prenatally in order to define the fundamentally important steps in the development of the phrenic nerve and diaphragm. However, much less was known concerning its embryonic development.Given this motor system's importance at birth, and implications to respiratory disorders, we believed that furthering our knowledge of the formation and maturation of this motor system prenatally would be beneficial. Thus, we initiated detailed studies of the embryogenesis of the phrenic nerve and diaphragm from the onset of axonal outgrowth at E11 to birth. As our results have been fully discussed within the relevant chapters, this general discussion will focus on the major findings and discuss them in relation to their contribution.

Phrenic nerve and diaphragm development

Our primary contributions with regards to the prenatal development of the phrenic nerve and diaphragm include: 1) Identification of the primordial diaphragm as the pleuroperitoneal fold, and description of how it differentiates into the substrate for the diaphragmatic neuromusculature. 2) Identification of a track of cells which appear to guide phrenic axons from the brachial plexus to their target. 3) Description of the formation of the diaphragmatic neuromusculature, from the timing and pathway of phrenic axon outgrowth and the elaboration of nerve and muscle from the pleuroperitoneal fold to the formation of an essentially complete neuromusculature by birth. 4) Discovery that the onset of functional respiratory drive immediately precedes dramatic changes in phrenic somatodendritic morphology that result in the features characteristic of mature phrenic motoneurons.

Embryonic Development

In relation to our basic understanding of the formation of neuromuscular systems during development, the phrenic nerve and diaphragm is poorly represented in both medical and embryological texts. In reading any number of these, it becomes apparent that no consistent picture backed by any direct evidence emerges. We anticipate that our findings shall be incorporated into future accounts of diaphragm embryogenesis. A recent review of respiratory development (Hilaire and Duron, 1999) has been the first to do so in its description of respiratory network development. Further, a detailed description of normal diaphragmatic development will have important implications for understanding certain respiratory disorders, most notably congenital diaphragmatic hernia (see below).

Neuromuscular Development

Investigation of factors controlling neuromuscular formation first requires a detailed understanding of the basic embryology of the system. These studies provide that basic understanding for future studies of phrenic-diaphragm development. Our findings are of interest from the standpoint of understanding axonal segregation at the mammalian forelimb in particular, and axonal pathfinding at plexi in general. First, we now have an account of phrenic axon segregation at the brachial plexus. Second, we have identified the primordial target for phrenic axons and found evidence that it may be derived from a population of cells which i) is appropriately positioned to perform a guidance role for phrenic axons, and ii) appears to form the mesodermal substrate for the diaphragm. Our working hypothesis that this track is formed by somatic mesodermal cells targeted to the diaphragm provides a basic rationale for studies of phrenic axon differential guidance brachial plexus. This is an attractive hypothesis for a number of reasons. The somatic mesoderm is implicated in the guidance of both nerve and muscle into limbs. Thus, phrenic axons are likely guided by a known guidance substrate. This implies that evolutionary addition of phrenic motoneurons to the plexus has resulted in the elaboration of existing guidance systems and re-emphasises the importance of the somatic mesoderm in differential guidance at plexus decision points. If the septum transversum were the principal target for phrenic axons, the possibility of primarily long distance chemotropic signaling in the selective guidance of phrenic axons

would have to be considered.

Recent advances in genetic technology are making great strides in defining the molecular regulatory mechanisms of neuromuscular development. However, in understanding the role of molecules implicated in particular developmental events, one must have an understanding of the environment in which the gene product acts. Deletion of a gene implicated in axonal pathfinding, the LIM homeobox transcription factor gene, *Hb9,* results in selective deletion of the phrenic nerve at the brachial plexus (Thaler et al., 1999; Arber et al., 1999). The authors speculate that phrenic axons misrouted into the limb. Understanding how this gene, and potentially others such as *Lhx3* and *Lhx4* (Sharma et al., 1998), promote selective axonal guidance will require an understanding of how their downstream effectors interact with the environment. Our studies provide the first indication as to what that environment might be. The benefits of such an understanding will likewise extend to understanding the control of muscle precursor migration at the forelimb. Interestingly, the role of the homeobox gene, *Lbx1*, in muscle precursor guidance appears to differ between the trifurcation at the forelimb and the bifurcation at the hindlimb (Schäfer and Braun, 1999).

Prospects

Now that we have identified the primordial diaphragmatic tissue, focus is now being turned to examining the formation of this tissue and testing a number of the hypotheses generated by these studies. One major step towards these goals is the adoption of a whole embryo culture system which will provide experimental access to early stages of the developing diaphragm. This would not otherwise be possible in mammalian embryos. A number of questions that immediately arise include: 1) What is the nature of this p75-expressing track of cells? Examination of p75 immunoreactivity in the track region in *HGF/SF* null mutant mice and *Splotch* mutant mice ought to clarify whether this tissue is indeed mesodermal. Further, co-labeling studies examining the correlation of HGF/SF and p75 expression may provide data regarding the putative guidance role of the track. We have obtained *HGF/SF* null mutant mice and probes for *in situ* hybridisation of HGF/SF. Further, *Splotch* mice can be obtained from Jackson Laboratories. Also, marking the cells of the track, such as by injection of a bolus of dye into cultured embryos, and inspection of subsequent

cellular migration ought to define whether the pleuroperitoneal fold does indeed develop from this track. 2) How does diaphragmatic muscle arise? We have followed muscle formation from the onset of myotube formation. Studies initiated in the laboratory (performed by Randal Babiuk, PhD student) are now examining the nature and timing of muscle precursor cells to the pleuroperitoneal fold, their proliferation, terminal differentiation and fusion into multinucleated myotubes. Further, it would be possible to selectively inject somites with DiI to determine the somitic origin of the diaphragmatic muscle. Such a methodology has been utilised to trace somitic cell fate in the chick (Hayashi and Ozawa, 1991) and rat (Lee and Sze). In order to label myogenic cells during specific stages of their development, several selective markers can be obtained. For migratory myogenic cells, the paired domain homeobox gene *Pax-3* (eg. Bober et al., 1994), the HGF/SF receptor tyrosine kinase *c-Met* (eg. Bladt et al., 1995), the homeobox gene *Msx1* (Houzelstein et al., 1999) and the homeobox gene *Lbx1* (Dietrich et al., 1998) are all expressed by migratory myogenic cells and provide clear labeling for these cells. For proliferating cells, immunohistology for the proliferating cell nuclear antigen, PCNA, provides adequate labeling of proliferating cells (Casasco et al., 1993). Helix-loop-helix (HLH) myogenic factors such as MyoD and Myf-5 label differentiating myoblasts (see Rudnicki and Jaenisch, 1995). The HLH myogenic factor, myogenin, as well as the intermediate filament desmin are good markers for early myotubes (see Capetanaki et al., 1997), as is PSA-NCAM.

Phrenic motoneuron development

The major contribution of this study is the finding that a major morphological reorganisation in phrenic motoneuron morphology directly follows the inception of respiratory drive to these motoneurons, implicating that drive in promoting these maturational changes. This study has been performed in parallel with an examination of the electrophysiological properties of phrenic motoneurons from E16 to birth and the contractile properties of the diaphragm from E18 to birth (performed by Miguel Martin Caraballo, PhD student). Taken together, these investigations are beginning to define the developmental profile of multiple aspects of an identified motor system. The next step is to start functionally

testing the role of descending drive on phrenic motoneuron and diaphragm development. Studies have been initiated in the laboratory in an attempt to uncouple the developing phrenic motoneuron pool from the descending respiratory drive during development by pharmacologically inhibiting respiratory drive. Attempts are also being made at spinal transection prior to the onset of functional drive, at E16. This data should provide evidence regarding which features of motoneuron development are coupled to their respective network, and which are not. It should be stressed that testing such aspects of mammalian motoneuron development is difficult to study in many other systems, primarily due to the close proximity of many motoneurons and local pattern generators.

The role of PSA-NCAM in axon guidance and myogenesis

The major contributions of these studies has been; 1) Finding that PSA-NCAM is selectively expressed by phrenic motoneurons at the brachial plexus. 2) Determining and testing the potential role of PSA-NCAM during muscle morphogenesis.

PSA-NCAM and phrenic axon guidance

PSA-NCAM is one of the only molecules demonstrated to play a role in selective axonal guidance at plexus decision regions in vertebrates, where it is postulated to act as a global defasciculator of axons, facilitating axonal pathfinding by attenuating contact between axons destined for different nerve trunks. We have found that the distribution of PSA-NCAM along axons at the brachial plexus is consistent with a selective role in phrenic axon pathfinding. This would be a novel finding concerning the role of PSA-NCAM in neuronal development and requires functional testing (see below). But why would phrenic axons selectively express PSA-NCAM and not the brachial axons? Evolutionarily, phrenic axons represent a more recent addition to the brachial plexus. It is tempting to speculate that the evolutionary addition of a third neuronal population at the forelimb plexus has resulted in the re-allocation of guidance resources at plexus regions. It is less likely that brachial axons would have undergone dramatic changes in their guidance systems than phrenic axons would

have devised a specialised system for their selective guidance. The use of PSA-NCAM to perhaps shield phrenic axons from the influence of these more established pathways in order to respond to unique cues towards the diaphragm is not inconceivable (and testable). In this regard, it would be of interest to perform the basic studies to determine the distribution of PSA-NCAM along bifurcating axons growing into the rodent hindlimb. We would postulate that it is more globally expressed, as at the chick crural plexus.

It will be important to test the functional role of PSA-NCAM at the brachial plexus. Two methods are being employed. 1) As demonstrated in chapter 9, trifurcation of axons at the brachial plexus occurs in whole rat embryos *in vitro*. This would make PSA removal by endoN injection simple, and testing the putative role of PSA-NCAM in selective axonal guidance feasible. 2) Mice null mutant for NCAM have been obtained and are now ready to examine for pathfinding defects in phrenic axon guidance. These mice have functionally innervated diaphragms as they survive birth, mature into adulthood and are fertile (Cremer et al., 1994; Ono et al., 1994; Moscoso et al., 1998). We postulate that outside of functional redundancy and compensatory mechanisms, phrenic axonal guidance in these mice is either retarded to an extent where there is reduction in axonal numbers, delayed in segregation from the brachial plexus or that early pathfinding errors may be corrected. These data shall be compared at the rat forelimb (trifurcation) and hindlimb (bifurcation).

Results from these studies should prove interesting with respect to the biology of PSA-NCAM in neuronal development. Demonstration of a role in selective pathfinding would certainly be an exciting new finding, but a negative result would re-emphasise the facilitatory role that PSA-NCAM plays.

PSA-NCAM and myotube separation

Previously, the role of PSA-NCAM in muscle morphogenesis had been proposed (Fredette et al., 1993) but neither expression data fully consistent with its proposed role nor functional data reporting the effects of PSA removal had been demonstrated. We have shown that PSA-NCAM is expressed in a manner indicative of a role in myotube separation in both the rat and chick and have begun to provide data demonstrating the potential functional role of this molecule. Differences between the rat and chick may also indicate a different balance

in the role of adhesive and repulsive factors in myotube adhesion/separation between these species. Ongoing studies which are aimed at further characterising the role and regulation of PSA-NCAM in muscle morphogenesis, particularly in relation to cadherins, are fully discussed in the relevant chapter. However, it is important to note here that whatever results are obtained, studies currently in progress shall provide a new understanding of the regulation of myotube separation.

Congenital Diaphragmatic Hernia

Our major contributions have been to: 1) Systematically test prevalent theories regarding the pathogenesis of a defect in diaphragm formation, finding that they are incorrect. 2) Utilise our data concerning normal diaphragm development to find which aspect of diaphragm development is abnormal. 3) Discover that the initial defect is due to abnormal formation of the pleuroperitoneal fold. Further, we are beginning to obtain data suggesting that the defect originates in the somatic mesoderm of that tissue. This work has prompted a number of ongoing studies aimed at furthering our understanding of the pathogenesis of this disorder:

1) We have determined that the pleuroperitoneal fold (PPF) is malformed by E13 to E13.5. But how does this defect arise? The ultimate question is, what and where is the initial insult? Structurally, the defect that we observe could arise by any number of mechanisms. Inadequate mesodermal invasion into the PPF, inadequate proliferation of the PPF mesoderm or inadequate expansion of the PPF mesoderm may be the simplest explanations. Closer examination of normal and abnormal embryos at ages prior to and during initial PPF formation may help to clarify these points and prompt further experimental work (currently being performed by Randal Babiuk, PhD student). Another possibility that should not be overlooked is the possibility that precocious proliferation or displacement of the liver may result in formation of a retarded PPF. Although there is no *a priori* reason to believe that the PPF would not just simply continue to develop and expand over an abnormally large liver,

we cannot discount this possibility. Further examination of normal and defective tissues to examine the dimensions of the liver as well as the potential use of proliferating cell markers (such as PCNA or BrdU) to examine growth within the liver will likely clarify these points.

2) Ongoing research is also aimed at investigating the potential role of abnormal retinoic acid signalling in CDH. Considerable circumstantial evidence points to a possible link between retinoid signalling and CDH. 1 out of 4 mice double null mutant for retinoic acid receptor subtypes α and β2 had CDH with subsequential lung hypoplasia, in addition to a number of other abnormalities (Mendelsohn et al., 1994). Further, vitamin A and retinol deficiency in the rat increases the incidence of CDH and lung maldevelopment in offspring, in addition to a number of other abnormalities (Wilson et al., 1953; Wellik et al., 1997). However, any significant reversal of CDH in the rat model required teratogenic levels of vitamin A (Thébaud et al., 1999). Further, despite some effort, no causal relationship has ever been found between vitamin A deficiency and human CDH. However, given the widespread and fundamental roles that retinoids play in embryonic development, this may be an important avenue for investigation (Armstrong et al., 1994; Mendelsohn et al., 1994; Ng et al., 1995; Shimeld, 1996). The laboratory has initiated a number of studies in this direction. Thus far, the most promising data has come from a collaboration with Dr. Claes Bavik (University of Texas, Austin, Texas). We have found that nitrofen induces a dramatic reduction in the expression of a retinoid response element (as detected by a fused lacZ reporter), of E8.5 to E9 murine embryos in whole embryo cultures, as previously described. This is an age at which we would postulate nitrofen to be acting to initiate abnormal diaphragmatic development.

3) We have not addressed the applicability of our data to the normal and abnormal development of the human diaphragm. Currently, these is no known environmental, dietary or genetic factor which causes CDH. It is important to emphasise that despite the use of a herbicide in producing CDH in rodent fetuses, we found no evidence for either seasonal and/or regional correlations with the incidence of CDH in infants from epidemiological data provided by Health and Welfare Canada, the Alberta Hereditary Diseases Program and the

California Birth Defects Monitoring Program. This does not rule out environmental causes but it does imply that CDH may be due to simple malregulation of some developmental step. As mentioned above, the possibility that abnormal retinoid signalling may be implicated is being pursued. It is pertinent to add here that recent studies by Migliazzi et al (1999, 2000a,b) show that there are remarkable similarities between the incidence and nature of cardiovascular and skeletal defects between CDH in humans and in nitrofen-induced rodent models. Our preliminary data that nitrofen appears to interfere with retinoid signalling, combined with the fundamental role that retinoids have in embryonic patterning, certainly provides circumstantial evidence for an intriguing link between the rodent model and human CDH. It is becoming more conceivable that nitrofen may be producing similar defects because it directly interferes with the same basic embryological systems. In this regard, the laboratory hopes to develop a method of determining the distribution of nitrofen in rodent fetuses.

Is diaphragmatic development similar in the human and rat fetus? Iritani (1984) showed one micrograph from a human fetus showing remarkable similarity between the rodent and human PPF at equivalent ages. Thus, given that the same initial structures are apparent, and the same outcome is apparent, we feel confident that a similar pathogenesis would result in CDH in these two species. Regardless, we have initiated a collaborative effort to reconstruct human diaphragm development from tissues provided by human embryo tissue banks, primarily the University of Alberta Embryo and Fetal Tissue Bank. Initially, we shall examine the morphology of these tissues and reconstruct 3-D renderings of the human PPF. Any success will be followed by direct, likely immunological, visualisation of cellular types or events of particular interest as elucidated by ongoing study of rodent fetuses. In relation to the pathogenic development of CDH in humans, it is currently impossible to detect CDH in human fetuses at early stages of PPF development (if we were to encounter an abnormal PPF, this would not necessarily mean that it would have contributed to CDH). However, we have obtained diaphragms from human perinates who died from CDH and these are being compared to nitrofen-induced rodent CDH diaphragms to look for similar characteristics (e.g., translocated intramuscular entry point of the nerve, increased myotube density near the herniation, phrenic nerve atrophy ipsilateral to the malformation).

REFERENCES

Arber S, Han B, Mendelsohn M, Smith M, Jessell TM and Sockanathan S (1999) Requirement for the homeobox gene *Hb9* in the consolidation of motor neuron identity. *Neuron* 23: 659-674.

Armstrong RB, Ashenfelter KO, Eckhoff C, Levin AA and Shapiro SS (1994) General and reproductive toxicology of retinoids. In: *The retinoids: Chemistry, Biology and Medicine.* 2nd Edition. Edited by MB Sporn, AB Roberts and DS Goodman. Raven Press Ltd. New York. pp 545-572.

Bladt F, Riethmacher D, Isenmann S, Aguzzi A, Birchmeier C (1995) Essential role for the c-Met receptor iin the migration of myogenic precursor cells into the limb bud. *Nature.* 376: 768-771.

Bober E, Franz T, Arnold HH, Gruss P, Tremblay. Pax-3 is required for the development of limb muscles: a possible role for the migration of dermomyotomal muscle progenitor cells. Development 1994;120:603-612.

Capetanaki Y, Milner DJ and Weitzer G (1997) Desmin in muscle formation and maintenance: knockouts and consequences. *Cell Struct. & Funct.* 22: 103-116.

Casasco A, Giordano M, Danova M, Casasco M, Cornaglia AI, Calligaro A. PC10 monoclonal antibody to proliferating cell nuclear antigen as probe for cycling cell detection in developing tissues. Histochem. 1993;99:191-199.

Cremer H, Lange R, Christoph A, Plomann M, Vopper G, Roes J, Brown R, Baldwin P, Kraemer P, Scheff S, Bathels D, Rajewsky K and Wille. (1994) Inactivation of the N-CAM gene in mice results in size reduction of the olfactory bulb and deficits in spatial learning. *Nature.* 367: 455-459.

Dietrich S, Schubert FR, Healy C, Sharpe PT, Lumsden A (1998) Specification of the hypaxial musculature. *Development.* 125: 2235-2249.

Fredette BJ, Rutishauser U and Landmesser L (1993) Regulation and activity-dependence of N-cadherin, NCAM isoforms and polysialic acid on chick myotubes during development. *J. Cell. Biol.* 6: 1867-1888

Hayashi K and Ozawa E (1991) Vital labelling of somite-derived myogenic cells in the chicken limb bud. *Roux's Arch. Dev. Biol.* 200: 188-192

Hilaire G and Duron B (1999) Maturation of the mammalian respiratory system. *Physiol. Rev.* 79: 325-360.

Houzelstein D, Auda-Boucher G, Chéraud Y, Rouaud T, Blanc I, Tajbakhsh S, Buckingham

ME, Fontaine-Perus J and Robert B (1999) The homeobox gene Msx1 is expressed in a subset of somites, and in muscle progenitor cells migrating into the forelimb. *Development.* 126: 2689-2701.

Iritani I (1984) Experimental study on embryogenesis of congenital diaphragmatic hernia. *Anat. Embryol.* 169: 133-139.

Lee KKH and Sze L-Y (1993) Role of brachial somites in the development of the appendicular musculature in rat embryos. *Dev. Dyn.* 198: 86-96

Mendelsohn C, Lohnes D, Décimo D, Lufkin T, LeMeur M, Chambon P and Mark M (1994) Function of the retinoic acid receptors (RARs) during development. II Multiple abnormalites at various stages of organogenesis in RAR double mutants. *Development.* 120: 2749-2771.

Migliazza L, Xia H, Alvarez JI, Arnaiz A, Diez-Pardo JA, Alfonso LF, Tovar JA. Heart hypoplasia in experimental congenital diaphragmatic hernia. J Pediat Surg, 1999; 34:706-10.

Migliazza L, Otten C and Xia H. (2000) Cardiovascular malformations in experimental diaphragmatic hernia. *J Pediatr Surg.* In press

Migliazza L., Xia H, Diez-Pardo JA. (2000) Skeletal malformations associated with congenital diaphragmatic hernia: experimental land human studies. *J Pediatr Surg*, in press

Moscoso LM, Cremer H and Sanes JR (1998) Organization and reorganization of neuromuyscular junctions in mice lacking neural cell adhesion molecule, tenasci-C, or fibroblast growth factor-5. *J. Neurosci.* 18: 1465-1477.

Ng KW, Zhou H, Manji S and Martin JT (1995) Regulation and regulatory role of the retinoids. *Crit. Rev. Eukaryotic Gene Expression.* 5: 219-253.

Ono K, Tomasiewicz H, Magnuson and Rutishauser U (1994) N-CAM mutation inhibits tangential neuronal migration and is phenocopied by enzymatic removal of polysialic acid. *Neuron.* 13: 595-609.

Rudnicki MA and Jaenisch R (1995) The MyoD family of transcription factors and skeletal myogenesis. *BioEssays.* 17: 203-209.

Schäfer K and Braun T (1999) Early specification of limb precursor cells by the homeobox gene *Lbx1h. Nature Gen.* 23: 213-216.

Sharma K, Sheng HZ, Lettieri K, Li H, Karavanov, Potter S, Westphal H and Pfaff SL (1998) LIM homeodomain factors LHX3 and LHX4 assign subtype identities for motor neurons. *Cell.* 95: 817-828.

Shimeld SM (1996) Retinoic acid, HOX genes and the anterior-posterior axis in chordates.

BioEssays. 18: 613-616.

Thaler J, Harrison K, Sharma K, Lettieri K, Kehrl J and Pfaff SL (1999) Active suppression of interneuron within developing motor neurons revealed by analysis of homeodomain factor HB9. Neuron. 23: 675-687.

Thébauld JF, Tibboel D, Rambaud C, Mercier J-C, Bourbon JR, Dinh-Xuan AT, Archer SL (1999) Vitamin A decreases the incidence and severity of nitrofen-induced congenital diaphragmatic hernia in rats. *Am. J. Physiol.* 277: L423-429.

Wellik DM, Norback DH and DeLuca HF 91997) Retinol is specifically required during midgestation for neonatal survival. *Am. J. Physiol. (Endocrinol. Metab.* 35:*)* 272: E25-29.

Wilson JG, Roth CB and Warkany J (1953) An analysis of the syndrome of malformations induced by maternAl vitamin A deficiency. Effects of restoration of vitamin A at various timjes during gestation. *Am. J. Anat.* 92: 189-217.